TUDelft

Arch of Glass-Concrete

Technische Universiteit Delft

Arch of Glass-Concrete

Design of Arch with Glass-Concrete Composite Components

Jinxuan He

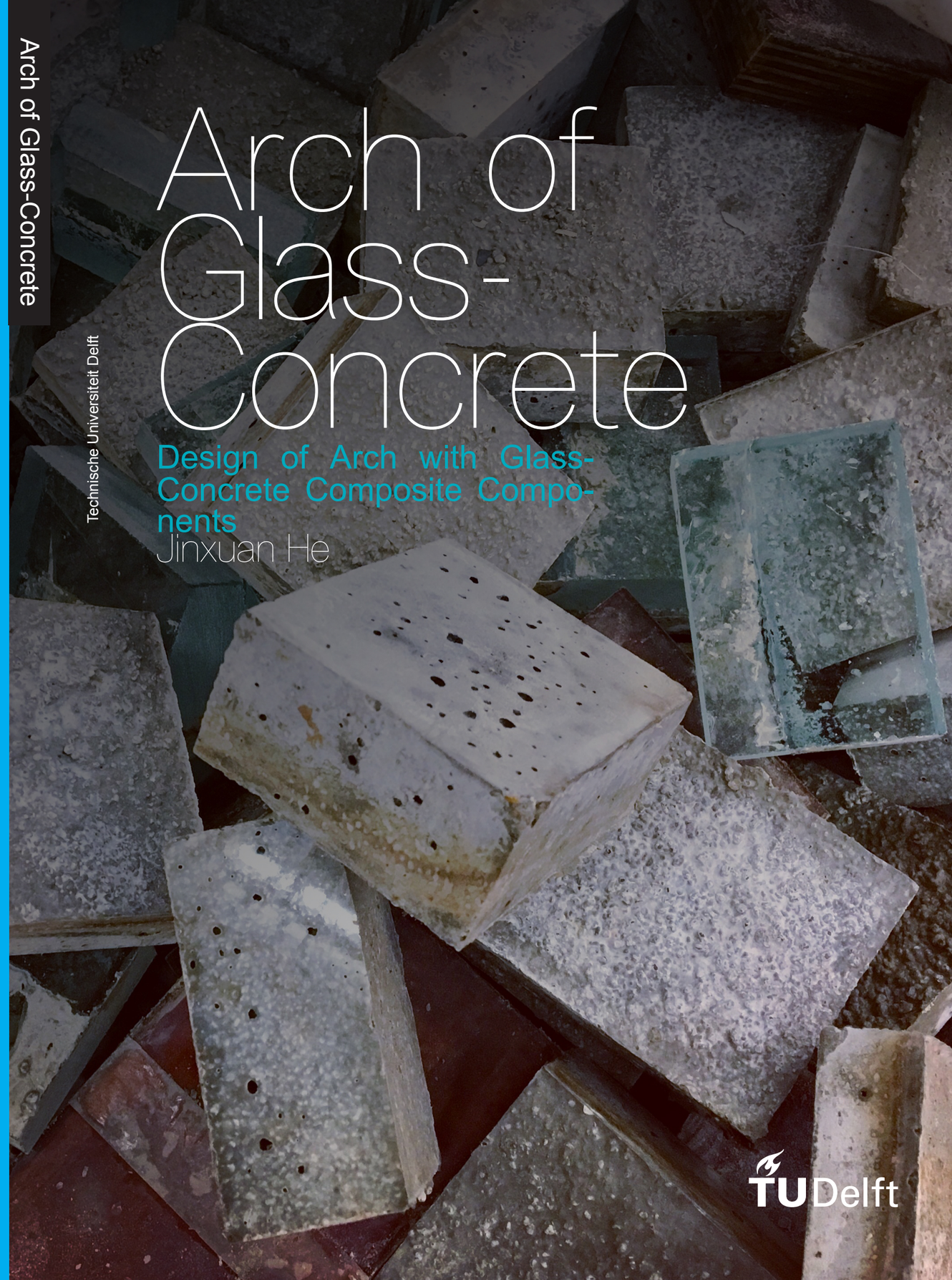

TUDelft

Arch of Glass-Concrete

Design of arch constructed with glass-concrete composoite components

by

Jinxuan He

To obtain the degree of Master of Science
in the faculty of Civil Engineering and Geosciences
at the Delft University of Technology,

Date:	February 2018		
Email:	J.He-9@student.tudelft.nl		
Student number:	4501438		
Thesis committee:	Prof. ir. Rob Nijsse	Chairman	Civil Engineering, Structural Design
	Ir. Telesilla Bristogianni	Daily Supervisor	Civil Engineering, Structural Design
	Dr. ir Fred Veer	Test,FEM Advisor	Architectural Engineering and Technology
	Dr. ir Christian Louter	Connection Advisor	Architectural Engineering and Technology
	Ir. Erwin ten Brincke	Structure Advisor	ABT

TU Delft Delft University of Technology

abt

Preface

This has been a unique and unforgettable experience for me to explore the possibilities of combing building materials glass and concrete. I have learned a lot and gained so much through this thesis, which gives me courage and keeps me cheerful along the journey. I know there is still much to improve in this thesis, but I am thankful and satisfied with the outcome, which is credited to the help from so many people during the thesis.

First of all, I would like to express my gratitude to all members in my thesis committee.

Prof. Nijsse answered my questions about thesis and arranged basic procedures of thesis start at our first meeting, which led me quickly into the research and to meeting other mentors. He is always glad to meet and provide support whenever I need advice from him.

As my supervisor, Telesilla is also a friend who is always supportive and helpful. She guided me through so many troubles, gave me many valuable advices on the basis of my thesis design. Since she is my supervisor, I throw quite a lot of detailed and amateur questions to her, but she was always patient and ready to solve my doubts.

I really appreciate my mentor Mr. Veer, the man who inspired me to start my thesis design from Nervi's work, for his selfless contribution to my thesis. I remember I really bothered him a lot after he just recovered from his illness. As my advisor for both experiment and FEM software, we spent much time together to discuss my problems in test, numerical calculation and other aspects. I deeply respect and thank him for helping me to make this thesis possible.

My gratitude also goes to Mr. Christian, for his insightful comment and suggestions on connection designs. I can still recall that afternoon I learned a lot when I struggled to explained my vague to him and Telesilla, which confused them but they were still very tolerant to give guidance.

It is a pity I could not work together much with my mentor Mr. Brincke. However, the discussions with him have been illuminating for his firm knowledge in both glass and structural design. I have greatly benefited from his practical feedbacks.

There are many people apart from my committee I am deeply grateful to. Mr. Baardolf in Dream hall, who managed to help me make test moulds and glass specimens even with his busy schedule. By his introduction, I got to know Mr. Blom and Mr. Leeuwen in concrete lab, who taught me so much in preparing, making and testing concrete specimens. Besides, I would like to offer my special thanks to talent and helpful Lida Barou, who guided and helped me to make test specimens even in her busies days. This thesis would not have been possible without their contribution and support.

Finally, to my dearest parents, and to all my supportive and beautiful friends, I love you.

感谢我的爸爸妈妈，我爱你们。

Jinxuan He
Delft, February 2018

Summary

The main topic of this thesis is the design of arch with components made up of glass and reinforced concrete. There is limited literature regarding the combing of glass and concrete, most examples of which use glass more like decorative material instead of load bearing elements. Some examples are discussed and introduced in both Chapter 1 and 2, where the functions of glass and concrete are explained. The important inspirational examples of Salone Agnelli and corrugated glass are briefly discussed in Chapter 1, which leads to the objectives and approaches of this thesis in section 1.4 and 1.5.

To define the reasons of combing glass and concrete, basic properties and possbile benefits are described in Chapter 2, where some background related to conceptual design, limitations, connection design and experiments will also be presented. Important theoretical supports for this design are given in Chapter 3 and the beginning of Chapter 4. Guidelines from Eurocodes, validation of FEM and principles for glass and arch design are explained in this part.

In Chapter 4 preliminary design of connection is also illustrated, which will be modified and further elaborated in Chapter 6. Parameters will be study in two levels of global and detailed models as is defined in section 4.3, of which the global parametric study will be carried out in Chapter 5, and the optimal choice will be made for the following design.

As for the mechanical and adhesive connections in Chapter 6, they will be discussed and compared to extract the required experimental data. Here mainly connections between glass and concrete, element and element are considered. The research of shear bond test will be depicted in Chapter 7, results of both concrete compression test and shear bond test are given and analysed in section 7.4.

Chapter 8 are composed of mainly two parts: global model and detailed mode. The behaviour of composite arch and pure glass arch, as well as parametric study of global level will be verified and compared in the first part. To validate the sufficiency of bond strength, the detailed model is built to study the shear stresses on the surfaces of bond between concrete and glass. Because of the problems occurred during the FEM simulations, we have the approximate results of stresses which exceed the range of experimental results. Therefore, two solutions are discussed to solve this problem in Chapter 9, either by increasing the bond strength or lowering the shear stress in this design, both of which will be validated.

Conclusions and recommendations will be made in the end of this report, to summarize the principal outcomes of this thesis, and what can be researched and improved further in the future.

Acronyms

2D	Two dimensional
3D	Three dimensional
Ansys WB	Ansys Workbench
ASR	Alkali Silicate Reaction
ASTM	ASTM International (originally called American Society for Testing Materials)
C-S-H	Calcium Silicate Hydrate
DM	DesignModeler
EPDM	Ethylene propylene diene monomer
EQU	Equilibrium of the structure
FEM	Finite Element Method
IGU	Insulating glazed units
MPC	Multi-point constraint
MS	Modified silicones
NEN	NEderlandse Norm
PC	Polycarbonate
PUR	Polyurethanes
SLS	Serviceability limit states
UDL	Uniformly distributed loading
UHPC	Ultra High Performance Fibre Reinforced Concrete
UHSC	Ultra High Strength Fibre Reinforced Concrete
ULS	Ultimate limit states

Symbols

Sign	Description	Unit
G_k	Total permanent load	
M_{arch}	Internal critical moment in the arch	$N \cdot mm / kN \cdot m$
$Q_{1;k}$	Characteristic value of the leading variable load	
$Q_{i;k}$	Characteristic value of variable load	
R_h	Thrust reaction force	kN
R_{moment}	Reaction moments at support	$kN \cdot m$
R_v	Vertical reaction force	kN
$\Psi_{Q;i}$	Factor for combination of variable load/ with the leading load	
γ_G	Partial factor for permanent loads	
$\gamma_{Q;i}$	Partial factor for variable loads	
μ_i	Shape coefficient for snow load	
σ_{c-b}	Maxmium/minmium bending stress in concrete part	N/mm^2
$\sigma_{f,f}$	Flexural strength from 3 point bending test	MPa
σ_{g-b}	Maximum/minimum bending stress in glass part	N/mm^2
τ_b	Shear bond strength from shear bond test	N/mm^2
τ_p	Shear strength from push out test	MPa
τ_{xy}	Shear stress in XY plane	N/mm^2
τ_{xz}	Shear stress in XZ plane	N/mm^2
τ_{yz}	Shear stress in YZ plane	N/mm^2
$c_{pe,10}$	External pressure coefficients	
$h_{ef;\sigma;j}$	Laminated glass effective thickness in terms of stress within a ply	mm
$h_{ef;w}$	Laminated glass effective thickness in terms of bending stress	mm
$q_p(Z_e)$	Peak velocity pressure for wind load	kN/m_2
s_k	Characteristic snow load on the ground	kN/m_2
w_{dl}	Linear dead load by multiplying pressure and component width	kN/m
w_{ds}	Surface pressure of dead load	N/mm^2
w_{sl}	Linear snow load by multiplying pressure and component width	kN/m
w_{ss}	Surface pressure of snow load	N/mm^2
w_{wl}	Linear wind load by multiplying pressure and component width	kN/m
w_{ws}	Surface pressure of wind load	N/mm^2

Contents

1 Introduction

Glass is being applied as part of building structure more frequently than before. As a structural material, its properties of high compressive strength and comparatively lower tensile strength are quite similar to concrete. However, the research between glass and normal concrete as well as UHSC is not much, which made me curious about the compatibility and possibility between these two materials. In this chapter, some study on glass combing concrete,the scope, objectives and methodology of this research will be defined.

1.1. Background

It has becoming increasingly common for the using glass as a load bearing material over the past couple of decades, while it has already been millennia for the using of concrete as normal load bearing material. Both materials are brittle before any improvement is made. A big difference between them is transparency, which gives the potential of combining them together as building components. In Figure 1.1 the Bruno Taut glass pavilion was built in 1914 at the Cologne Deutscher Werkbund Exhibition.Here concrete structure behaved like a skeleton where coloured glass plates on the façade inlying into(Richards, 2006).

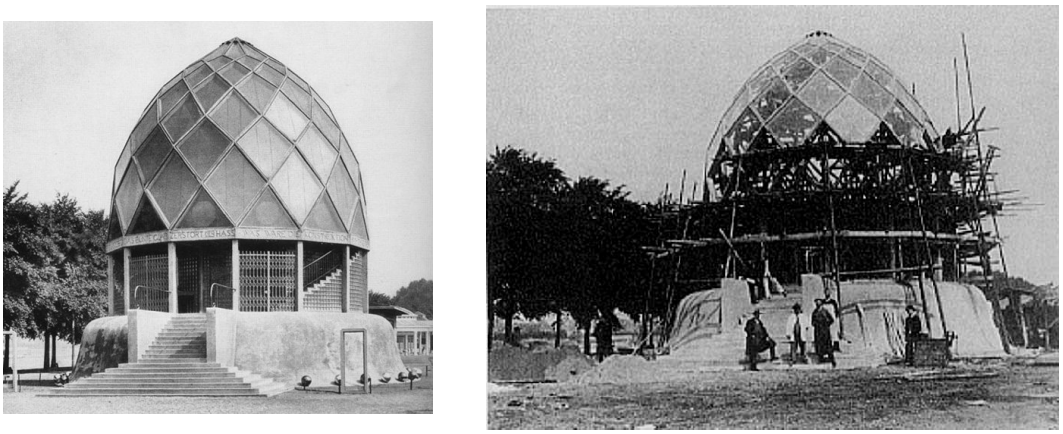

Figure 1.1: Glass Pavilion

The slender staircase of glass and concrete created by ABT[1] is another example combing UHPC and glass. In Figure 1.2a the stair is so slender that the mould for it to fill in is just 5 centimetres deep, where innovative pouring process should be applied. The close up in Figure 1.2b shows an

[1]Source: https://www.abt.eu/en/expertise/innovations/ultra-thin-hybrid-staircase.aspx

invisible connection between the glass balustrade and concrete plate, in which case steel strips are prefabricated and bonded onto the glass. Small notches on these steel strips are bolted almost invisibly onto the concrete from underneath.

(a) Sideview

(b) Detail of stair

Figure 1.2: Ultra-slim hybrid staircase

1.2. Motivation

With the advice from Mr. Fred Veer, I found myself some inspirations from one of the masterpieces designed by Pier Luigi Nervi, the Salone Agnelli hall of Turin Exhibition Building (Figure 1.3). This famous vault shape hall with its undulating corrugated roof surly had its influence on the folded surface concept developing(Schueller, 1996).

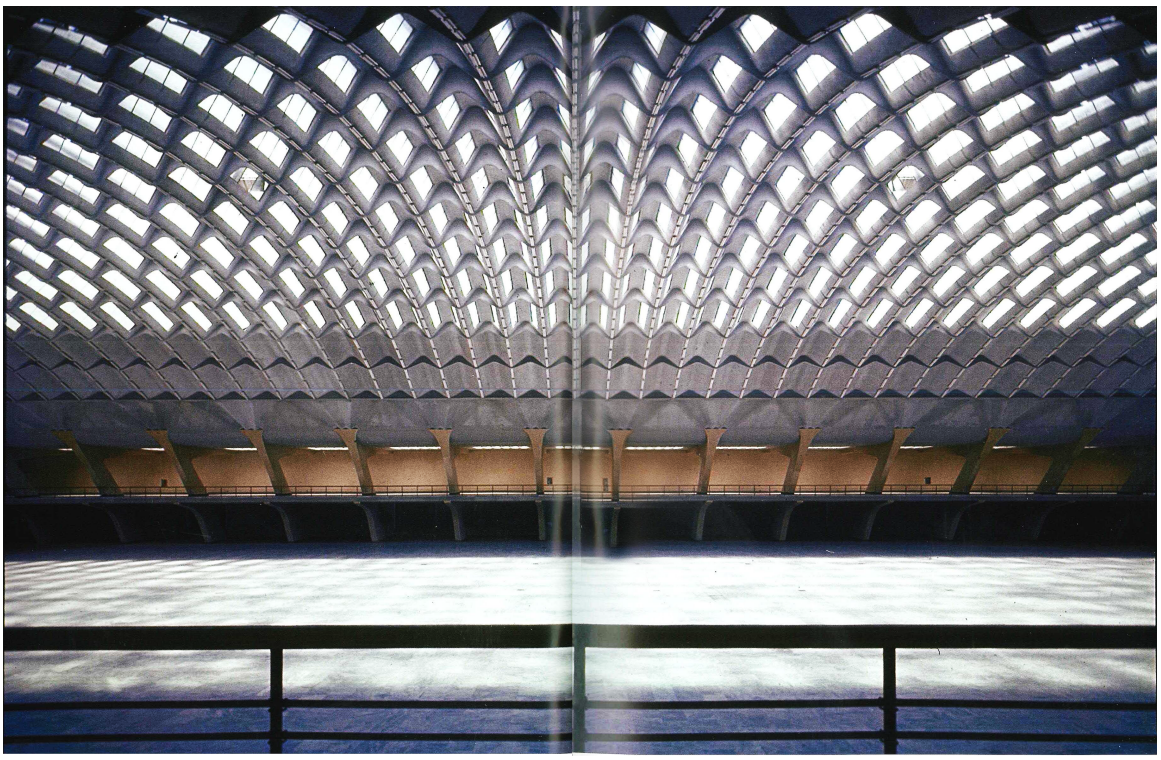

Figure 1.3: Turin Exhibition Building: Salone Agnelli (1948)

The longitudinal and transverse section of this hall are shown in the following pictures(Nervi and Einaudi, 1965), where the length of this vault is about 75 metres. The span of vault is 95.1 metres while the height of it is 18.4. The folded (corrugated) component section can be seen along the undulating roof of Salone Agenlli in Figure 1.4.

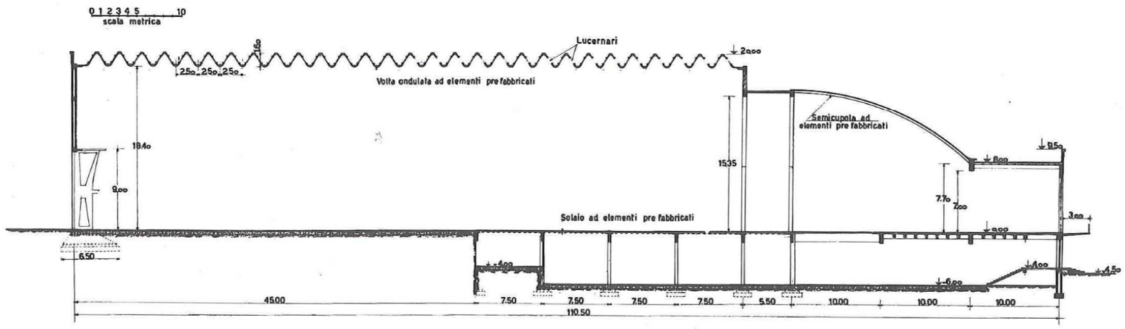

Figure 1.4: Longitudinal section of Salone Agnelli

On the other hand, components constituting the arch section are straight lines as showing in Figure 1.5.

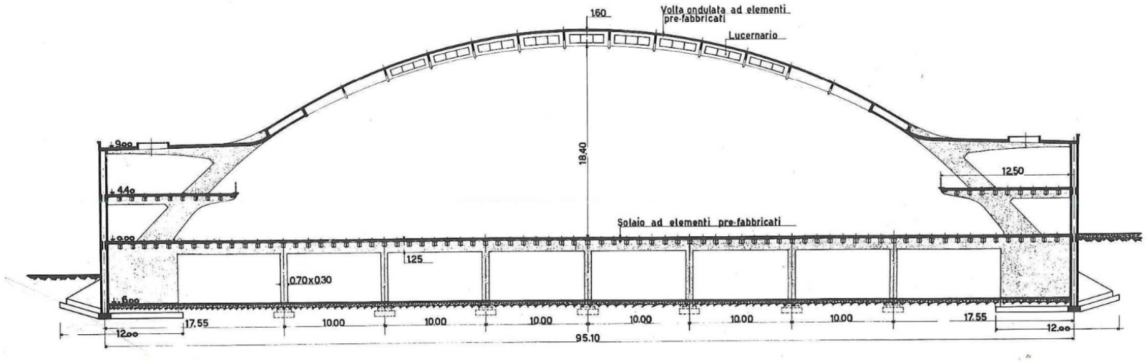

Figure 1.5: Transverse section of Salone Agnelli

The site photo of Figure 1.6a shows the comparatively large dimension of one single component. Figure 1.6b gives an idea about installing components in site with the assistance of falsework. After the instalment of elements, in place concrete is poured to obtain a perfect connection which makes the connecting arch work as a monolithic structure(Nervi and Einaudi, 1965).

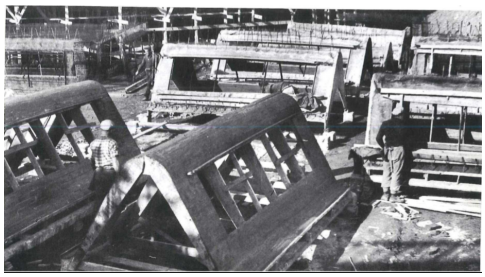

(a) Site photo of elements

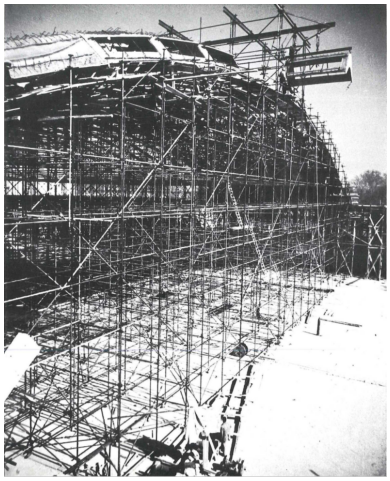

(b) Site photo of elements erecting

Figure 1.6: Site photos

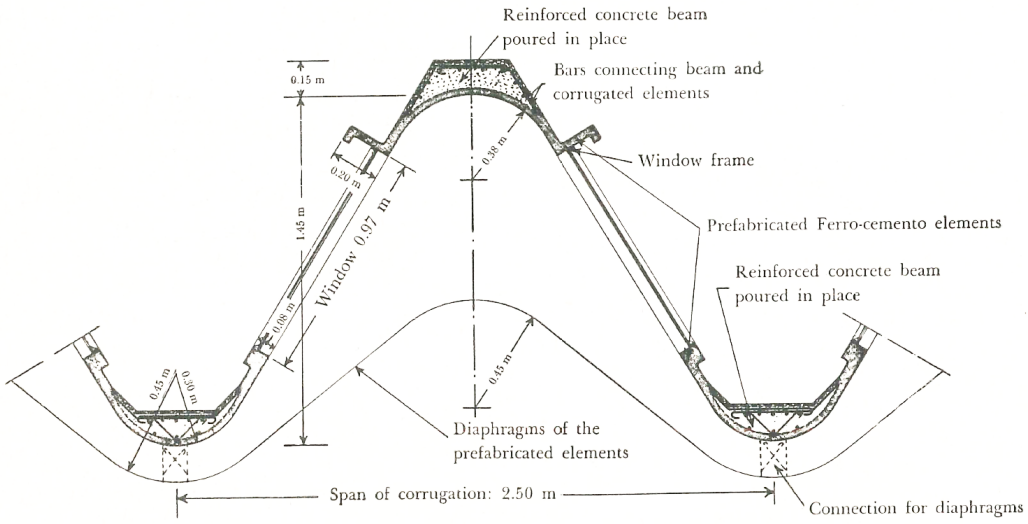

Figure 1.7: Roof beam for the main hall

The section of one component is demonstrated in Figure 1.7. This element is 1.5 inch thick ferro-cemento concrete plate in sinusoidal shape.The height of single element is 1.6 metres with the length of one unit being 2.5. The concrete ribs along the top and bottom of the corrugated element are cast in place to achieve the static collaboration between each unit rings(Nervi, 1956).

It turns out to be a very creative and beneficial way to fold a plate, and use it as a load bearing element. By applying the Huygens–Steiner theorem, such element becomes stronger with little more material.

Glass was not used as a load bearing material but more like a functional composition in the example shown above in Salone Agnelli. However, there are two remarkable projects deploying corrugated glass as part of structural system in the façade: Casa da Musica in Porto (Figure 1.8) and Museum aan de Stroom in Antwerp(Figure 1.9).

Figure 1.8: Casa da Musica

If one component is taken out of the undulating façade, an asymmetrical corrugated panel is presented in the Figure 1.10. Here this type of glass is applied on façade and in compression. There is possibility we can apply this structurally favourable folded element on the roof similar to the one in

Salone Agnelli.

Figure 1.9: Museum aan de Stroom

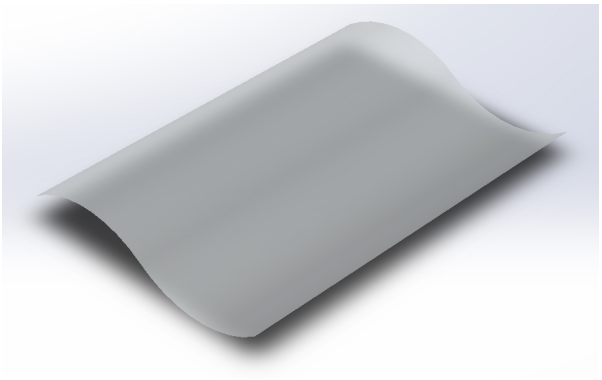

Figure 1.10: One panel of corrugated glass

1.3. Scope

According to the introduction in motivation, it can be easily related between Salone Agnelli roof beam and corrugated glass in the way of structural typology. Integrating concrete and corrugated glass can be a workable direction, which may be simply described as transforming the functional glass in Nervi's example into both functional and structural one.

Many aspects need to be taken into consideration in this possible design as following (not all aspects are covered):

- Arch (vault) design
- Connection design

- Foundation design
- Climate design
- Maintenance and replacement
- Structure redundancy design (safety design)
- Fire safety and accidental design
- Inner space use
- ...

This thesis will mainly cover the aspects of arch design and connection design. Other aspects will be further studied if possbile.

1.4. Research objectives

As being said in the scope discussion, the object of this thesis is to design an arch composed of glass-concrete composite element. In this case, glass area in Nervi's roof beam will be expanded to resist more force while concrete is still integrated to reach a better structural or functional performance. A parametric way of research will be carried out in the design of both arch and component.

Some important questions are to be answered in this thesis:

1. What advantages does concrete bring into this design both functionally and structurally?
2. The same applies to glass in question 1.
3. What connections will be used and reasons for that?
4. What data is needed in this design?

These questions will be answered in terms of different design stages in following chapters.

1.5. Approach

Time plans and processing approaches were modified frequently in this thesis. Figure 1.11 is a diagram briefly illustrating the stages and process through my research.

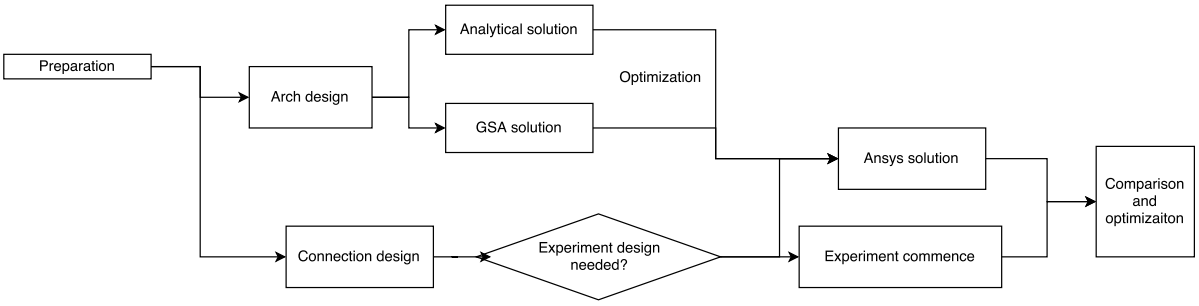

Figure 1.11: Approach plan for thesis

In Chapter 2 reviews over the literature study and preparation related to this thesis are depicted. Several new concepts and important support theories will be listed in Chapter 3, which provides the theoretical framework for this research. Basic and simple designs conceived in the preliminary period as well as some conceptual directions for this thesis are described in Chapter 4.

Two important branches in Figure 1.11 are elaborated in Chapter 5 and 6: Arch and connection design, which will be both influenced a number of common parameters and studied parametrically. For the shear bond strength data required in the design from Chapter 6, an experiment shall be carried out and analysed in Chapter 7. To validate this research, Finite Element Method (FEM) is introduced to assist both global and detailed designs, which will be stated in the Chapter 8. Some discussions to solve current problems and achieve this design is presented in Chapter 9 thereafter. Finally, some comparisons and possible improvements are discussed in Chapter 10. To conclude this research, recommendations will also be added in Chapter 10.

2

Background

Arch of glass and concrete involves as least three topics: Arch, glass and concrete. Basic information and literature study is required before combining them together in this research. Some theories about shell structures and design of glass as well as concrete will be covered in this chapter. Besides, previous application and research of corrugated glass is summarized here. Instead of using normal concrete or UHSC for further study, fly ash concrete (technically named fly ash mortar or Hoogeovens mortel in Dutch) will be applied, which is discussed in this chapter.

2.1. Material of composite component

2.1.1. Properties

The history of using glass as building material to enclose space can date back to almost two millennia ago, while the discovery of glass was even earlier. In Table 2.1 some physical properties of normal building materials, glass, concrete and steel are listed. We can see glass and concrete have similar density while glass is stiffer and higher in tensile strength, there is possibility to save material and improve structural performance by combining them.

	Material		
Properties	Glass (Soda-lime)	Concrete (C25/30)	Steel (S355)
Young's Modulus $[N/mm^2]$	70000	27000	210000
Poisson's ratio	0.2	0.2	0.3
Tensile strength $[N/mm^2]$	20	2.2	235
Density $[kg/m^3]$	2500	2500	7850
Coefficient of thermal expansion $[K^{-1}]$	8.6×10^{-6}	10×10^{-6}	12×10^{-6}
Thermal conductivity $[Wm^{-1}m^{-1}]$	1	1	50.2

Table 2.1: Properties comparison

Glass does not yield like steel or aluminium, which means it is a brittle material resembling concrete. It is also clearly shown in Figure 2.1 (Haldimann et al., 2008). Therefore, attention needs to be paid to stress concentration when designing glass elements. However, post breakage behaviour can be alleviated by laminating layers of glass panels. Laminated glass shall be deployed in this research for safety reason, whereas long-term loading and thermal shock behaviour is worth further studied.

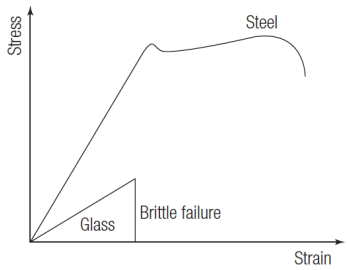

Figure 2.1: Stress/strain curves for steel and float glass

2.1.2. Advantages of combing

Improvements can be achieved if certain properties of glass and concrete are extracted to be taken advantage of, which mainly depends on specific design. In this research, improvements glass and concrete will possibly bring into this design are summarized in Table 2.2. Since glass has better performance in certain mechanical properties, material saving becomes practical by expanding glass as load bearing material. With the nearly same density, it is lighter to hoist one component, which also saves the cost of falsework and labour. By applying an interlayer of certain material or air, the thermal performance of glass panels is also controllable.

The increase of glass areas will provide better daylight environment to inner space, while concrete parts work as necessary sun shading as the same time. It is feasible for concrete to work as compensation for the tolerance due to the manufacture of curved glass (will be described in the section of corrugated glass), when concrete is casted in connection or diaphragm. In addition, functional space such as pipes or gutter is also convenient to make with the help of concrete. Different types of concrete such as UHSC is promising to improve the performance of component. Last but not the least, post-tension concrete to maintain compression both in concrete and glass will be a big benefit.

Glass	Concrete
• Material saving • Transparency/Daylight • Thermal performance / Climate design • Falsework / Construction effort • Load bearing • Typology • ...	• Beam and diaphragm • Stiffener / connection • Tolerance compensation • Water tightness • Sun shading • Gutter / Functional space • Prestressing • UHSC • ...

Table 2.2: Feasible introduced improvements

2.2. Fly ash concrete

2.2.1. Definition and specification

Fly ash is a term referred to any solid, fine-grained particulate material precipitated from the combustion of pulverized coal in industrial power station furnaces.This term is not applied to the extracted residue from the bottom of boilers, while fly ash is collected in electrostatic or mechanical separators (Wesche,

2004).

Fly ashes may be categorized into two types according to ASTM (Wesche, 2004):

- *Class F: Fly ash normally produced by burning anthracite or bituminous coal which meets the requirements applicable to this class. Class F fly ash has pozzolanic properties.*
- *Class C: Fly ash normally produced by burning lignite or sub-bituminous coal which meets the requirements applicable to this class. In addition to pozzolanic properties, Class C fly ash also possesses some cementitious properties. Some Class C fly ashes may have lime contents in excess of 10%.*

2.2.2. Composition and reaction

SiO_2, Al_2O_3 and Fe_2O_3 are particularly rich in fly ash, and along with other oxides such as CaO, MgO, MnO, TiO_2,Na_2O,K_2O,SO_3,etc (Wesche, 2004). Chemical composition examples of cement, fly ash (Bendapudi and Saha, 2011) as well as glass (Haldimann et al., 2008) are illustrated and compared in Table 2.3.

	Chemical composition (%)							
Materials	SiO_2	Al_2O_3	Fe_2O_3	CaO	MgO	SO_3	Na_2O	LOI
Cement	19.61	7.33	3.32	63.15	2.54	2.13	-	2.97
Fly ash 1	55.3	25.70	5.3	5.6	-	1.4	-	1.9
Fly ash 2	56.79	28.21	5.31	<3	5.21	0.68	-	3.9
Soda-lime glass	69-74	0-3	-	5-14	0-6	-	10-16	-

Table 2.3: Chemical composition

As a member of pozzolanic material, fly ash will react with calcium hydroxide to form a reaction product that is similar in composition and properties to C-S-H (Bumrongjaroen et al., 2007), which can be written as equation 2.1:

$$SiO_4^{4-} + xCa(OH)_2 + (y - 2x)OH^- + nH_2O \rightarrow Ca_xSi(OH)_y \cdot nH_2O \tag{2.1}$$

Leaching will form if a film of water retains on the surface of glass for a long time, the reason for which is that the bond between silicon and the oxygen in the water is stronger than that to the components in the lattice interstices in the glass (Schittich and Institut für Internationale, 2007). The diagram of this process is described in Figure 2.2. For normal wet concrete, leaching from glass is likely to happen which is similar to the alkalis attack process in Figure 2.3 (Schittich and Institut für Internationale, 2007).

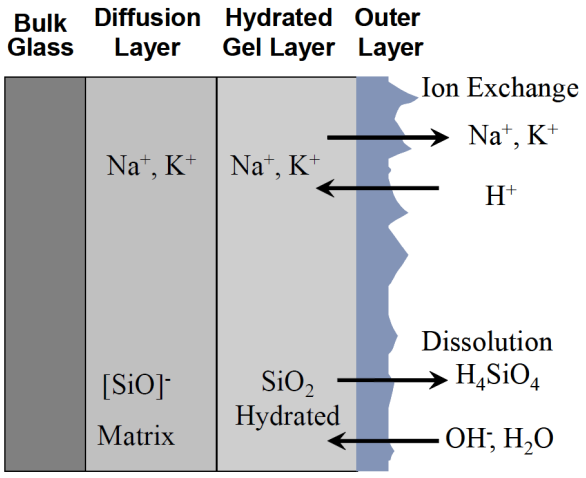

Figure 2.2: Schematic diagram of glass hydration surface layers

2.2.3. Related reasons and test

Recycling and using glass in concrete is an economical way of waste disposal. From Table 2.3 it is clear that high silica content existing in glass, making it a potentially pozzolanic material when it is in particle and size smaller than 75 μm(Chandrusha et al., 2017).

There is a major concern when applying glass in concrete that Alkali Silicate Reaction (ASR) will occur. As mentioned in last section, the reaction is between alkali inside concrete pore solution and silica-rich glass particles. However, by including fly ash in glass concrete, this reaction is suppressed or reduced, which results in a more workable and durable concrete(Chandrusha et al., 2017).

a Alkaline solution:
Film of water on glass surface

b Alkali as a reaction product in solution:
Alkali diffusing out of glass surface into water (leaching)

c Alkali as a reaction product in solution:
Alkali reaction particles on the glass surface after drying (leaching)

d Sketch of glass cross-section reduced (corroded) by alkalis

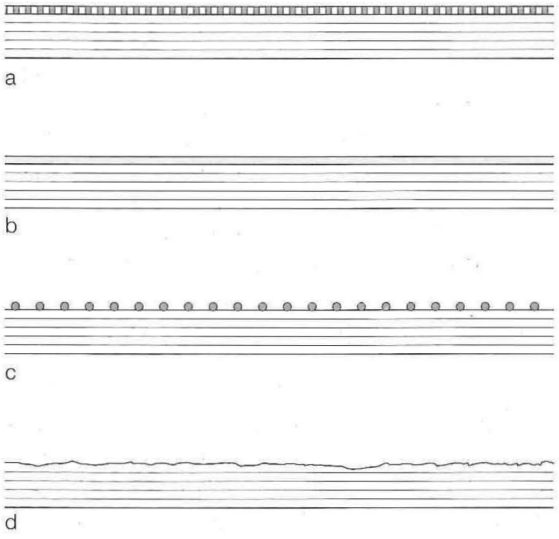

Figure 2.3: Reaction caused by alkalis attacking glass

We utilize fly ash concrete in this research for mainly three reasons:

- Its property to reduce the ASR between normal concrete and glass, in this way surface and strength of glass can be stabilized.
- Research predicted through computer simulation that inter-facial strength is improved by replacing 20% of cement with smaller particle fly ash comparing to control Poland cement paste. Because small particle size and pozzolanic reactivity can generate denser micro-structures thus stronger inter-facial bond (Wong et al., 1999a).
- It is a problem to dispose millions of tons fly ash per year. The high environmental pollution of green gas pollution caused by producing and using cement is significant. By replacing part of cement with fly ash, not only some properties of concrete are refined, but also the environmental and economical benefits can be accomplished(Bendapudi and Saha, 2011).

The shear bond test related to fly ash concrete will be further described in the chapter of experiment.

2.3. Corrugated glass

2.3.1. Curved glass production

To make curved glass, hot bending and cold bending are two common methods. Cold forming is forcing a flat glass plate into a desired shape, by clamping or point fixing on a sub-construction. The stresses caused by cold bending remain in the glass after production(Nijsse, 2009). This method limits the degree for a single curved surface up to half. Besides, it can be less curved if glass sheet is thicker and stiffer, the minimum radius of which is many times larger than hot deformed one for cylindrical curvature(Wurm, 2007).

Therefore, it is preferable to hot bend and produce curved glass sheets in this case. Through heating a flat glass panel in a furnace to hot viscous state, it will sag on to a fire resistant metal or ceramic mould by the gravity of its mass. Figure 2.5 presents one proceeding method of thermal bending curved glass (Molter and Wolf, 2011).Before any prestressing, laminated safety glass can be made by placing several panels one upon each other in a single thermal bending process.It is also achievable to manufacture curved glass with straight extensions (Figure 2.4) and multiple curvatures in an S-shape or U-shape, and the straight extension can be on one side or both sides(Wurm, 2007).

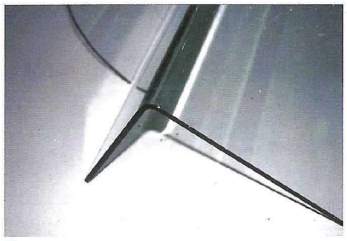

Figure 2.4: Example of bent glass with straight extensions

(a) Mother mould for hot-bent glass

(b) Using hot-bent glass panes to make insulating glazing

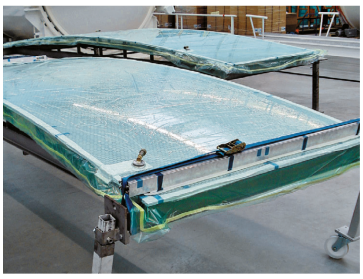

(c) Laminated bends of glass panes

Figure 2.5: Hot bending

2.3.2. Restrictions

During the process of making corrugated glass, residual stresses may still exist despite tempering is to be avoided. The stress can be up to $30 N/mm^2$ according to the study and experiments done by the RWTH Aachen University, which is due to the gravity variant of moulding process(Nijsse, 2009).

The exactness for the dimensions of corrugated glass is also critical. On the one hand, the thickness can differ along the curvature of one glass panel. This is because the heated glass sags differently at different spot of curvature, where a weaker spot may develop, the average tolerances for bent glass is summarized in Figure 2.6.

On the other hand, the length, width and curvature of various panels are unlikely to be the same, the tolerance in the examples of Porto (Figure 1.8) and Antwerp (Figure 1.9) can be +/- 2mm from experience(Nijsse, 2009).

The size of one glass panel has its limitations too. In the case of corrugated glass in Antwerp, the upper bound of length of one panel is 6 metres due to the limitation of production and transportation (Nijsse, 2009). The height of "wave" of curved glass is more flexible with the changing of width. In Figure 2.7 [2]it is clear that for annealed glass maximum "wave height" is 1000mm, where the thickness of various heights are also various.

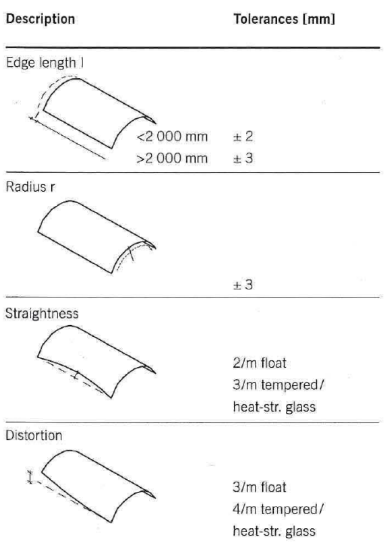

Figure 2.6: Summary of average tolerances in mm for bent glass

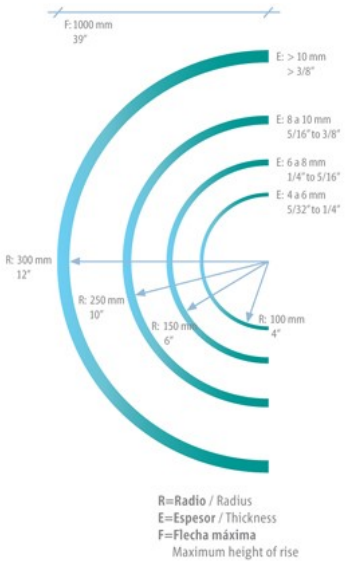

Figure 2.7: Limitation of curved annealed glass

[2]Source: http://www.cricursa.com/segur/prinproductos.aspx?Cerca=1&PerTip1=101

Another important aspect considering the asymmetrical shape of one corrugated glass panel is the discrepant structural behaviour, which is depicted in Figure 2.8 (Nijsse, 2009). The concave shape is weaker, likely to move more and flatten out under loading. Moreover, the overall shape of the profile can rotate in the direction of the convex part.

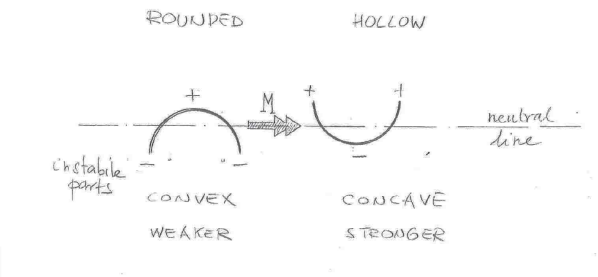

Figure 2.8: The structural effect of being concave or convex for a corrugated surface

2.4. Glass shell structure (Arch)

2.4.1. Waterloo International Terminal

This asymmetrical terminal extends its way for 400 metres through London with its volumetric form (Figure 2.9) . 2,520 panes of glass are fixing on the perforated aluminium section(Figure 2.10), with the triangulated trusses running below the roof covering to the east and above the covering to the west, in the latticework form (Wessely, 2011).

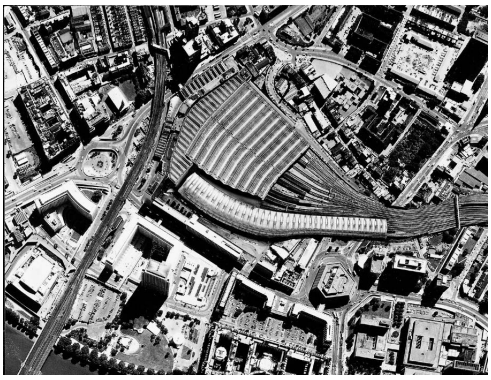

(a) Aerial view of Waterloo regional station with the new Waterloo International Terminal, 1994

(b) View from above of the deserted terminal, 2011

Figure 2.9: Waterloo International Terminal

(a) Section scale 1:500

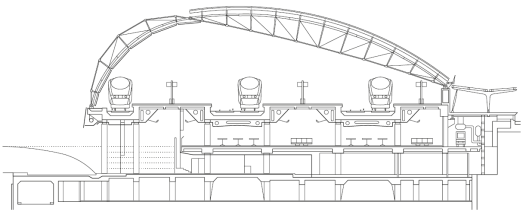

(b) Interior of deserted terminal, 2011

Figure 2.10: Section and interior

2.4.2. Maximilian Museum in Augsburg

The self-supporting barrel-vault roof over the central courtyard of the museum comprises total of 527 panes of glass(Figure 2.11), the dimension of which is 37m × 14m, with a rise of 4 metres [3]. Only a minimum number of other components are required in this shell. The edges of it is supported by a tubular frame resting on the slender pedestals which are adapted to the complicated support situation of the courtyard. Glass panes of this barrel shell are identical along the single-curvature, makes it easier to prefabricate. Each panes is made of 2 × 12 heat-strengthened laminated safety glass and measures 1.16 × 0.95m.

Figure 2.11: Side and interior view of structure

To stabilize the entire structure, a network of prestressed steel cables and additional cable trusses (totally 9) at every fifth transverse axis are deployed (Figure 2.12) (Ludwig and Weiler, 2000). The star-shaped nodes between the panes are composed of four shoes secured by clamping stainless steel caps, the detail of which is shown in Figure 2.13 and 2.14 (Weiler and Schiele, 2001).

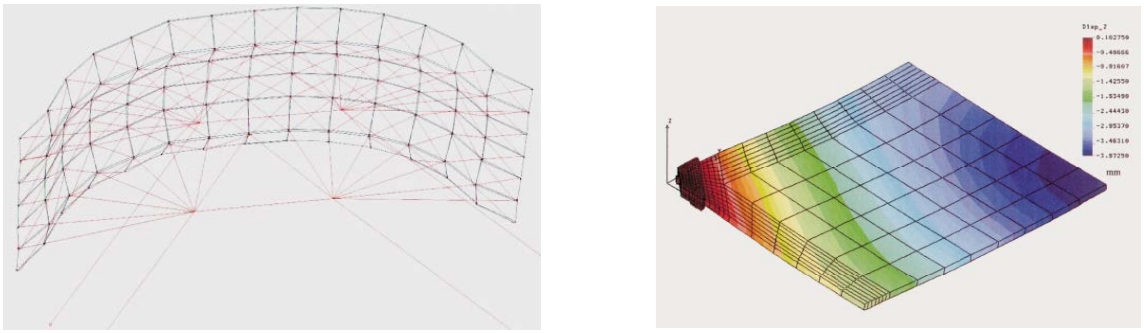

(a) Section of the strut and tie model –deformations

(b) Finite element model –deformations

Figure 2.12: Stabilization of vault

[3]Source: https://seele.com/references/maximilianmuseum/

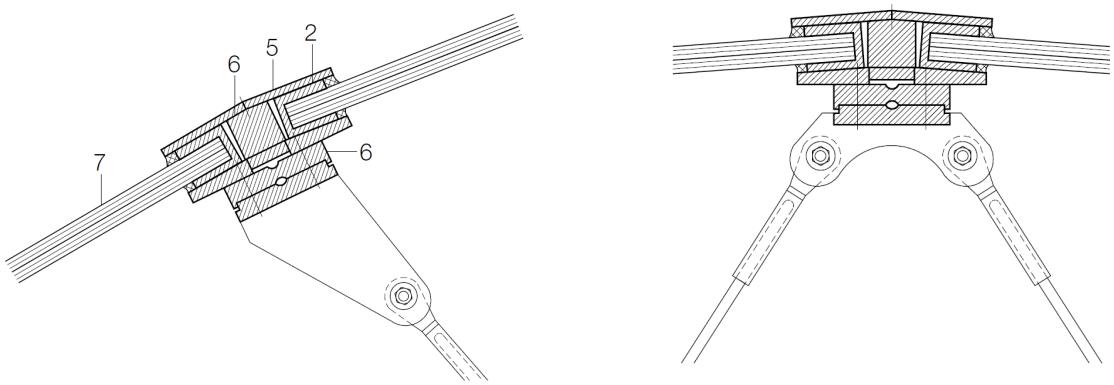

Figure 2.13: Nodes details

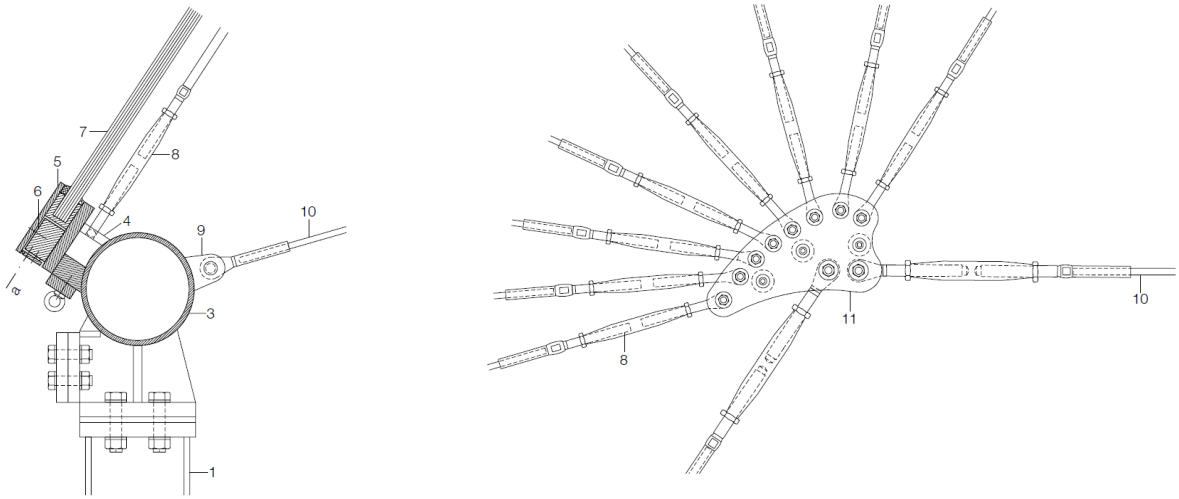

Figure 2.14: Edge and gussets details

2.4.3. Tetra glass arch

The semicircular arch consists of twelve equilateral tetrahedra with a span of 8 metres and apex height of 4. The dimensions can be seen from Figure 2.15. Because of the modularity of this geometry system, all connections of elements are identical, which allows for high level of prefabrication. Detail 1 and Detail 2 in Figure 2.15 are zoomed in and illustrated in Figure 2.16 and Figure 2.17.All glass elements are laminated panes made of 2 x 6 mm heat-strengthened glass in this arch (Wurm, 2007).

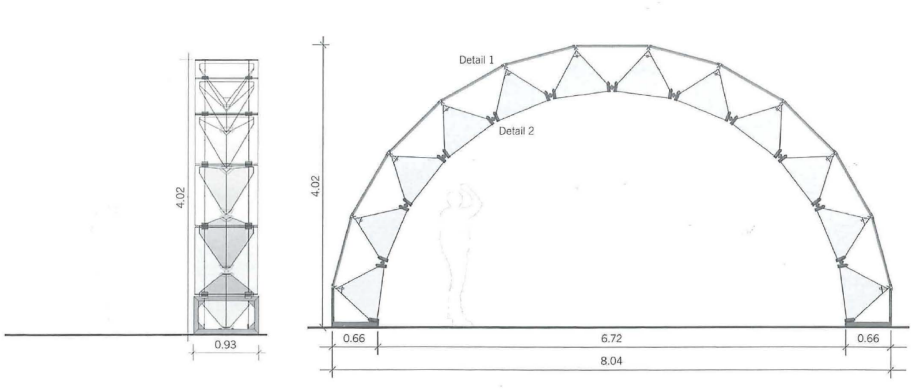

Figure 2.15: Side views of built Tetra Arch with a span of 8 m (dimensions in metres)

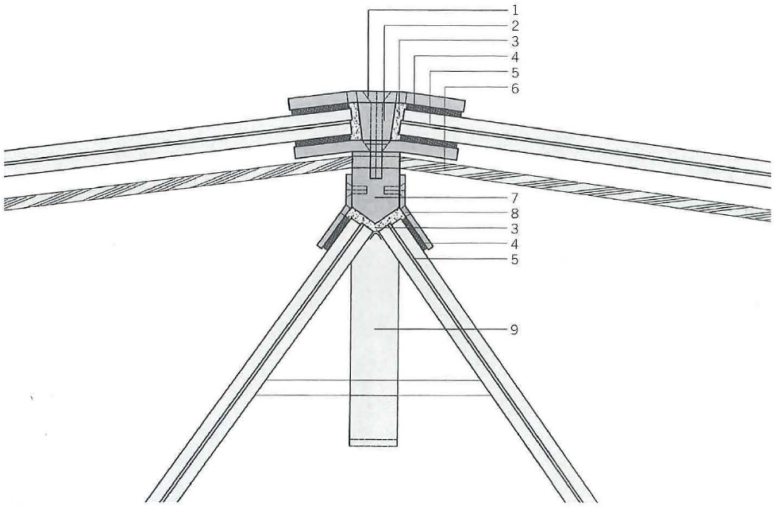

Connection edge fitting to top chord
(see "detail 1" in Fig. 50)
1 100 mm x 100 mm clamping plate, F28 aluminium alloy, anodised, with 6 mm injection holes for position 3
2 Aluminium block-profile, approx. 20 mm x 20 mm
3 Injection mortar Hilti Hit-HY 50
4 3 mm hard rubber strip
5 2 x 6 mm laminated glass of heat-treated glass, SGG Contrasplit
6 6 mm Inox cable
7 Aluminium prismatic rod
8 Aluminium edge plate
9 Clamp for securing the glass

Figure 2.16: Detail 1: Connection edge fitting to top chord

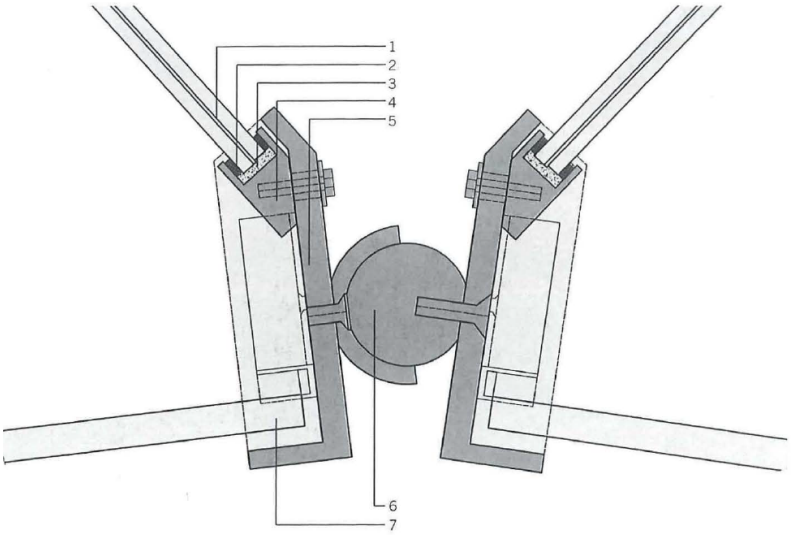

Connection between node and bottom chord
(see "detail 2" in Fig. 50)
1 2 mm x 6 mm laminated glass of heat-treated glass, SGG Contrasplit
2 3 mm cellular rubber
3 Injection mortar Hilti Hit-HY 50
4 U-profile, milled, F28 aluminium alloy, anodised
5 Aluminium cap, milled
6 Articulated joint, milled
7 GFRP edge pultrusion

Figure 2.17: Detail 2: Connection between node and bottom chord

In order to compensate for all the possible combinations of load cases, two parallel, prestressed cables are applied along the semicircular polygonal. These cables are guided through grooves in this profile beneath the roof top chord, to ensure that all the forces resulting from dead load, snow and prestressing load will be transferred linearly to the glass edges of the upper tetrahedron plates. The intensity of prestressing is 6 kN per cable, resulting in a semicircular line of pressure corresponding to the geometry of load-bearing structure. Radial force as a result is 1 kN per top chord node, which guarantees glass is in compression under all combinations of load cases(Wurm, 2007). The schematic diagram is in Figure 2.18.

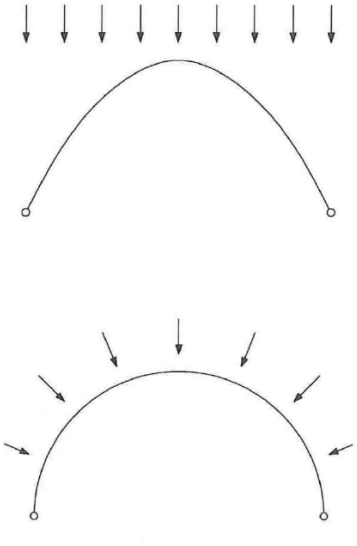

(a) Line of pressure for evenly distributed vertical forces and evenly distributed radial forces

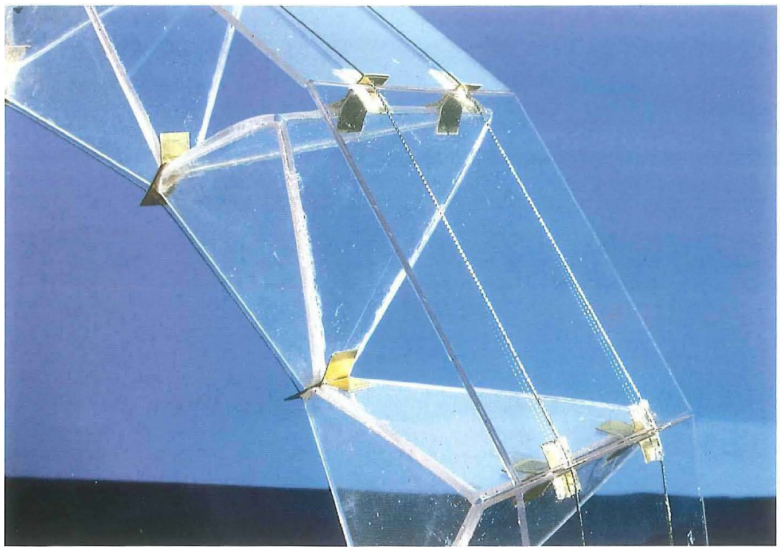

(b) Detail model

Figure 2.18: Prestressing description

3

Design Philosophy (Theoretical framework)

During the design of glass arch, standard and empirical regulations should be taken into consideration and applied. Attention needs to be paid also to performance requirements associated with this research during design. In this chapter, the outline of essential aspects related to glass structure design will be explained. Basic building norms from Eurocodes as well as NEN will be used as guide for design. Finally, the usage of FEM shall be validated.

3.1. Design of glass structure

3.1.1. Strength of glass

The strength of glass varies significantly in real design, which is influenced by many factors: flaws in glass, glass type, structural element type, manufacturer, quality control etc. Generally speaking, we use low maximum tensile strength 20 MPa for annealed glass (6 MPa for allowing corrosion), 40 MPa for heat strengthened glass and 60 MPa for fully tempered glass. As for the compressive strength, 200 MPa will be used normally. Based on the risk and consequences, safety factor for glass design can be different. Usually 5 to 7 is used. [4]

3.1.2. Performance requirements

1. Overhead glazing

   The self-weight of overhead glazing represents a permanent out-of-plane loading, under which circumstance laminated safety glass must be used if it is single glazing or for the inner pane of IGU. Residual load-bearing capacity should be considered for design thereby tempered glass alone is inadvisable. If glass is supported on two opposite edges instead of four, there will still be the risk of folding in the centre of the pane even with laminated safety glass. Therefore, it is recommended to use all-side support in German technical rules for linearly supported glazing. Besides, for spans greater than 1200 millimetres, a maximum side length ratio of 3:1 is advised(Wurm, 2007).

2. Plates loaded in compression

   The strength of plate element is barely reduced by the brittleness of glass. Glass plates can be utilized as wall panels, struts and shell elements, although the stability should be considered when load is transferred linearly. Plates may buckle about the weaker axis when load is transferred in the unsupported edge direction. The critical load does not tie to compressive strength but rather to tensile bending strength, when lateral displacement occurs in the middle region of glass cross section. In fact, many other factors are related to critical buckling loads, such as geometrical slenderness,supports conditions, load eccentricity, initial imperfections etc.(Wurm, 2007).

[4] Sources: Lecture notes from CIE4285 Structural Glass

In this case, similar to the examples introduced in corrugated glass, it is favourable for our theoretical component to be loaded in compression, which is also the reason why arch and prestress may be integrated into this design. Compression forces can be transferred by contact, bolted or friction grip connections, where imposed deformation shall be accommodated with bearing and articulated connections at the supports.

3. Weather protection

   Weather protection, solar control, undrifted snow and cleaning is noticeable for glazed roof with very little slope. Because standing water/snow or pond can happen and be detrimental to structure or climate performance. The minimum fall for the panes with clamped bars is 15 degrees in the direction of flow, 7.5 degrees for the ones with internal drainage. When the fall is even smaller, glazing should be watertight with permanently elastic sealed joints. Rainwater drains from ridge (apex) to the eaves in a controllable manner for gabled and vault, in which case prefabricated elements can be used to secure watertight seal at the ridge(Wurm, 2007).

4. Continuous linear supports

   Continuously linearly supporting a glass pane is the easiest and most pervasive way of stabilizing glass. Usually the out-of-plane load of the pane is transferred through gaskets or structural sealant while in-plane load is transferred through setting blocks. Ethylene propylene diene monomer (EPDM) rubber, gaskets or silicone can be used into supporting frame peripherally around glass pane, to transfer lateral loads. Diaphragm action load can also be transmitted through continuous linear supports, where the fixing between glass and the frame requires careful design. Machining edges of panes, isolation of corners of panes from in-plane load and influence of thermal movement should be taken into consideration. Finally, it is important to understand and account for the issue of inconstant stress distribution along the line of support in design.(Haldimann et al., 2008)

3.2. Load cases and limit states

3.2.1. Ultimate limit states (ULS) and Serviceability limit states (SLS)

The ULS concern about safety issues while SLS concern about functionality issues. For this research, ULS of static Equilibrium of the structure (EQU) will be verified. The load combination is as follows:

$$\gamma_G \cdot G_k + \gamma_{Q;i} \cdot Q_{1;k} + \sum(\gamma_{Q;i} \cdot \Psi_{Q;i} \cdot Q_{i;k}) \tag{3.1}$$

where γ_G is 1.35 and $\gamma_{Q;i}$ is 1.5 in this case.

For certain cases it is physically not possible for two loads to simultaneously act in their extreme or zero in the same load combination. So $\Psi_{Q;i}$ will set to zero for wind and snow load when the leading variable load is the other one(NEN-EN 1990).

3.2.2. Dead load

Self-load of component will be calculated by multiplying the unit width area with the density mentioned in the properties of materials.

3.2.3. Snow load

Under the condition of cylindrical roof, without snow fences hindering, the snow load shape coefficients are given in the following expressions (also in Figure 3.1)(NEN-EN 1991-1-3):

$$For \beta > 60°, \qquad \mu_3 = 0 \tag{3.2}$$

$$For \beta \leq 60°, \qquad \mu_3 = 0,2 + 10h/b \tag{3.3}$$

Here the recommended upper value for μ_3 is 2,0.

- The Undrifted load arrangement which should be used is shown in Figure 3.2 , case (i).
- The Undrifted load arrangement which should be used is shown in Figure 3.2 , case (ii),unless specified for local conditions.

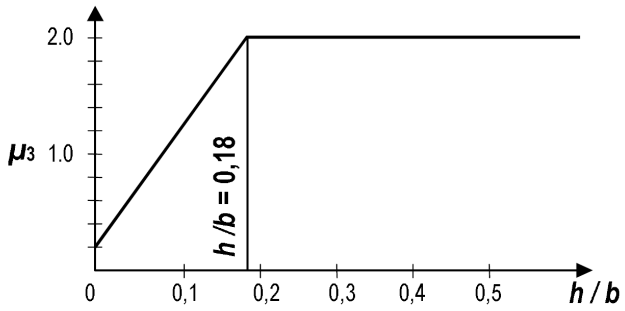

Figure 3.1: Recommended snow load shape coefficient for cylindrical roofs of differing rise to span ratios (for $\beta \leq 60°$)

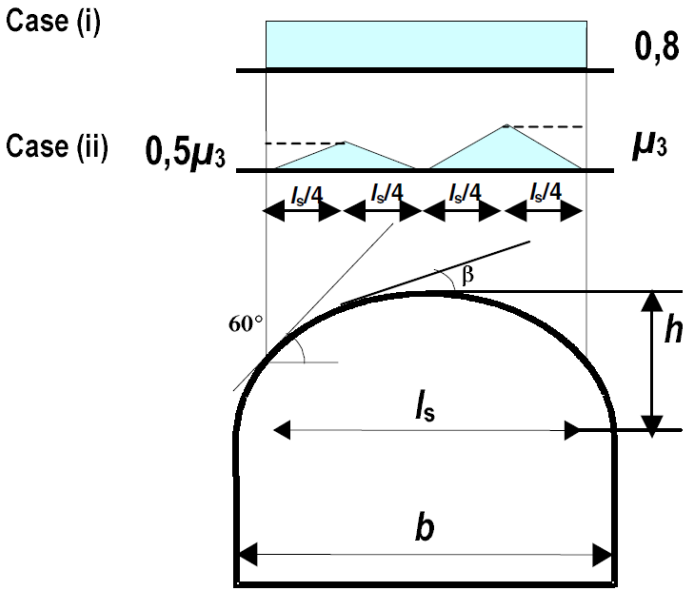

Figure 3.2: Snow load shape coefficients for cylindrical roof

For the calculation in this research, snow loading is calculated by $s = s_k \cdot \mu_i \cdot C_e \cdot C_t$, where Exposure coefficient C_e and Thermal coefficient C_t are both set to 1,0. Value of μ_i is as described above. The value of s_k of Central West in Europe is decided by $s_k = 0.164Z - 0.083 + A/944$, where Z is usually 2 or 3 for Netherlands, and A is the site altitude above sea level. The vault roof in this research has its limitation of height, which does not have much influence on the altitude level. Therefore, we take 0.7 kN/m_2 as s_k value (NEN-EN 1991-1-3).

3.2.4. Wind load

Section 7.2.8 in (NEN-EN 1991-1-4) gives the recommended values of external pressure coefficient $c_{pe,10}$ for circular cylindrical roof. This is shown in Figure 3.3, that vault roof has been divided into three wind zones A, B and C.

- For $0 < h/d < 0.5$, $c_{pe,10}$ is obtained by linear interpolation.
- For $0.2 \leq f/d \leq 0.3$, two values of $c_{pe,10}$ have to be considered.

Here we have h equal to zero, so we only have to take into account one condition of $c_{pe,10}$ value. By applying different wind pressure of different heights, to the formula $w_e = q_p(Z_e) \cdot c_{pe,10}$, the wind pressure $w_e$on the external surfaces can be calculated. The values used for parametric modelling will be defined in the following chapters.

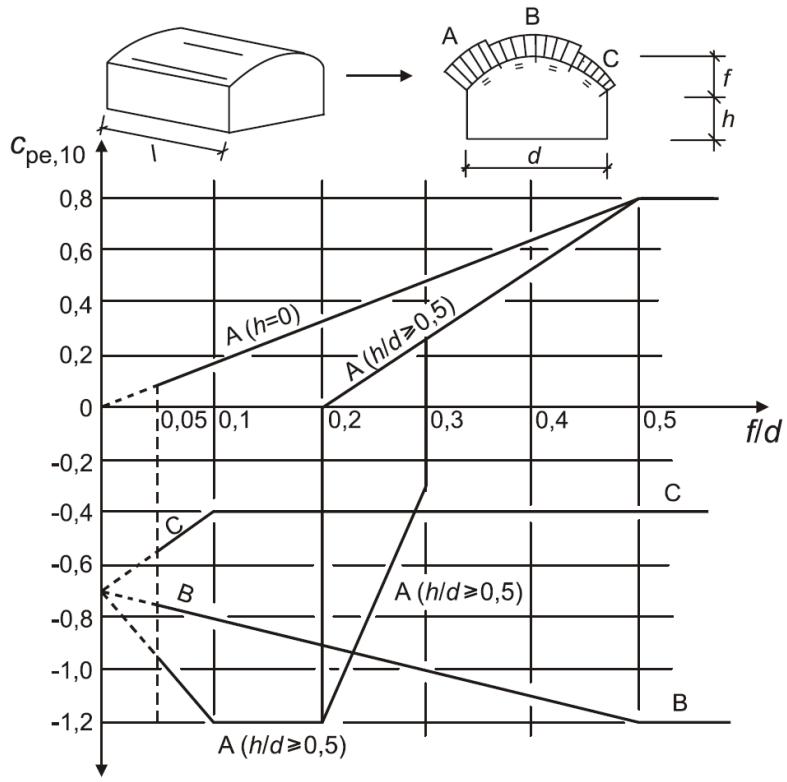

Figure 3.3: Recommended values of external pressure coefficients $c_{pe,10}$ for vaulted roofs with rectangular base

3.3. Validation of FEM

3.3.1. Methodology

Two approaches can be adopted to control the level of modelling accuracy for the purpose of the model, which is relevant to the scale of the glass structure(Haldimann et al., 2008):

1. A relatively simple global model and a set of detailed local models can be built, which are complementary for the analysis. Iteratively analyses can be carried out.

2. A single detailed global will do the job which concerns all the structural aspects.

By making advantage of the time efficient analyses of global modelling, the global behaviour, deflection and reaction force are to be obtained and evaluated from the studying in approach 1. The other aspects such as stress distribution will be complemented by partially detailed local modelling. The one single detailed model in approach 2 is not easy to model and modify afterwards, which also requires high computational capability. Moreover, it will not be straightforward to make detailed modelling in the early design phases, which may be altered all the time. Therefore, approach 1 is adopted in this research.

For the specific design in this thesis, attention should be paid to the contact area of concrete and glass. Non-linear contact element (such as COMBIN39 spring element in Ansys[5]) should be used if possible. Different deflected shapes of glass and supporting structure can be displayed under different load cases.

3.3.2. Simple global model

In the global arch model, it is suitable to model glass with 2D or 3D shell elements. When laminated glass is used, the thickness of shell element can be calculated and applied as the effective thickness. The effective thickness of laminated glass is calculated as follows(Haldimann et al., 2008):

[5]Ansys, Inc. is a public company developing and marketing engineering simulation software.
Official website:`https://www.ansys.com/`

In terms of bending stress:

$$h_{ef;w} = \sqrt[3]{\sum_k {h_k}^3 + 12\omega(\sum_i h_k {h_{m,k}}^2)} \tag{3.4}$$

In terms of stress in a ply:

$$h_{ef;\sigma;j} = \sqrt{\frac{(h_{ef;w})^3}{(h_j + 2\omega h_{m;j})}} \tag{3.5}$$

where:

ω	is the coefficient of shear transfer of the interlayer, which varies from 0 to 1.
h_k and h_j	are the thicknesses of the plies of glass within a laminated sheet, as defined in Figure3.4.
$h_{m;i}$	is the distance to the mid-plane of the glass piles

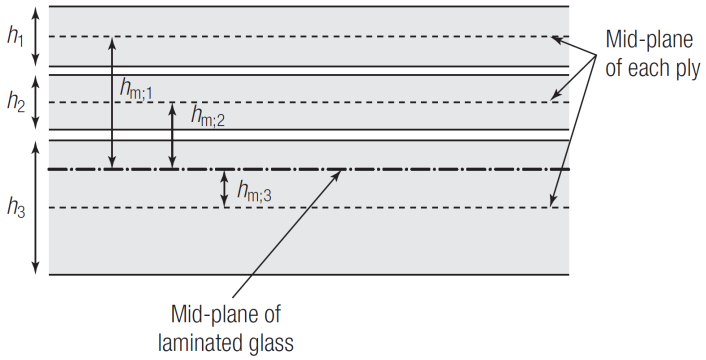

Figure 3.4: Laminated glass thickness dimensions

During the following simulations in FEM software, the initial effective thickness will be assumed as 16 millimetres.

3.3.3. Analysis types

Linear elastic analysis will be carried out in this research since the material stress-strain relationship is linear before breaking, which also need less time even to solve large models. Load cases of this analysis are simply superposition of load combinations. However, the deformation of structure should be 'small' to verify the credibility of such analysis.

When the deflection is approaching the thickness of glass plate, transition will occur where the stresses redistribute from bending to membrane action. Linear elastic analysis may over-estimate the stress in plates for this large deflection. Consequently, a geometrical,materially or boundary-condition non-linear analysis may be necessary corresponding to various conditions(Haldimann et al., 2008).

3.3.4. Ansys and GSA

GSA[6] and Ansys Workbench (Ansys WB) will both be utilized for analyses in this research. Global model are built in GSA for bending moment and reaction force analysis, which concerns less about the component of glass-concrete. When model is built in Ansys WB, CAD parameters are included with the help of Solidworks[7]. Approach 1 described in methodology is used in Ansys WB here: Global modelling → sub-modelling analyses.

[6]GSA Suite from Oasys Software.
Official website: `http://www.oasys-software.com/products/engineering/gsa-suite.html`

[7]A solid modelling computer-aided design (CAD) and computer-aided engineering (CAE) computer program published by Dassault Systèmes. Official website: `http://www.solidworks.com/`

4

Conceptual Design

Designs and ideas come up and change frequently in preliminary design stage. Many theoretical proposals have been brought up during this phase, not all of which are adopted and proceeded further. But some of them are innovative and promising, where more research are executed. Some essential sequences of arch and connection conceptual designs, and some related literature study will be covered in this chapter. A basic parameter summary will be stated in the end.

4.1. Arch

Nowadays surface structure can have almost any shape compared to traditional forms of domes, vaults etc. The main characteristic of the shell is its surface shape, whose capacity is higher than a structure built with single linear elements of similar dimensions. Surface structure can be categorized into soft and rigid shells, in addition to the traditional vaults. Soft shells are tensile membrane structure in prestressing, which is flexible and light-weighted. On the other hand, rigid shell can be either thick or thin, but still thicker than membrane structure. When bending stiffness is needed, thick shells can be used. Thin shells will be sufficient regarding purely axial and shear loading.

For material of low tensile strength, tension can be resisted by reinforcement, as reinforced-concrete shells is such case. Moreover, reinforced-concrete tensile shells are often prestressed to keep concrete in compression and uncracked. Here, compressive shells is in fact achievable by hanging membranes inversely so that it is in compression under its own weight. While tension caused by asymmetrical loading can be resisted by prestressing, the advantages of which also includes keep concrete uncracked and tight, so hardly any coating and waterproofing is required (Schueller, 1996).

4.1.1. Shell typology

The definition of surfaces is closely connected to all kinds of curves. Therefore, some special curves are to be classified as follows:

- Principal curvature

  The maximum and minimum curvatures respectively at any point on the surface, where the two curvatures are perpendicular to each other.

- Gaussian curvature

  The outcome of multiplying principal curvatures $K = 1/R_x R_y$ at a point, where R_x, R_y are the radii corresponding to the principal curvatures.

- Mean curvature

  The arithmetic average of the principal curvatures $1/2 \cdot (1/R_x + 1/R_y)$ at a point.

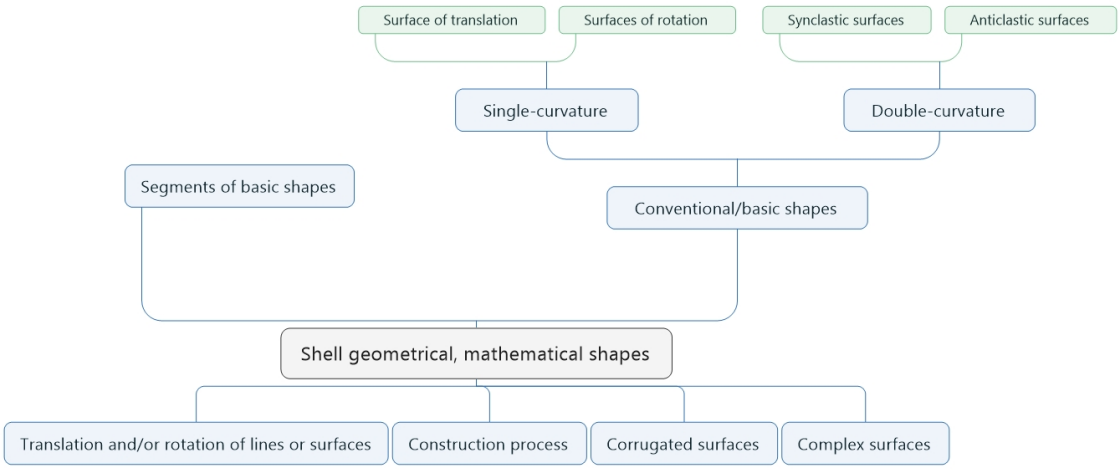

Figure 4.1: Surfaces classification

From the perspective of geometrical, mathematical classification, shell shapes are categorized in Figure 4.1. In the part of conventional/basic shapes, single and double-curvature systems can be identified by the three curvatures referred to above. For double-curvature surface, there are two subdivision listed: synclastic and anticlastic surfaces. Gaussian curvature K is =0 for singly curved surfaces and >0 for doubly curved synclastic surfaces respectively. While for anticlastic surfaces K would be <0 , since curvatures of which are adversed to each other (Schueller, 1996).

The geometry of basic surfaces can also be categorized as surfaces of revolution(rotation)(Figure 4.2 left)and surfaces of translation(Figure 4.2 right).

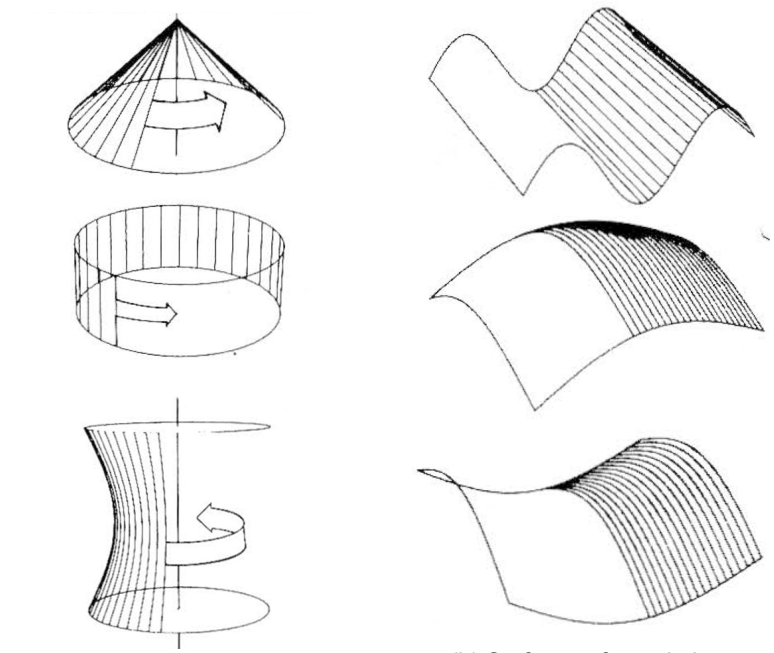

(a) Surfaces of revolution: Surfaces formed by rotating a plane curve around a fixed axis.

(b) Surfaces of translation: Surfaces formed by sliding a plane curve alone another curve which is not on the same plane.

Figure 4.2: Generation of basic surfaces

Surface of translation of single curvature surface (Cylinder) is chosen for further design in this research.The reason for this choice is that it is a ruled surface, which means the surface can be generated by moving a straight line along two fixed end curves. The tangential edge of one component section will be straight in the longitudinal direction. With the straight lines showing Figure 4.3, it is more practical to simply connect components horizontally along the straight lines to keep modularization and avoid high labour intensity. Besides, one feature distinguishes singly curved surfaces from doubly curved surfaces is that only single-curvature surfaces are developable, that is, surfaces can be flattened without stretching or tearing(Schueller, 1996). In this case, this feature ensures the modularization of component, which will be corrugated transversely and straight longitudinally.

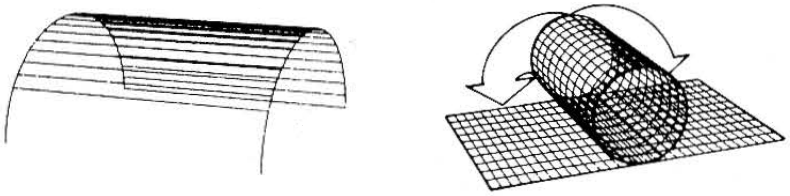

(a) Singly ruled surface: cylinder (b) Developable surfaces

Figure 4.3: Single curvature surface

4.1.2. Barrel shells

If we elaborate on single-curvature cylindrical shells, many various types of curves may be involved in the geometry defining. The basic defined geometries of curves may range from (left to right in Figure 4.4) the circular segment, the parabola, ellipse, hyperbola, and cycloid, to the corresponding geometry of funicular curve(Schueller, 1996).

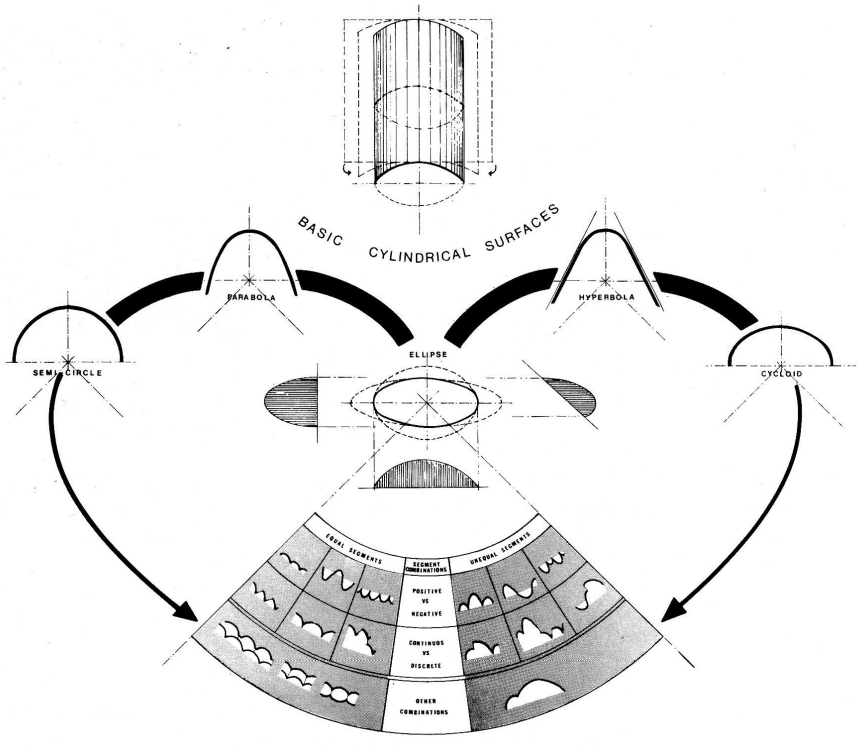

Figure 4.4: Basic concepts related barrel shells

These basic shapes may be connected in countless ways to produce cross sections of all kinds of forms, as in this case it will be single shell constructed from multiple segments. Besides, segment

may be organized in a parallel, radial or intersecting forms, where single unit may be straight, bent or folded(Schueller, 1996). Single shell composed of corrugated segmental units which are arranged in a parallel manner.

Segmental circular cylindrical shell will be picked and further proceed in the research. For the reasons that its possibility of modular instalment and labour ease. Besides, radial pressure can be applied on this structure by prestressing. However, parabola shell will be kept as an option for its favourable structural behaviour and better inner space utilization(Milošević et al., 2014).

4.1.3. Support conditions

When considering cylindrical shells, not only the shape of cross section is one of their characterizations, but also other factors are included: the longitudinal and transverse support types of shells, diaphragm type, conditions of edge beams, and the consecutiveness of multi-bay or multi-span shells(Schueller, 1996). There are mainly three categories of barrel shells as is illustrated in Figure 4.5(left to right):

1. Long barrel shells or shell beams:

   When shell is only supported in the transverse direction, but has no supports in the longitudinal direction. It will act like a longitudinal beam without arch action. Longitudinal beam action will dominate when its span in that direction is longer than its width. Such shell beams can be considered as continuous shallow beams with curved cross section, which is simply supported.

2. Short barrel shells:

   If the support conditions of long barrel shells change, or the chord width of shells is larger compared to longitudinal span, the primary action becomes transverse arch action.

3. Vaults:

   The behaviour of barrel shells may be reckoned as parallel arches when they are continuously supported in the longitudinal direction by foundations,walls,frames or (prestressed) deep beams. The behaviour of transmitting force directly to the supports in the transverse direction, may be visualized as the behaviour of parallel arches of per unit width. Since these shells may resist both bending and axial forces, they should be thick enough and designed as if they were arches.

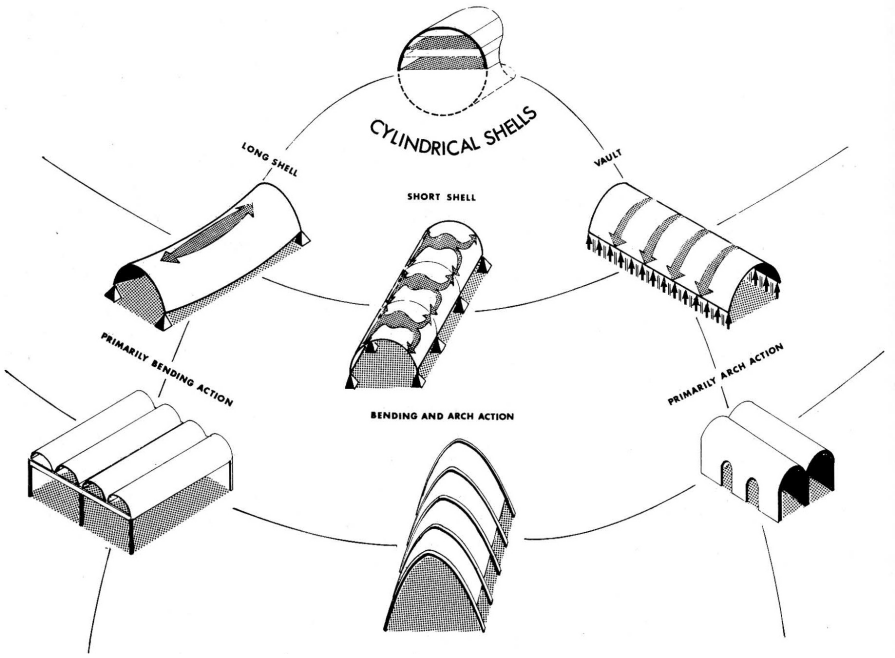

Figure 4.5: Barrels

In the field of this research, edge beams are selected, narrowing down the scale of this design to an arch of component width. Further study of arch design will be elaborated below.

4.1.4. Arch supports and Load cases defining

When it comes to the design of a single arch, we divide arches into 3 categories in terms of height-to-span ratio:

Steep roof arches:	$h/L \geq 1/3$
Intermediate roof arches:	$1/8 < h/L < 1/3$
Shallow roof arches:	$h/L \leq 1/8$

where h is the height and L is the span of arches. Unless specifically explained, in the following text, h and L will always refer to the height and span of arches respectively.

We will discuss three conditions of supports for most arches: three hinged, two hinged and fixed, where the hinges are located at two end nodes and middle node of arch curves(Figure 4.6). According to Sonavane (2014), under self-weight load or Uniformly distributed loading (UDL) conditions, arches of three hinged tend to have the largest internal bending moment and deflection among three support conditions, whereas large deformation would be unfavourable for elastic glass structure analyses. Therefore, two-hinged and fixed arches will be further explored in this research.

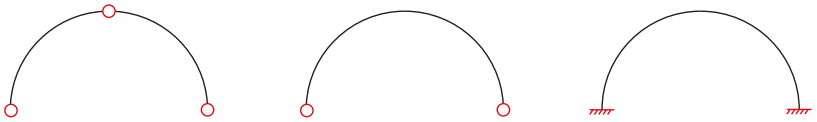

Figure 4.6: From left to right: Three-hinged, two-hinged and fixed arches

Concluded from the book of Schueller (1996), intermediate circular roof arches can be reckoned as parabolic arches for early stage design purposes, while the bending effect due to dead load must be taken into account. In addition to that, two-hinged parabolic, flat circular or even the corresponding fixed arches can be considered as three hinged ones, for the preliminary design intention. Although the approximation can be used for two-hinged and fixed arches with certain conditions, there are some certain rules applied to critical moment by safety issues:

Steep roof arches:	$M_{arch} \times (1 + 10\%)$	Due to axial action
Shallow roof arches:	$M_{arch} \times (1 + 30\%)$	Due to larger thrust force
Intermediate roof arches:	$M_{arch} \times (1 + 20\%)$	Medium thrust forces

4.1.5. Moment calculation

After the simplification in the last section, calculation and superposition become easier after the approximation. Given by Schueller (1996), moment calculations for the circular arches in Figure 4.7(left to right):

Uniform loading		M_{max}Location:
Full gravity:	$M_{max} = -wh^2/8$	Mid-height of arch
Asymmetrical vertical:	$M_{max} = \pm w_L L^2/64$	Quarter span ($x = L/4$) of arch
Asymmetrical lateral:	$M_{max} = qh^2/8$	Approximately mid-height of arch projection

where w is the dead load, w_L is the vertical live load and q is the lateral live load.
For analytical calculations, three types of arches will be checked as follows:

- Steep arches: Uniform full gravity loading will dominate during design, but result of uniform lateral (wind) load should be checked.
- Intermediate arches: Uniform full gravity loading plus asymmetrical vertical loading will dominate during design, but result of purely dead loading should be checked.
- Shallow arches: Asymmetrical vertical loading will dominate during design.

Four load cases will be examined under ULS in GSA and Ansys as is shown in Figure 4.8:

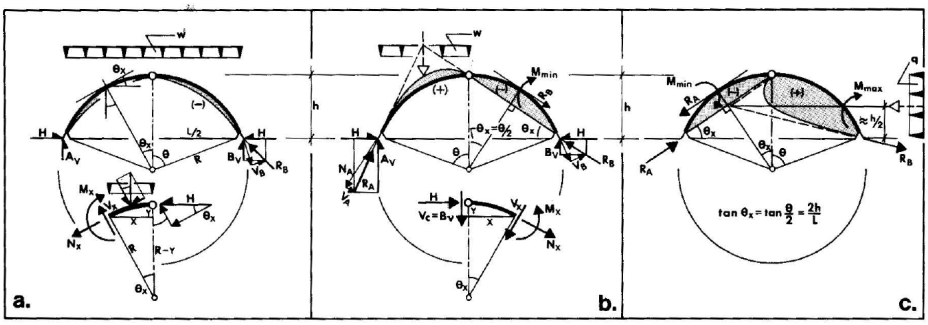

Figure 4.7: Circular arch under uniform load action

- **Load case 1: uniform dead load**
  $1.35 \cdot w_{dl}$ for analytical and GSA solution, $1.35 \cdot w_{ds}$ for Ansys solution.
- **Load case 2: uniform dead load + arch wind load**
  $1.35 \cdot w_{dl} + 1.5 \cdot w_{wl}$ for analytical and GSA solution, $1.35 \cdot w_{ds} + 1.5 \cdot w_{ws}$ for Ansys solution.
- **Load case 3: uniform dead load + uniform snow load**
  $1.35 \cdot w_{dl} + 1.5 \cdot w_{sl}$ for analytical and GSA solution, $1.35 \cdot w_{ds} + 1.5 \cdot w_{ss}$ for Ansys solution.
- **Load case 4: uniform dead load + asymmetrical snow load**
  $1.35 \cdot w_{dl} + 1.5 \cdot w_{sl}$ for analytical and GSA solution, $1.35 \cdot w_{ds} + 1.5 \cdot w_{ss}$ for Ansys solution.

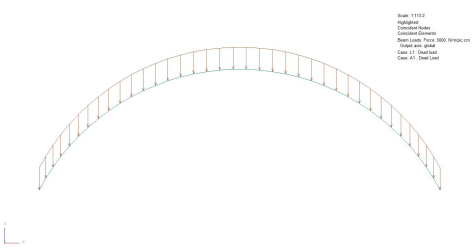

(a) Load case 1

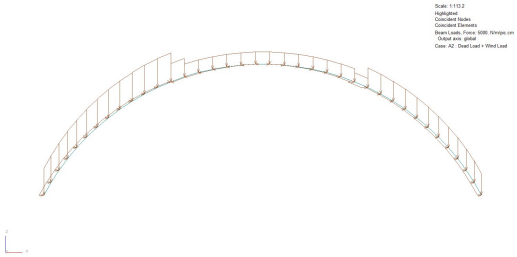

(b) Load case 2

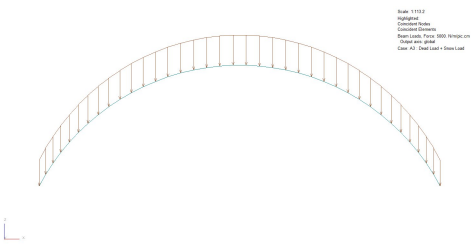

(c) Load case 3

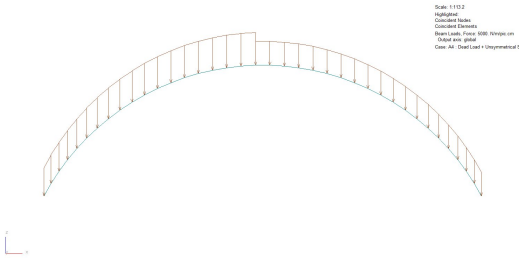

(d) Load case 4

Figure 4.8: Four load cases

4.1.6. Prestressed arch

Similar to the example of Tetra glass arch in section 2.4.3, prestressing is included in this conceptual design of glass-concrete arch. The difference in this case is that prestressing is transmitted to whole structure by post-tensioning the segmental arch, which also means that prestressing force will be transmitted through the connections of concrete and glass. Asymmetrical loading is thus possibly compensated by prestressing. Because the shape of load-bearing arch is corresponding to the radial

pressure, entire structure will be in compression, which should be favourable for glass and concrete. Conceptual process of this prestressing is described in Figure 4.9, where glass-concrete component will be installed in place and connected, after which the post-tensioning in concrete will be implemented.

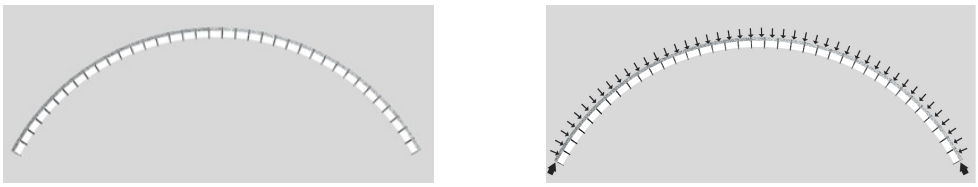

(a) Installed in place (b) Post-tension

Figure 4.9: Prestress and radial pressure

4.2. Preliminary connection design

4.2.1. Reinforced glass

'Residual stability' is vital for overhead glass. The term 'residual stability' generally denotes that the glass component can still provide some resistance after breakage, to prevent whole structure system failure. This structure safety redundancy can also be enhanced by including reinforcement into glass, thus adding more safety. Reinforced glass is involved in the preliminary conceptual design, some examples of this are summarized below:

Accurate alignment is required for the area to transmit post-tensioning force into glass-beam. Residual stability is obtained by post-tensioning steel tendons at the beam ends, without bonding which to the annealed glass beam. In this case a perfect alignment is achieved by edges cutting and grinding following the process of laminating.

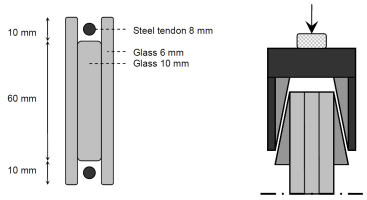

Figure 4.10: Post-tensioned glass beams by Louter et al. (2006)

As illustrated in the **left** laminated glass panel of Figure 4.11: 1 glass pane, 2 PVB membrane, 3 armour, 4 PVB membrane, 5 glass pane. For the **right** panel: 1 glass monolithic, 2 interlayer (PVB or SG), 3 perforated metal plate with 1 mm. An interesting design point here is that armour can also work as sun-screening for overhead glazing.

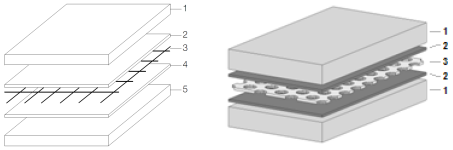

Figure 4.11: Armoured laminated glass by Kaltenbach (2004) and embedding perforated stainless steel plates by Cruz and Valente

By extending the steel plate of the right panel in Figure 4.11, the concept of connecting glass panels by metal bridges emerges. Perforated steel is used here to optimize transparency. Two symmetrical polycarbonate bars are inserted from upper and lower sides, where the inner gap space and contact between PC and glass will be filled with silicone for sealing purpose.

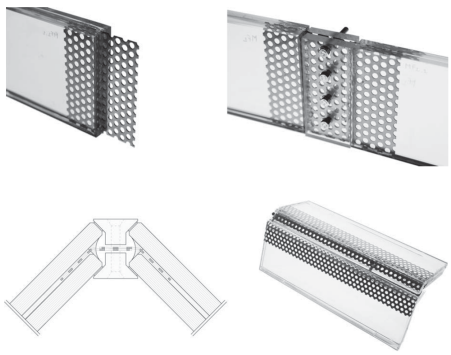

Figure 4.12: Protruding the steel plate out of the laminated glass to establish connection between two panels by Carvalho et al. (2014).

Freytag (2004) presents a new approach to construct by using vastly transparent building elements, where the glass is connected to UHPC by direct contact. Large scale experiments are carried out to testify the structural behaviour and failure mechanisms in their research.
In their research, the glass edges are positioned into a fitting slot of the relating concrete part, which is formed by liquid concrete covering the glass edges. This means the glass is placed before concreting starts. Another kind of pozzolanic material silica fume is added into conrete composition to achieve higher shear strength. Here the glass surfaces of contact part are pre-treated with specially roughing and enamelled coating before thermal toughing process. Three shear transferring mechanisms are obtained in this case: Adhesion, interlocking and clamping friction, where the clamping effect is attained by shrinkage of the concrete part by adding certain amount of fine steel fibres into concrete. Experiments have proved that the brittleness of glass can be compensated by a clever composition with UHSC.

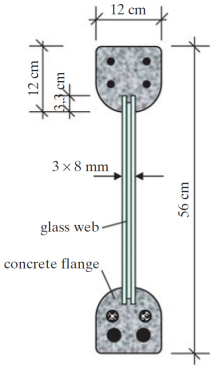

(a) Cross section

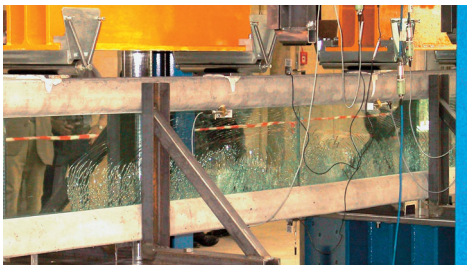

(b) Crack initiation

Figure 4.13: Glass-Concrete Composite(Freytag, 2004)

4.2.2. Mechanical connection

In this design, laminated corrugated annealed glass will be used for component. By extending reinforcement steel or steel plate from interlayer of glass, the reinforcement frame between glass panels will be built. Concrete will be cast in plate to achieve connection and sealing function. The diagram of this hypothetical design and connection section is depicted in Figure 4.14 and Figure 4.15. Tolerances of curved glass panel for laminating should be considered in this case. Moreover, there is possibility that glass panels can be used as permanent formwork for concrete casting.

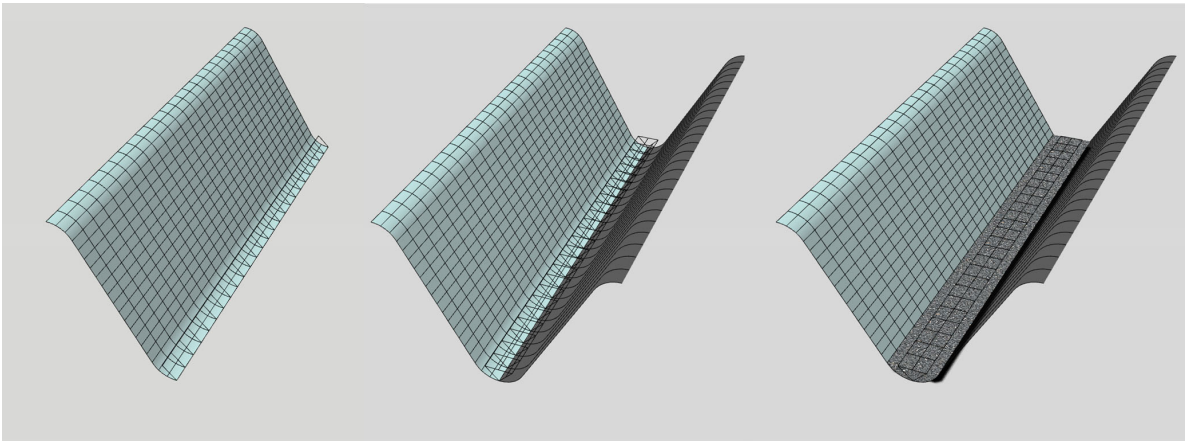

Figure 4.14: Diagram of casting concrete

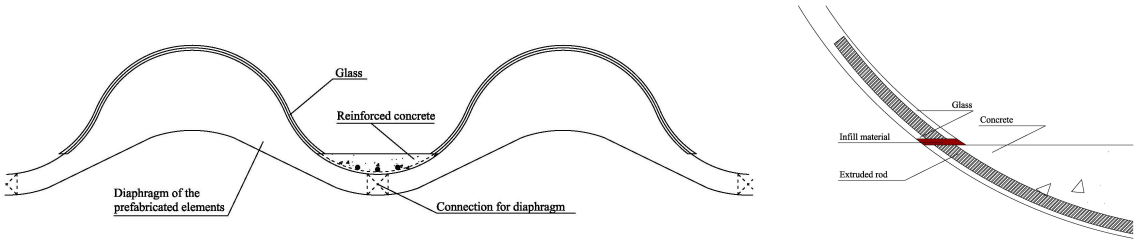

(a) Section of mechanical connection

(b) Detail of connection

Figure 4.15: Corrugated component

4.2.3. Adhesive connection

For this part, concrete and glass will be connected in a hard adhesive system, where stiff adhesive material, such as epoxy ,acrylate, polyester etc., will be applied here (Figure 4.16). Attention should be paid to the curing condition and long-term as well as thermal loading for adhesive connection. Besides, the cement-rich skin or laitance on the concrete surface, especially on the casting side sometimes absorb part of the adhesive, in which case the second layer of adhesive may be needed. The second coat of adhesive should be applied when the first layer is still viscous(Engineers and ., 1999).

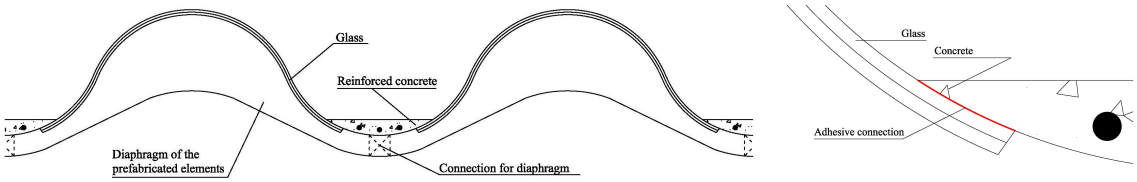

(a) Section of connection

(b) Detail of adhesive connection

Figure 4.16: Corrugated component

4.3. Parameters study

Many parameters in global model and detailed model will influence the output results in different levels. Simply divided them into input and output is not easy, since some parameters are entwined with both input and output as described in Figure 4.18. For example, in Figure 4.17, when the spans of arches are assumed to be identical, it would be better for the thrust line to stay within the arch geometry(Varma et al.). But when the thickness of arch is altering the self-weight of arch is also altering, which changes the internal moment and axial force of structure. Since thrust distance equals to resultant moment/resultant axial force at the location of arches, which means the thrust line will shift as well, causing the stress within component to change. Besides, the cost will also be different.

Therefore, the viable approach would be study and optimize parameters and make necessary estimation in models of different levels, which will be elaborated in arch and connection simulations.

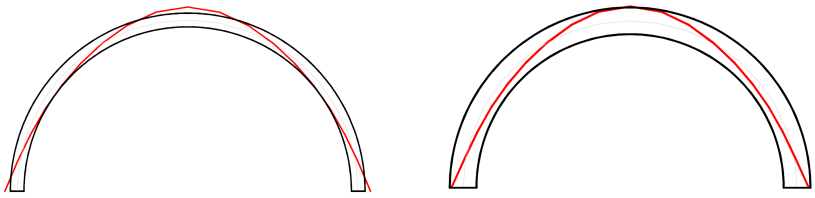

(a) Thrust line for thin arch

(b) Thrust line for thick arch

Figure 4.17: Thrust lines research

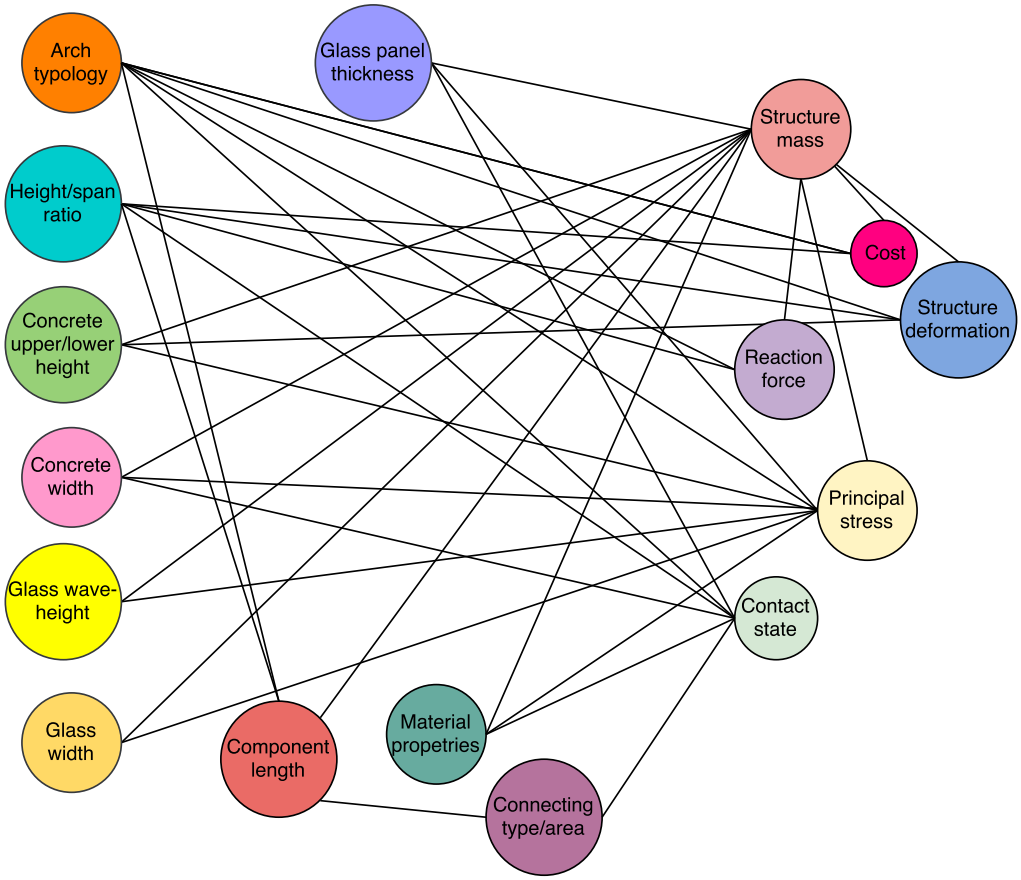

Figure 4.18: Parameters relation

5

Arch Design

Global arch behaviour has been studied in lots of literature already. In this chapter, the structure behaviour of different height to span ratios of arches will be studied and optimized. Besides, a case study of cost estimation is alos carried out to make further optimization. Analytical and GSA solutions are presented inside this chapter, while Ansys analysis related to arch design will be dicussed in the chapter 8 of FEM simulations, where the conclusion of this chapter will be compared and used.

5.1. Parameters define

As is described in the above chapters, the arch will consist of modular straight components made of glass and concrete. In this chapter, we set the span of this arch to 30 metres while changing the height of it. Figure5.1 shows the height ranges from 1 to 15 metres which means it ranges from shallow, intermediate, to steep circular arches.

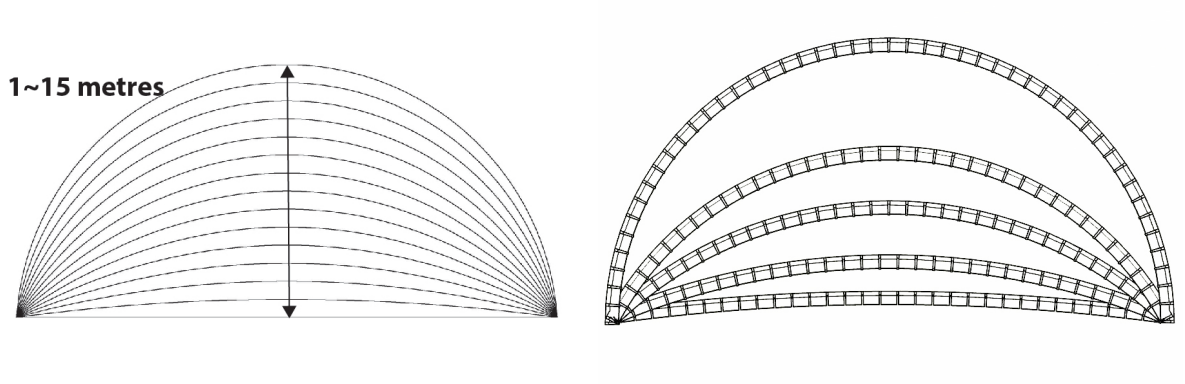

Figure 5.1: Different height to span ratios

GSA is used to calculate reaction force and bending moment for preliminary design purpose. However, a hypothetical section is needed for the dead load calculation in analytical solution. The dimensions of symmetrical glass-concrete component section is shown in Figure 5.2, where the tangential curves represent glass as the rectangles represent concrete parts. One aspect concerning the reason for the location of concrete parts will be given in following section 5.2.2.

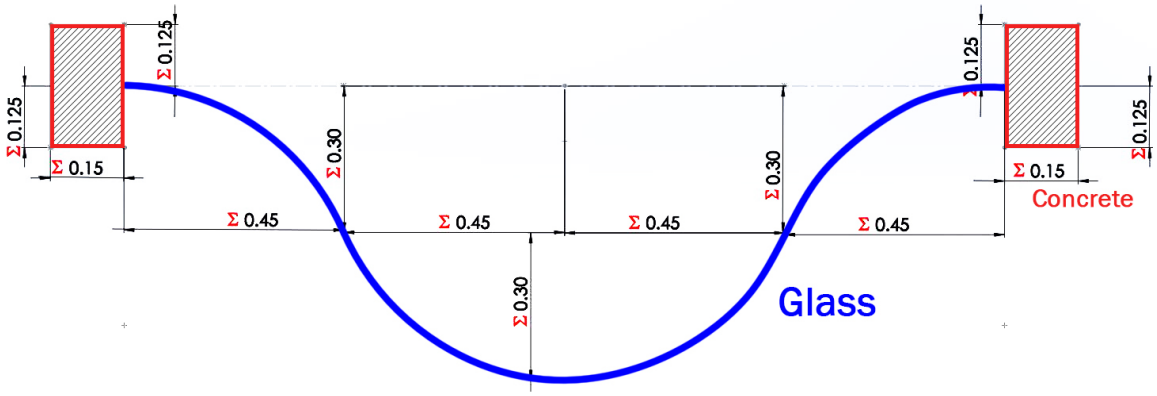

Figure 5.2: Hypothetical section

5.2. Analytical solution

5.2.1. Critical load case

It has been mentioned that different types of load can dominate design under different types of arches in section 4.1.5. During this analytical calculation, height ranging from 1 to 9 metres of arches are calculated, the critical load case for which will be Load case 4: uniform dead load + asymmetrical snow load ($1.35 \cdot w_{dl} + 1.5 \cdot w_{sl}$). According to NEN-EN 1991-1-3, the snow load is functional on either asymmetrical side because of shape coefficient μ_i as is described in section 3.2.3. Here we simply this load by setting uniform distributed load on one side of arch with $\mu_i = 0.1$, which value is half of largest $\mu_3 = 2.0$.

5.2.2. Moment and stress comparison

Comparison of concrete locations

The dead load of one component is unchanged when we consider the component is reversed upside down as we shift the location of concrete parts from top to bottom. Assumed that the height of arch is 9 metres and the results of the analytical solution are as follows:

At the point of critical moment (at quarter of span according to section 4.1.5):

Concrete at top: $\sigma_{c-b} = 1.81\ MPa, \quad \sigma_{g-b} = 2.70\ MPa$

Concrete at bottom: $\sigma_{c-b} = -1.81\ MPa, \quad \sigma_{g-b} = 6.95\ MPa$

Where σ_{c-b} is the largest bending stress in concrete, similar for σ_{g-b} in glass panels. Concrete is in compression when it is located downside of the component. The cause of this is that under load case 4, the critical moment will always tend to push arch outward. The out layer of arch inside component will always be in tension in this case. Thereby, concrete parts shall be at upside of component in the following design.

Comparison of concrete integration

To verify the structural advantage of concrete integration, both the stress inside glass-concrete component and pure glass component for arch of same dimensions will be calculated. Again assumed that the height of arch is 9 metres and the results of the analytical solution are as follows:

With concrete: $\sigma_{c-b} = 1.81\ MPa, \quad \sigma_{g-b} = 2.70\ MPa$

without concrete: $\sigma_{g-b} = 3.59\ MPa$

It can be seen that by integrating concrete, tensile stress inside glass at critical point is reduced. This means apart from other benefits, it is beneficial in terms of structural behaviour.

5.2.3. Parametric study

By altering the height of arches but limited inside range of shallow and intermediate, the critical bending moment and stress will be calculated. Both situations of arch made of pure glass components and composite components will be calculated. In Figure 5.3 the bending stresses of pure glass situation (top) and composite situation (bottom) are given. We can tell from this diagram that the moment stresses increase with the height increasing, in both situations, also in both concrete and glass.

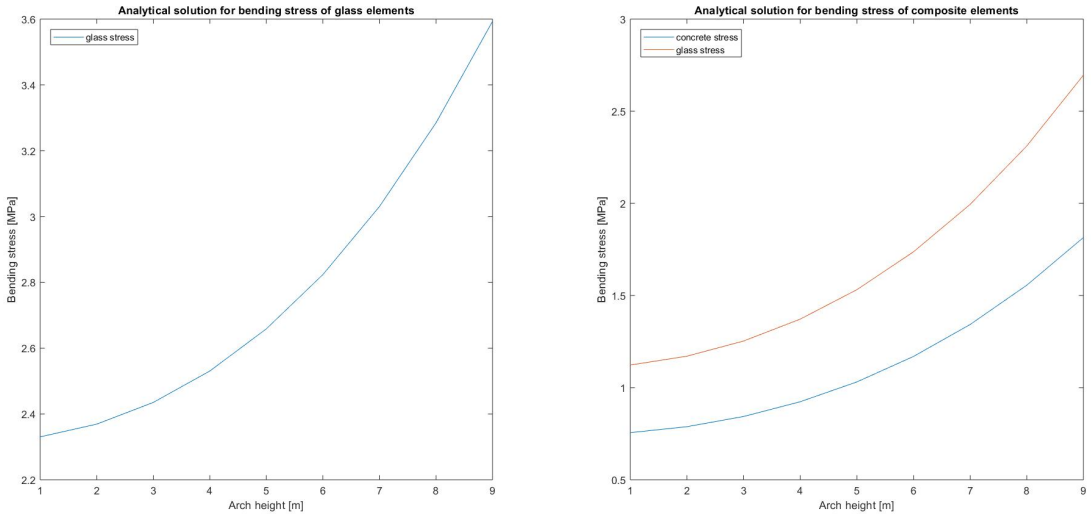

(a) Pure glass component (b) Composite component

Figure 5.3: Stresses of analytical solution

5.2.4. Behaviour analysis

The comparison of bending moments and stresses in two situations are plotted in Figure 5.4 and 5.5.

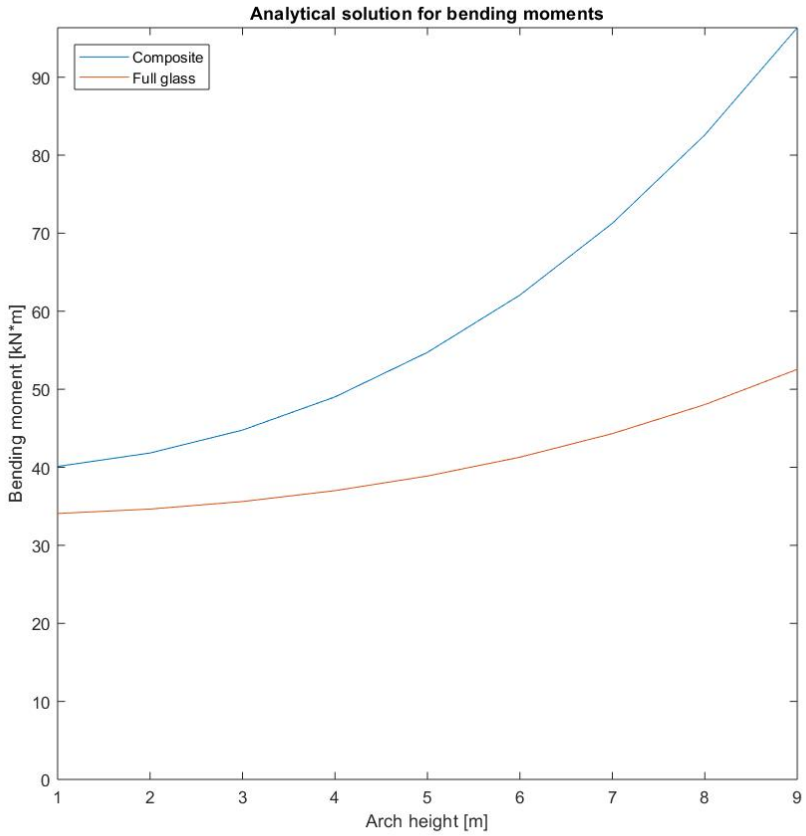

Figure 5.4: Comparison of bending moments

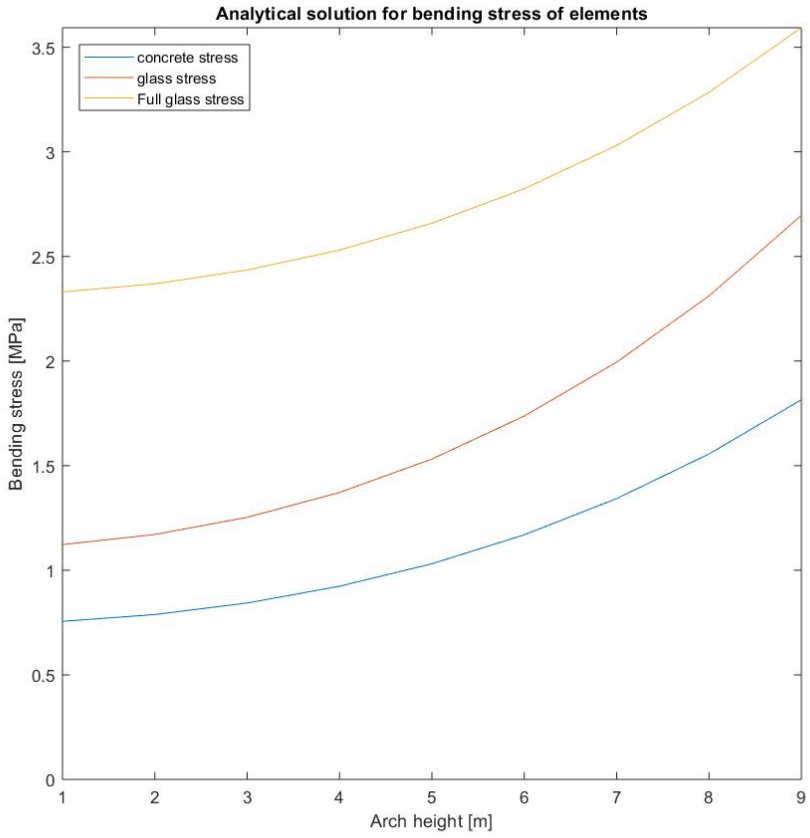

Figure 5.5: Comparison of pure glass and ending stresses

It can be inferred from the Figure 5.4 that the critical bending moment of composite arch is always higher than pure glass arch. For both arches the bending moments are raising with height increment, and the curve of composite arch is steeper than pure glass arch when the height is approaching height of 9 metres.

On the other hand, stress increment of composite component is also slightly larger than pure glass arch when height is escalating. But the maximum stress of glass inside the composite arch is overall lower than the one inside pure glass arch.

5.3. GSA solution

5.3.1. Approach

Geometry Gym[8] plug-ins for Rhino[9] Grasshopper[10] is used to connect GSA software with arch geometries. By altering the parameters in Grasshopper (Figure 5.6) and transferring data into GSA, results can be obtained both in GSA and Grasshopper. The data then will be collected inside Microsoft Excel to do further analysis.

[8]Geometry Gym provides OpenBIM software tools and support for Architects and Engineers amongst others in the Built Environment.
Website:https://geometrygym.wordpress.com/

[9]Rhinoceros 3D is a commercial 3D computer graphics and computer-aided design (CAD) application software.
Official website:https://www.rhino3d.com/

[10]Grasshopper is a graphical algorithm editor tightly integrated with Rhino’s 3-D modelling tools.
Website:http://www.grasshopper3d.com/

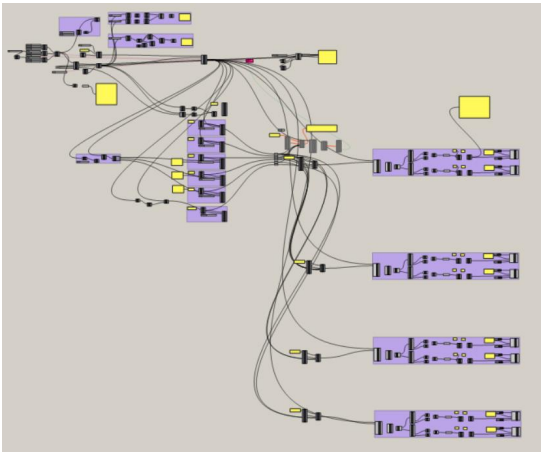

Figure 5.6: Script in grasshopper

5.3.2. Numerical modelling

According to NEN-EN 1991-1-4 in section 3.2.4, the $c_{pe,10}$ for different wind zones as well as the peak velocity pressures will be changing to various heights. The wind load inputs shall be calculated and used in modelling. Here the input for GSA calculation is listed in Appendix C section C.1, where the load is listed in column of $Zone\ A\ [kN/m]$.

Four load cases in section 4.1.5 will be simulated under the supports conditions of both two-hinged and fixed arches. Here the snow load will be applied as projected in global coordinate while wind load will be applied in local coordinate, both of which will be applied in the direction of Y axis.

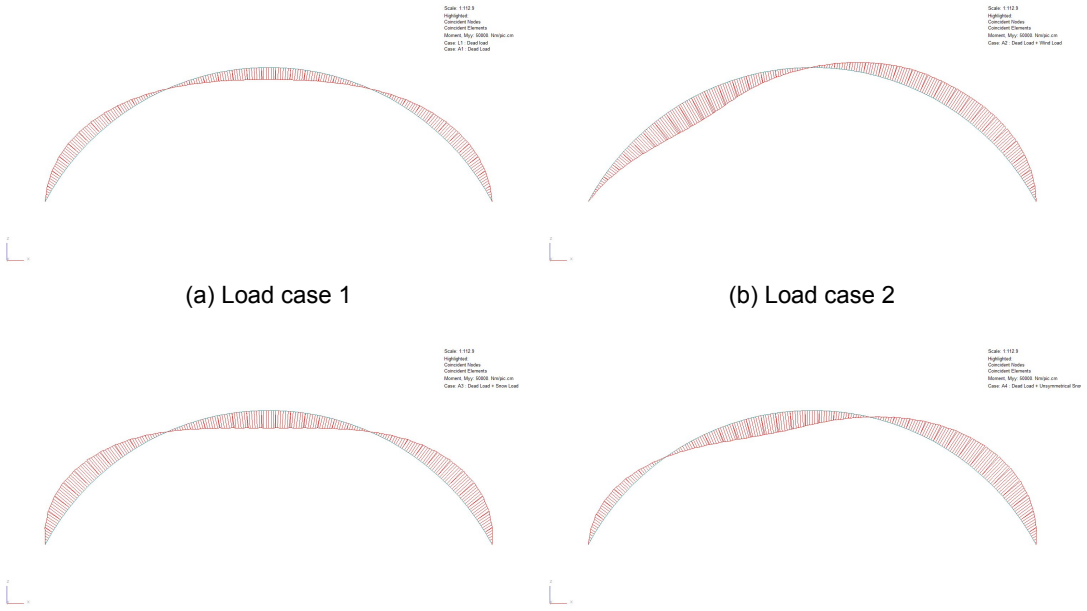

(a) Load case 1

(b) Load case 2

(c) Load case 3

(d) Load case 4

Figure 5.7: Bending moments of two-hinged arch

5.3.3. Results of GSA

Assumed the height of arch is 9 metres, the bending moments of two-hinged arch under 4 load cases are plotted in Figure 5.7 while the ones for fixed arch are in Figure 5.8.

Figure 5.7 indicates that critical bending moments for both load case 2 and load case 4 occur at one fourth of the arch span. The moment distributions for load case 1 and load case 3 are similar, only different in values. On the other hand, the critical bending moments in fixed arches occur at the

supports. It can be derived from the scale of both diagrams that the overall bending moment of the fixed arch within the arch roof is smaller than that of two-hinged arch, which means the cost of arch is lower while the cost of supports is higher compared to two-hinged arch.

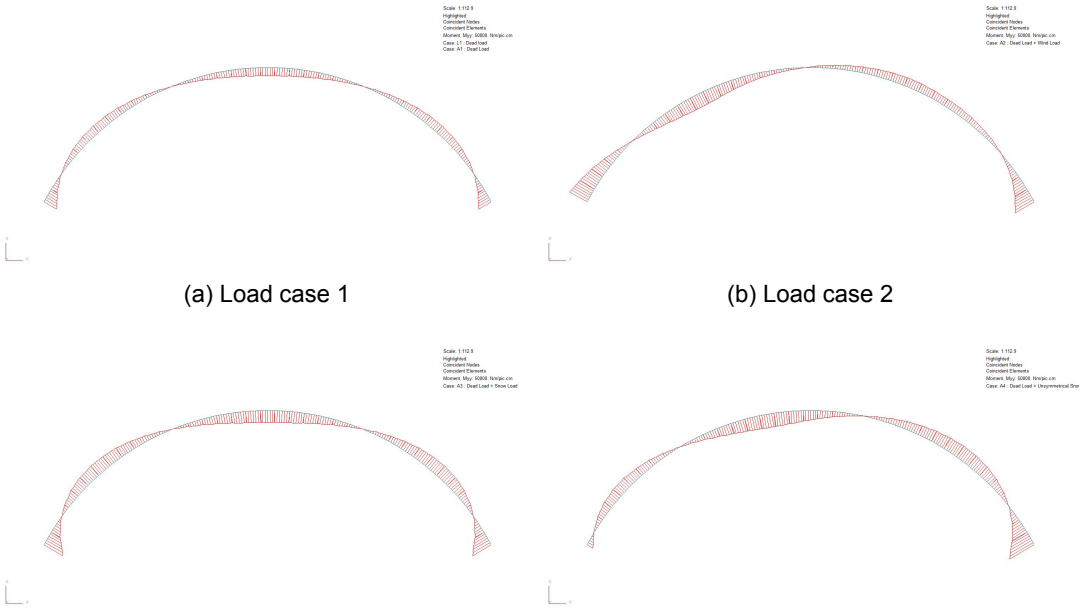

(a) Load case 1 (b) Load case 2

(c) Load case 3 (d) Load case 4

Figure 5.8: Bending moments of fixed arch

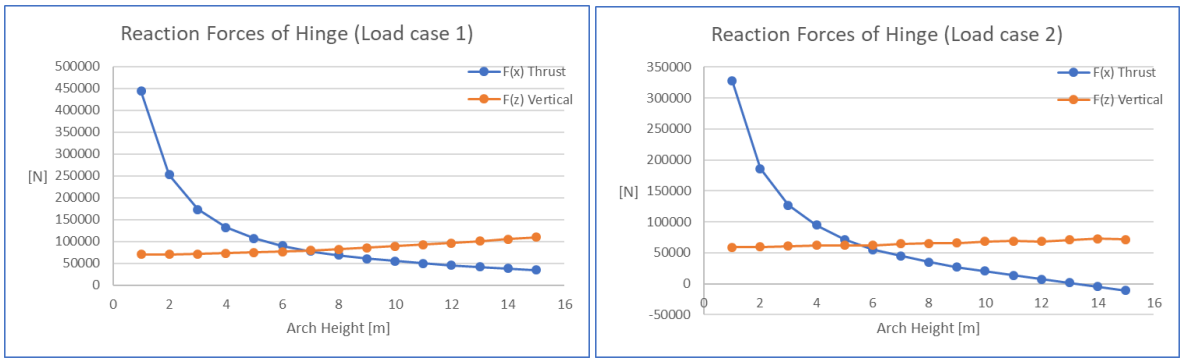

(a) Load case 1 (b) Load case 2

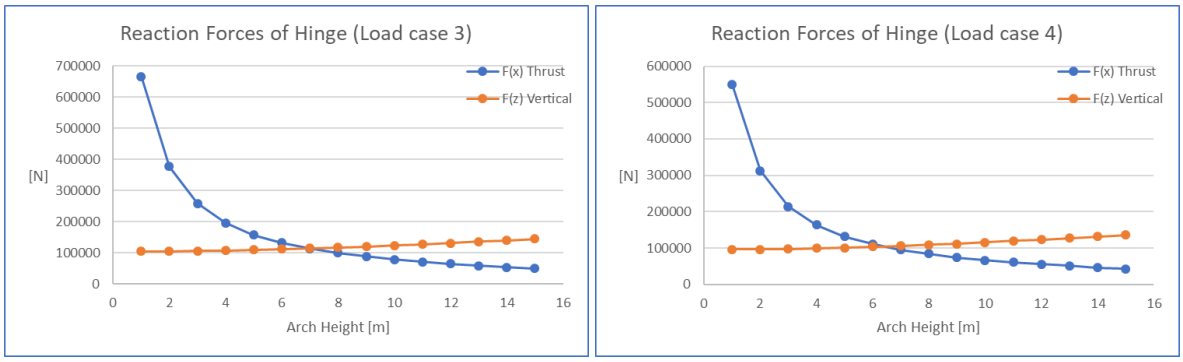

(c) Load case 3 (d) Load case 4

Figure 5.9: Reaction forces of two-hinged arch

5.3.4. Parametric study

By collecting the results of horizontal (thrust) reaction force R_h and vertical reaction force R_v from GSA solution for arches of all parametric heights, the charts are given in Figure 5.9 for two-hinged arches and Figure 5.10 for fixed arches. Besides, the reaction forces for four load cases are gathered and compared in terms of two-hinged arches and fixed arches in Figure 5.12. The additional reaction moments R_{moment} at supports of fixed arches are illustrated in Figure 5.13.

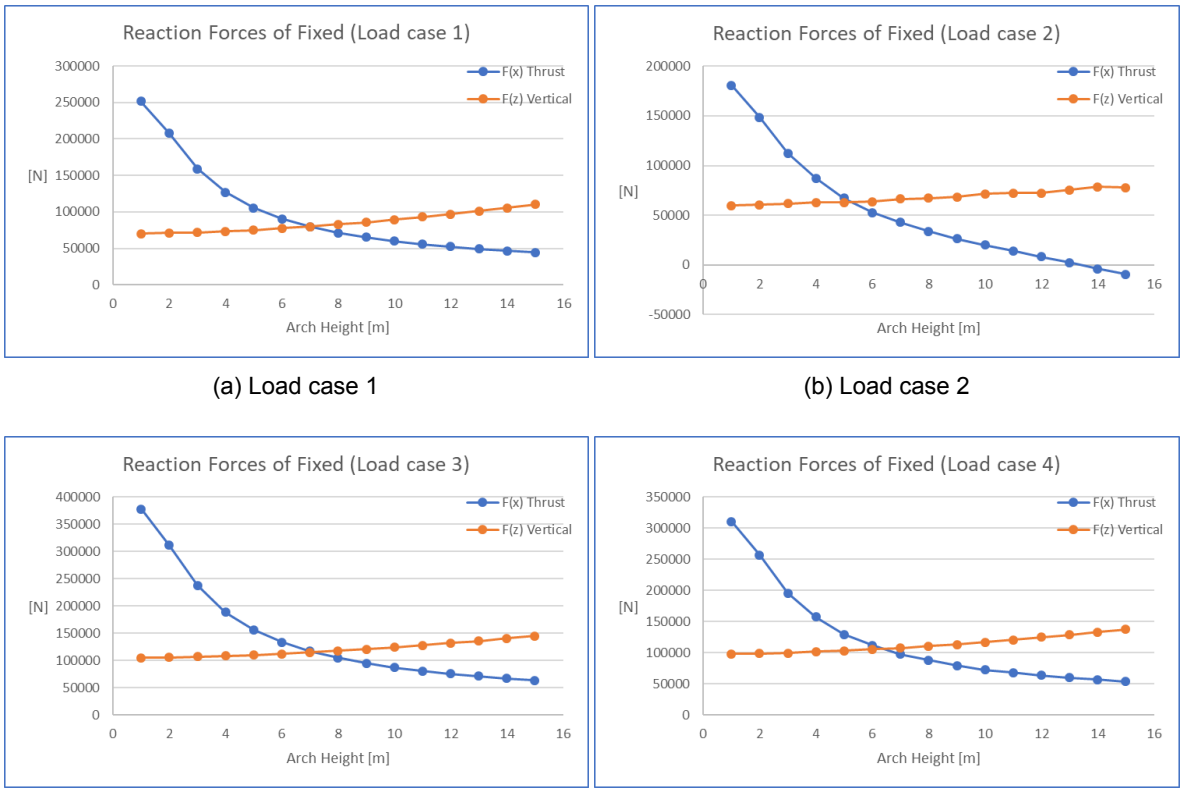

(a) Load case 1 (b) Load case 2

(c) Load case 3 (d) Load case 4

Figure 5.10: Reaction forces of fixed arch

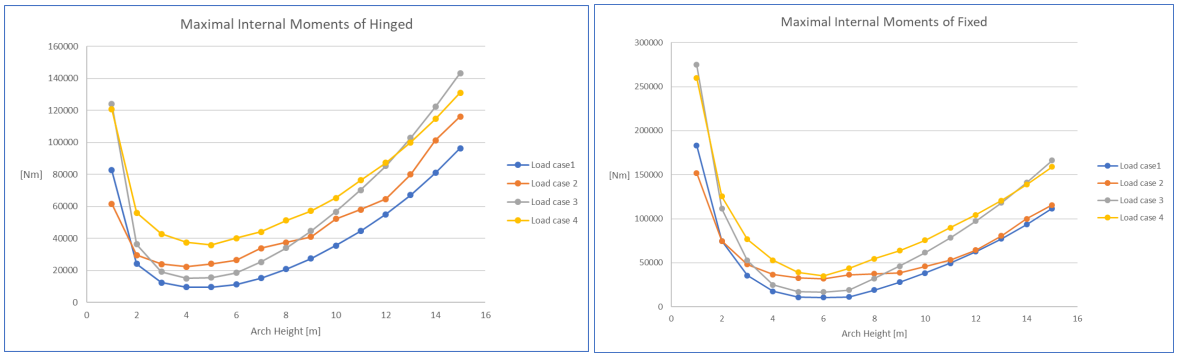

(a) Internal moments of two-hinged arches (b) Internal moments of fixed arches

Figure 5.11: Maximum internal moments

It can be found that in both in two-hinged and fixed arches the R_h declines and R_v rises with height-to-span ratio developing. The slope of R_h declining is steeper than the slope of R_v rising. Obviously load case 3 is the dominating case of R_h, R_v and most results of R_{moment}. The internal bending moments of arches on the other hand diminish first then climb back after certain height in Figure 5.11, this implies that cost of arch will also follow these curves globally. It is clear that there is an optimal height of arch

to balance the cost of supports and arch components in this case.

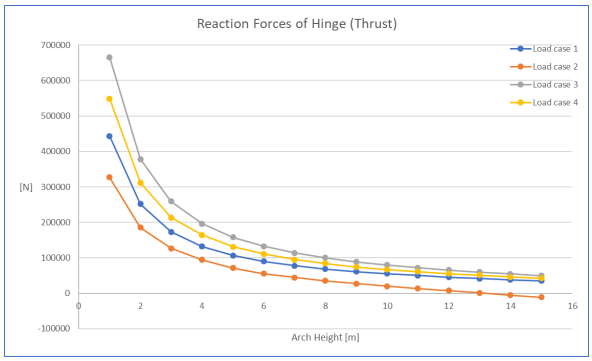

(a) Thrust reaction forces of two-hinged arches

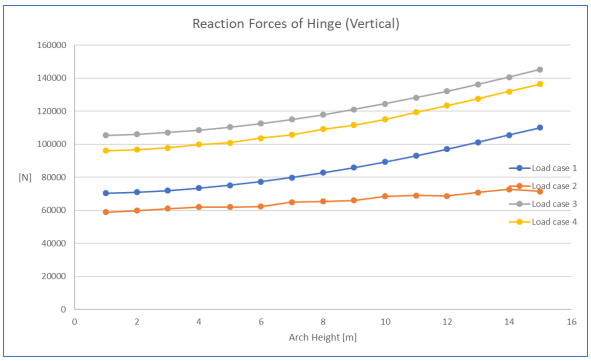

(b) Vertical reaction forces of two-hinged arches

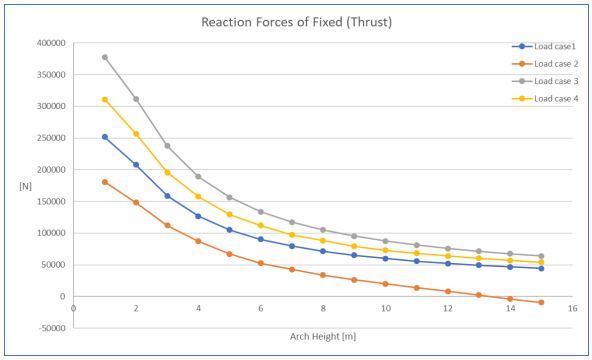

(c) Thrust reaction forces of fixed arches

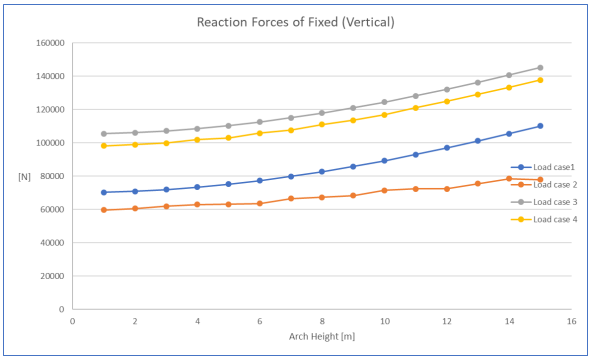

(d) Vertical reaction forces of fixed arches

Figure 5.12: Reaction forces comparison

Figure 5.13: Reaction moments at supports of fixed arches

5.3.5. Behaviour analysis

To study the cause for the behaviour of internal moments of arches, the internal moments as well as axial forces along the arches are gathered from GSA. The bending moments results of different heights under different load cases are shown in Figure 5.14 for two-hinged arches and Figure 5.15 for fixed arches. More clear figures will be attached at Appendix C section C.2 and C.3.

By comparing these figures with the results in section 5.3.3, we can infer that when the height of arch becomes too small, the arch action tends to disappear, where the two-point supported flat beam action is dominating. This is the reason that bending moment is larger in the beginning of height parameters.

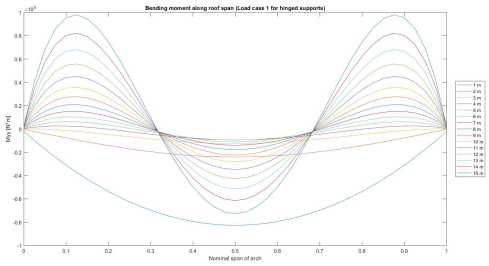

(a) Load case 1

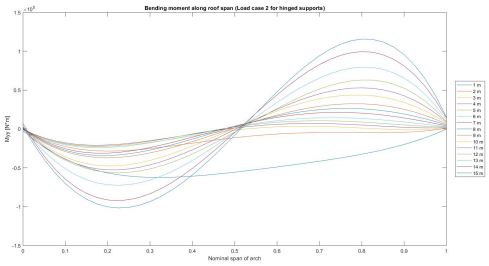

(b) Load case 2

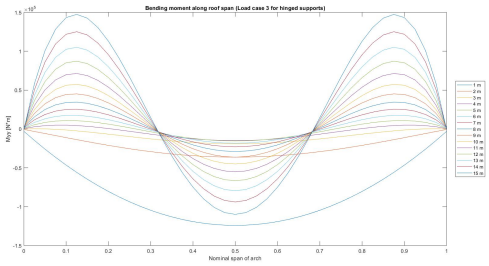

(c) Load case 3

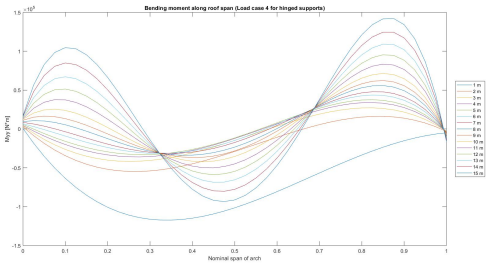

(d) Load case 4

Figure 5.14: Internal moments of two-hinged arch

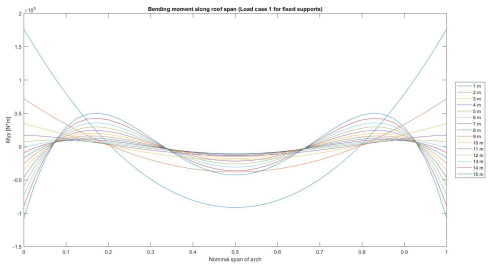

(a) Load case 1

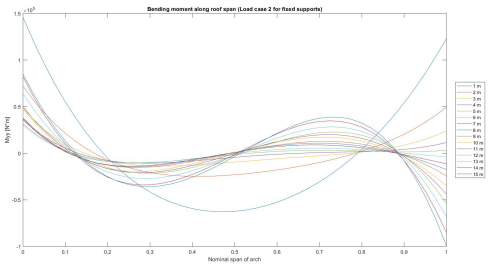

(b) Load case 2

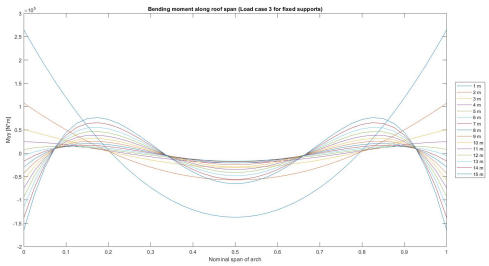

(c) Load case 3

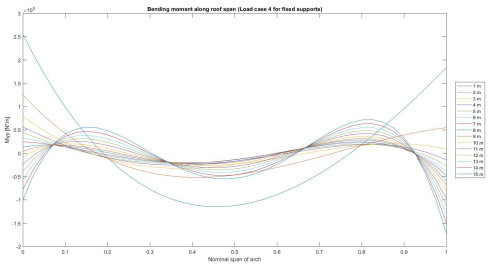

(d) Load case 4

Figure 5.15: Internal moments of fixed arch

5.3.6. Cost estimation case study

Because it is not easy to find some general guide on the cost estimation for arch building, and the design here only includes the arch roof with considering other aspects such as inner space,labour costs, site-works, maintenance cost etc. During this case study, the Gateway Bridge in Michigan is used for rough cost estimation according to the cost analysis table (Figure 5.16) in (Chapman and Kasi, 2012).

From Figure 5.16 and Figure 5.17we can get following information for cost estimation:

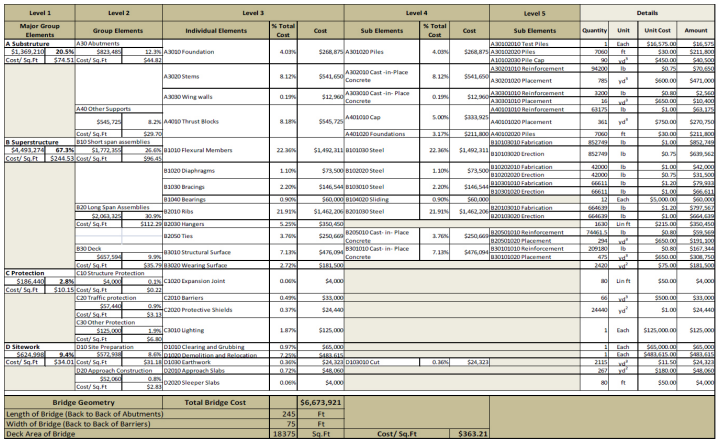

Level 1	Level 2	Level 3		Level 4			Level 5	Details			
Major Group Elements	Group Elements	Individual Elements	% Total Cost	Cost	Sub Elements	% Total Cost	Cost	Sub Elements	Quantity	Unit	Unit Cost	Amount
A Substructure	A30 Abutments							A30102010 Test Piles	1	Each	$16,575.00	$16,575
$1,369,210 20.5%	$823,485 12.3%	A3010 Foundation	4.03%	$268,875	A301020 Piles	4.03%	$268,875	A30102020 Piles	7060	ft	$30.00	$211,800
Cost/ Sq.Ft $74.51	Cost/ Sq.Ft $44.82							A30102030 Pile Cap	90	yd³	$450.00	$40,500
		A3020 Stems	8.12%	$541,650	A302010 Cast -in- Place Concrete	8.12%	$541,650	A30201010 Reinforcement	94200	lb	$0.75	$70,650
								A30201020 Placement	785	yd³	$600.00	$471,000
		A3030 Wing walls	0.19%	$12,960	A303010 Cast -in- Place Concrete	0.19%	$12,960	A30301010 Reinforcement	3200	lb	$0.80	$2,560
	A40 Other Supports							A30301010 Placement	10	yd³	$650.00	$10,400
	$545,725 8.2%	A4010 Thrust Blocks	8.18%	$545,725	A401010 Cap	5.00%	$333,925	A40101010 Reinforcement	63175	lb	$1.00	$63,175
	Cost/ Sq.Ft $29.70							A40101020 Placement	361	yd³	$750.00	$270,750
B Superstructure	B10 Short span assemblies				A401020 Foundations	3.17%	$211,800	A40102020 Piles	7060	ft	$30.00	$211,800
$4,493,274 67.3%	$1,772,350 26.6%	B1010 Flexural Members	22.36%	$1,492,311	B101030 Steel	22.36%	$1,492,311	B10103010 Fabrication	852749	lb	$1.00	$852,749
Cost/ Sq.Ft $244.53	Cost/ Sq.Ft $96.45							B10103020 Erection	852749	lb	$0.75	$639,562
		B1020 Diaphragms	1.10%	$73,500	B102020 Steel	1.10%	$73,500	B10202010 Fabrication	42000	lb	$1.00	$42,000
								B10202020 Erection	42000	lb	$0.75	$31,500
		B1030 Bracings	2.20%	$146,544	B103010 Steel	2.20%	$146,544	B10301010 Fabrication	66611	lb	$1.20	$79,933
								B10301020 Erection	66611	lb	$1.00	$66,611
		B1040 Bearings	0.90%	$60,000	B104020 Sliding	0.90%	$60,000		12	Each	$5,000.00	$60,000
	B20 Long Span Assemblies							B20103010 Fabrication	664639	lb	$1.20	$797,567
	$2,063,325 30.9%	B2010 Ribs	21.91%	$1,462,206	B201030 Steel	21.91%	$1,462,206	B20103020 Erection	664639	lb	$1.00	$664,639
	Cost/ Sq.Ft $112.29	B2030 Hangers	5.25%	$350,450					1630	Lin ft	$215.00	$350,450
		B2050 Ties	3.76%	$250,660	B205010 Cast -in- Place Concrete	3.76%	$250,660	B20501010 Reinforcement	74461.5	lb	$0.80	$59,569
								B20501020 Placement	299	yd³	$650.00	$193,309
	B30 Deck	B3010 Structural Surface	7.13%	$476,094	B301010 Cast -in- Place Concrete	7.13%	$476,094	B30101010 Reinforcement	209180	lb	$0.80	$167,344
	$657,594 9.9%							B30101020 Placement	470	yd³	$650.00	$308,750
	Cost/ Sq.Ft $35.76	B3020 Wearing Surface	2.72%	$181,500					2420	yd²	$75.00	$181,500
C Protection	C10 Structure Protection											
$186,440 2.8%	$4,000 0.1%	C1020 Expansion Joint	0.06%	$4,000					80	Lin ft	$50.00	$4,000
Cost/ Sq.Ft $10.15	Cost/ Sq.Ft $0.22											
	C20 Traffic protection	C2010 Barriers	0.49%	$33,000					66	yd³	$500.00	$33,000
	$57,440 0.9%	C2020 Protective Shields	0.37%	$24,440					24440	yd²	$1.00	$24,440
	Cost/ Sq.Ft $3.13											
	C30 Other Protection											
	$125,000 1.9%	C3010 Lighting	1.87%	$125,000					1	Each	$125,000.00	$125,000
	Cost/ Sq.Ft $6.80											
D Sitework	D10 Site Preparation	D1010 Clearing and Grubbing	0.97%	$65,000					1	Each	$65,000.00	$65,000
$624,998 9.4%	$572,998 8.6%	D1020 Demolition and Relocation	7.25%	$483,615					1	Each	$483,615.00	$483,615
Cost/ Sq.Ft $34.01	Cost/ Sq.Ft $31.18	D1030 Earthwork	0.36%	$24,323	D103030 Cut	0.36%	$24,323		2115	yd³	$11.50	$24,323
	D20 Approach Construction	D2010 Approach Slabs	0.72%	$48,060					267	yd²	$180.00	$48,060
	$52,060 0.8%	D2020 Sleeper Slabs	0.06%	$4,000					80	ft	$50.00	$4,000
	Cost/ Sq.Ft $2.83											

Bridge Geometry	Total Bridge Cost		$6,673,921			
Length of Bridge (Back to Back of Abutments)		245	Ft			
Width of Bridge (Back to Back of Barriers)		75	Ft			
Deck Area of Bridge		18375	Sq.Ft	Cost/ Sq.Ft		$363.21

Figure 5.16: Cost Analysis of the Gateway Arch Bridge Using the UNIFORMAT II Elemental Classification and Example Sub Classification

Element	% of total cost
Thrust Blocks	8.18
Foundation in Thrust blocks	3.17
Ties	3.76
Ribs	21.91

Table 5.1: Cost proportions

By substituting cost of ribs with cost of arch, cost of thrust blocks and ties with cost of fixed supports, cost of thrust blocks and ties minus cost of foundation with cost of two-hinged supports, the cost estimation is as follows:

- Two-hinged:
  Nominal arch length× Nominal M_{arch}× 21.91%+Nominal resultant reaction force× 8.77%
- Fixed:
  Nominal arch length× Nominal M_{arch}× 21.91%+(Nominal resultant reaction force× 0.5+Nominal reaction moment × 0.5)× 11.94%

Where nominal values denote that it is divided by the value of same term from arch of 11 metre high, whose height-to-span ratio is same as the Gateway Arch Bridge.

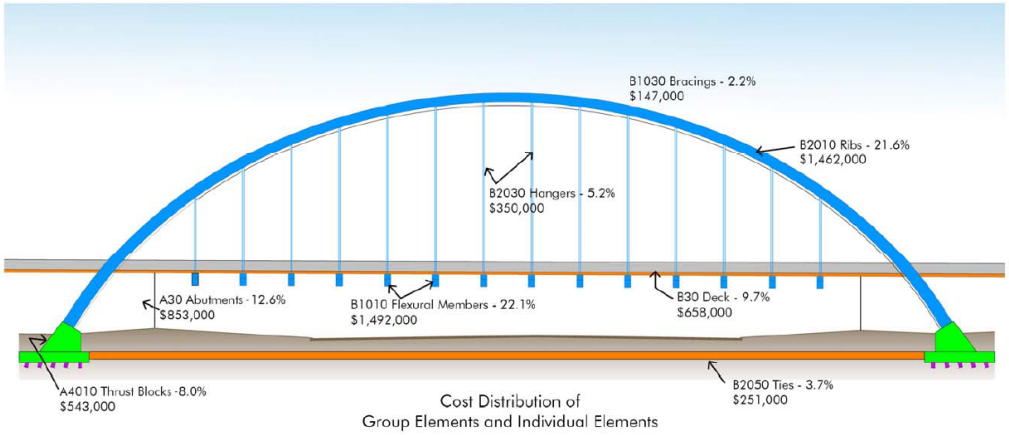

Figure 5.17: Cost Distribution of Selected Group Elements and Individual Elements for the Gateway Arch Bridge

The plot of nominal costs can be seen in Figure 5.18. After comparing the highest cost for all load cases of all heights, the optimal result is that 5 metres for two-hinged support and 6 metres for fixed support. Sonavane (2014) gives advice on economical rise-to-span ratio of 0.2 to 0.3, so we set height of arch at 6 metres to do further study.

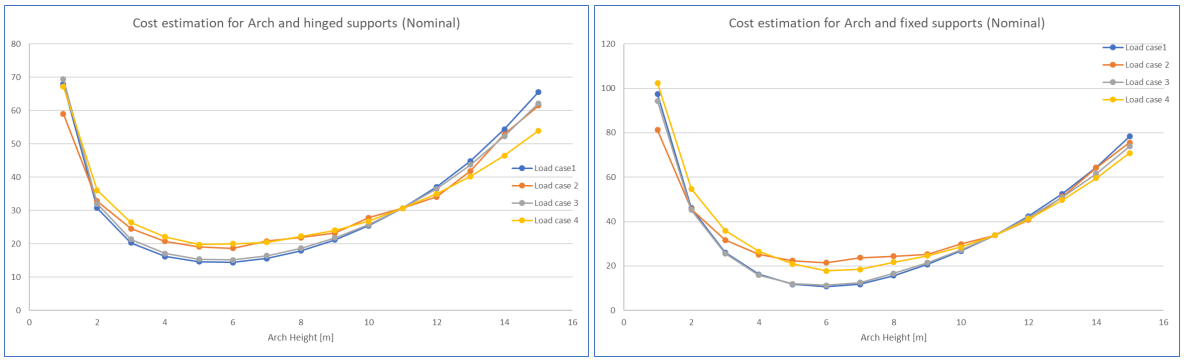

(a) Nominal cost of two-hinged arches (b) Nominal cost of fixed arches

Figure 5.18: Cost estimation

5.3.7. Final design

In accordance with the example of Museum aan de Stroom (Figure 1.9), the length of corrugated glass is limited within 6 metres(Nijsse, 2009). After the global dimension of arch is set, the results of () for element length from 0.5 to 6 metres are gathered and plotted in Figure 5.19.

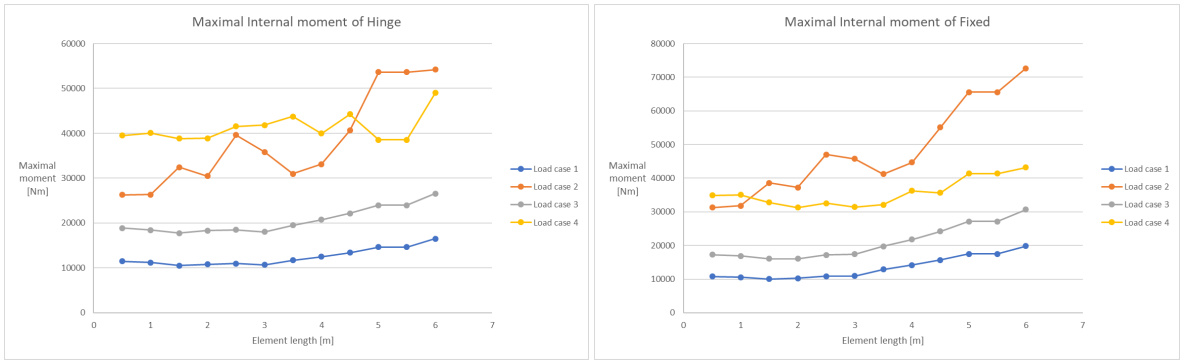

(a) Two-hinged arch (b) Fixed arch

Figure 5.19: Comparison of different element lengths

The fluctuation in the diagram can be explained by Figure 5.20. If the element becomes longer, each element works more like an individual beam which weakens the arch action to some extent.

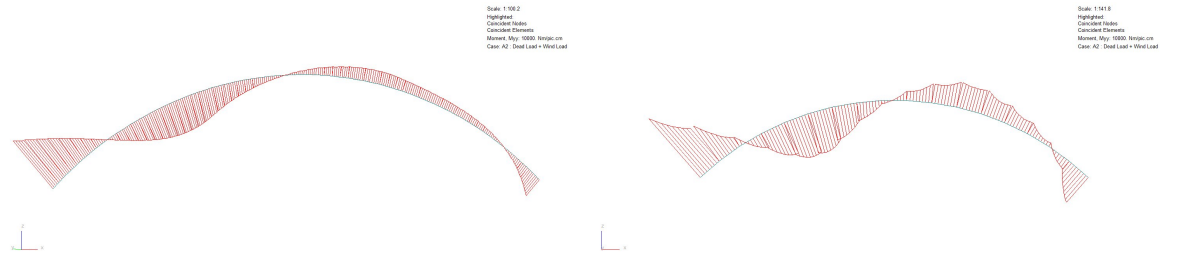

(a) Elements of 0.5 metre (b) Elements of 2 metres

Figure 5.20: Moment distribution along fixed arches

We can deduce from Figure 5.19 that 1.5 metres is the optimal length for single element of two-hinged arch where load case 4 is dominating. While for fixed arch, the lowest value occurs at 0.5 metre. However, for both supports conditions, there is possibility that the lowest value merges at somewhere between 1 to 1.5 metres. Because of the declining slope within 1 and 1.5 metres of two-hinged arch, the intersection of load case 2 and load case 4 with 1 and 1.5 metres of fixed arch. Under this circumstance, we limit out element length around 1 and 1.5 metres for following research.

In conclusion, the final choices for global arch design are as follows:

Parameter	Selection
Arch shape	Circular
Arch span	30 m
Arch height	6 m
Support condition	Two-hinged and fixed
Length of element	Around 1 to 1.5 metres

Table 5.2: Cost proportions

6

Connection Design

The importance of connection design cannot be emphasized more during the design of glass structure. Concentrated load should not be neglected because of the brittleness of glass material. In this chapter, classifications of connection will be discussed first, after which some modified and new connection designs will be listed and analysed together with the assembling order scheme. Finally, choices will be made, where experiment verification is needed and proceed.

6.1. Classification of connection

There are mainly four types of connections in this design as described in Figure 6.1.

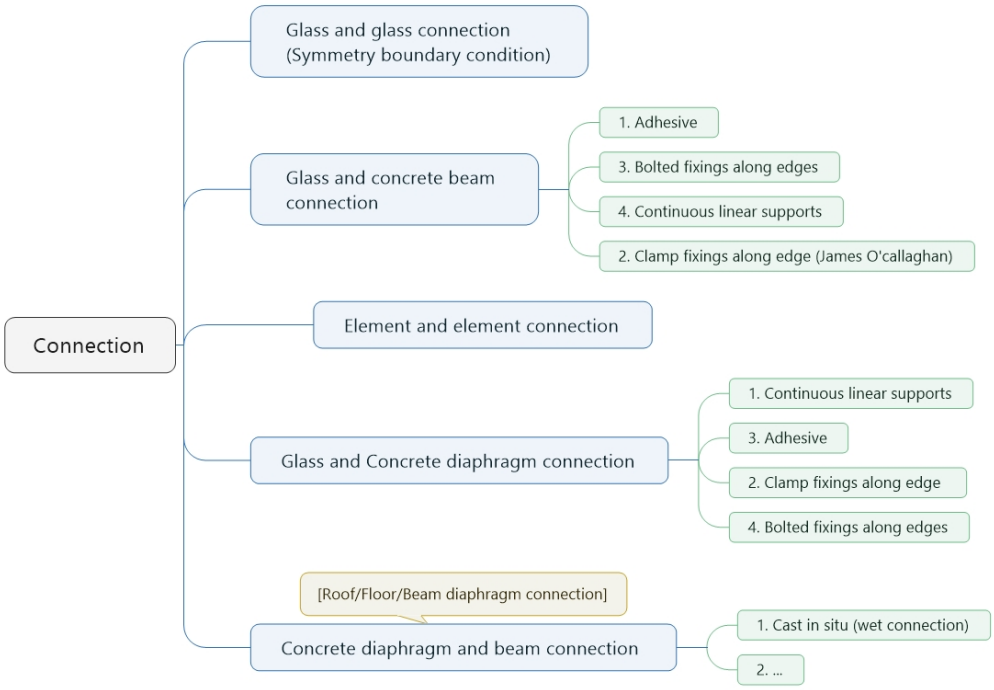

Figure 6.1: Connection classification

When element made of corrugated glass panels in Figure 5.2 needs an intermediate break along the curve, a glass-to-glass connection is required which is usually jointed by silicone. Here in this case we assume that the corrugated glass panel can be produces as a whole piece if it is within the dimensions mentioned in section 2.3.2, where the largest possible wave-height is 1000 millimetres.

If we take the upper concrete parts in Figure 5.2 as arch beams, the diaphragm and concrete beam connection depends quite on the type of diaphragm. Normally in-plane shear plates can be utilized as is shown in the element of Salone Agenlli (Figure 1.7), where the diaphragm is prefabricated in the element before installing to preventing cross-sectional deformation of element. Here in this case we prefer to prefabricate whole corrugated elements at manufacturer places than in-site casting, so if the diaphragm is required in this design, two favourable options will be available here: Prefabricated concrete plate, or prestressed steel cables used as horizontal tie.

After all these presupposed conditions, the following context will mainly focus on the design of three types of connections:

- Connection between glass panels and concrete beams
- Connection between glass panels and element junctions
- Connection between modular elements

6.2. Connection between glass and concrete beams

As indicated in section 5.2.2, concrete is shifted to the upside of the component. Design will still be classified into mechanical and adhesive connections listed in the following sections.

6.2.1. Mechanical connection

6.2.1.1. Interlocking:

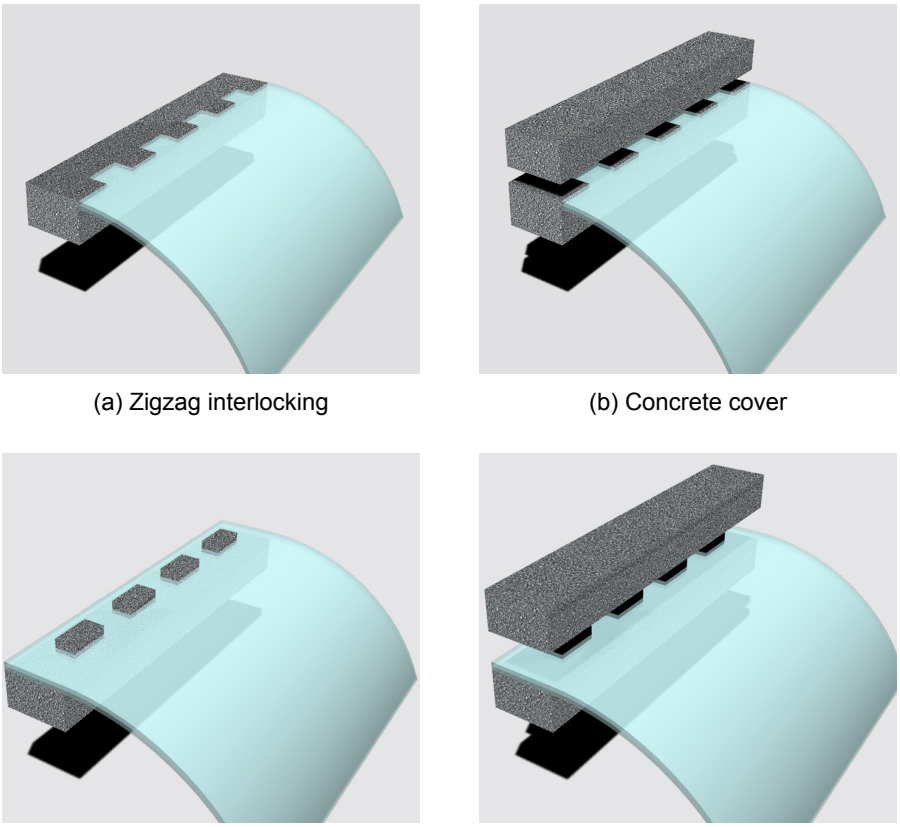

(a) Zigzag interlocking

(b) Concrete cover

(c) Protruded interlocking

(d) Concrete cover

Figure 6.2: Interlocking connection

In this connection both glass and concrete is connected in linear interlocking way. Concrete will be prefabricated in desired shape, after which the glass panels will be placed on top of it. The process of drilling or cutting glass should be implemented before any hot bending, coating or laminating, therefore the tolerance and alignment here shall be controlled. In the upper connection of Figure 6.2, the inserted sticking out parts of glass should be smaller than notches in concrete, so that soft infill material can be used to compensate dimensional variation, thermal movement. The same principal goes for the lower connection of Figure 6.2 where the notches in glass should be slightly larger than the concrete extruded blocks.

6.2.1.2. Shear connector

Point fixings of undercut anchors are used in this case similar to the way shear connectors are used in composite steel-concrete beams(NEN-EN 1994-1-1). Undercut holes can be manufactured by the diamond drilling process by local grinding in non-tempered single or laminated glass(Wurm, 2007). The drilling process likewise shall be conducted before hot-bending and laminating process where the alignment and tolerance condition will be critical. In Figure 6.3, after the production of curved glass panels, they will be placed onto the prefabricated concrete frame. The concrete will be casted in place subsequently.

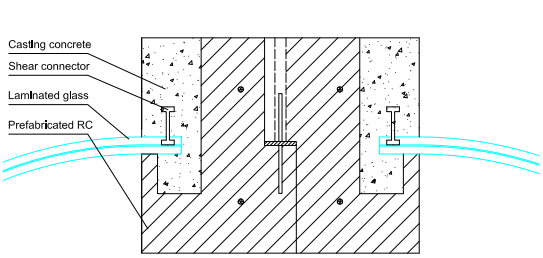

(a) Connection between glass and concrete beams

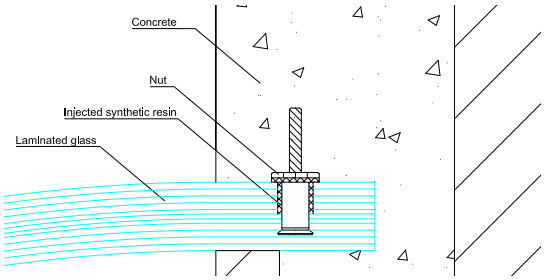

(b) Detail of undercut anchor

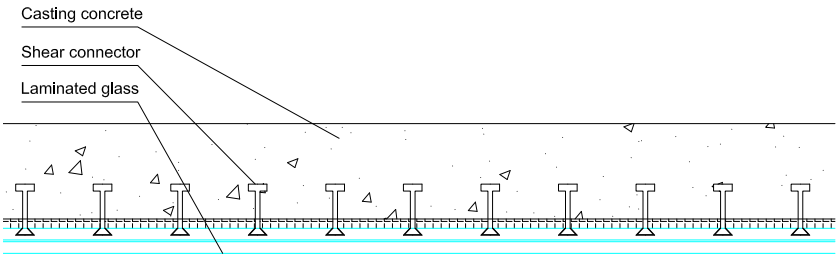

(c) Longitudinal section

Figure 6.3: Shear connectors

Figure 6.4: Undercut anchors [11]

[11] Source: https://www.glaswelt.de/Archiv/Heftarchiv/article-247734-104870/kleiner-halter-grosse-wirkung-.html

6.2.1.3. Friction connection

Friction connections can be applied when some form of diaphragm action and in plane loading is required in this case (Haldimann et al., 2008). As is illustrated in Figure 6.5, stresses are transferred with clamping plates with or without drilled holes. When drilled holes used, these bolt holes should be oversized to avoid any contact between the bolt and the glass. An intermediate pad is inserted between clamp and glass to distribute forces uniformly and form necessary friction. Besides, for laminated glass, local interlayer material in the area of contact edges may be needed. This is to prevent the interlayer material from being squeezed out from the laminated glass, which is detrimental to connection effectiveness because of the weakening of clamping force. The interlayer material should be resistant to creep and have the matched thickness to that of glass interlayer(Haldimann et al., 2008).

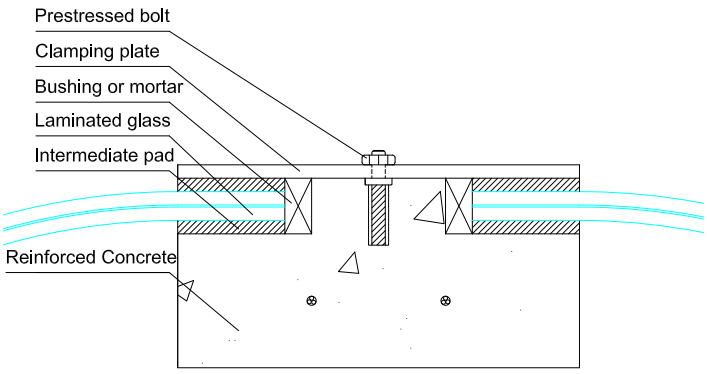

(a) Clamped 1

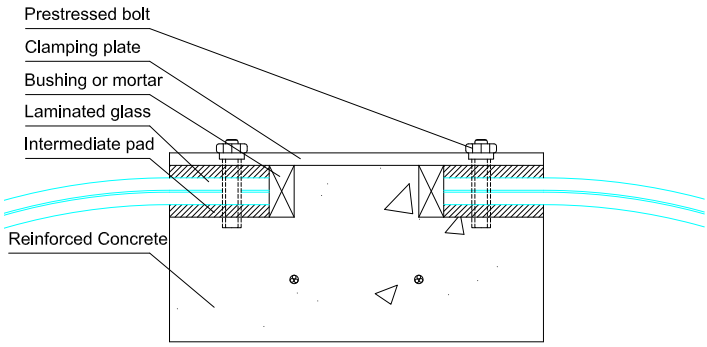

(b) Clamped 2

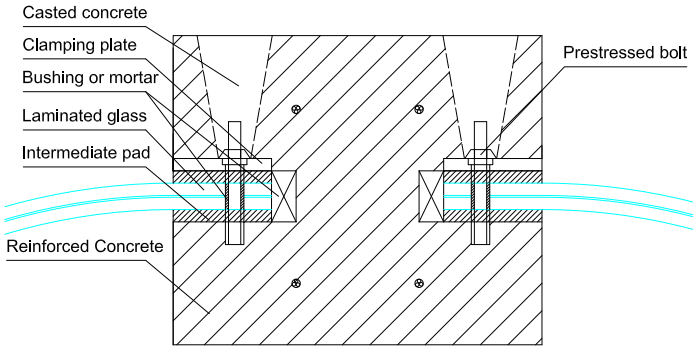

(c) Clamped and casted

Figure 6.5: Friction connections

6.2.2. Adhesive connection

According to section 2.2.3, fly ash concrete generates denser micro-structures which results in stronger inter-facial bond. When we cast fly ash concrete along the concrete frame, assuming that concrete and glass is bonded, this produces a connection effect similar to linear adhesive bond. For example, the adhesive systems of Silicone, MS polymers and Polyurethanes (PUR). The difference is that the thickness of adhesive layer can be zero or not constant in this case.

Normally only low strength is needed due to large bonded area of linear adhesive connection. Diaphragm action can also transmitted through linear supports, but attention must be paid to pane's edge machining, isolating the corners of the pane from the in-plane forces and the influence of thermal movement(Haldimann et al., 2008).

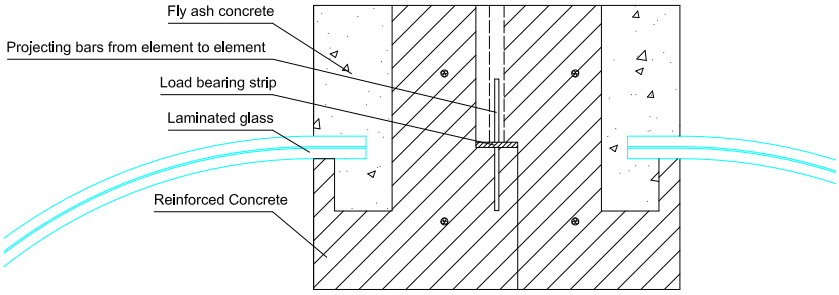

Figure 6.6: Adhesive connection between concrete and glass

6.2.3. Comparison and decision

To enhance residual loading bearing capacity, it is better in this design to four-sided support corrugated glass panels according to the general rule from Wurm (2007)(Table 6.1), because of the high safety requirement for overhead glazing glass structure. Therefore, prefabricated concrete frame with or without steel strips for corrugated glass panel will be used in this component.

Residual load-bearing capacity on breakage of all panes	Low	Medium	Good	Very good
Four-sided supported				×
Two-sided supported	×			
Point supports with button fixings			×	
Point supports with countersunk fixings		×		

Table 6.1: Residual load-bearing capacity of laminated safety glass with various types of support

	Connection type			
	Interlocking	Shear connector	Friction connection	Adhesive connection
Aspects				
Stress distribution	++	+++	+++	++++
Transparency	+++	++++	++++	+++
Assembly ease	++	+++	+	++++
Durability	-	+++	+++	-
Climate isolation	+++	++++	+++	++++
Maintenance	+	+	+++	+
Aesthetics	++++	++++	++	++++
Cost	++	+	+	++++

Table 6.2: Comparisons of connection designs
(+ means better performance while - means not applicable or data needed)

Some empirical comparisons between connections are listed in Table 6.2 to help make further research. Stress will distribute more evenly under the condition of no point fixings through drilled holes being used. Besides, drilling or cutting curved glass panels implicates high cost. On the other hand, assembling process can be challenging due the tolerance of drilled or cut corrugated glass as well as prestressing bolts. Climate isolation of the roof will also be crucial due to its geometry complication. It would be much easier to simply cast concrete in place to achieve sealing and connecting purpose, and additionally to compensate possible tolerances.

Take into consideration all the above listed reasoning, as well as personal interest, we would like to proceed design further with the option adhesive connection. However thermal performance, long-term loading performance and maintenance method should be investigated undoubtedly when it is possible.

6.3. Assembling order

After choice is made for the concrete frame and glass connection, the conceptual assembling order should be clarified to check the feasibility of building process. Here in this design, as is demonstrated in Figure 6.7, prefabricated concrete frame will be used as fitting support for glass and permanent formwork for fly ash concrete casting. Concrete will be poured around the periphery of glass panels along red lines in Figure 6.7. After the concreting and curing process, glass and concrete works as a whole component.

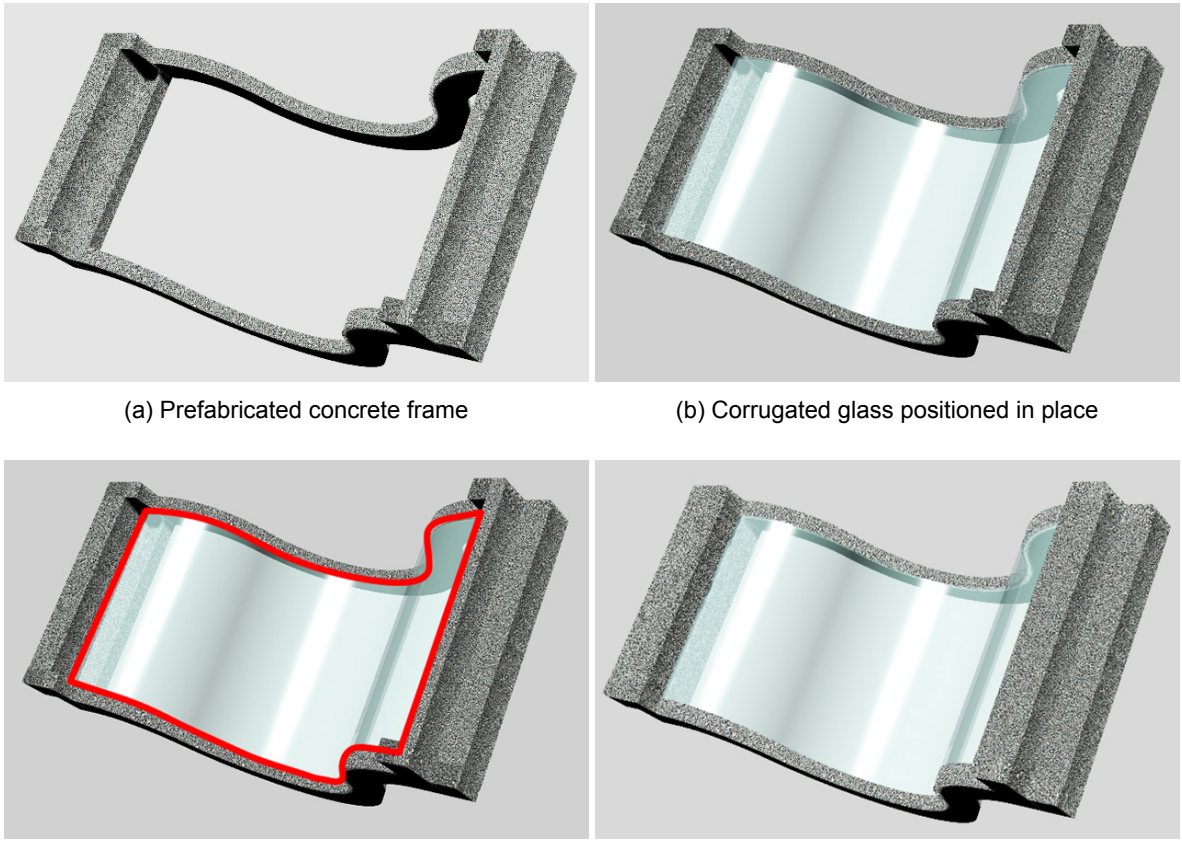

(a) Prefabricated concrete frame

(b) Corrugated glass positioned in place

(c) Edges where concrete will be casted

(d) Concrete casted in places

Figure 6.7: Element prefabrication

As for the assembling in construction site, elements will be positioned in place with the help of falsework. Mortar should be applied to rigidly connect between elements in the longitudinal section so that multi-elements turn into an arch system. While the connection between elements of two adjacent arches will be grouted in the gaines as shown in Figure 6.6.

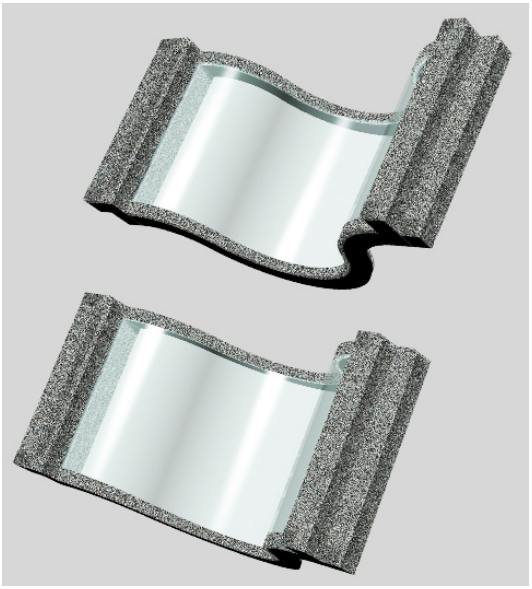

(a) Elements aligned and installed in place

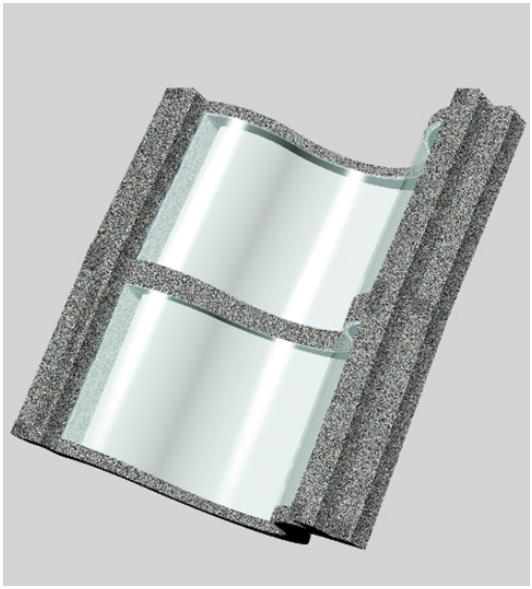

(b) Mortar applied into fitting boundaries

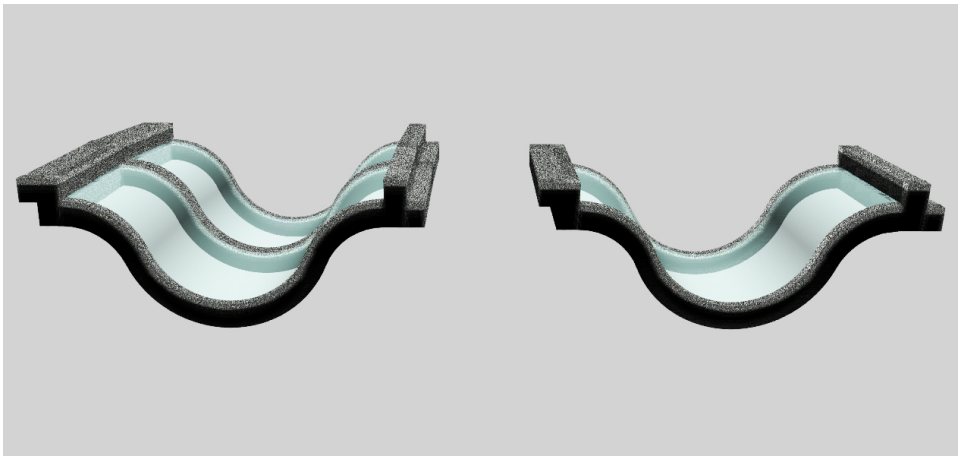

(c) Adjacent arch element put in place

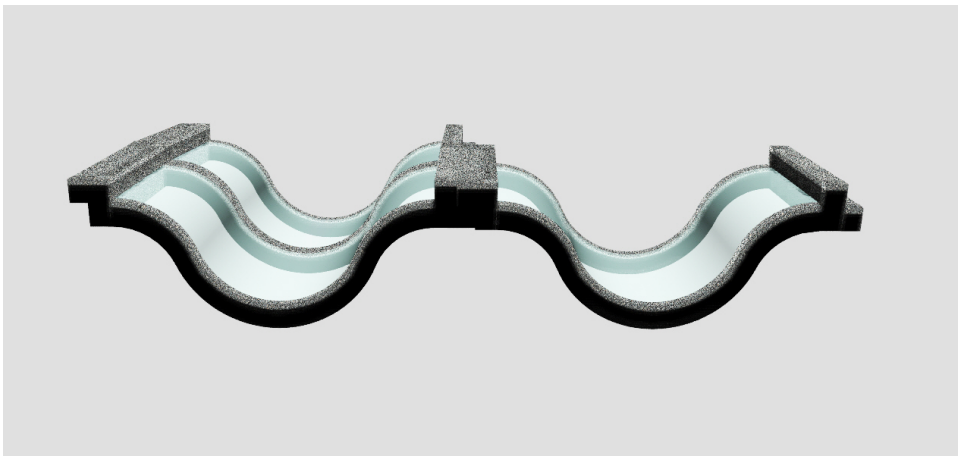

(d) Concrete casted in place for arch-to-arch joint

Figure 6.8: Element instalment

6.4. Connection between elements

Since concrete frame will be utilized as described in section 6.2.3, the connection design between elements can be allocated to concrete connection design, or prestressed concrete connection design in specific case. Assuming that concrete without prestressing is used here, wet connection of tooth-shaped connection is applied here(Figure 6.9 (c), (d)) for better sealing results. Protruding bars from prefabricated elements can be joined in the gaps which will be casted afterwards. When prestressing is introduced, tongue-and-groove system (Figure 6.9 (f)) will be applied to reach a high level liquid tightness.

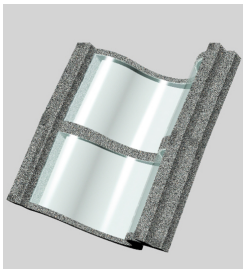

(a) Two elements connecting

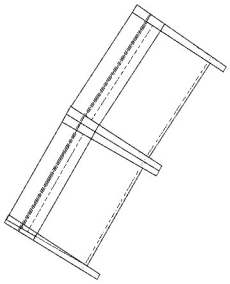

(b) Section of connection

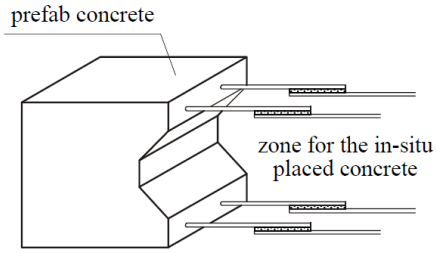

(c) Connection by welding reinforcement bars[12]

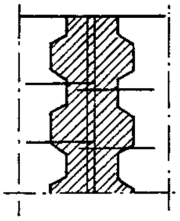

(d) Tooth-shaped connection[13]

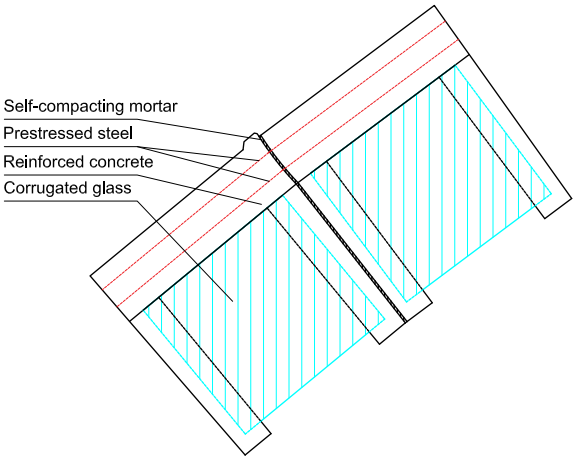

(e) Section of connection

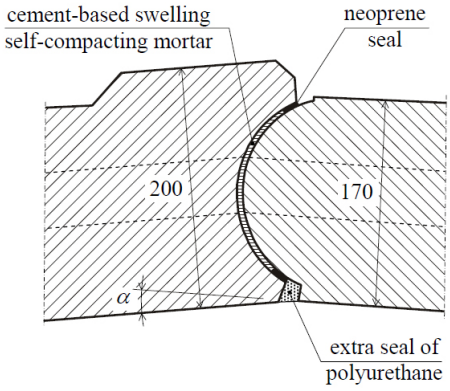

(f) Tongue-and-groove system[14]

Figure 6.9: Connection between elements

[12]Source: Lecture notes from CIE5110 Concrete-Science and Technology
[13]Source: Lecture notes from CIE4281 Building Structures 2
[14]Source: Lecture notes from CIE5110 Concrete-Science and Technology

6.5. Experimental data define

In this multi-straight-component arch design, the glass-concrete component may resist axial force and bending moment at the same time. When an individual element is in bending with glass and concrete working together, flexural shear stress and pull out shear will develop within the component. Thereby experimental data of this structural value will be needed in this calculation and analysis. Shear bond test design will be elaborated in Chapter 7.

6.6. Possibilities

If it is the case that shear bond strength from obtained from experiments appears to be not sufficient for the design. Mechanical connectors such as in section 6.2.1.2 can be modified by using fly ash concrete or other special concrete to improve the shear bond strength. Besides, one essential advantage of this pure concrete connection is its ability to achieve complicated geometries, which provides the opportunity to make further typology optimization.

7

Experimental Research

During the connection design of conrete and glass, pure bond between these two materials has been chosen to be further experimented. Normal soda-lime glass brick and fly ash concrete is used for this experiment, where the push out test will be carried out. In this chapter, experiment design and results analysis will be explained and analysed. Possible improvements to increase the shear bond strength will also be discussed.

7.1. Coupling parameters

Wong et al. (1999b) investigated the mortar-aggregate interfaces properties of fly ash-modified cement. According to their research, interfacial bond strength and interfacial fracture toughness is enhanced with the replacement 15% fly ash concrete. Besides, by computer simulation studies,(Dale, 1991) predicted that 20% replacement of fly ash of smaller particle size generated higher interfacial strength than control Portland cement paste.

Accordingly, levels of fly ash replacement is one of the chosen coupling parameters to be studied, The other parameter is the bond length between the glass and concrete.

7.2. Experiment design

7.2.1. Dimensions of moulds

Soda-lime glass brick dimensions are illustrated in Figure 7.1. Timber moulds will be used for concrete casting in this test (Figure 7.2). After three series of wooden moulds are assembled, glass brick will be taped to bottom wood panel. Before casting concrete, pre-treatment of glass surface and wooden panel should be done. Glass surfaces should be cleaned with 2-propanol while oil should be applied on wooden inner surfaces to make it easier to demould.

To research on the parameters affecting the bond strength as well as the coupling effects, specimens of concrete with various replacement levels and various bond lengths will be made. In this test, we use vliegas smz for fly ash concrete making, 3 series of concrete mixtures will be prepared, with proportions of 0%, 15% and 30% fly ash being used. 3 series of bond length will be prepared likewise, as is shown from top to bottom in Figure 7.2.

Besides, $100mm \times 100mm \times 100mm$ cube specimens (NEN-EN 12390-1) for compression test will also be prepared at the same time. For each group of test, 3 specimens will be made to get reliable result(Table 7.1).

	Fly ash proportion		
	0%	15%	30%
Bond length			
10mm	3	3	3
20mm	3	3	3
30mm	3	3	3
Cubes	3	3	3

Table 7.1: Specimens amount for test

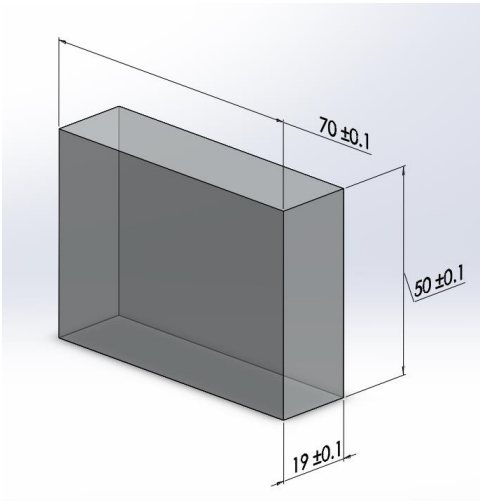

Figure 7.1: Dimensions of soda-lime glass

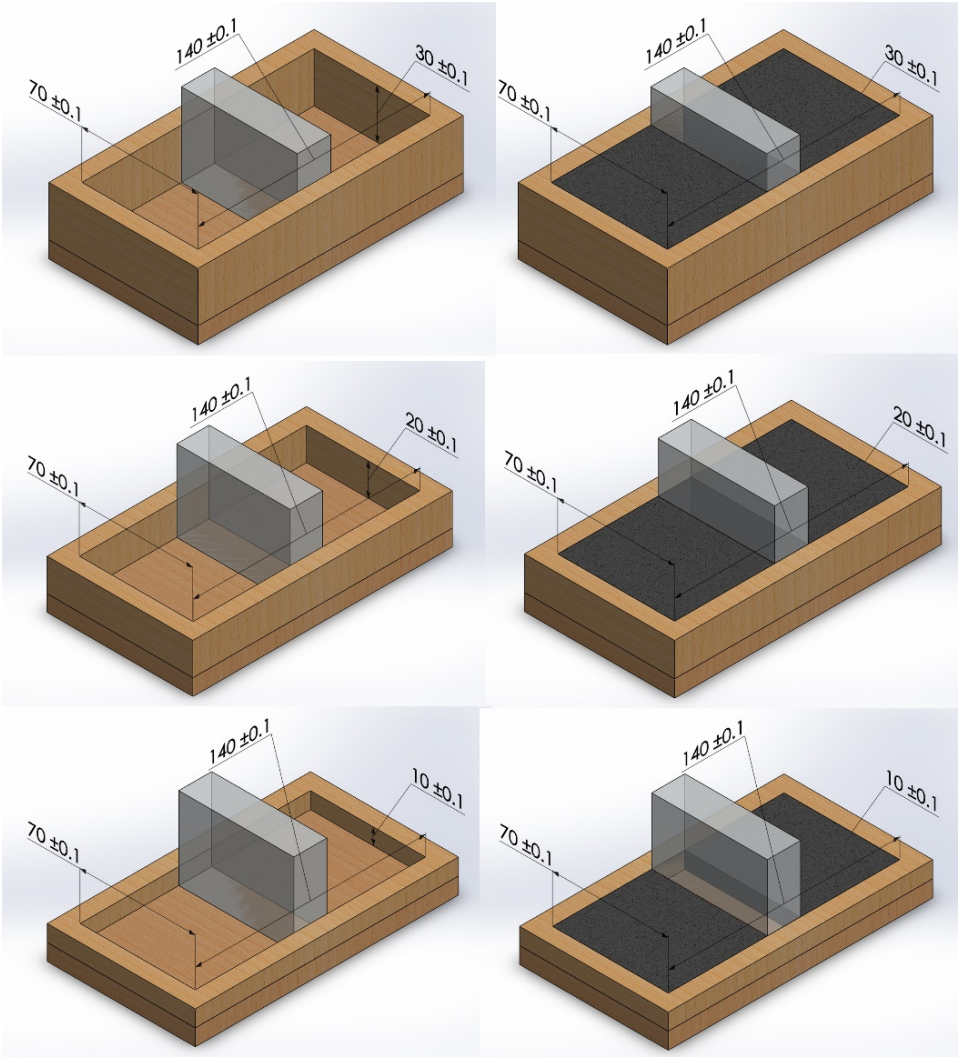

Figure 7.2: Moulds design

7.2.2. Test procedure

After sufficient cure time(28 days), put each specimen on the apparatus to implement test. Carefully alignment upper and lower specimen surface along support and load plates. Load the specimen smoothly using a constant cross-head speed of 1 mm/min(Figure 7.3). Record the maximum load in Newtons. Calculate the static shear strength τ_b,expresssed in mega-pascals, using formula:

$$\tau_b = \frac{F}{A}$$

Where:
F is the maximum load, in Newtons;
A is the bond area, in square millimetres.
Slip and load curve can be recorded within this test.

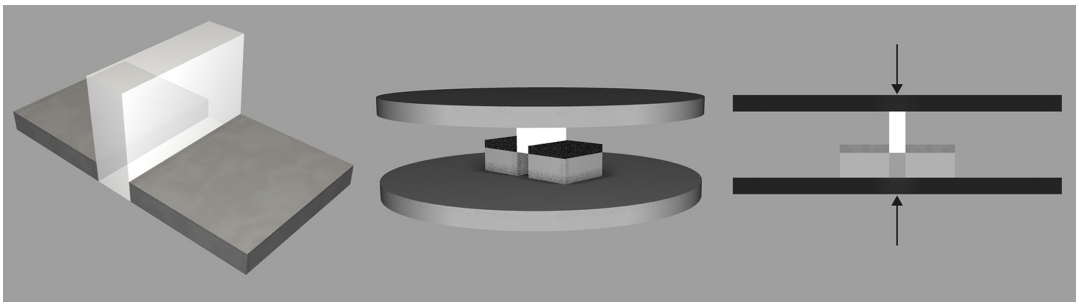

(a) Test procedure

Key
1. upper compression plate
2. glass brick
3. concrete block
4. specimen support
5. lower compression plate

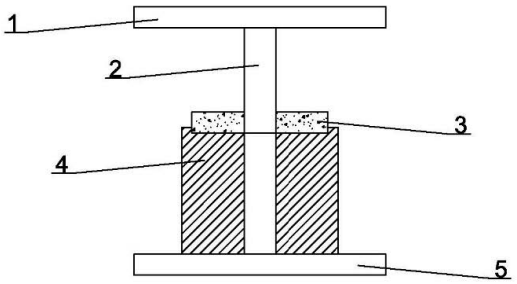

(b) Push out test

Figure 7.3: Push out test procedure

7.3. Experimental process

7.3.1. Material preparation

According to (NEN-EN 450-1):

"The k-value concept is a prescriptive concept. It is based on the comparison of the durability performance (or strength as a proxy-criterion for durability where appropriate) of a reference concrete with cement "A" against a test concrete in which part of cement "A" is replaced by an addition as function of the water/cement ratio and the addition content."

In this case we choose K-value = 0.2, and Water/(cement + k × fly ash) = 0.5. The total usage of material is listed in Table 7.2.

	Fly ash proportion		
	0%	15%	30%
Recipe (g)			
CEM I 52.5R	3150	2677.5	2205
Sand 1-2mm	9450	9450	9450
Water	1575	1386	1197
Fly ash	0	472.5	945

Table 7.2: Total usage of material

7.3.2. Specimens making

Before making the specimens, 27 timber moulds should be prepared. Each glass brick was attached to mould with bottom tape, where the thickness of tape should be smaller enough to prevent concrete from forming a bottom layer under glass brick. Because in this test moulds will be used only once, no de-mould oil was applied to avoid contaminating glass surface. The surface of both glass and timber moulds were cleaned carefully with 2-propanol before mixing the concrete.

(a) Timber mould

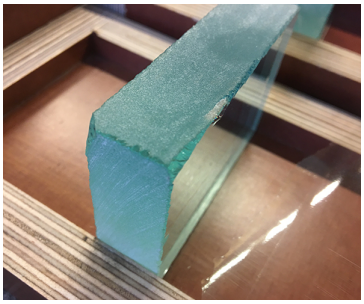

(b) Glass fits into mould

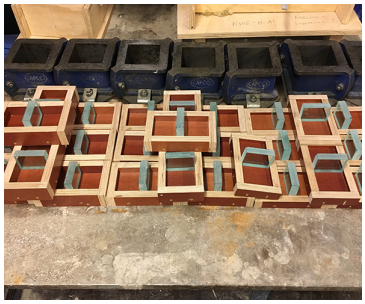

(c) Glass taped onto moulds

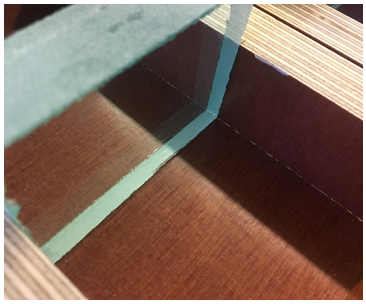

(d) Surface cleaning

(e) Fly ash and cement mix

(f) Water and sand adding

(g) Check workability

(h) Moulds filling

(i) Into moisture chamber

Figure 7.4: Samples making procedure

Firstly we weighed the cement and water by means of the balance. Before adding water into mixer, cement and fly ash were blended to mix them together. After sand was added, water was pouring in slowly while check the workability at the same time. Specimens were moulded immediately after the preparation of concrete, after which the concrete in moulds was compacted with vibrating table. Meanwhile, we scraped the extra concrete above the depth of moulds with steel trowels to ensure the flatness of the bond surface.

After the samples making was finished, they were clearly labelled and photographed. Then all specimens were transported to the curing room in the same day. In this case we chose to remove specimens from the moulds after one week because the reaction between glass and fly ash concrete can be slow.

7.3.3. Shear bond and compression test

After curing of 28 days, compression test was carried out for concrete cubes. The shear bond test was implemented after a curing of 30 days. The test set up and procedure of compression test followed NEN-EN 12390-3. Machine Zwick/Z100 was used to perform the push out test as presented in Figure 7.5. The function of bottom steel supports and top timber rod here in this test was to behaviour rigidly and distribute force uniformly onto the specimens. The load speed of all shear bond tests were set at 1 mm/min.

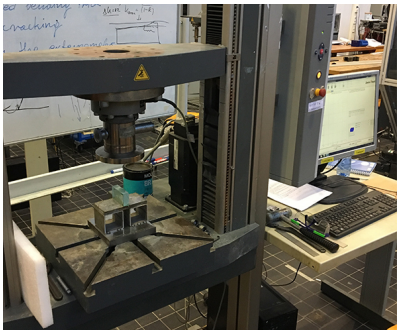

(a) Apparatus for push out test

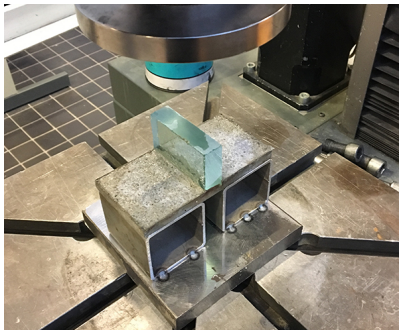

(b) Steel supports for specimens

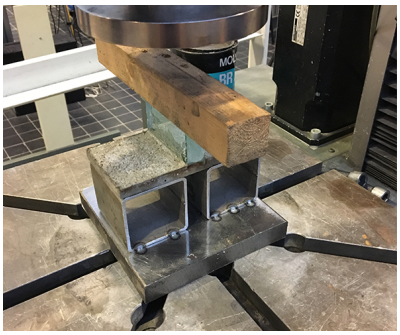

(c) Timber strip to keep rigid

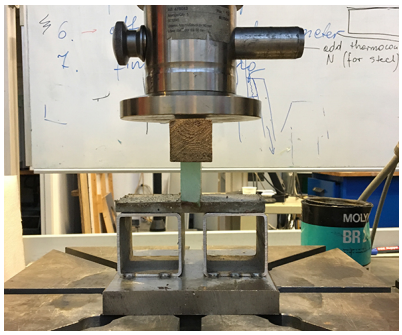

(d) Front view of test

Figure 7.5: Set up for push out test

7.4. Results analysis

7.4.1. Compression test

Results of compression test are described in Table 7.3 and Figure 7.6. It is indicated by the results that by replacing 15% of concrete with fly ash, the compressive strength of concrete was improved by 6.9% compared to normal concrete. The strength of group 30% on the hand reduced by 3.8% compared to control group. While the density for three group stayed almost the same. From the test photos in Figure 7.6 we can tell that failure mode of group 30% is unsatisfactory with two specimens failing under tensile crack.

Test results	Fly ash proportion		
	0%	15%	30%
Mean compressive strength [MPa]	54.03	57.81	51.98
Mean density $[kg/m^3]$	2230	2240	2230

Table 7.3: Results of compression test

(a) Concrete of 0% fly ash (b) Concrete of 30% fly ash (c) Concrete of 30% fly ash

Figure 7.6: Results of compression test

7.4.2. Shear bond test

Shear bond strength results are plotted in Figure 7.7 in terms of fly ash portion and Figure 7.8 in terms of bond length.

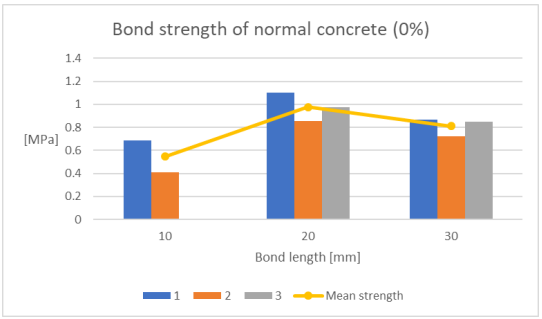

(a) Mean value: 0.808 MPa
Standard deviation: 0.208 MPa

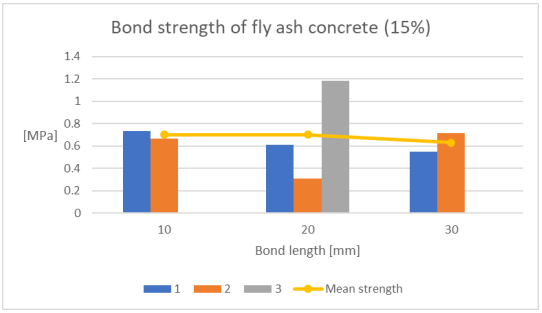

(b) Mean value: 0.682 MPa
Standard deviation: 0.265 MPa

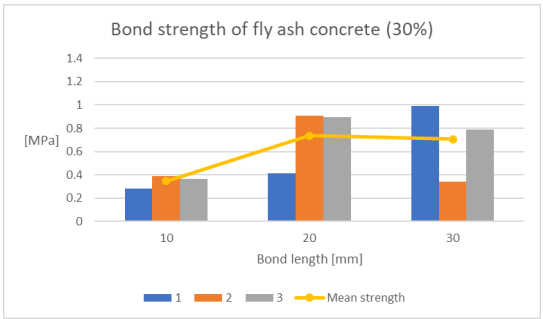

(c) Mean value: 0.596 MPa
Standard deviation: 0.290 MPa

Figure 7.7: Shear bond strength

According to the bar charts, where the yellow scatter line curves represent the mean values, obviously the control group obtain the highest mean shear bond strength. However, the specimen of the highest shear strength occurred in the group 15%. The highest value is 1.19 MPa, which is comparable

to normal silicone shear strength of around 1 MPa in an adhesive system(Wurm, 2007).

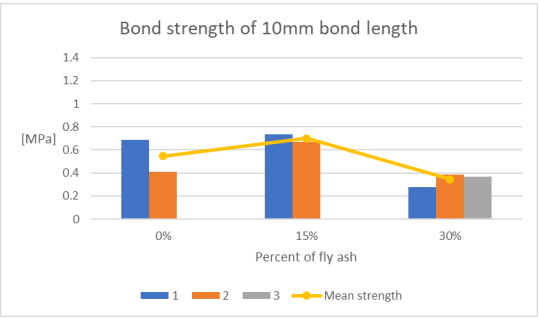

(a) Results of 10mm

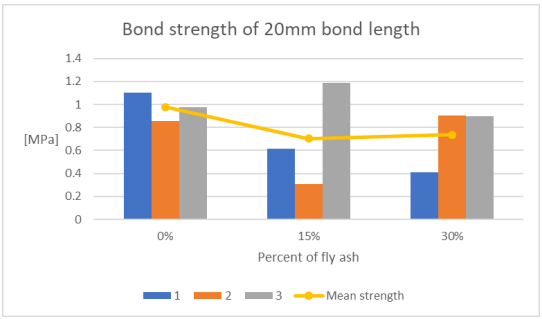

(b) Results of 20mm

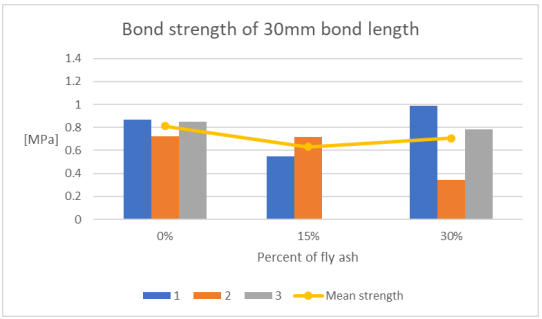

(c) Results of 30mm

Figure 7.8: Shear bond strength

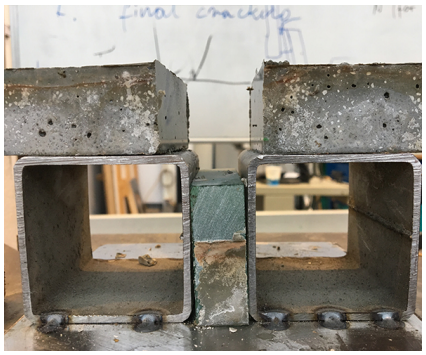

(a) Two-sided failure

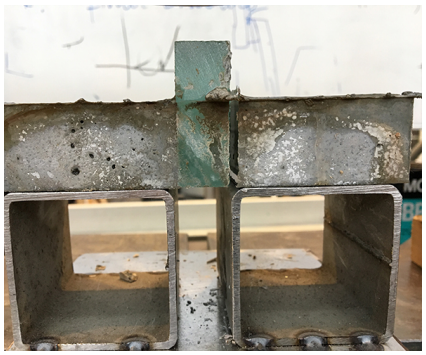

(b) One-sided failure

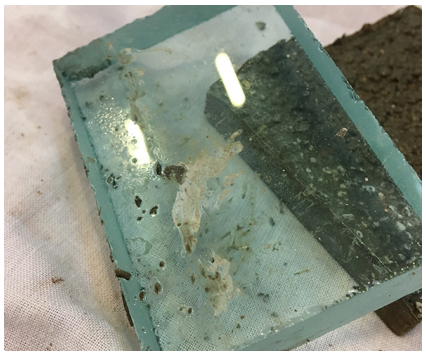

(c) Surface of glass after failure

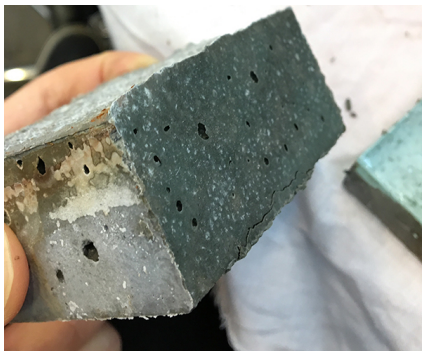

(d) Surface of concrete after failure

Figure 7.9: Set up for push out test

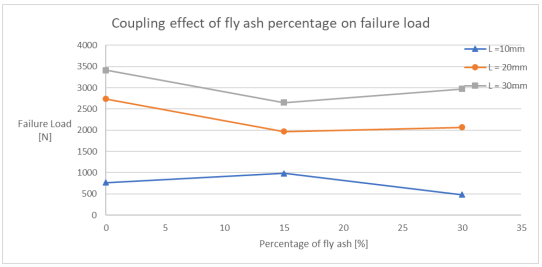

(a) Fly ash percentage

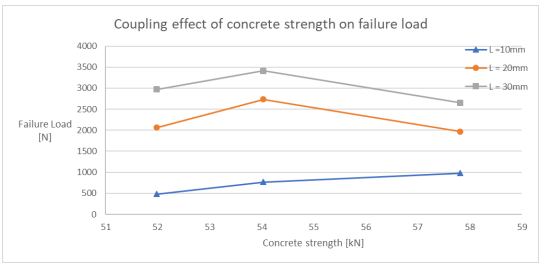

(b) Concrete strength

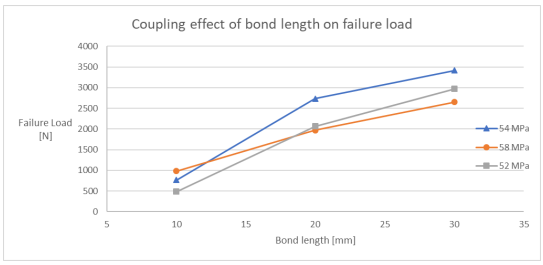

(c) Bond length

Figure 7.10: Coupling effect

The failure modes of this test can be divided into mainly two types: Bi-suface shear and one-sided shear as is described in Figure 7.9. The possible reasons for one-sided shear failure is load eccentricity, deviance of bond length or the discrepancy between micro-structures of bond surfaces.

Through plotting the relations between failure loads and concrete strength (compressive strength), fly ash proportion as well as bond length, we got the charts in Figure 7.7. Charts (a), (b) illustrate that for bond length of 20mm and 30mm, failure loads rises then falls with concrete strength increasing, and with proportion of fly ash increasing it is the other around. This indicates that there can be an optimal composition between the replacement of 0% and 15%.

Chart (c) shows that load increment is declining with the bond length increasing, there is possibly an effective length in this case.

7.5. Conclusions

Although the results from this experiment can not prove the advantages of applying fly ash concrete instead of normal concrete, the sear bond strength of concrete and glass is comparable to normal silicone material, and the highest value occurs in 15% group. According to Wong et al. (1999b), longer curing time of fly ash concrete such as 90 days will also have positive impact on the shear bond strength. Some other evidences also indicate that groups of smaller fly ash percentage intervals may reach an optimal results. More samples and research are needed to obtain a better quality control and reliable value.

8

Finite Element Analysis

Finite element software Ansys Workbench (Ansys WB) is used in this design. Both global and detailed model are built to study the behaviour of the glass-concrete arch. In the first part of this chapter, the simplified global model will be used to investigate the global behaviour, compare with analysis from Chapter 5,and optimize for the detailed model. In the second part, detailed model will be made to verify the adequacy of experiment results. Some possible improvements are proposed in the end.

8.1. Approach

As mentioned in section 3.3.4, Solidworks is used to help import CAD parameters into Ansys. Global variable (Figure 8.1) are established inside Solidworks. These variables are parameters depicted by section drawing in Figure 8.3. Besides, span and height of arch is also parametrized into CAD parameters. The whole global model in Solidworks is shown in Figure 8.2

Global Variables	
"DS_half_span_of_arch"	= 15
"DS_height_of_arch"	= 9
"DS_Upper_part_concrete_height"	= 0.125
"DS_Lower_part_concrete_height"	= 0.125
"DS_Prestressing_steel_horizontal_distance'	= 0.075
"DS_Prestressing_steel_vertical_distance"	= 0.0625
"DS_Upper_part_concrete_half_width"	= 0.15
"DS_Lower_part_concrete_half_width"	= 0.15
"DS_one_fourth_length_glass_panel"	= 0.45
"DS_Height_of_half_glass_panel"	= 0.3

Figure 8.1: Global variables in Solidworks

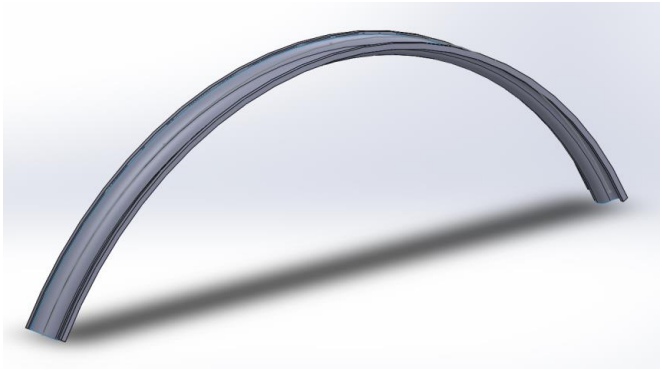

Figure 8.2: Global model in Solidworks

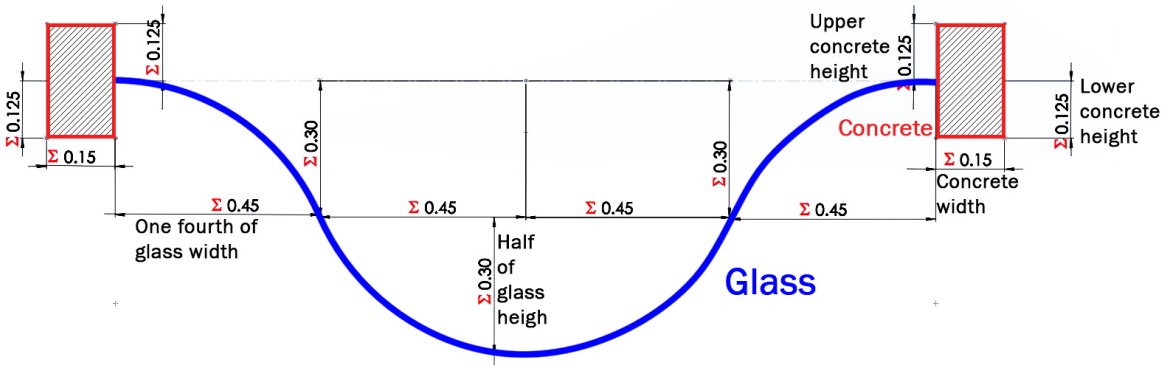

Figure 8.3: Parameters in section

After the model is built in Soliworks, it will be transferred into the geometry module in Ansys WB. Some selections and operations will be done inside DesignModeler (DM) in Ansys WB, which can be used in the static structural analysis system (Figure 8.4 (a)). Parameter set (Figure 8.4 (b)) is utilized here to change inputs of geometry and gather the update outputs from static structural as is shown in the work flow in Figure 8.4 (a).

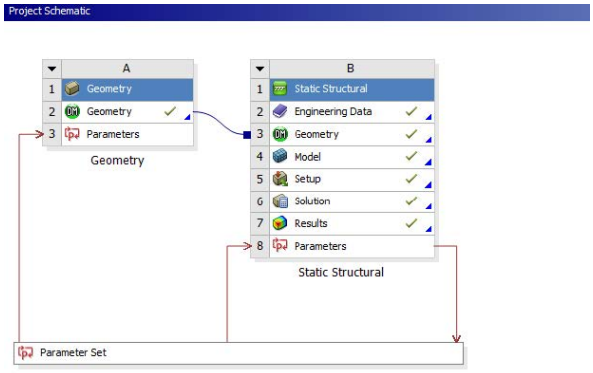

(a) Parameter set work-flow

Outline of All Parameters

	A	B	C	D
1	ID	Parameter Name	Value	Unit
2	Input Parameters			
3	Geometry (A1)			
4	P1	P3@DS_half_span_of_arch	15	
5	P2	P3@DS_height_of_arch	6	
6	P3	P3@DS_Upper_part_concrete_height	0.125	
7	P4	P3@DS_Lower_part_concrete_height	0.125	
8	P5	P3@DS_Upper_part_concrete_half_width	0.15	
9	P6	P3@DS_Lower_part_concrete_half_width	0.15	
10	P7	P3@DS_one_fourth_length_glass_panel	0.45	
11	P8	P3@DS_Height_of_half_glass_panel	0.3	
12	Static Structural (B1)			
13	P9	Glass_panel_surface Thickness	16	mm
*	New input parameter	New name	New expression	
15	Output Parameters			
16	Static Structural (B1)			
17	P10	Total Deformation Maximum	6.6414	mm
18	P11	Maximum Principal Stress Maximum	4.6561	MPa
19	P12	Normal Stress Maximum	4.6562	MPa
20	P13	Total Deformation 2 Maximum	6.4581	mm
21	P14	Total Deformation 3 Maximum	6.4581	mm
22	P15	Normal Stress 2 Maximum	1.2584	MPa
23	P16	Normal Stress 3 Maximum	1.259	MPa

(b) Input and output in parameter set

Figure 8.4: CAD parameters in Ansys WB

8.2. Numerical modelling

For the comparison and arch study, both pure glass arch model and composite arch were built in solidworks and transferred into Ansys WB. In this case we compare the global deformation and maximum principal stress between composite arch and pure glass arch. The parametric arch study will be processed in the model of pure glass arch for its clean and simple arch parameters. While the parametric study of components will take place in composite arch model.

8.2.1. Pure glass arch model

8.2.1.1. Elements

Element shell181 is used for this pure glass 3D modelling. Since it is suitable for moderately-thick shell structures, where we set the thickness of glass at 2 ×8 millimetres. It is a four-node element with six degrees of freedom at each node: translations in the x, y, and z directions, and rotations about the x,

y, and z-axes. According to Nelson and Wang, shell181 is based on the REISSNER-MINDLIN theory and take into account the shear stress distribution over the thickness, which is more accurate for this simulation.

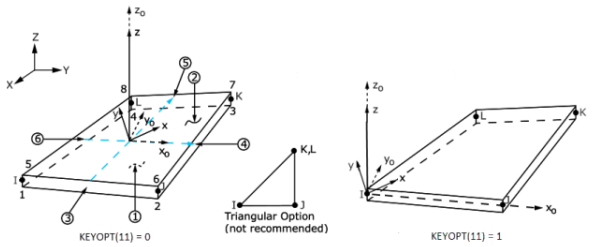

Figure 8.5: SHELL181 Geometry

8.2.2. Engineering data

Glass properties in Table 2.1 will be defined for engineering data here in Figure 8.6

	A	B	C
1	Property	Value	Unit
2	Material Field Variables	Table	
3	Density	2500	kg m^-3
4	Isotropic Elasticity		
5	Derive from	Young's Modulus and Poisson...	
6	Young's Modulus	7E+10	Pa
7	Poisson's Ratio	0.22	
8	Bulk Modulus	4.1667E+10	Pa
9	Shear Modulus	2.8689E+10	Pa

Figure 8.6: Engineering data for glass

8.2.2.1. Boundary conditions and load applying

The glass panel arch edges are modelled as symmetry regions to simulate the behaviour of two connecting arches (Figure 8.7). A symmetric structural boundary condition means that out-of-plane displacements and in-plane rotations are set to zero, which in this case means that the displacement in the x direction and the rotation around y and z is restrained.

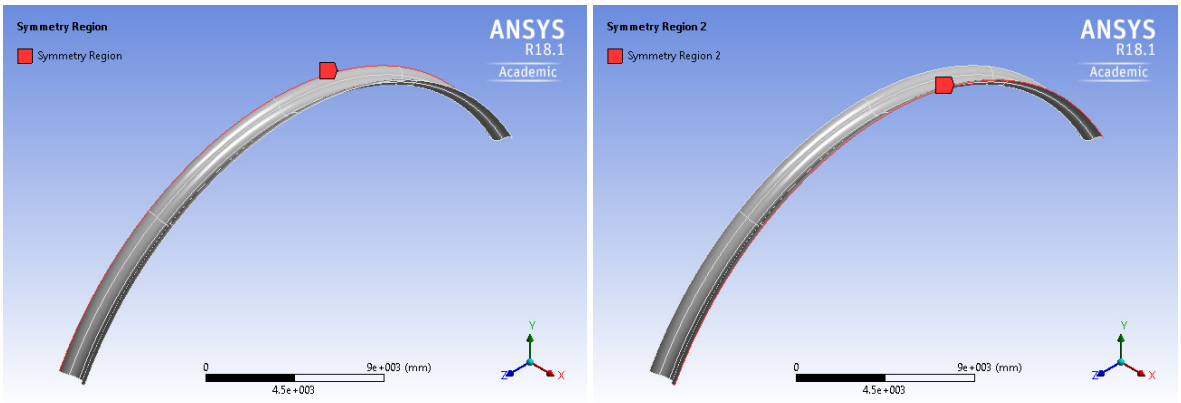

Figure 8.7: Symmetry regions

Supports and load conditions are depicted in Figure 8.8. Remote supports at two ends of arch are adopted in this model, where the support points will at the centroid of edges of arch edges. XYZ components will be set at zero with free rotations for hinged supports, while rotation will also be limited for rigid supports. Acceleration is applied to simulate gravity by accelerating a structure in the direction opposite of gravity whose value is multiplied with γ_G already. Snow load and wind load are applied on

the shell as pressure load of the value multiplying with $\gamma_{Q;i}$. The direction of snow load is in -Y while the direction of wind is normal to the surface onto surface effect elements.

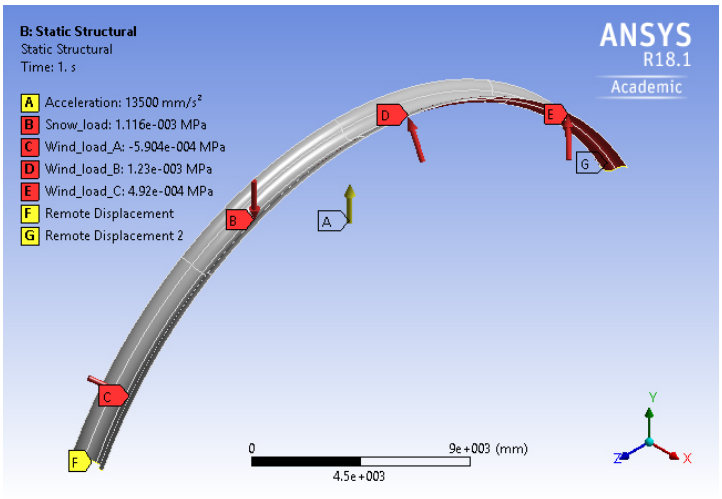

Figure 8.8: Supports and loads

8.2.3. Composite component model

8.2.3.1. Elements and contact

Shell181 is still used for glass panels here while solid186 is assigned to concrete parts here. Solid186 is a quadratic 3D element with 20 nodes. Each node has three degrees of freedom: translations in the nodal x, y, and z directions.

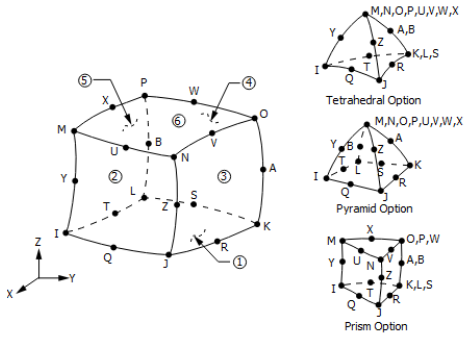

Figure 8.9: SOLID186 Homogeneous Structural Solid Geometry

Conta175 is used for the modelling of contact between shell181 edges and solid186 faces. Here it works as a node-to-surface contact element.It supports large sliding, large deformation, and different meshes between the contacting components.

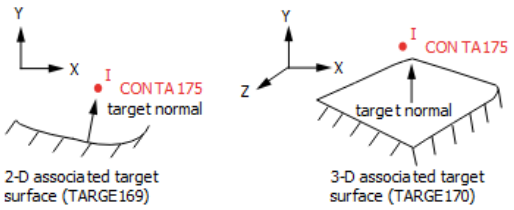

Figure 8.10: CONTA175 Geometry

8.2.4. Engineering data

Concrete properties in Table 2.1 will be defined for engineering data here in Figure 8.11. Glass will be defined same as in section 8.2.2.

	A	B	C
1	Property	Value	Unit
2	Material Field Variables	Table	
3	Density	2500	kg m^-3
4	Isotropic Secant Coefficient of Thermal Expansion		
6	Isotropic Elasticity		
7	Derive from	Young's Modulus and Poisson...	
8	Young's Modulus	2.7E+10	Pa
9	Poisson's Ratio	0.18	
10	Bulk Modulus	1.4063E+10	Pa
11	Shear Modulus	1.1441E+10	Pa
12	Tensile Yield Strength	0	Pa
13	Compressive Yield Strength	0	Pa
14	Tensile Ultimate Strength	5E+06	Pa
15	Compressive Ultimate Strength	4.1E+07	Pa

Figure 8.11: Engineering data for concrete

8.2.4.1. Boundary conditions and load applying

Similar to section 8.2.2.1, the symmetry regions here will be the two outermost surfaces of concrete parts on two sides.

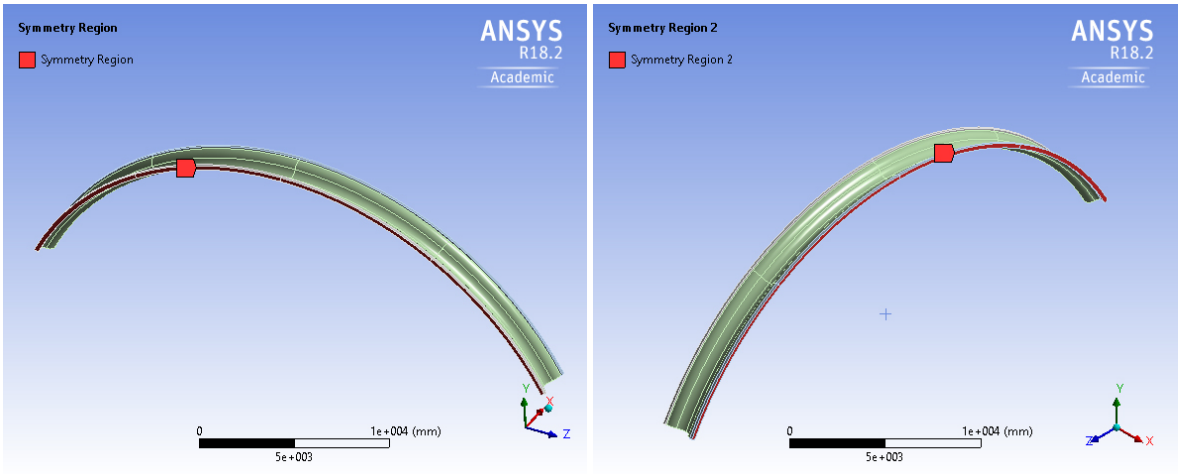

Figure 8.12: Symmetry regions

Load and supports conditions will be applied similarly to section 8.2.2.1 likewise. The difference here is that for wind load zone ABC, we used concrete uppermost faces to apply load, where the normal directions of faces are opposite to the glass panel normal directions. It should be noticed that here load case 2 and load case 4 will be simulated separately, Figure 8.8 and 8.13 are used to show all loading for combinations.

8.2.4.2. Contact regions

Multi-point constraint (MPC) formulation for contact regions will be used in this model. Its formulation of transferring action can be described as constrain equation between ROTZ at node 2 and UY at nodes 1 and 3 of Figure 8:

$0 = UY_3 - UY_1 - 10 \times ROTZ_2$

By internally adding this such equation to ”tie” the displacements between contacting surfaces, it is a sufficient way to bond surfaces of contact regions. In this case, the contact edge is on glass edges and target surfaces are concrete surfaces. They are bonded using MPC and constrained in all directions along the whole arch (Figure 8.15).

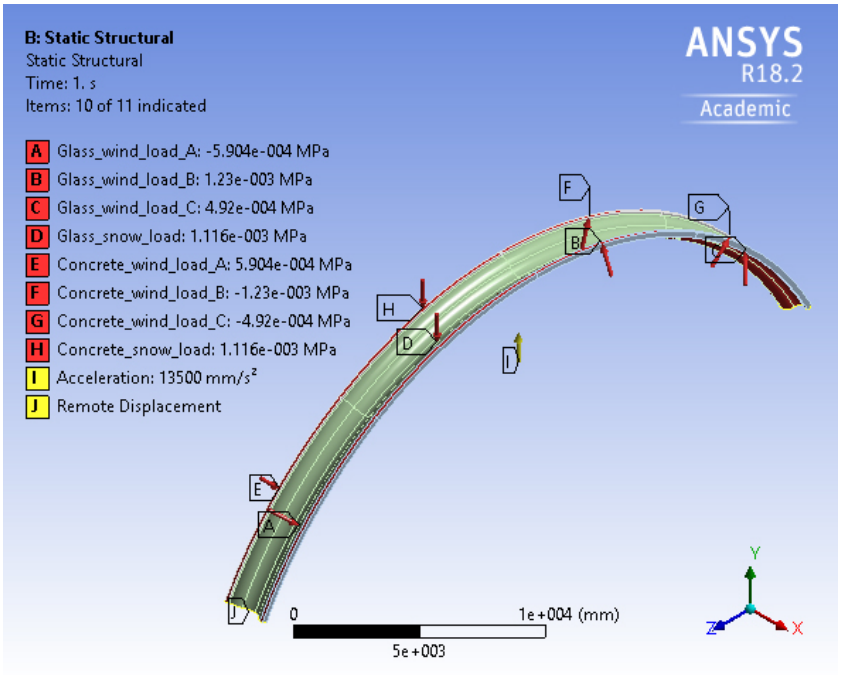

Figure 8.13: Supports and loads

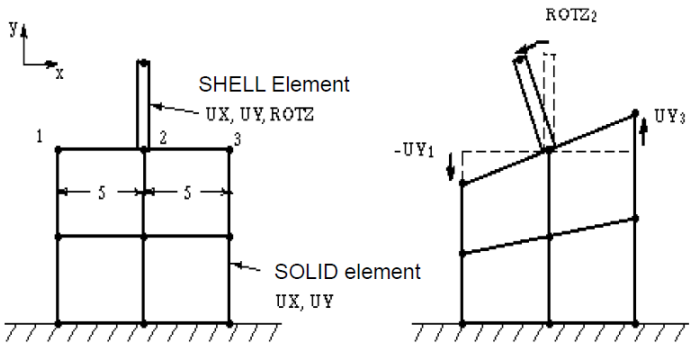

Figure 8.14: MPC formulation

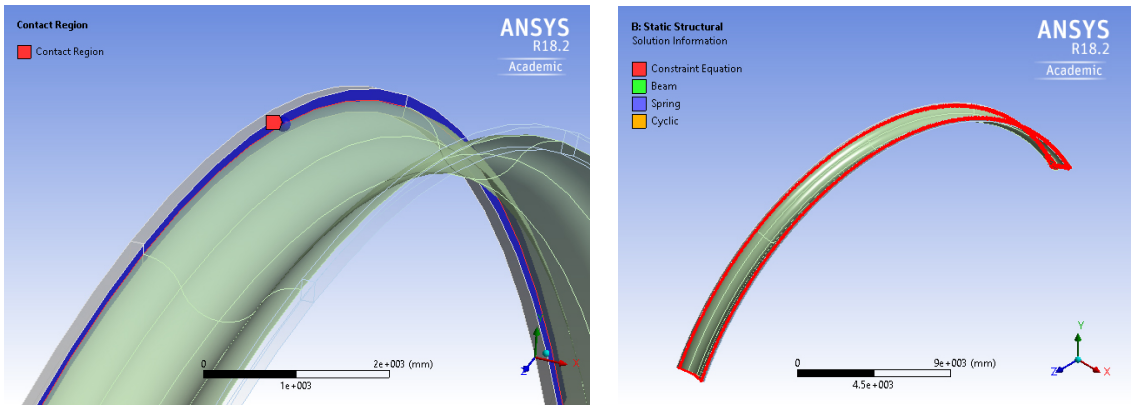

(a) Contact region between shell edges and solid faces (b) MPC formulation

Figure 8.15: Bond contact between concrete and glass

8.3. Comparisons of global models

8.3.1. Comparison between GSA and Ansys

By setting the height of arch at 9 metres and the dimensions of pure glass section same as the one in Figure 8.3. The results of two-hinged and fixed arches under load case 4 are demonstrated in

Figure 8.16 and compared to the results from GSA solution. By comparing these two FEM results, we can see the similarities. Under load case4, the largest bending moment occurs at around L/4 of arch for two-hinged arch and at supports for fixed arch. The largest tensile stress locates in the outer fibre for two-hinged arch and inner fibre for fixed arch.

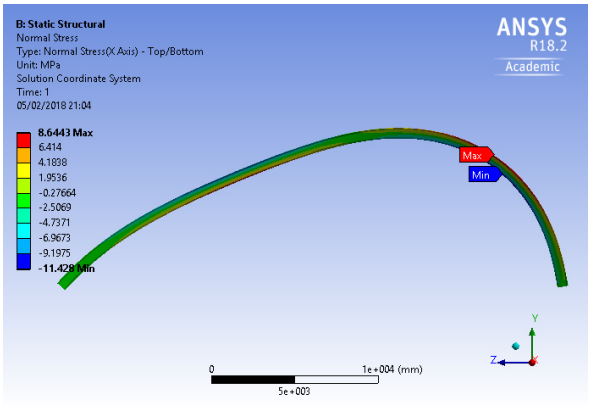

(a) Normal stress of two-hinged arch in Ansys

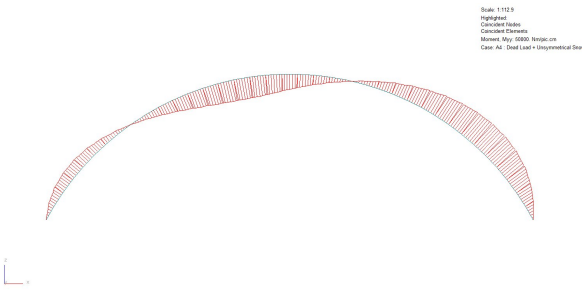

(b) Bending moment of two-hinged arch in GSA

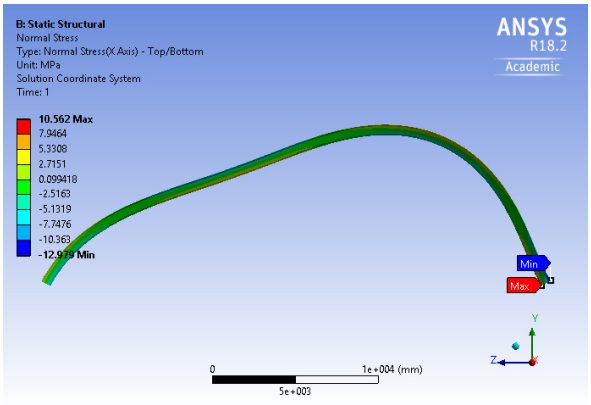

(c) Normal stress of fixed arch in Ansys

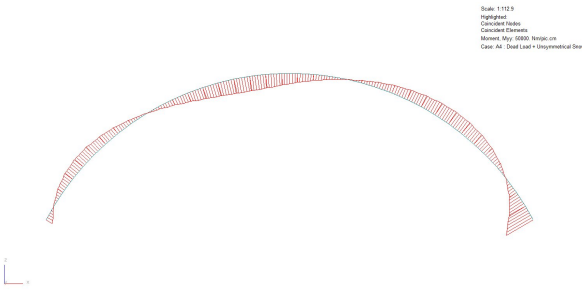

(d) Bending moment of fixed arch in GSA

Figure 8.16: Results comparing of load case 4

8.3.2. Comparison between pure glass and concrete arches

Again set the height of arch at 9 metres, and the section dimensions of pure glass component or composite component same as Figure 8.3. To verify the structural advantage in Ansys WB, simulations of composite arch and pure glass arch with both two-hinged supports and fixed supports under load case 4 are implemented. The comparisons are displayed in Figure 8.17 and Figure 8.18.

From Figure 8.17 we can see that for two-hinged arches under load case 4, the total deformation of glass in composite arch is 10.574 mm. This is much smaller than the one in pure glass arch where the result 17.024 mm has exceeded the thickness of glass panels. At the location of critical moment M_{arch}, the outer fibre in concrete is in tensile through glass and concrete working together. Therefore the maximum principal stress of glass in composite arch is located at where second largest bending moment occurs, which is smaller than that in pure glass arch.

Similar results apply to the ones from fixed arch under load case 4. Although the deformation within fixed arch is smaller than the one in two-hinged, the maximum principal stress of both glass and concrete at the supports is larger compared to two-hinged one, which is crucial for concrete. Attention needs to be paid for this aspect.

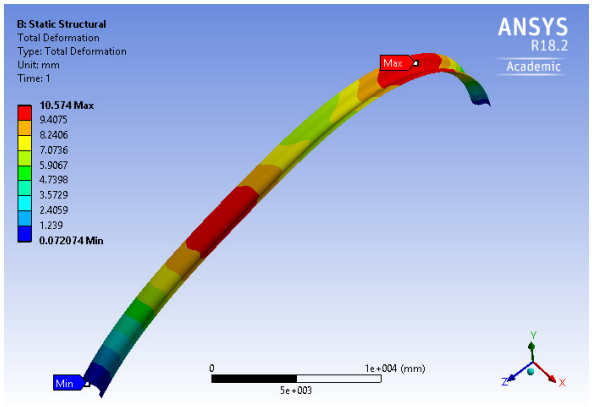

(a) Total deformation of glass in composite arch

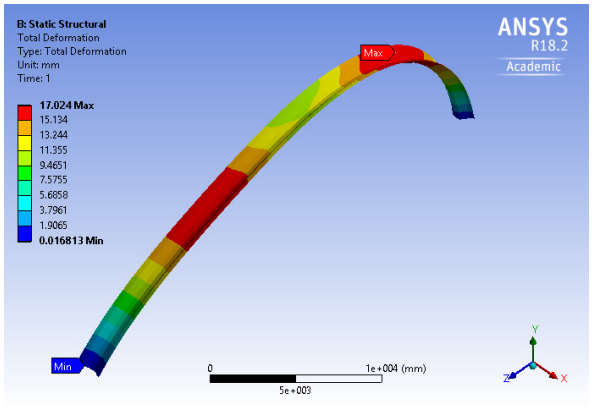

(b) Total deformation of glass in pure glass arch

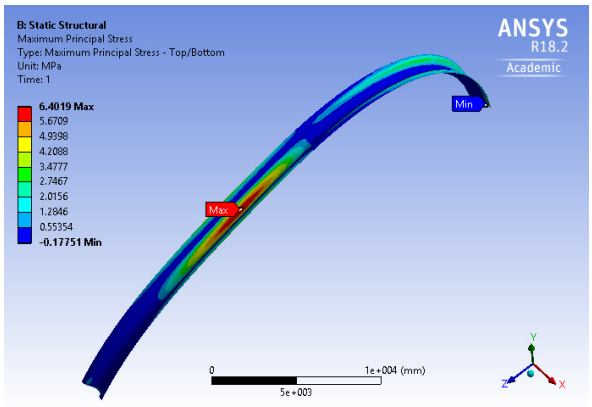

(c) Maximum principal stress of glass in composite arch

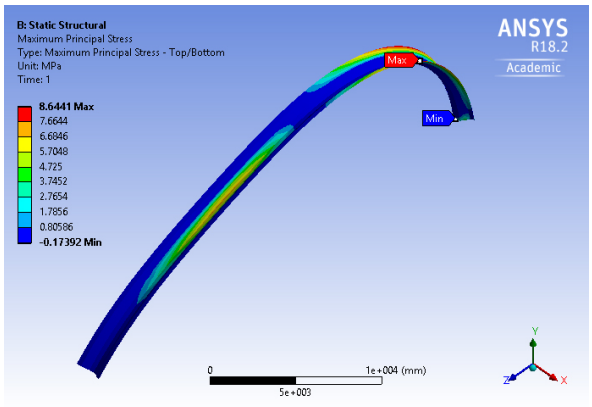

(d) Maximum principal stress of glass in pure glass arch

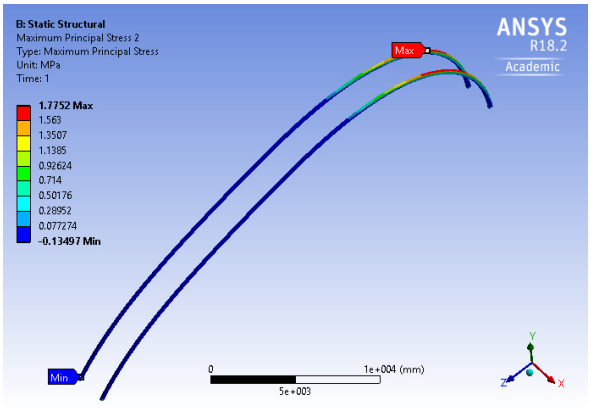

(e) Maximum principal stress of concrete in composite arch

Figure 8.17: Results comparing of two-hinged arches under load case 4

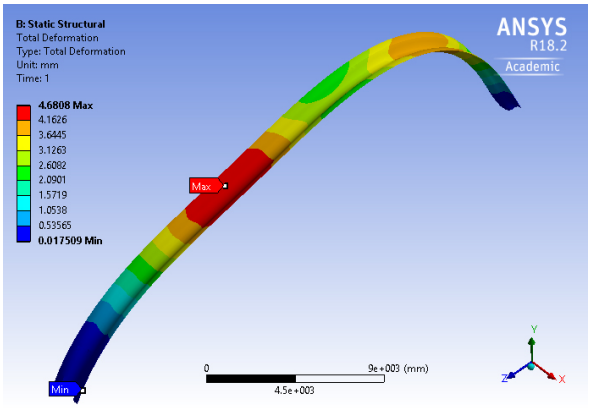

(a) Total deformation of glass in composite arch

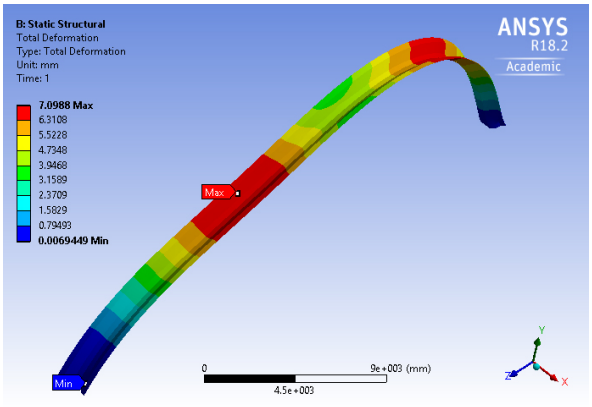

(b) Total deformation of glass in pure glass arch

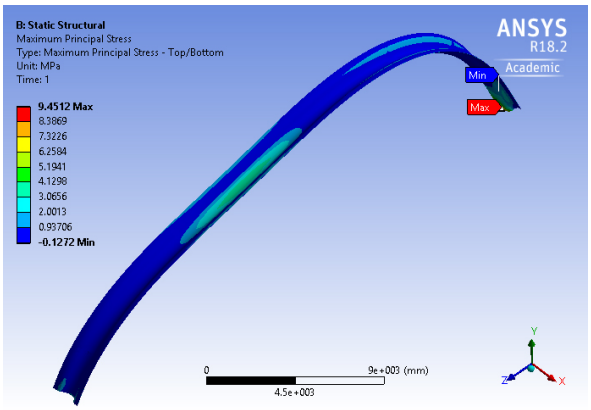

(c) Maximum principal stress of glass in composite arch

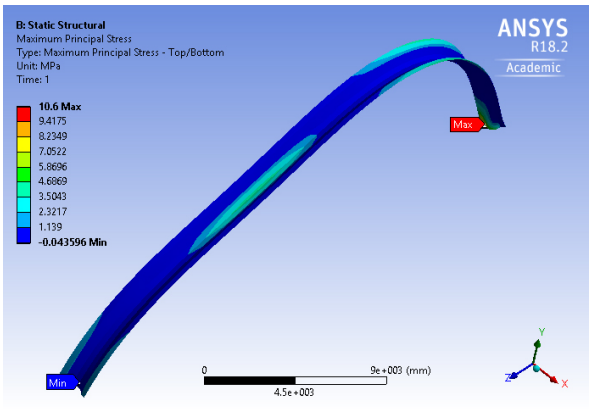

(d) Maximum principal stress of glass in pure glass arch

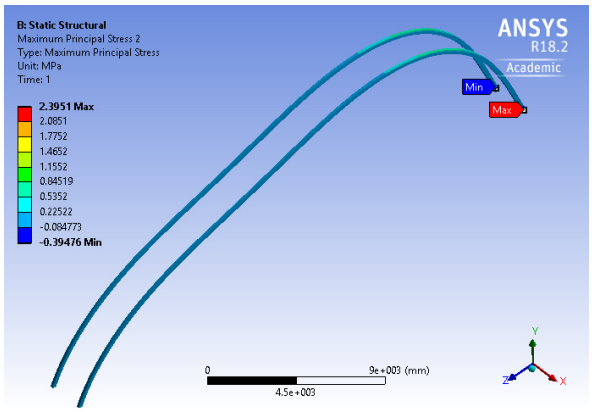

(e) Maximum principal stress of concrete in composite arch

Figure 8.18: Results comparing of fixed arches under load case 4

8.4. Parametric study

8.4.1. Height/span ratio

By changing the parameter height of arch in Figure 8.4 from 1 to 15 metres, we will get the results of defined outputs from Ansys WB mechanical. Here the input for Ansys WB calculation is listed in Appendix C section C.1, where the load is listed in column of $Zone\ A\ [MPa]$. The results were obtained in the model of pure glass arch and plotted in Figure 8.19. We can see there are some deviances between it and Figure 5.11, but the tendency of curves are similar. The total deformation of glass at 6 metres is smaller than half of glass thickness which is satisfactory for linear analysis. The rest of the result plots are in Appendix C section C.8.

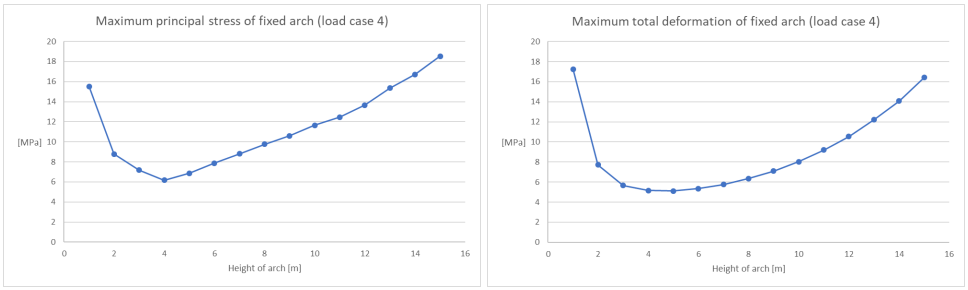

(a) Maximum principal stress (b) Maximum total deformation

Figure 8.19: Results of fixed arches with different heights under load case 4

8.4.2. Component dimension

To prepare for the detailed model in Ansys WB we set the height of arch at 6 metres and change the parameters in Figure 8.4 which means the changes of dimensions in cross section of Figure 8.3. Figure 8.20 indicates that load case 4 is dominant for composite arch of 6 metre high, because the maximum principal stress in glass is higher overall. The fluctuation of these curves is possibly due to the complicated intertwining of many parameters. For example the altering of width changes dead load, loading area and neutral axis at the same time. In this case, we choose to change the height of upper concrete to 300mm while the rest parameters stay the same but open to any possible changes.

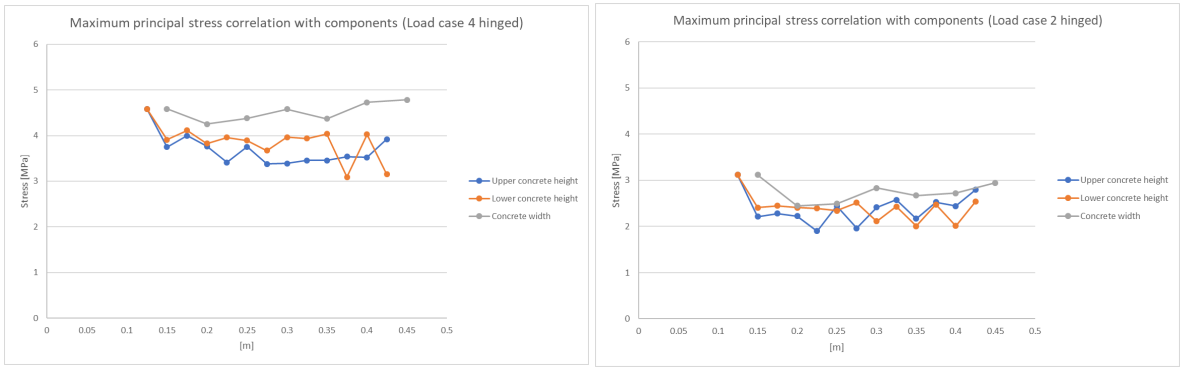

(a) Load case 4 (b) Load case 2

Figure 8.20: Glass maximum principal stress correlate with dimensions of concrete

According to section 2.3.2 the wave height of corrugated glass is limited inside 1000 millimetres, in this study we simulated the range of wave-height from 100 to 450 mm and plotted the results in Figure 8.21. It can be seen from these diagram that the load case 4 is dominating for most situations. As the width and height of glass panel rise, the stress inside glass increases generally for load case 2. But the distribution is more complicated and random for load case 4. For following design we choose the lowest stress parameters of two-hinged arch under load case 4: half height = 400 mm, 1/4 width = 450mm to do detailed modelling. But keep these parameters open to any possible changes.

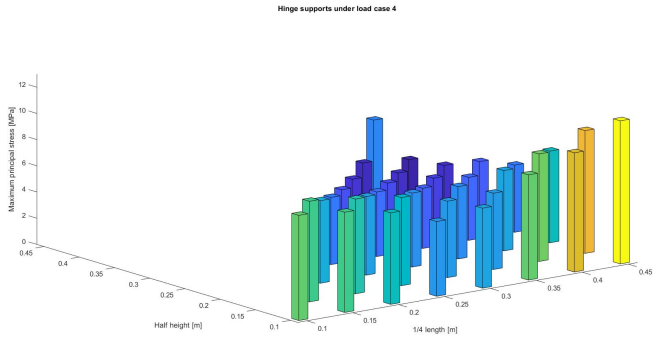

(a) Load case 4 of two-hinged

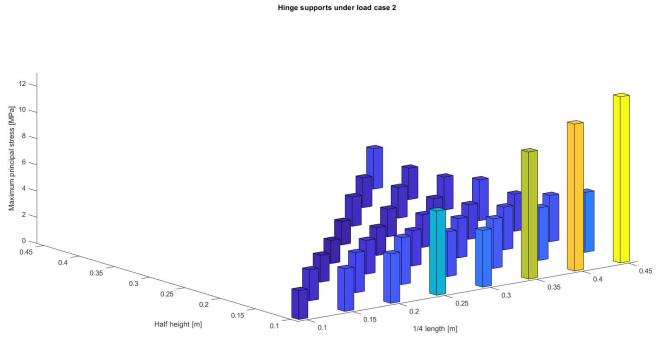

(b) Load case 2 of two-hinged

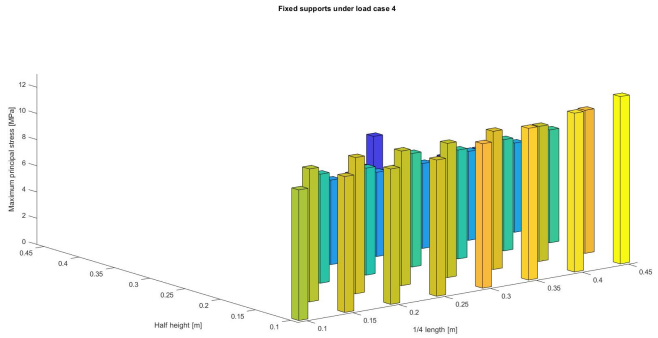

(c) Load case 4 of fixed

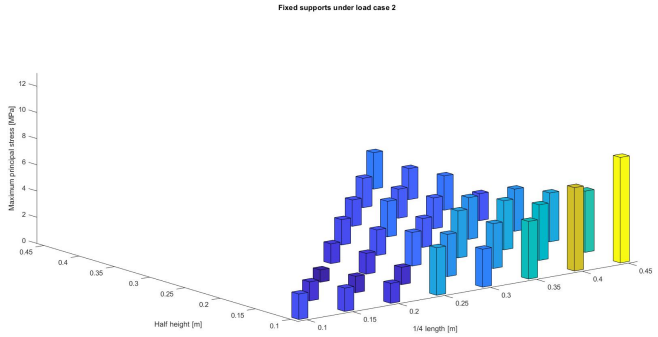

(d) Load case 2 of fixed

Figure 8.21: Glass maximum principal stress correlate with dimensions of glass

8.5. Detailed global model

8.5.1. Approach

For the student version of Ansys WB there is a limit of 32K nodes/elements for structural physics, so the mesh of large-scale model cannot be very dense. Therefore the detailed sub-modelling is needed in this design. Firstly the global model will be calculated with a coarse mesh, then the local sub-model will be calculated with a finer mesh. The process is shown in Figure 8.22

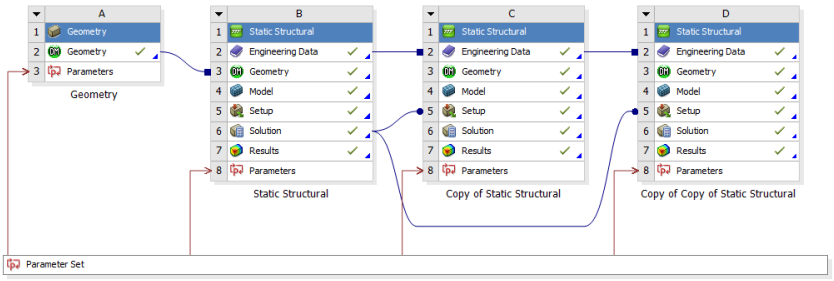

Figure 8.22: Sub-modelling work-flow

8.5.1.1. Parameters defining

Similar to section 8.1, parameters are defined in Solidworks and transferred into Ansys Workbench (Ansys WB) (Figure 8.23 (a)). Some new detailed parameters are added this time. The bond length between glass and concrete (Figure8.24), diaphragm upper and lower thickness, length of glass panel and concrete cover (Figure 8.25) are defined in Solidworks part. This part will be assembled into an arch (Figure 8.23 (b)).

Outline of All Parameters

	A	B	C	D
1	ID	Parameter Name	Value	Unit
2	Input Parameters			
3	Geometry (A1)			
4	P1	A1@DS_length_of_glass	900	
5	P2	A1@DS_length_of_side_concrete	1500	
6	P3	A1@DS_connection_bond_length	100	
7	P4	A1@DS_length_of_one_fourth_glass	450	
8	P5	A1@DS_height_of_half_glass	400	
9	P6	A1@DS_height_of_upper_concrete	300	
10	P7	A1@DS_height_of_lower_concrete	125	
11	P8	A1@DS_width_of_upper_concrete	150	
12	P9	A1@DS_width_of_lower_concrete	150	
13	P10	A1@DS_thickness_of_one_glass	8	
14	P11	A1@DS_upper_rebate_thickness	40	
15	P12	A1@DS_lower_rebate_thickness	80	
16	P13	A1@DS_length_of_cut_concrete_body	700	
17	Copy of Static Structural (C1)			
18	P14	A1@DS_length_of_glass	900	
19	P15	A1@DS_length_of_side_concrete	1500	
20	P16	A1@DS_connection_bond_length	100	
21	P17	A1@DS_length_of_one_fourth_glass	450	
22	P18	A1@DS_height_of_half_glass	400	
23	P19	A1@DS_height_of_upper_concrete	300	

(a) Imported CAD parameters

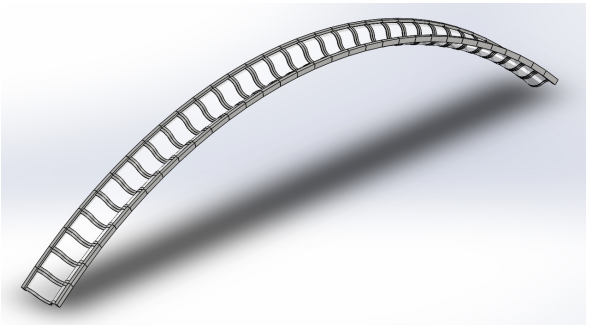

(b) Detailed arch model

Figure 8.23: Parameters and whole arch

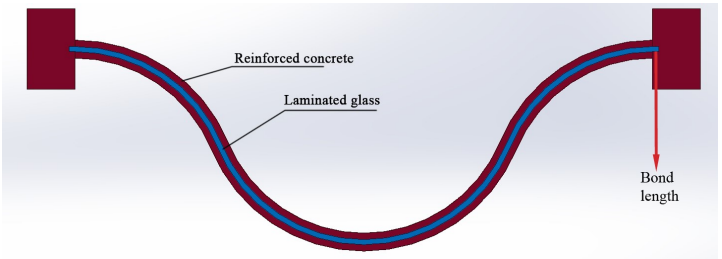

Figure 8.24: Bond length

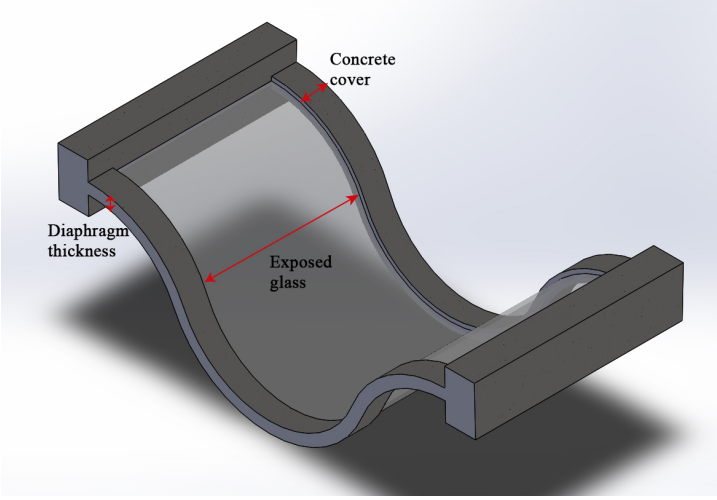

Figure 8.25: Part for assembling

8.5.2. Numerical modelling

8.5.2.1. Elements

Solid186 in Figure 8.9 will be used to model glass and both Solid186 and Solid187 (Figure 8.26) will be used to model concrete parts. Solid187 is a 3D 10-node-element with three degrees of freedom at each node: translations in the nodal x, y, and z directions. 3D 8-Node surface-to-surface contact element Conta174 is used for the contact regions between solid glass and solid concrete elements, In this case, the contact bodies are glass panels and target bodies are concrete parts. They are bonded using MPC and constrained in all directions along the arch(Figure 8.27).

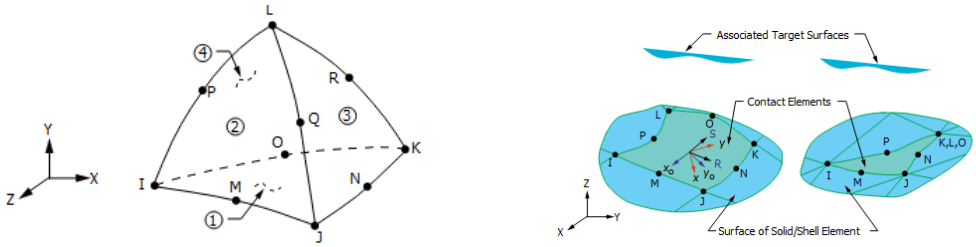

(a) SOLID187 Geometry

(b) CONTA174 Geometry

Figure 8.26: Elements choice

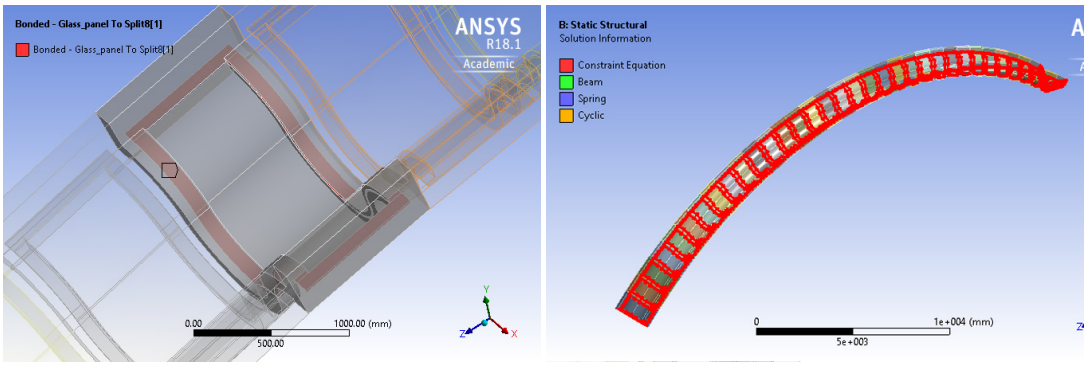

(a) surface to surface contact regions

(b) MPC formulation along whole arch

Figure 8.27: Contact regions

8.5.3. Global modelling

The supports,symmetry boundaries conditions and loading cases are defined similarly to as mentioned in previous sections. In this case two-hinged arch under load case 4 is checked. By plotting the shear stresses τ_{xy}, τ_{yz} and τ_{xz} of XY, YZ, XZ planes in local solution coordinates. We can check the shear stress distribution in glass and concrete bodies. By some slowly increasing the value of new defined parameters, we find that bond length of 100 mm, thickness of diaphragm of 120mm and concrete cover length of 100mm is getting closer to adequate results, so we try to refine mesh by division of 10, 20, and 30 of glass panel edges before moving into sub-modelling.

From Figure 8.28 we can infer that structural singularity or FEM errors occurs because the stress is developing with the mesh refining, and the stress concentrations and localizations are quite random and dispersive. Besides, maximum and minimum of stress locations are shifting around the model in unaveraged results. The reason for this singularity is possibly the sharp edges and the contact formulation in this model. After changing contact elements into node-to-surface contact or contact restrains into projected displacement only, the singularity problem will still exist. Under this circumstance, we decided to move on to detailed sub-modelling study.

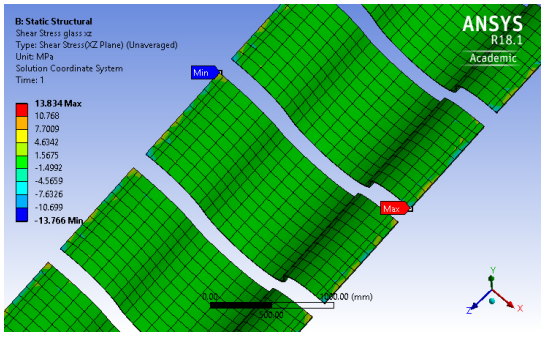

(a) Division of 10

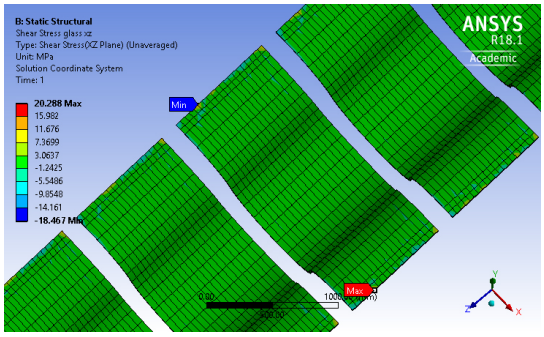

(b) Division of 20

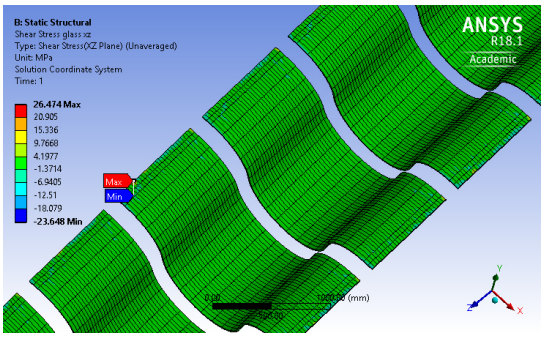

(c) Division of 30

Figure 8.28: Mesh refinement

8.5.4. Sub-modelling

The largest shear stresses of glass and concrete in global modelling tend to appear around the location of the largest deformation,(Figure 8.29 (a)) where the element is selected out to be sub-modelled.

The cut boundary conditions are applied on the cutting out surface of geometry (Figure 8.29 (c)) to replace the original load condition of this sub-model in global model. It should be noticed that with this method the results close to cut boundary can be inaccurate. In this case we will study the middle component in Figure 8.29 (c). The local coordinates set for each element are shown in Figure 8.29 (d), where positive y direction will follow along the curve of glass panels as is shown of the green arrows, positive z direction is shown as blue arrows normal to glass panel surfaces, and the red arrows depict the positive x direction. Figure 8.30 gives the unaveraged results of τ_{xy}, τ_{yz} and τ_{xz}, where the scoped surfaces have been selected and plotted.

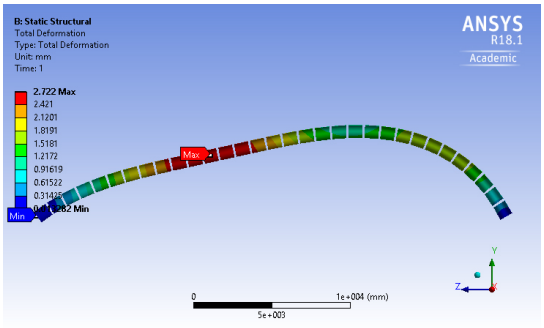

(a) Total deformation of glass

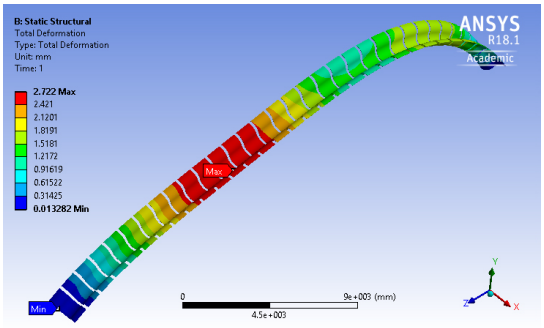

(b) Perspective view of total deformation of glass

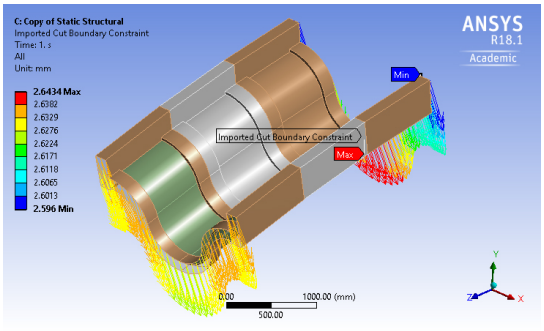

(c) Imported cut boundary conditions

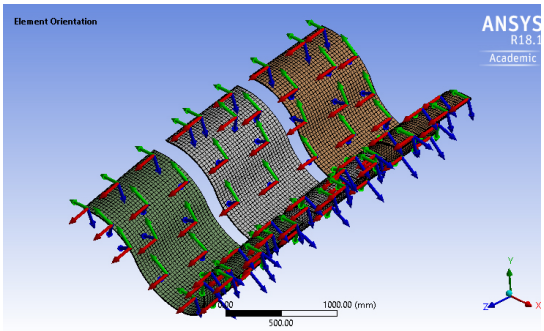

(d) Local coordinates of elements

Figure 8.29: Sub-modelling elements

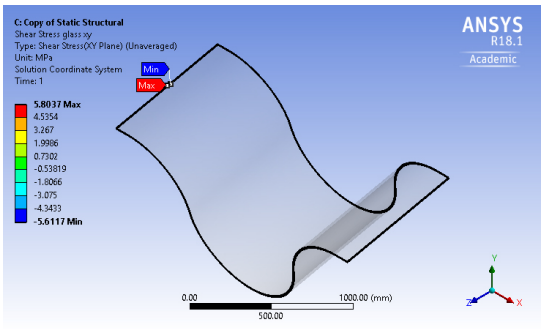

(a) Division of 10

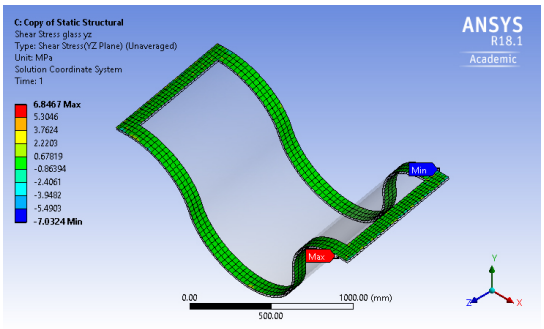

(b) Division of 20

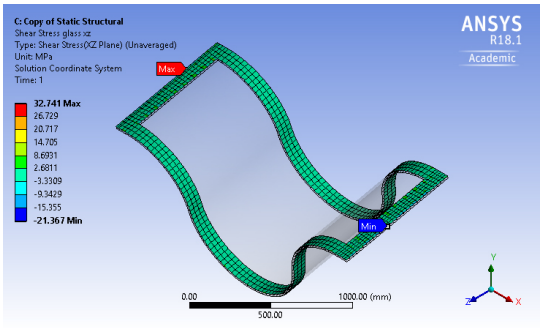

(c) Division of 30

Figure 8.30: Mesh refinement

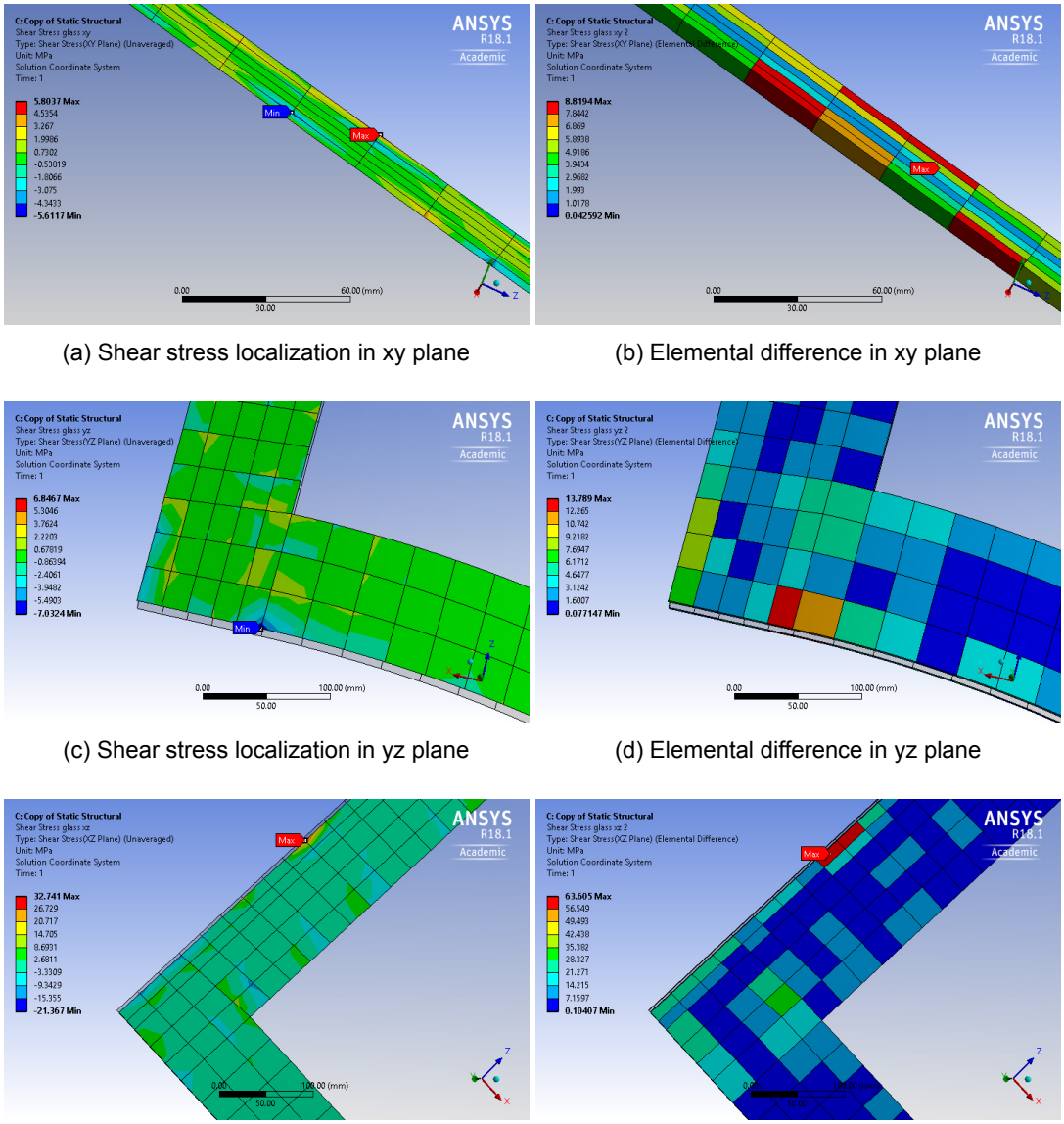

(a) Shear stress localization in xy plane

(b) Elemental difference in xy plane

(c) Shear stress localization in yz plane

(d) Elemental difference in yz plane

(e) Shear stress localization in xz plane

(f) Elemental difference in xz plane

Figure 8.31: Shear stress localization in glass

Because the shear stresses on glass surface are higher than the ones on concrete surfaces, we check the unaveraged values of stresses on glass surfaces, it is clear that singularity problems are quite dispersive and random which is shown in results of Figure 8.31. Here the elemental difference calculates the maximum difference between the unaveraged computed result for for all nodes in an element, including midside nodes. Clearly the elemental difference is larger when the stress is more localized, where the gradients are huge in one single element, and the results will be inaccurate in this case. Normally for such stress concentration a brittle material may crack, causing a local redistribution of the stresses in most cases.

8.5.4.1. Approximate results ruling out stress localization

To obtain approximate results in this model, one solution is to look at the stress in one element away from the element of the maximum singularity. This is shown in Figure 8.32. Here we use path plot of unaveraged results in figures of left column, and probe plot of averaged results in figures of right column.

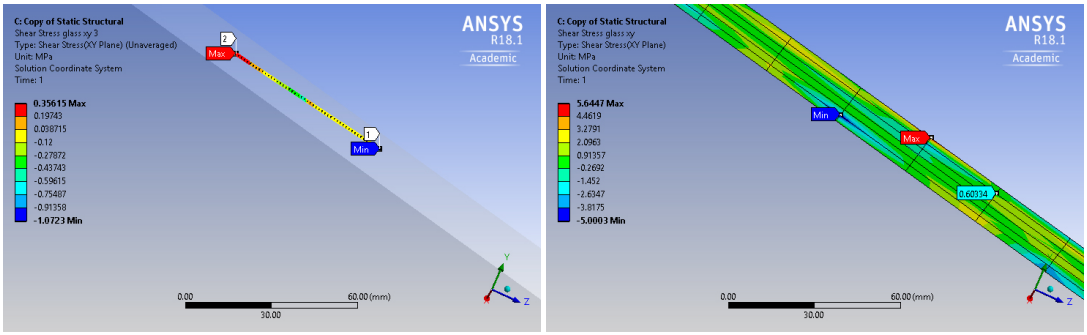

(a) Unaveraged result of shear stress in xy plane τ_{xy}= 1.07 MPa

(b) Averaged result of shear stress in xy plane τ_{xy}= 0.60 MPa

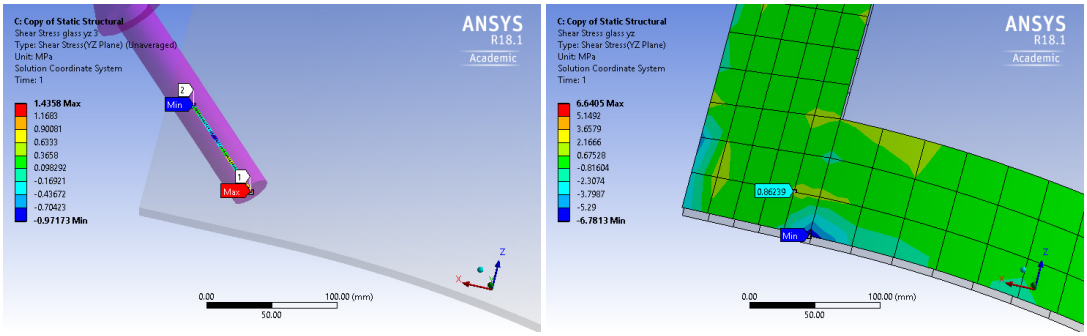

(c) Unaveraged result of shear stress in yz plane τ_{yz}= 1.44 MPa

(d) Averaged result of shear stress in yz plane τ_{yz}= 0.86 MPa

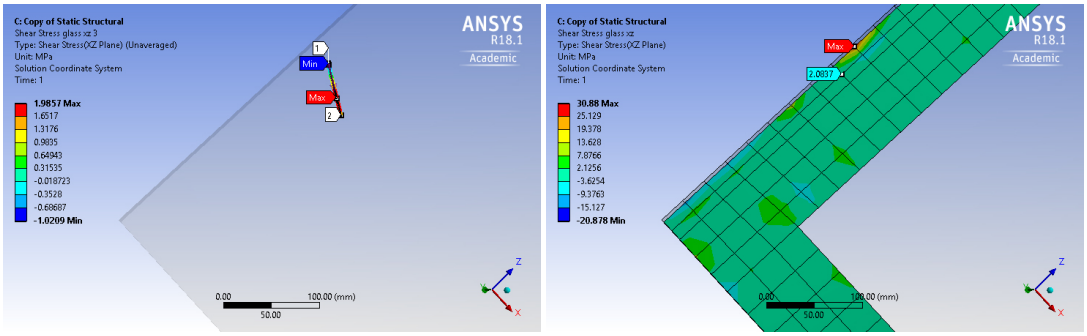

(e) Unaveraged result of shear stress in xz plane τ_{xz}= 1.99 MPa

(f) Averaged result of shear stress in xz plane τ_{xz}= 2.08 MPa

Figure 8.32: Shear stresses in glass

8.5.5. Comparison with experimental data

The results indicate that τ_{xy}e lies within the shear bond strength from experiment, but quality control of this connection is needed. For τ_{yz} and τ_{xz} the highest data is exceeded. As is illustrated in Figure 8.33, the shear stresses in this design locates in the blue shadowed area, which is beyond the results of all specimens. However, due to the random and dispersive singularity in this model, this result may not be realistic. Therefore, a new model is needed to obtain more accurate and reliable results.

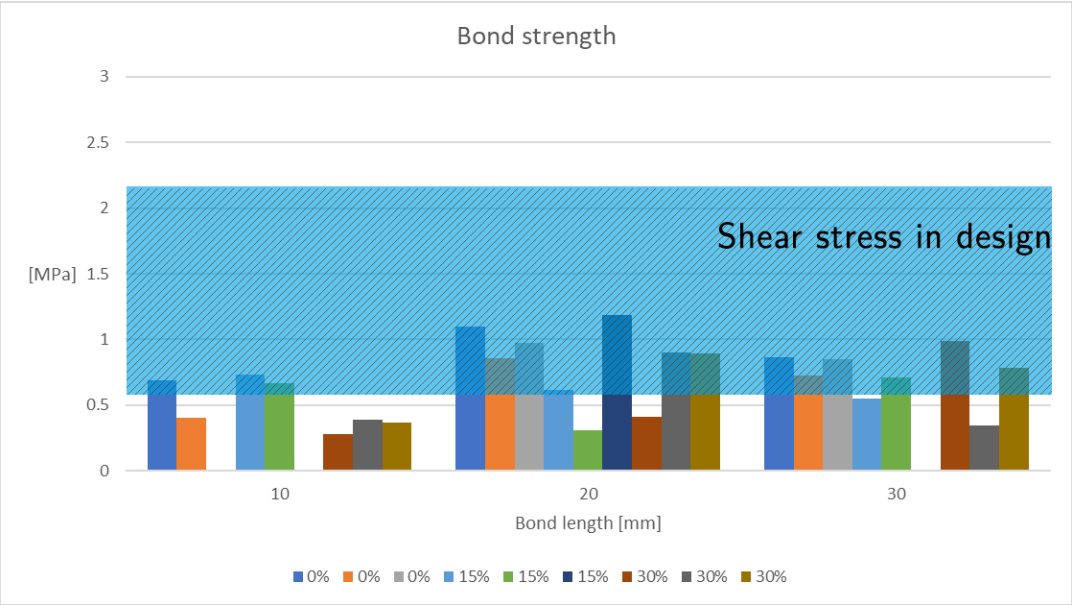

Figure 8.33: Shear stress comparison

9 Discussion

From chapter 8 we conclude that the experimental data is not sufficient for the current design. Therefore, two solutions are provided in this chapter of discussion. One approach is improving the shear strength between glass and concrete to suffice our design, the other way is optimizing our design to control shear stress below our existing data. These two methods will be explained and proved either with the data from Veer et al. or with the simulation analysis from Ansys WB. Finally, an example of typology optimization is carried out to verify the possible of this connection.

9.1. Improvement on shear bond strength

Since the largest shear stress in Figure 8.32 from Chapter 8 is 2.08 MPa, the goal in this method is enhancing the bond strength between concrete and glass to outdo the value from design. However, the safety factor for design should be considered.

According to Veer et al., in order to check the adequacy of adhesion when using the glass as reinforcement in concrete, the test of pushing the glass out of the concrete was carried out. The specimens made of rectangular pieces of normal and sandblast glass embedding in concrete were tested, and the results are shown in Table 9.1.

The flexural strength $\sigma_{f,f}$ in Table 9.1 is the test result by 3 point bending rectangular specimens of dimension 1000×100×40 mm, where the composition is B25 concrete mixture with aggregates made of normal and sandblasted glass rods.

Surface condition	τ_p (MPa)	$\sigma_{f,f}$ (MPa)
Normal	0.98	16.2
Sand blasted	2.95	16.6

Table 9.1: Effect of glass surface treatment

Here we can see the shear strength by using glass of sandblasted surface is three times high as using normal glass. Comparing the shear strength in Table 9.1 with the results of normal concrete group from Chapter 7, it can be seen that τ_p of 0.98 MPa is higher but still not suffices this design.

However, if we use sandblasted glass in our design that the shear stresses from design will probably locate inside the range of τ_p as is described in Figure 9.1. In this case, more research should be performed to validate this assumption.

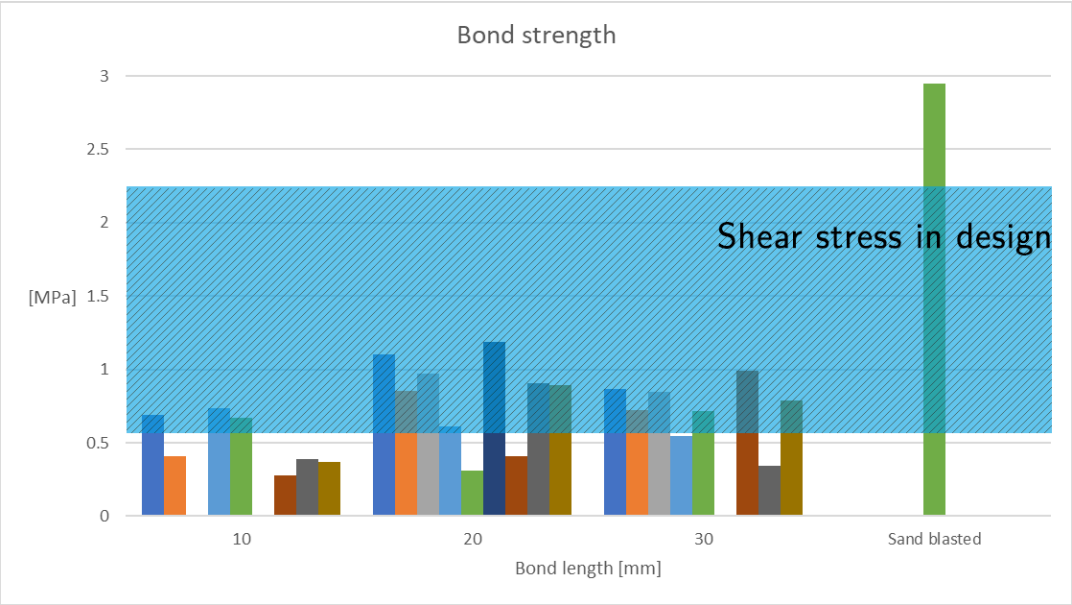

Figure 9.1: Result of using sandblasted glass

9.2. Improvement on structure design

The solution of this section is to lower the shear stress in this design to reach a acceptable range as is shown in Figure 9.2. Because of the existing problem of FEM model in Chapter 8, we will do the parameters correlation analysis in global detailed model instead of previous method of optimal parameter study.

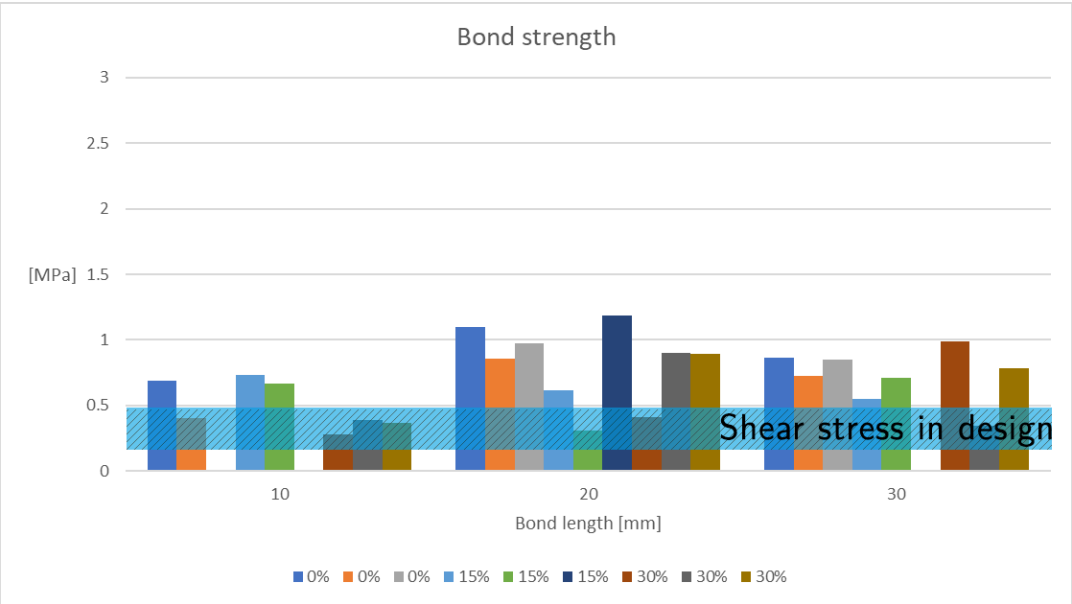

Figure 9.2: Result of optimize design

By the correlation simulation of the parameters in Figure 8.3 ,Figure 8.2, maximum and minimum τ_{xy}, τ_{yz}, τ_{xz}, we get the correlation chart in Figure 9.3. It can be seen that there is a positive correlation between bond length and minimum τ_{xy}, glass thickness and minimum τ_{yz}, τ_{xz}, while there is a negative correlation between bond length and maximum τ_{xy}, glass thickness and maximum τ_{yz}, τ_{xz}, which means the absolute values of τ_{xy}, τ_{yz} and τ_{xz} are becoming smaller with the increasing of bond area.

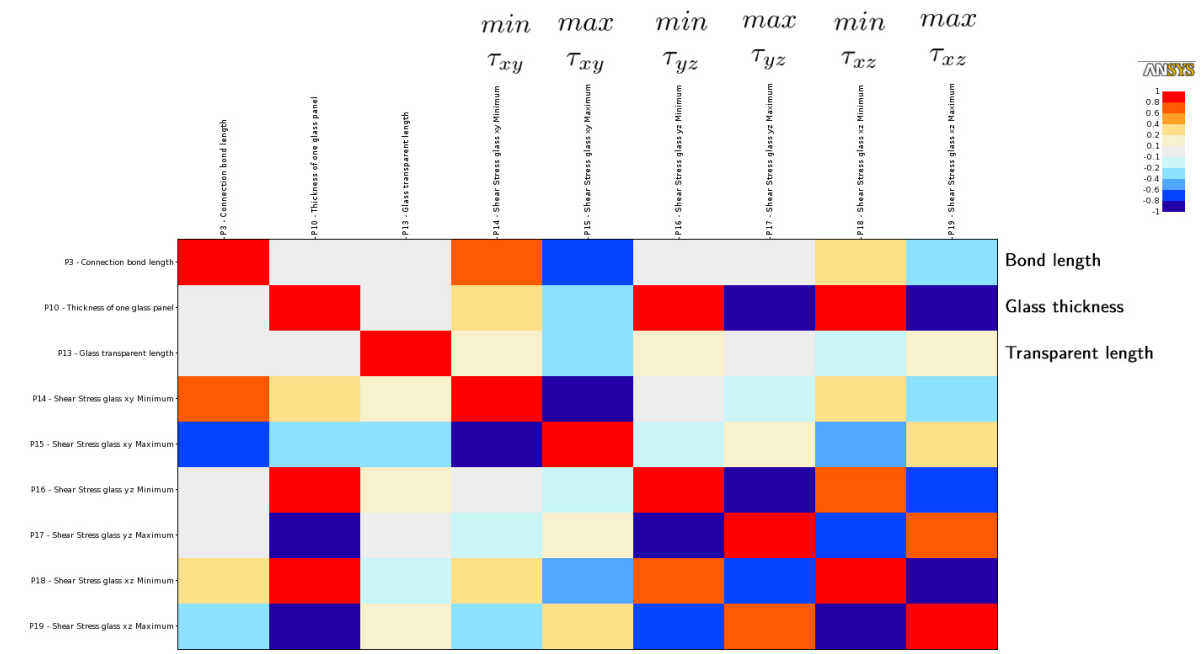

Figure 9.3: Correlation matrix

To illustrate the relation more clearly, the correlation scatter charts are plotted in Figure 9.4, 9.5 and 9.6, where the shear stresses are reducing with the rising of bond area. Other correlation curves can be found in Appendix C section C.10. There are still in fact stress concentration in these global models, where the accurate shear stresses can be lower. Therefore, we can conclude that τ_{xy}, τ_{yz} and τ_{xz} can be controlled into the range of Figure 9.2 with further optimization of this design.

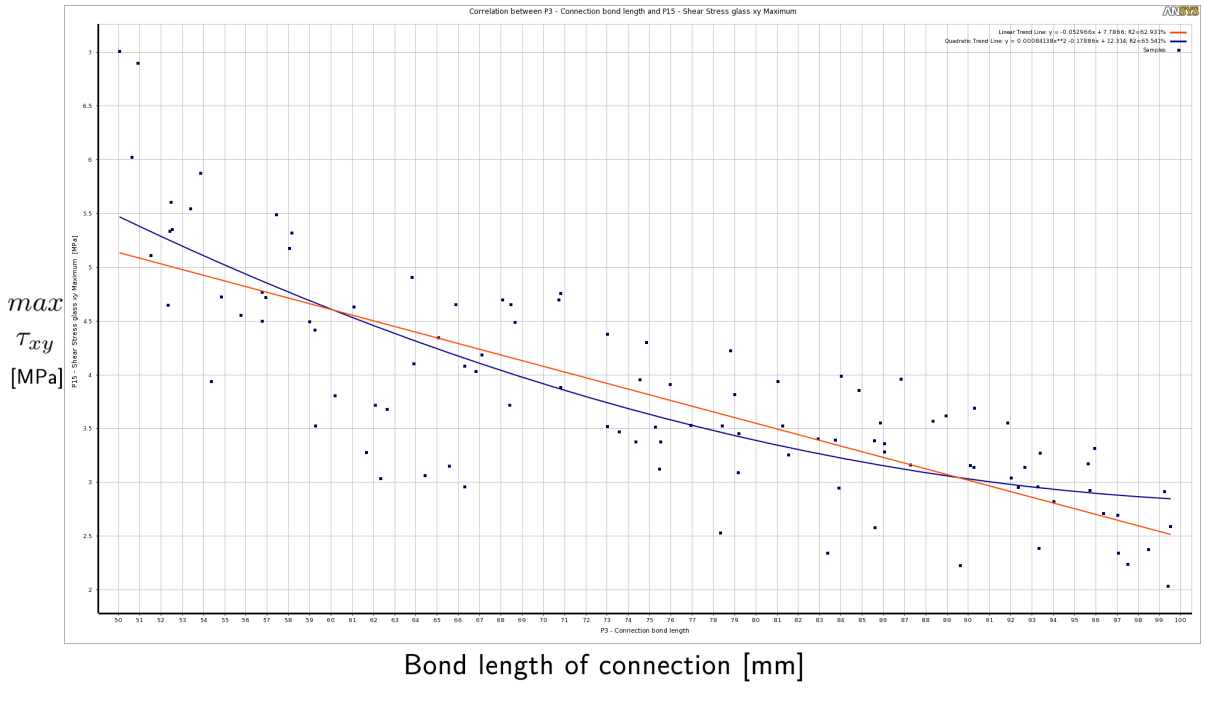

Figure 9.4: Correlation curve of bond length and maximum τ_{xy}

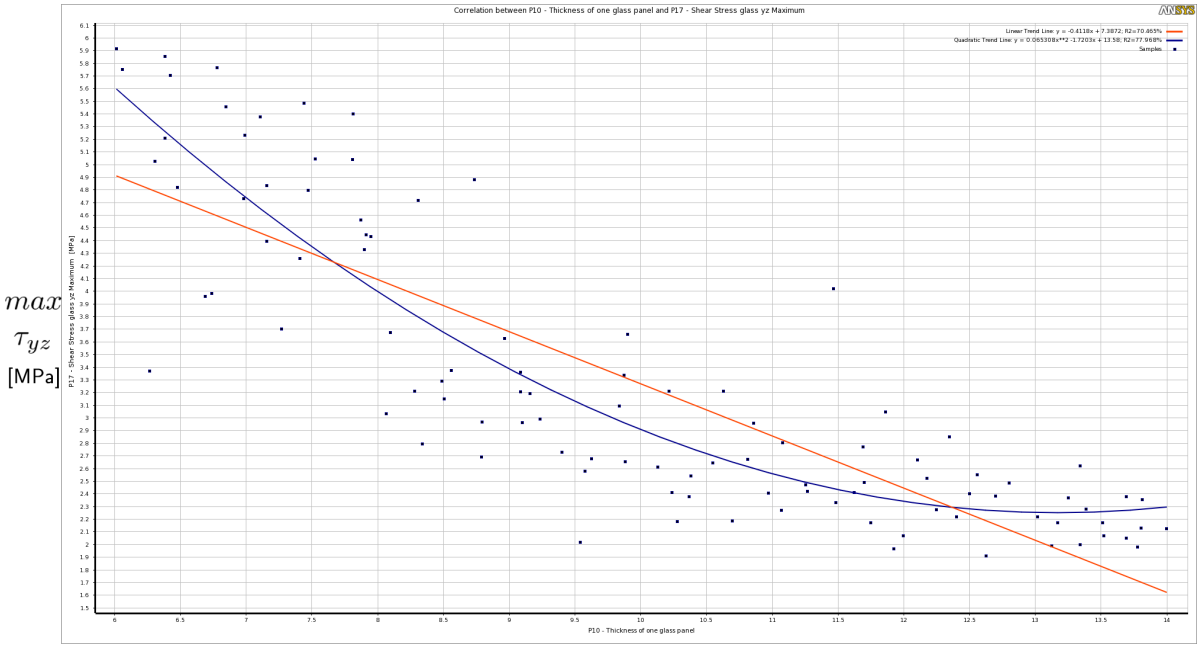

max
τ_{yz}
[MPa]

Figure 9.5: Correlation curve of glass thickness and maximum τ_{yz}

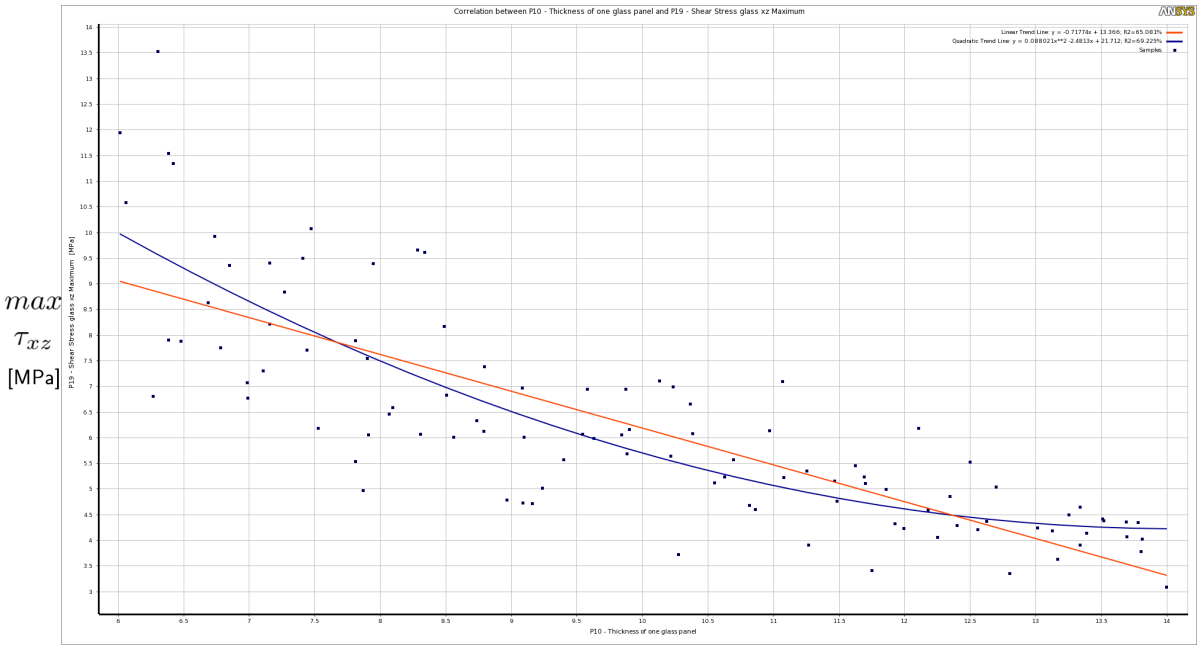

max
τ_{xz}
[MPa]

Figure 9.6: Correlation curve of glass thickness and maximum τ_{xz}

9.3. Typology simulation

To explore the possibility of typology optimization, one component is studied by the loading intensity of snow and wind load. The result is shown in the Figure 9.7， where the usage of concrete is decreased by 22.8% while the deformation in glass is increased by 24.5%. This will depend on the limitation of deformation and choice of safety factor here, but this is still an interesting prove of possible typology optimization.

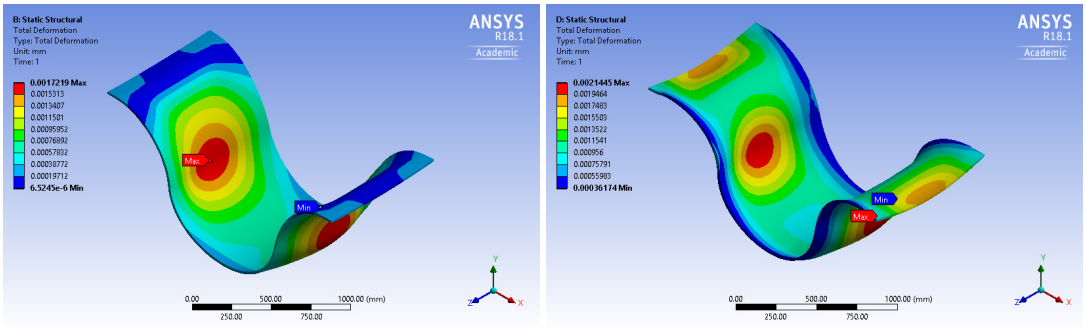

(a) Before simulation (b) After simulation

Figure 9.7: Typology comparison

10

Conclusion and recommendations

Within this chapter, conclusions of this thesis will be summarized. Some limitations and problems occurred during this research, and solutions are not straightforward but may need more research or help of experts in certain fields. Recommendations are discussed in the end to bring up challenges, possibilities and even more questions.

10.1. Conclusion

10.1.1. Parametric behaviour of arch and the economical arches

- Shape typologies and support conditions are important to arch design and should be considered before further parametric studying. In this case, circular cylindrical shells of two-hinged and fixed supports were chosen for further optimization, which narrows down the scope of parametric analysis inside arch structures.

- For most alterations of height-to-span ratios, the dominating load cases are dead load + unsymmetrical snow load in terms of internal bending moments, dead load + full uniform snow load in terms of reaction forces, dead load + unsymmetrical snow or wind load in terms of cost estimation.

- As the height of arch rises, the decreasing of thrust reaction forces is much faster than the increasing of vertical reaction, which means the cost of supports reduces at the same time. On the other hand, the arch length is larger as height increases while the internal bending moment is a parabolic curve, which means the cost of arch is also changing. All these behaviours implies that there is an optimal height-to-span ratio from a material efficiency point of view.

- From the cost estimation results of this case study, the most favourable height-to-span ratios of economical arches will lie in the range of 0.13 ~ 0.3 for two-hinged and fixed arches.

10.1.2. Integration of glass and concrete

- Since both glass and concrete are brittle materials, it would be best for them to be loaded in compression. This is the reason for including shell structure and prestress in this design. The ideal situation in shell design is to load components in pure compression. However, due to unsymmetrical loading and typology limitations, shear and bending do occur inside the component.

- By integrating corrugated glass in this design, the risk of component buckling is lowered when loaded in compression. The load transmit mechanism between glass and concrete is mainly shear of the contact surfaces between glass and concrete. On the hand hand, by integrating concrete into corrugated glass, in addition to some functional advantages, the structural performance is also improved as is described in section 8.3.2 (Figure).

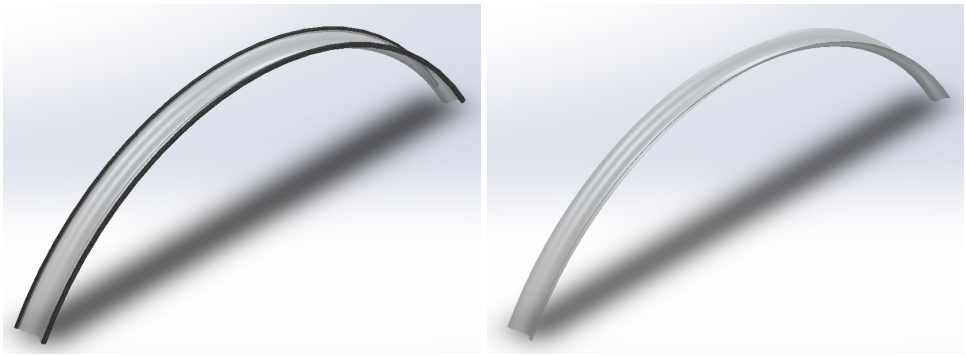

(a) Composite arch (b) Pure glass arch

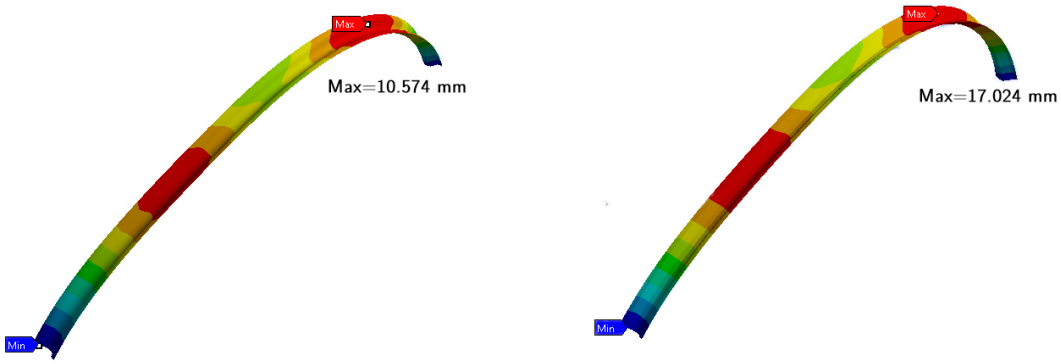

(c) Deformation of glass in composite arch (d) Deformation of glass in pure glass arch

Figure 10.1: Integration of glass and concrete

- The results of shear bond test of smooth soda-lime glass and concrete indicates that it is possible to utilize this connection as linear bond connection. Because the shear bond strength of normal concrete and glass without any surface pre-treatment, is comparable to 2-part silicone SG 500 in an adhesive system.
- Applying pozzolanic material in concrete is promising, as the highest bond result from test is one specimen from the group of 15% fly ash replacement. The value of bond strength is 1.18 MPa.

10.1.2.1. Solutions to realize this design

- The feasibility of adhesive connection needs more research and experiments to make the FEM solutions as well as test results more reliable. In this case, the data from experiment shows the bond strength is not enough for this design.
- According to Veer et al., the shear strength between normal concrete and sandblasted glass (Table 10.1) is strong enough to cover the range of shear stresses from this design. Therefore, one solution here is to use sandblasted glass for bond area before casting concrete.

Surface condition	τ_p (MPa)	$\sigma_{f,f}$ (MPa)
Normal	0.98	16.2
Sand blasted	2.95	16.6

Table 10.1: Effect of glass surface treatment （2004）

- The other solution is verified in Chapter 9 that the optimization of existing parameters can actually reduce the shear stresses in global detailed model, by enlarging the shear bond area between

glass and concrete. The aim here is to control the range of τ_{xy}, τ_{yz} and τ_{xz} inside the results from experiments.

10.1.3. Comparisons of solutions

- There are some deviances between the solutions of analytical calculation, GSA and Ansys WB. The possible reasons for that are the axial forces inclusion, supports and boundary condition settings and safety factors during calculation.

- In this case, we make decisions in accordance with GSA solutions in global model and Ansys WB solutions in detailed model. The verification of similar arch behaviours between different solutions are also carried out.

10.2. Recommendations

10.2.1. Possibilities of arch design

- Other than arch structure, alternatives such as double curved shell structure can also be considered in this design. However, the design of the component needs to be adjusted accordingly.

- Prestressing is not studied further in this design due to time limit. But the benefits of realizing the prestressed arch will be tremendous as mentioned in the conclusion with components resisting compression. Therefore, pre or post-prestressing concrete combined with glass is an interesting direction to investigate. It is noticed that concrete shape and location should be changed according to the kern area calculation.

10.2.2. Bond of glass and concrete

- The amount of specimens is restricted in terms of coupling parameters. More specimens are needed to get a reliable results. Moreover, quality control is also needed since the results in the test varies a lot. More sets of groups can be studied in terms of coupling parameters in this test, because there is a possible optimal portion of replacement and effective bond length as described in Chapter 7.

- Beside the coupling parameters studied in this thesis, many aspects are also quite related to the bond between glass and concrete: The particle sizes of fly ash and sand, loading rate, glass types and environment temperature etc. Furthermore, the thermal shock, time dependent effects and other durability tests should be verified.

- To improve the shear bond strength, many methods can be tested in this case. Other pozzolanic material such as silica fume may be applied instead of fly ash in concrete. UHPC or UHSC can be used as an alternative. Surface treatment such as rough on glass surfaces or edge can probably increase the bond strength.

- Injected mortar or other soft material such as neoprene or aluminium may be utilized around the sharp corners or edges to avoid stress concentration, which is shown in the results of Ansys WB modelling.

10.2.3. Components of concrete and glass

- Both the shape of glass panels and concrete can be irregular for the component design, where the free form of concrete is more intuitive due to its properties. For the glass panels, gradually varied thickness along the cross section curves can be a way to optimize this component.

- Replacement and maintenance design is an important aspect and should be designed carefully and thoroughly in the future. Residual loading design considering structure safety redundancy is also very essential in this overhead glazing system.

- For laminated glass, the glass composite behaviour shall be studied if possible, especially if the friction connections are adopted.

Figure 10.2: Component of glass-concrete

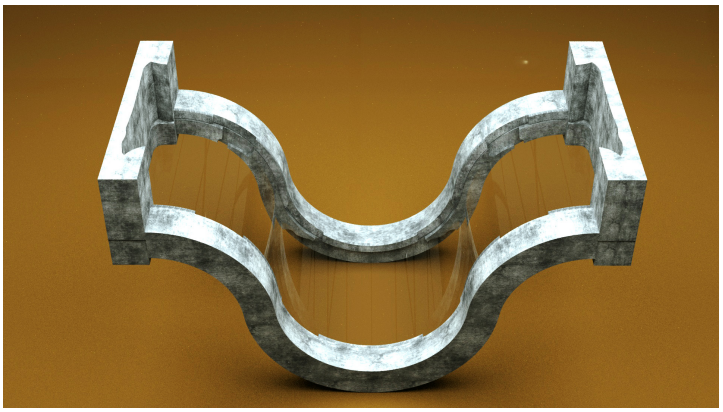

Figure 10.3: Possible typology optimization

10.2.4. Numerical calculations

- Geometrical non-linear analysis is needed when the displacement it was larger than half of glass thickness in this case.
- The detailed model encountered some errors which remained unsolved here. The temporary solution in this case can be unreliable and dangerous, thereby further modification or a new model is required to study the shear stress on the contact surfaces.

10.2.5. Possible applications of integration of glass concrete

- Using concrete as functional space, sun-shading or a sealing material for the connections in glass. Tolerances can also be compensated by casting concrete.
- Concrete can even be used as a repair material for glass when the bond is strong enough, because of its good property of handling irregular shapes. Besides, for the design where fire safety is important, concrete can also work as part of the protection material in the combination with glass.

10.2.6. Visions of arch

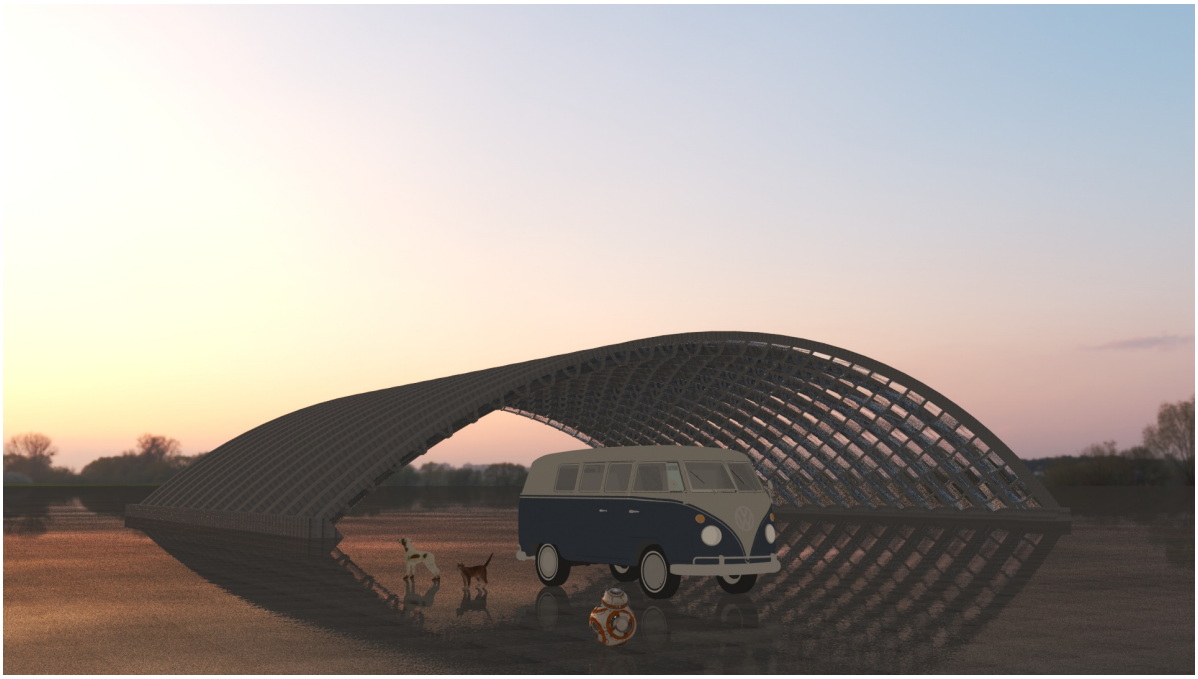

Figure 10.4: Arch of day time

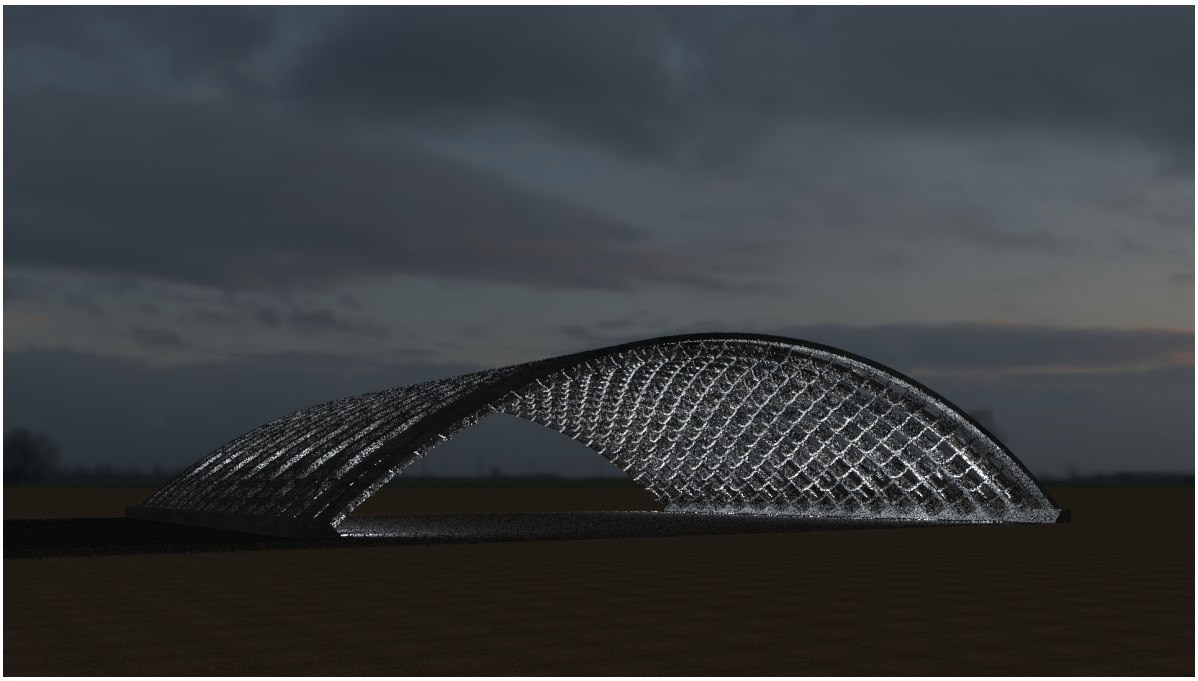

Figure 10.5: Arch of night hours

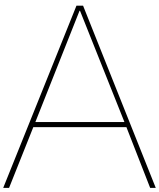

Appendix A - Calculations

A.1. Composite arch calculation

```
function [arch_maximoment, c_stress, g_stress] = Arch_calculation( ...
h_upper_concrete,w_upper_concrete, h_lower_concrete, w_lower_concrete,...
t_glass, h_half_glass, w_fourth_glass,span_arch, h_arch)
% Noticed that t_glass is half the thickness of the whole glass pane

% The method of calculation is from 'The Design of Building Structures' by
% Wolfgang Schueller
% Wind load and snow load is referred to Eurocode

% For shallow cicular arch (H/L<3), three-hinged and two-hinged arches can
% be treated as parabolic arches for the first approximation
% but the effect of dead load must be considered

% The slope at the supports
tan_slope = 4*h_arch/(2*span_arch);

% The length of arch
len_arch = span_arch * (1+8*(h_arch/span_arch)^2/3);

% The uniform gravity loads
%% Self weight of component
% radius of glass panel
r_glass = (w_fourth_glass^2+h_half_glass^2)/(2*h_half_glass);

% angle radians of one fourth glass
radians_glass = asin(w_fourth_glass/r_glass);

% total length of glass panel
length_glass = 4*r_glass*radians_glass;

% area of glass
area_glass = length_glass*2*t_glass;

% area of concrete
area_concrete = h_upper_concrete*w_upper_concrete*2+h_lower_concrete*
    w_lower_concrete*2;

% self weight calculation(kN/m)
```

```
% resolving the total load again into a uniform load on the horizontal
    roof
% projection by dividing it through the span
self_weight_span = 25 *(area_glass+area_concrete)/10^6;
self_weight_char = self_weight_span*len_arch/span_arch;

% multiply with the partial factor
self_weight = self_weight_char*1.35;
%% Varible load according to Eurocode

% In this situation wind load depends on the height of the arch as well as
% the zone A B C of the surface. To make a rough calculation, the pressure
% will be set at height of 9 meters, and the factor for combining the
% leading varible load will be 1.5

% snow load calculation: \mu 3 will be 2.0 accroding to Eurocode. For
% uniform load distribution \mu will be set at 1.0
% the unit is kN/m by multiply the length of the component
snow_load = 1.5 *0.744*(4*w_fourth_glass+2*w_upper_concrete)/1000;

% wind load will be set at the average value of the half span of roof
% the unit is kN/m by multiply the length of the component
wind_load = 1.5*(0.98+0.392)/2*(4*w_fourth_glass+2*w_upper_concrete)/1000;
wind_load_A = 1.5*0.47*(4*w_fourth_glass+2*w_upper_concrete)/1000;
wind_load_B = 1.5*-0.98*(4*w_fourth_glass+2*w_upper_concrete)/1000;
wind_load_C = 1.5*-0.392*(4*w_fourth_glass+2*w_upper_concrete)/1000;
element_length = 4*w_fourth_glass+2*w_upper_concrete;
%% Moment calculation
% with respect to shallow arch the maximum moment takes into account the
% dead load and unsymmetrical half span snow load
max_moment = self_weight*h_arch^2/8+snow_load*span_arch^2/64;

% using a 20% increasing of moment for shallow arch to take into account
% axial action
% the unit is N*mm
arch_maximoment_1 = 1.2*max_moment*10^6;

% Convert it to unit kN*m
arch_maximoment = 1.2*max_moment;
%% Neutral axis calculation
% Given the condition that the common modulus of elasticity of glass and
% concrete is 70000 and 27000 N/mm2

% centroid of concrete away from the component bottom
Centroid_c = (h_upper_concrete*w_upper_concrete*(h_half_glass*2+...
h_upper_concrete/2) + h_lower_concrete*w_lower_concrete*(h_half_glass
    *2-...
h_lower_concrete/2))/( h_upper_concrete*w_upper_concrete+h_lower_concrete*
    w_lower_concrete);

% solve the equation for the neutral axis
% neutral line away from the bottom
syms h
eqn = 70000*(h-h_half_glass)*area_glass-27000*(Centroid_c-h)*area_concrete
    == 0;
h_na = double(subs(solve(eqn,h)));
```

```
90
91 %% Moment of inertia calculation
92 % moment of inertia of one fourth glass panel
93 inertia_fourth_glass = integral2(@(r,a) (r.*sin(a)).^2.*r,r_glass-t_glass
       ,...
94     r_glass+t_glass,pi/2-radians_glass,pi/2);
95
96 % by using Parallel Axis Theorem one fourth glass Ix is
97 % unit is mm4
98 inertia_move_f_glass = inertia_fourth_glass - r_glass*radians_glass*...
99     2*t_glass*(r_glass-h_half_glass)^2;
100
101 % moment of inertia of total glass panel
102 % unit is mm4
103 inertia_glass = 4*inertia_move_f_glass+area_glass*(h_na-h_half_glass)^2;
104
105 % moment of inertia of left concrete part
106 % unit is mm4
107 inertia_l_concrete = w_upper_concrete*h_upper_concrete^3/3+...
108     w_lower_concrete*h_lower_concrete^3/3;
109
110 % moment of inertia of total concrete
111 % unit is mm4
112 inertia_concrete = inertia_l_concrete*2+area_concrete*(2*h_half_glass-h_na
       )^2;
113
114 % moment of inertia of whole component
115 % unit is mm4
116 inertia_component = inertia_glass+inertia_concrete;
117
118 %% Stress calculation
119 % stress at the bottom point of glass
120 % unit is N/mm2
121 g_stress = arch_maximoment_1*70000*(2*h_half_glass-h_na)/(70000*
       inertia_glass+...
122     27000*inertia_concrete);
123
124 % stress at the top point of concrete
125 % unit is N/mm2
126 c_stress = arch_maximoment_1*27000*(h_upper_concrete+2*h_half_glass-h_na)
       /...
127     (70000*inertia_glass+27000*inertia_concrete);
128 end
```

A.2. Pure glass arch calculation

```
1 function [arch_maximoment, g_stress] = Arch_calculation_g(t_glass,...
2  h_half_glass, w_fourth_glass,span_arch, h_arch)
3 % Noticed that t_glass is half the thickness of the whole glass pane
4
5 % The method of calculation is from 'The Design of Building Structures' by
6 % Wolfgang Schueller
7 % Wind load and snow load is referred to Eurocode
8
9 % For shallow cicular arch (H/L<3), three-hinged and two-hinged arches can
10 % be treated as parabolic arches for the first approximation
```

```
% but the effect of dead load must be considered

% The slope at the supports
tan_slope = 4*h_arch/(2*span_arch);

% The length of arch
len_arch = span_arch * (1+8*(h_arch/span_arch)^2/3);

% The uniform gravity loads
%% Self weight of component
% radius of glass panel
r_glass = (w_fourth_glass^2+h_half_glass^2)/(2*h_half_glass);

% angle radians of one fourth glass
radians_glass = asin(w_fourth_glass/r_glass);

% total length of glass panel
length_glass = 4*r_glass*radians_glass;

% area of glass
area_glass = length_glass*2*t_glass;

% self weight calculation(kN/m)
% resolving the total load again into a uniform load on the horizontal
    roof
% projection by dividing it through the span
self_weight_span = 25 * area_glass/10^6;
self_weight_char = self_weight_span*len_arch/span_arch;

% multiply with the partial factor
self_weight = self_weight_char*1.35;
%% Varible load according to Eurocode

% In this situation wind load depends on the height of the arch as well as
% the zone A B C of the surface. To make a rough calculation, the pressure
% will be set at height of 9 meters, and the factor for combining the
% leading varible load will be 1.5

% snow load calculation: \mu 3 will be 2.0 accroding to Eurocode. For
% uniform load distribution \mu will be set at 1.0
% the unit is kN/m by multiply the length of the component
snow_load = 1.5 *0.744*(4*w_fourth_glass)/1000;

% wind load will be set at the average value of the half span of roof
% the unit is kN/m by multiply the length of the component
wind_load = 1.5*(0.98+0.392)/2*(4*w_fourth_glass)/1000;
wind_load_A = 1.5*0.47*(4*w_fourth_glass)/1000;
wind_load_B = 1.5*-0.98*(4*w_fourth_glass)/1000;
wind_load_C = 1.5*-0.392*(4*w_fourth_glass)/1000;
element_length = 4*w_fourth_glass;
%% Moment calculation
% with respect to shallow arch the maximum moment takes into account the
% dead load and unsymmetrical half span snow load
max_moment = self_weight*h_arch^2/8+snow_load*span_arch^2/64;

% using a 20% increasing of moment for shallow arch to take into account
```

```
% axial action
% the unit is N*mm
arch_maximoment_1 = 1.2*max_moment*10^6;

% Convert it to unit kN*m
arch_maximoment = 1.2*max_moment;

%% Moment of inertia calculation
% moment of inertia of one fourth glass panel
inertia_fourth_glass = integral2(@(r,a) (r.*sin(a)).^2.*r,r_glass-t_glass
    ,...
    r_glass+t_glass,pi/2-radians_glass,pi/2);

% by using Parallel Axis Theorem one fourth glass Ix is
% unit is mm4
inertia_move_f_glass = inertia_fourth_glass - r_glass*radians_glass*...
    2*t_glass*(r_glass-h_half_glass)^2;

% moment of inertia of total glass panel
% unit is mm4
inertia_glass = 4*inertia_move_f_glass;

%% Stress calculation
% stress at the bottom point of glass
% unit is N/mm2
g_stress = arch_maximoment_1*h_half_glass/inertia_glass;
end
```

A.3. Input plot for bending stress of composite element

```
%Create an array of different heights of the arches
h_arch = zeros(9,1);
%Create a matrix for the result output from functions
r_arch = zeros(9,3);
for i = 1:1:9
    h_arch(i,1) = i;
    [m,c,g]=Arch_calculation(125,150,125,150,8,300,450,30,i);
    r_arch(i,1) = m;
    r_arch(i,2) = c;
    r_arch(i,3) = g;
end
plot(h_arch',r_arch(:,2:3));
legend('concrete stress','glass stress','Location','northwest');
xlabel('Arch height [m]');
ylabel('Bending stress [MPa]');
title('Analytical solution for bending stress of composite elements');
```

A.4. Input plot for bending stress of pure glass element

```
%Create an array of different heights of the arches
h_arch = zeros(9,1);
%Create a matrix for the result output from functions
r_arch = zeros(9,3);
for i = 1:1:9
    h_arch(i,1) = i;
```

```
    [m,g]=Arch_calculation_g(8,300,450,30,i);
    r_arch(i,1) = m;
    r_arch(i,2) = g;
end
plot(h_arch',r_arch(:,2));
legend('glass stress','Location','northwest');
xlabel('Arch height [m]');
ylabel('Bending stress [MPa]');
title('Analytical solution for bending stress of glass elements');
```

A.5. Input plot for bending stress comparison

```
%Create an array of different heights of the arches
h_arch = zeros(9,1);
%Create a matrix for the result output from functions
r_arch = zeros(9,3);
for i = 1:1:9
    h_arch(i,1) = i;
    [m,c,g]=Arch_calculation(125,150,125,150,8,300,450,30,i);
    [m2,g2]=Arch_calculation_g(8,300,450,30,i);
    r_arch(i,1) = m;
    r_arch(i,2) = c;
    r_arch(i,3) = g;
    r_arch(i,4) = m2;
    r_arch(i,5) = g2;
end
plot(h_arch',r_arch(:,[2 3 5]));
ylim([0,inf]);
legend('concrete stress','glass stress','Full glass stress','Location','
    northwest');
xlabel('Arch height [m]');
ylabel('Bending stress [MPa]');
title('Analytical solution for bending stress of elements');
```

A.6. Input plot for bending moment comparison

```
%Create an array of different heights of the arches
h_arch = zeros(9,1);
%Create a matrix for the result output from functions
r_arch = zeros(9,3);
for i = 1:1:9
    h_arch(i,1) = i;
    [m,c,g]=Arch_calculation(125,150,125,150,8,300,450,30,i);
    [m2,g2]=Arch_calculation_g(8,300,450,30,i);
    r_arch(i,1) = m;
    r_arch(i,2) = c;
    r_arch(i,3) = g;
    r_arch(i,4) = m2;
    r_arch(i,5) = g2;
end
plot(h_arch',r_arch(:,[1 4]));
ylim([0,inf]);
legend('Composite','Full glass','Location','northwest');
xlabel('Arch height [m]');
ylabel('Bending moment [kN*m]');
```

```
20 title('Analytical solution for bending moments');
```

B

Appendix B - Experiments

B.1. Plot Force-deformation curves

Plot Force-deformation curves of 0% fly ash

```
for iSheet = 1:3
    s_array = xlsread('Speciment_results.xls',iSheet);
    x = s_array(:,1);
    y = s_array(:,2);
    h1 = plot(x,y,'color',[0.0    0.447    0.741]);
    hold on;
end
for iSheet = 4:7
    s_array = xlsread('Speciment_results.xls',iSheet);
    x = s_array(:,1);
    y = s_array(:,2);
    h2 = plot(x,y,'color',[0.85    0.325    0.098],'linestyle','--');
    hold on;
end
for iSheet = 8:10
    s_array = xlsread('Speciment_results.xls',iSheet);
    x = s_array(:,1);
    y = s_array(:,2);
    h3 = plot(x,y,'color',[0.929    0.694    0.125],'linestyle','-.');
    hold on;
end
hold off;
ylim([0,inf]);
xlabel('Derformation [mm]');
ylabel('Standard Force [N]');
legend([h1 h2 h3],{'10mm bond','20mm bond','30mm bond'},...
    'Location','best');
title('Force-deformation curves of 0% fly ash bond')
```

Plot Force-deformation curves of 15% fly ash

```
for iSheet = 11:14
    s_array = xlsread('Speciment_results.xls',iSheet);
    x = s_array(:,1);
    y = s_array(:,2);
    h1 = plot(x,y,'color',[0.0    0.447    0.741]);
```

```
    hold on;
end
for iSheet = 15:19
    s_array = xlsread('Speciment_results.xls',iSheet);
    x = s_array(:,1);
    y = s_array(:,2);
    h2 = plot(x,y,'color',[0.85    0.325    0.098],'linestyle','--');
    hold on;
end
for iSheet = 20:22
    s_array = xlsread('Speciment_results.xls',iSheet);
    x = s_array(:,1);
    y = s_array(:,2);
    h3 = plot(x,y,'color',[0.929    0.694    0.125],'linestyle','-.');
    hold on;
end
hold off;
ylim([0,inf]);
xlabel('Derformation [mm]');
ylabel('Standard Force [N]');
legend([h1 h2 h3],{'10mm bond','20mm bond','30mm bond'},...
    'Location','best');
title('Force-deformation curves of 15% fly ash bond')
```

Plot Force-deformation curves of 30% fly ash

```
for iSheet = 23:27
    s_array = xlsread('Speciment_results.xls',iSheet);
    x = s_array(:,1);
    y = s_array(:,2);
    h1 = plot(x,y,'color',[0.0    0.447    0.741]);
    hold on;
end
for iSheet = 28:30
    s_array = xlsread('Speciment_results.xls',iSheet);
    x = s_array(:,1);
    y = s_array(:,2);
    h2 = plot(x,y,'color',[0.85    0.325    0.098],'linestyle','--');
    hold on;
end
for iSheet = 31:33
    s_array = xlsread('Speciment_results.xls',iSheet);
    x = s_array(:,1);
    y = s_array(:,2);
    h3 = plot(x,y,'color',[0.929    0.694    0.125],'linestyle','-.');
    hold on;
end
hold off;
ylim([0,inf]);
xlabel('Derformation [mm]');
ylabel('Standard Force [N]');
legend([h1 h2 h3],{'10mm bond','20mm bond','30mm bond'},...
    'Location','best');
title('Force-deformation curves of 30% fly ash bond')
```

Plot Force-deformation curves of 0% fly ash 10mm

```
1
2  for iSheet = 1:3
3      s_array = xlsread('Speciment_results.xls',iSheet);
4      x = s_array(:,1);
5      y = s_array(:,2);
6      plot(x,y);
7      hold on;
8  end
9  hold off;
10 ylim([0,inf]);
11 xlabel('Derformation [mm]');
12 ylabel('Standard Force [N]');
13 legend('Specimen 1','Specimen 2','Specimen 3');
```

Plot Force-deformation curves of 0% fly ash 20mm

```
1
2  for iSheet = 4:7
3      s_array = xlsread('Speciment_results.xls',iSheet);
4      x = s_array(:,1);
5      y = s_array(:,2);
6      plot(x,y);
7      hold on;
8  end
9  hold off;
10 ylim([0,inf]);
11 xlabel('Derformation [mm]');
12 ylabel('Standard Force [N]');
13 legend('Specimen 4','Specimen 5','Specimen 6','Specimen 7',...
14     'Location','northwest');
```

Plot Force-deformation curves of 0% fly ash 30mm

```
1
2  for iSheet = 8:10
3      s_array = xlsread('Speciment_results.xls',iSheet);
4      x = s_array(:,1);
5      y = s_array(:,2);
6      plot(x,y);
7      hold on;
8  end
9  hold off;
10 ylim([0,inf]);
11 xlabel('Derformation [mm]');
12 ylabel('Standard Force [N]');
13 legend('Specimen 8','Specimen 9','Specimen 10','Location','northwest');
```

Plot Force-deformation curves of 15% fly ash 10mm

```
1
2  for iSheet = 12:14
3      s_array = xlsread('Speciment_results.xls',iSheet);
4      x = s_array(:,1);
5      y = s_array(:,2);
```

```
    plot(x,y);
    hold on;
end
hold off;
ylim([0,inf]);
xlabel('Derformation [mm]');
ylabel('Standard Force [N]');
legend('Specimen 12','Specimen 13','Specimen 14','Location','northwest');
```

Plot Force-deformation curves of 15% fly ash 20mm

```

for iSheet = 15:19
    s_array = xlsread('Speciment_results.xls',iSheet);
    x = s_array(:,1);
    y = s_array(:,2);
    plot(x,y);
    hold on;
end
hold off;
ylim([0,inf]);
xlabel('Derformation [mm]');
ylabel('Standard Force [N]');
legend('Specimen 15','Specimen 16','Specimen 17','Specimen 18',...
    'Specimen 19','Location','northwest');
```

Plot Force-deformation curves of 15% fly ash 30mm

```

for iSheet = 20:22
    s_array = xlsread('Speciment_results.xls',iSheet);
    x = s_array(:,1);
    y = s_array(:,2);
    plot(x,y);
    hold on;
end
hold off;
ylim([0,inf]);
xlabel('Derformation [mm]');
ylabel('Standard Force [N]');
legend('Specimen 20','Specimen 21','Specimen 22','Location','northwest');
```

Plot Force-deformation curves of 30% fly ash 10mm

```

for iSheet = 23:27
    s_array = xlsread('Speciment_results.xls',iSheet);
    x = s_array(:,1);
    y = s_array(:,2);
    plot(x,y);
    hold on;
end
hold off;
ylim([0,inf]);
xlabel('Derformation [mm]');
ylabel('Standard Force [N]');
```

```
13 legend('Specimen 23','Specimen 24','Specimen 25','Specimen 26',...
14     'Specimen 27','Location','northwest');
```

Plot Force-deformation curves of 30% fly ash 20mm

```
1
2 for iSheet = 28:30
3     s_array = xlsread('Speciment_results.xls',iSheet);
4     x = s_array(:,1);
5     y = s_array(:,2);
6     plot(x,y);
7     hold on;
8 end
9 hold off;
10 ylim([0,inf]);
11 xlabel('Derformation [mm]');
12 ylabel('Standard Force [N]');
13 legend('Specimen 28','Specimen 29','Specimen 30','Location','northwest');
```

Plot Force-deformation curves of 30% fly ash 30mm

```
1
2 for iSheet = 31:33
3     s_array = xlsread('Speciment_results.xls',iSheet);
4     x = s_array(:,1);
5     y = s_array(:,2);
6     plot(x,y);
7     hold on;
8 end
9 hold off;
10 ylim([0,inf]);
11 xlabel('Derformation [mm]');
12 ylabel('Standard Force [N]');
13 legend('Specimen 31','Specimen 32','Specimen 33','Location','northwest');
```

Force-deformation curves

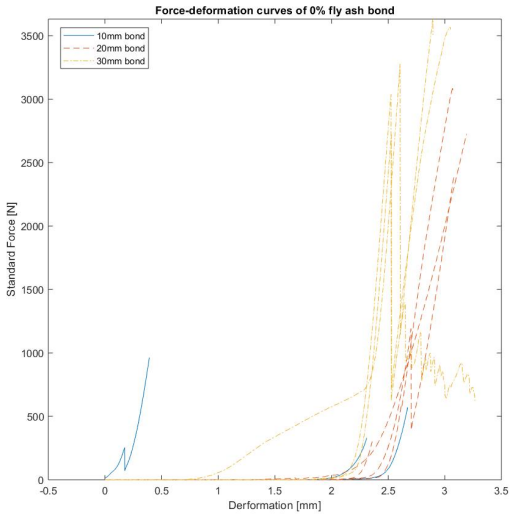
Force-deformation curves of 0% fly ash bond
10mm bond
20mm bond
30mm bond
Standard Force [N]
Derformation [mm]

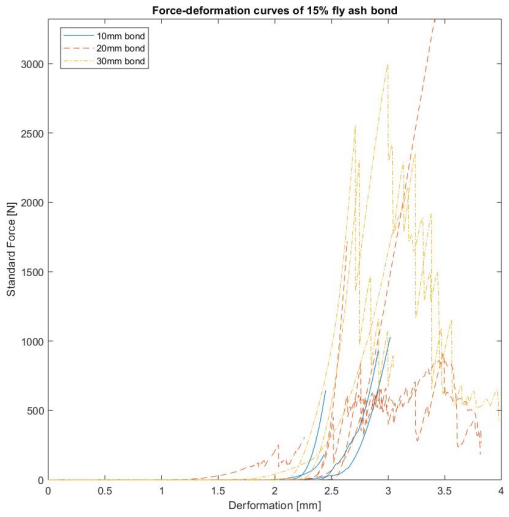
Force-deformation curves of 15% fly ash bond
10mm bond
20mm bond
30mm bond
Standard Force [N]
Derformation [mm]

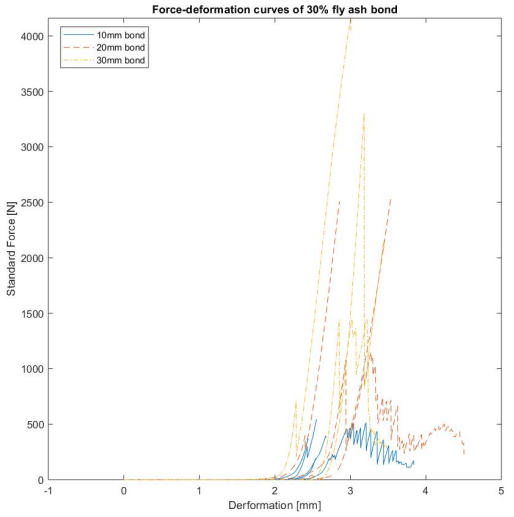
Force-deformation curves of 30% fly ash bond
10mm bond
20mm bond
30mm bond
Standard Force [N]
Derformation [mm]

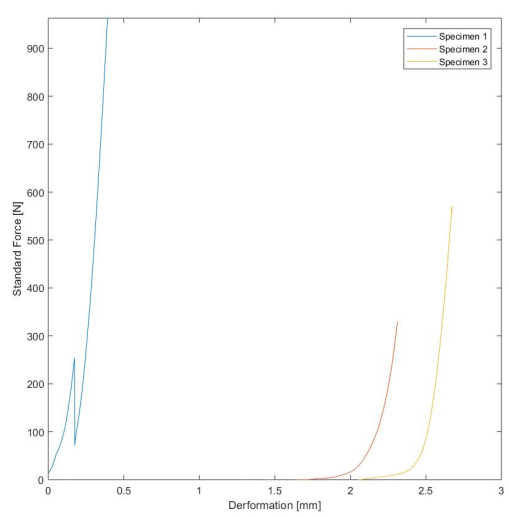
Specimen 1
Specimen 2
Specimen 3
Standard Force [N]
Derformation [mm]

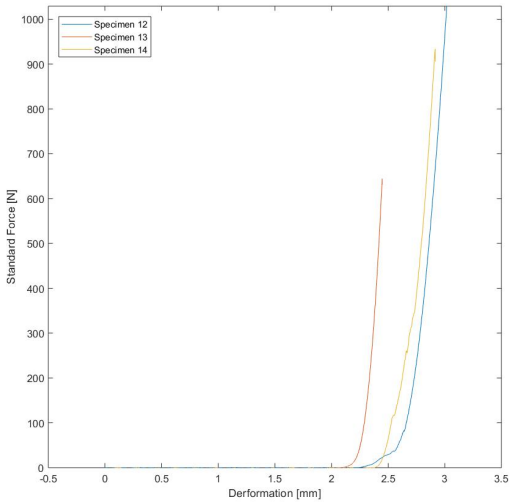
Specimen 12
Specimen 13
Specimen 14
Standard Force [N]
Derformation [mm]

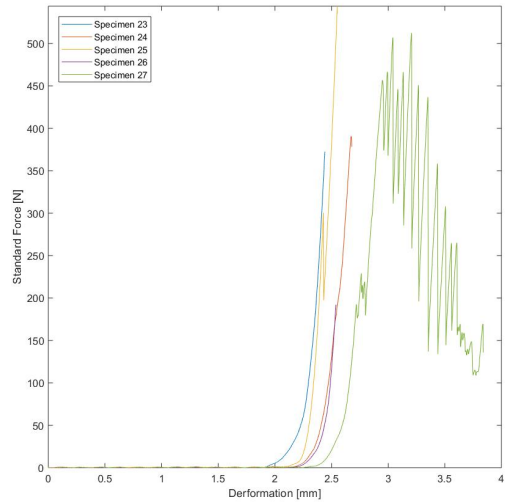
Specimen 23
Specimen 24
Specimen 25
Specimen 26
Specimen 27
Standard Force [N]
Derformation [mm]

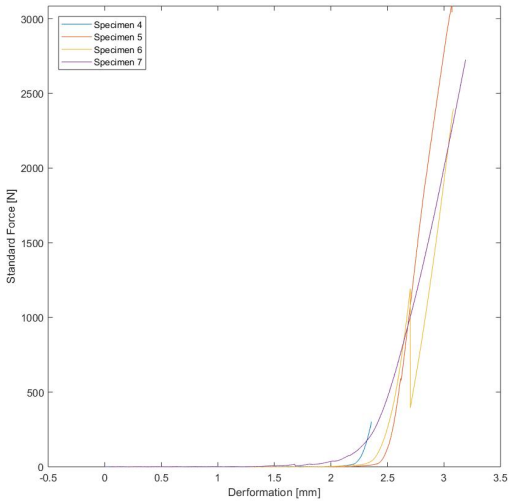
Specimen 4
Specimen 5
Specimen 6
Specimen 7
Standard Force [N]
Derformation [mm]

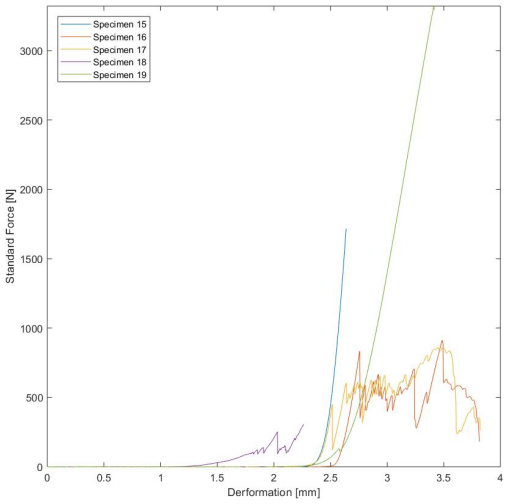
Specimen 15
Specimen 16
Specimen 17
Specimen 18
Specimen 19
Standard Force [N]
Derformation [mm]

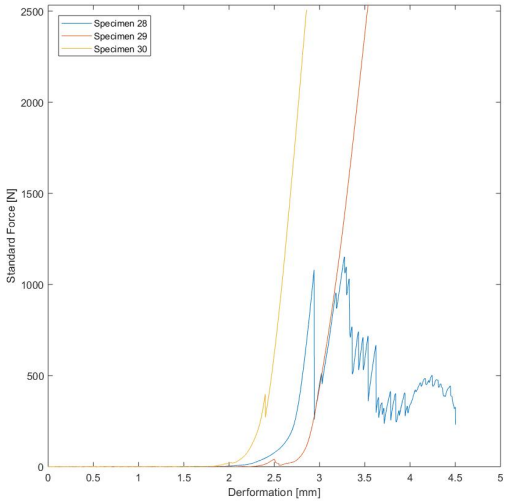
Specimen 28
Specimen 29
Specimen 30
Standard Force [N]
Derformation [mm]

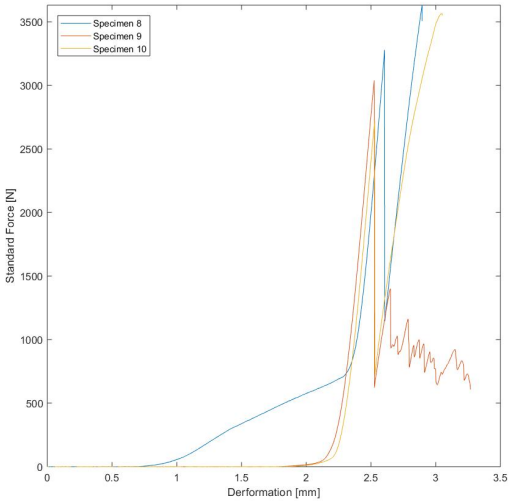
Specimen 8
Specimen 9
Specimen 10
Standard Force [N]
Derformation [mm]

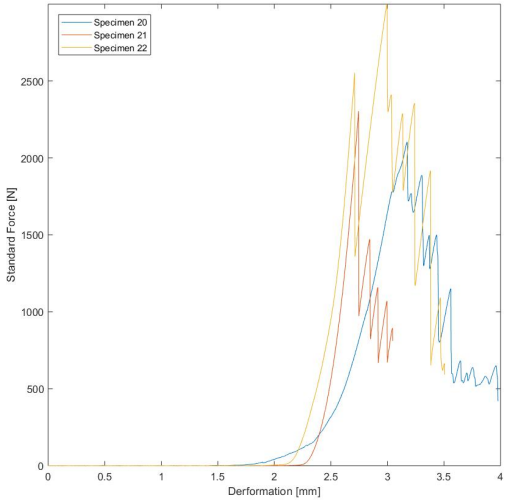
Specimen 20
Specimen 21
Specimen 22
Standard Force [N]
Derformation [mm]

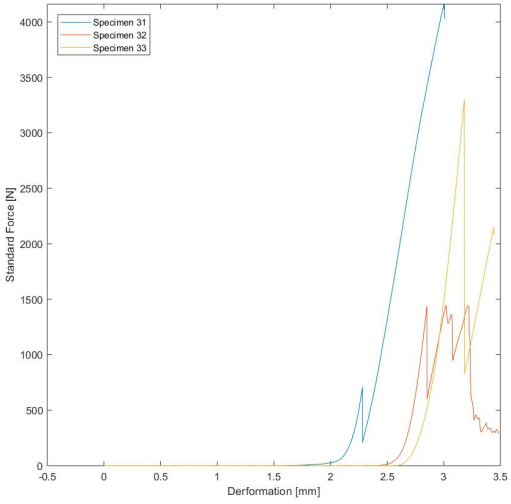
Specimen 31
Specimen 32
Specimen 33
Standard Force [N]
Derformation [mm]

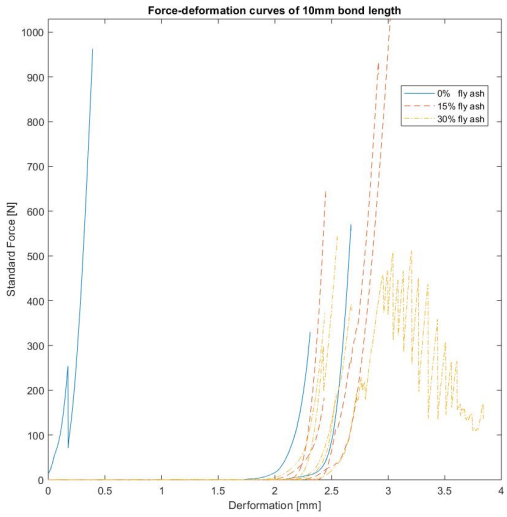
Force-deformation curves of 10mm bond length
Standard Force [N]
Derformation [mm]
0% fly ash
15% fly ash
30% fly ash

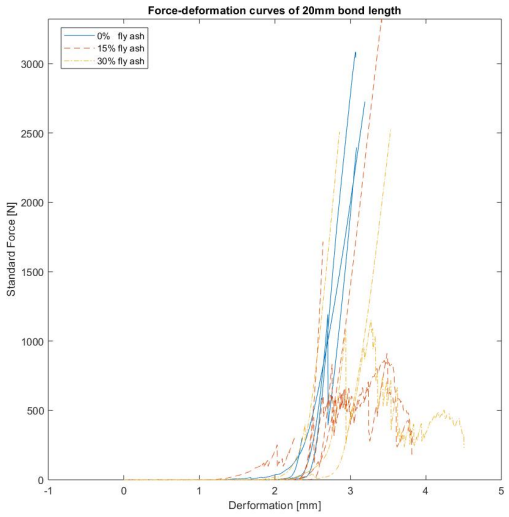
Force-deformation curves of 20mm bond length
Standard Force [N]
Derformation [mm]
0% fly ash
15% fly ash
30% fly ash

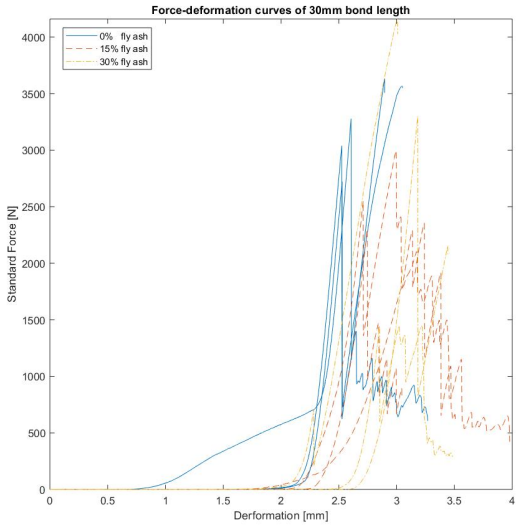
Force-deformation curves of 30mm bond length
Standard Force [N]
Derformation [mm]
0% fly ash
15% fly ash
30% fly ash

C

Appendix C - Numerical Calculations

C.1. Wind load inputs

Height [m]	Pressure coefficient	Times partial factor	Peak velocity pressure	Zone A [MPa]	Zone A [kN/m]
1	-0.053333	-0.0799995	0.6	-4.79997E-05	-0.10079937
2	-0.106667	-0.1600005	0.6	-9.60003E-05	-0.20160063
3	-0.16	-0.24	0.6	-0.000144	-0.3024
4	-0.213333	-0.3199995	0.6	-0.000192	-0.40319937
5	-0.266667	-0.4000005	0.66	-0.000264	-0.554400693
6	-0.32	-0.48	0.71	-0.0003408	-0.71568
7	-0.373333	-0.5599995	0.75	-0.00042	-0.881999213
8	-0.426667	-0.6400005	0.79	-0.0005056	-1.06176083
9	-0.48	-0.72	0.82	-0.0005904	-1.23984
10	-0.533333	-0.7999995	0.85	-0.00068	-1.427999108
11	-0.586667	-0.8800005	0.876	-0.00077088	-1.61884892
12	-0.64	-0.96	0.902	-0.00086592	-1.818432
13	-0.693333	-1.0399995	0.928	-0.00096512	-2.026751026
14	-0.746667	-1.1200005	0.954	-0.00106848	-2.243809002
15	-0.8	-1.2	0.98	-0.001176	-2.4696

Figure C.1: Wind load inputs for zone A of arch

Height [m]	Pressure coefficient	Times partial factor	Peak velocity pressure	Zone B [MPa]	Zone B [kN/m]
1	0.733333	1.0999995	0.6	0.00066	1.38599937
2	0.766667	1.1500005	0.6	0.00069	1.44900063
3	0.8	1.2	0.6	0.00072	1.512
4	0.833333	1.2499995	0.6	0.00075	1.57499937
5	0.866667	1.3000005	0.66	0.000858	1.801800693
6	0.9	1.35	0.71	0.0009585	2.01285
7	0.933333	1.3999995	0.75	0.00105	2.204999213
8	0.966667	1.4500005	0.79	0.0011455	2.40555083
9	1	1.5	0.82	0.00123	2.583
10	1.033333	1.5499995	0.85	0.0013175	2.766749108
11	1.066667	1.6000005	0.876	0.0014016	2.94336092
12	1.1	1.65	0.902	0.0014883	3.12543
13	1.133333	1.6999995	0.928	0.0015776	3.312959026
14	1.166667	1.7500005	0.954	0.0016695	3.505951002
15	1.2	1.8	0.98	0.001764	3.7044

Figure C.2: Wind load inputs for zone B of arch

Height [m]	Pressure coefficient	Times partial factor	Peak velocity pressure	Zone C [MPa]	Zone C [kN/m]
1	0.6	0.9	0.6	0.00054	1.134
2	0.5	0.75	0.6	0.00045	0.945
3	0.4	0.6	0.6	0.00036	0.756
4	0.4	0.6	0.6	0.00036	0.756
5	0.4	0.6	0.66	0.000396	0.8316
6	0.4	0.6	0.71	0.000426	0.8946
7	0.4	0.6	0.75	0.00045	0.945
8	0.4	0.6	0.79	0.000474	0.9954
9	0.4	0.6	0.82	0.000492	1.0332
10	0.4	0.6	0.85	0.00051	1.071
11	0.4	0.6	0.876	0.0005256	1.10376
12	0.4	0.6	0.902	0.0005412	1.13652
13	0.4	0.6	0.928	0.0005568	1.16928
14	0.4	0.6	0.954	0.0005724	1.20204
15	0.4	0.6	0.98	0.000588	1.2348

Figure C.3: Wind load inputs for zone C of arch

C.2. Internal moments of arches from GSA solutions

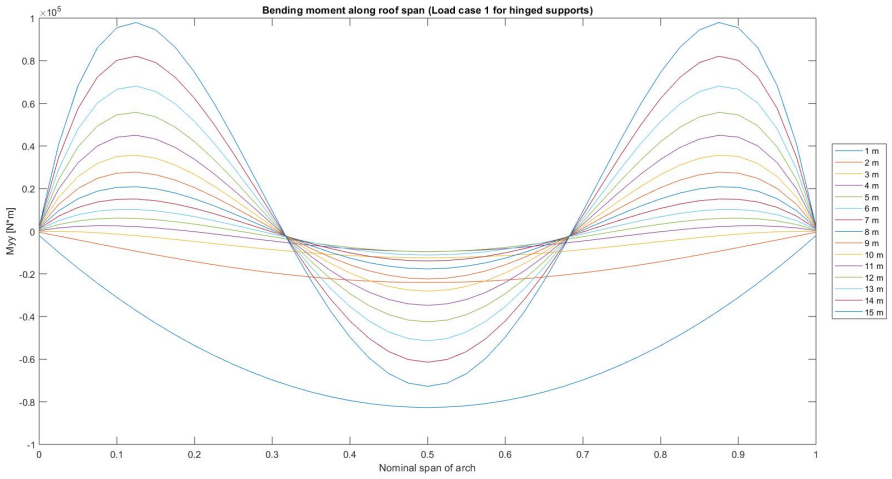

Figure C.4: Load case 1 for two-hinged arches

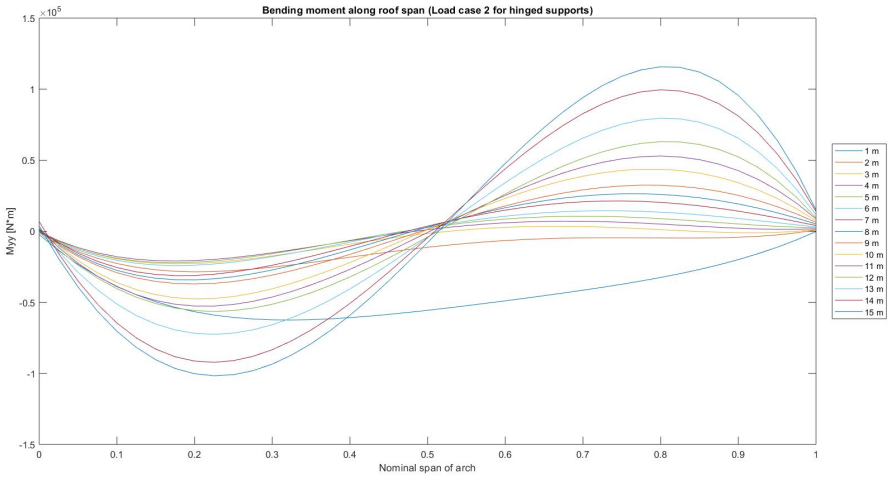

Figure C.5: Load case 2 for two-hinged arches

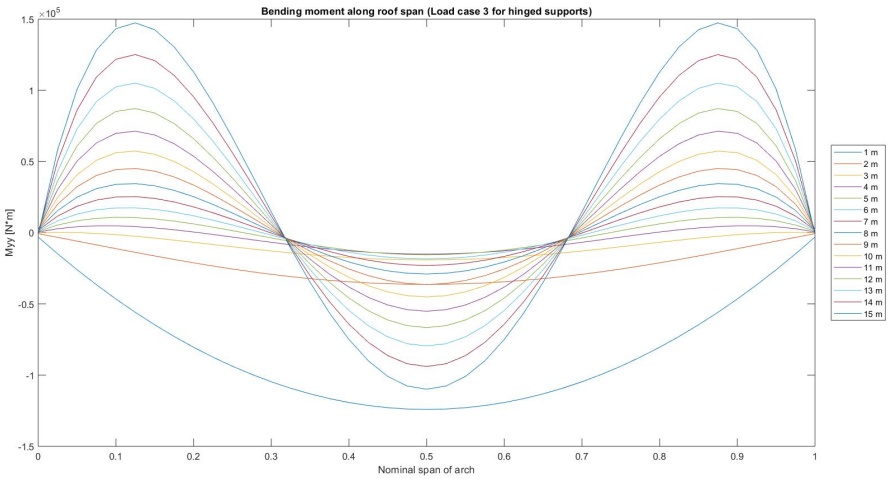

Figure C.6: Load case 3 for two-hinged arches

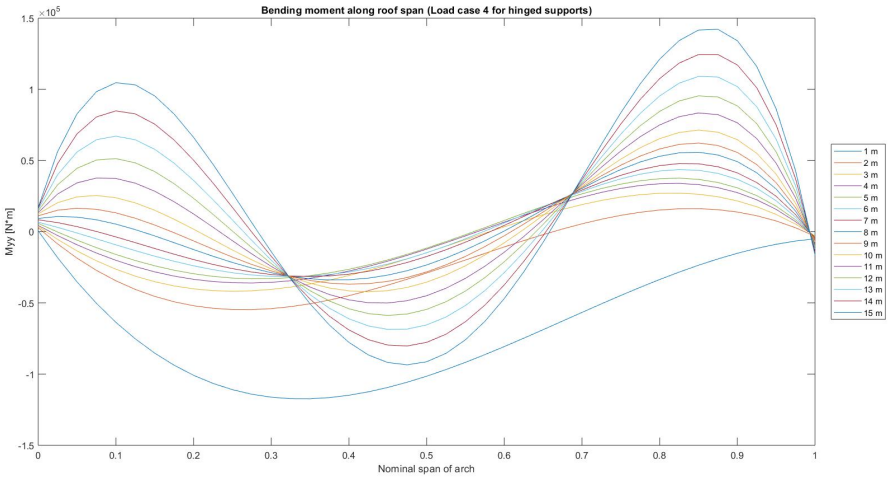

Figure C.7: Load case 4 for two-hinged arches

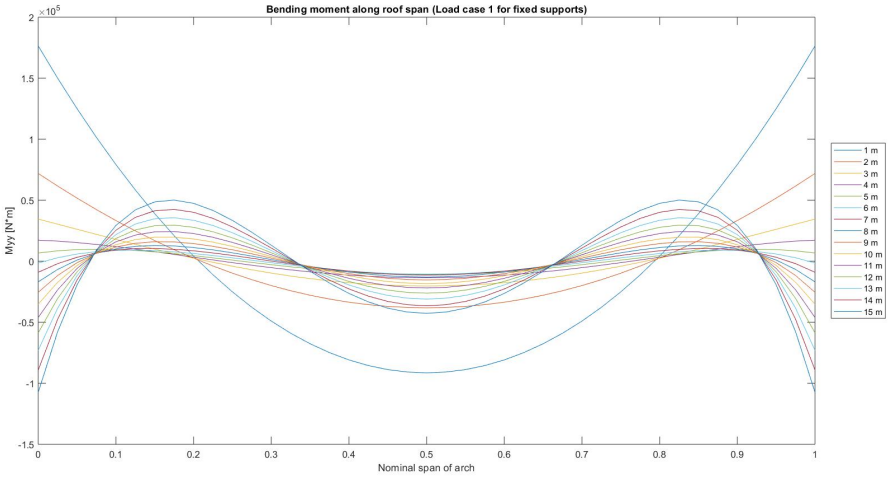

Figure C.8: Load case 1 for fixed arches

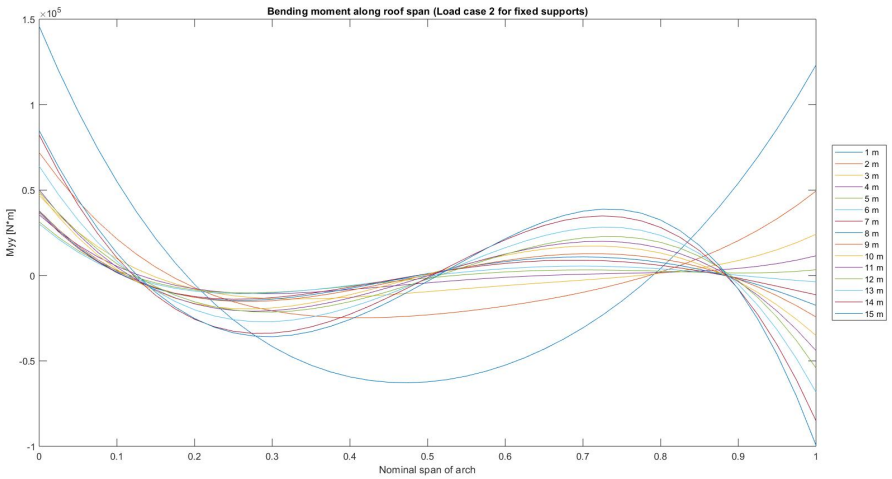

Figure C.9: Load case 2 for fixed arches

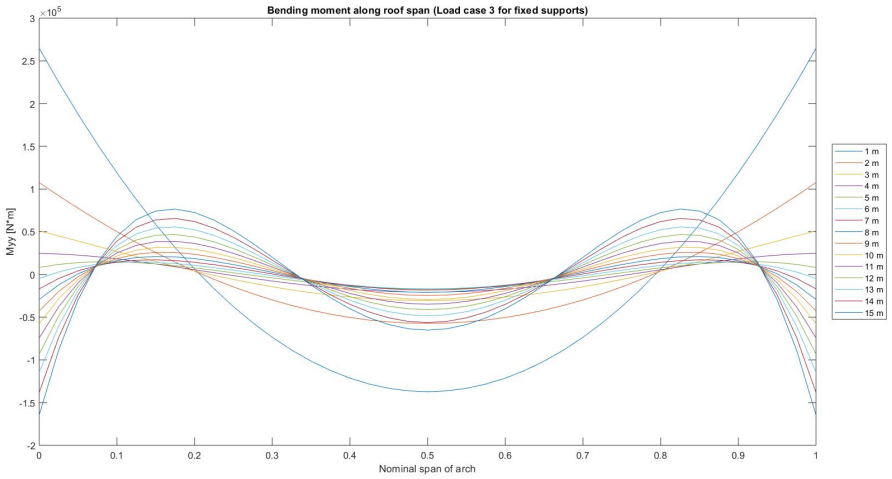

Figure C.10: Load case 3 for fixed arches

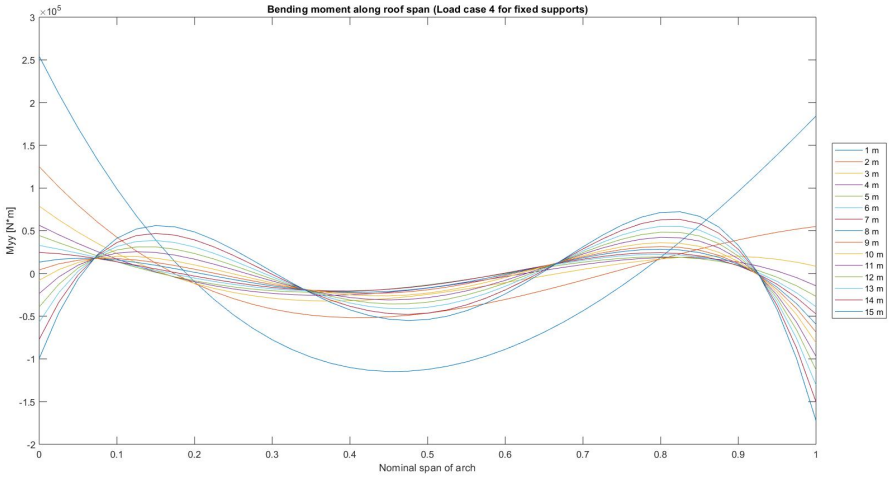

Figure C.11: Load case 4 for fixed arches

C.3. Internal axial forces of arches from GSA solutions

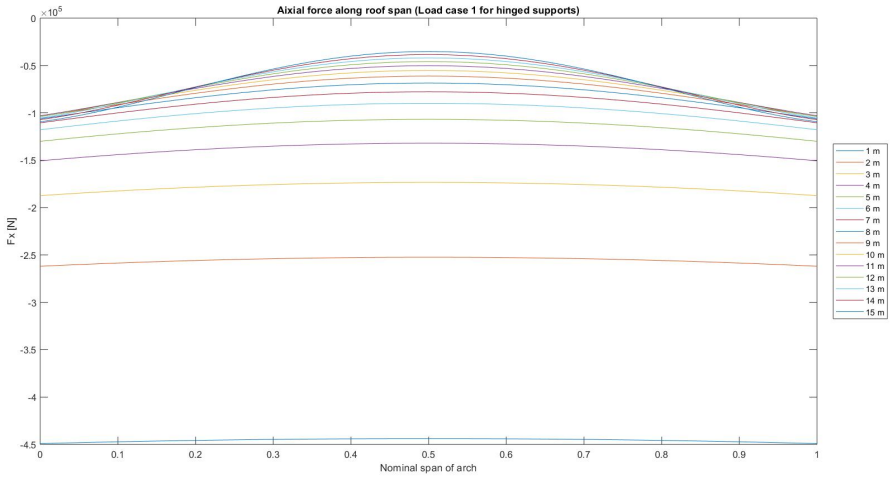

Figure C.12: Load case 1 for two-hinged arches

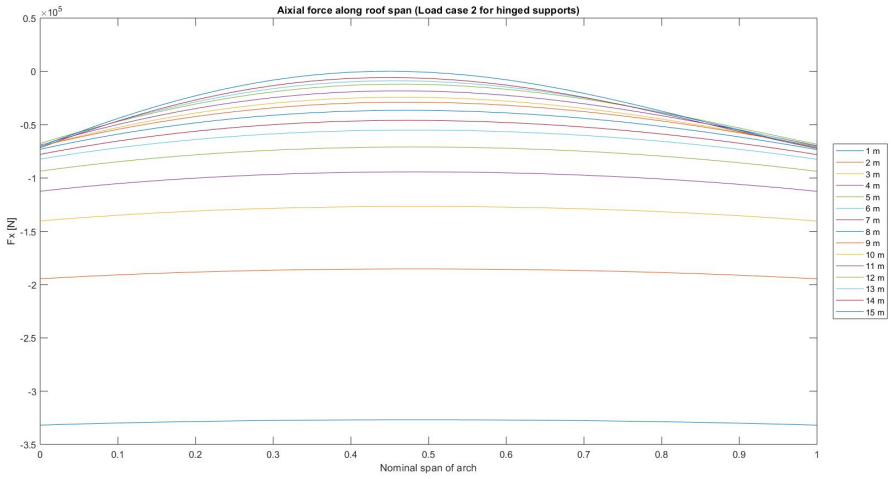

Figure C.13: Load case 2 for two-hinged arches

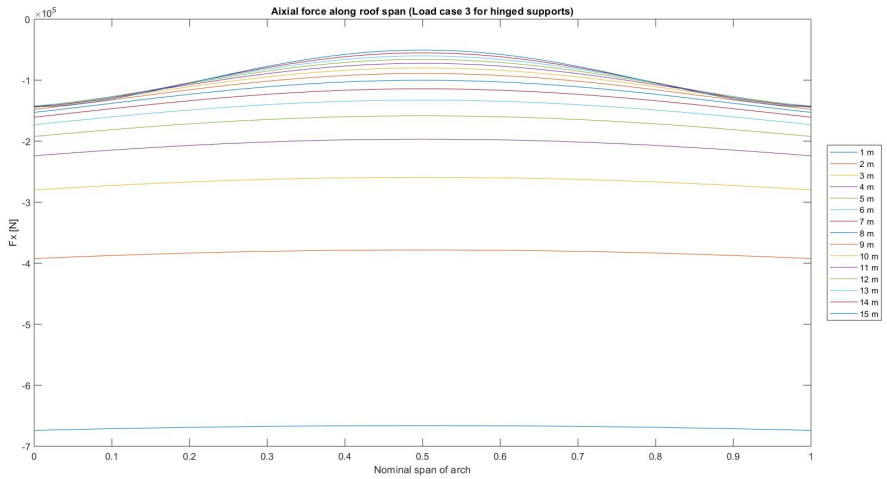

Figure C.14: Load case 3 for two-hinged arches

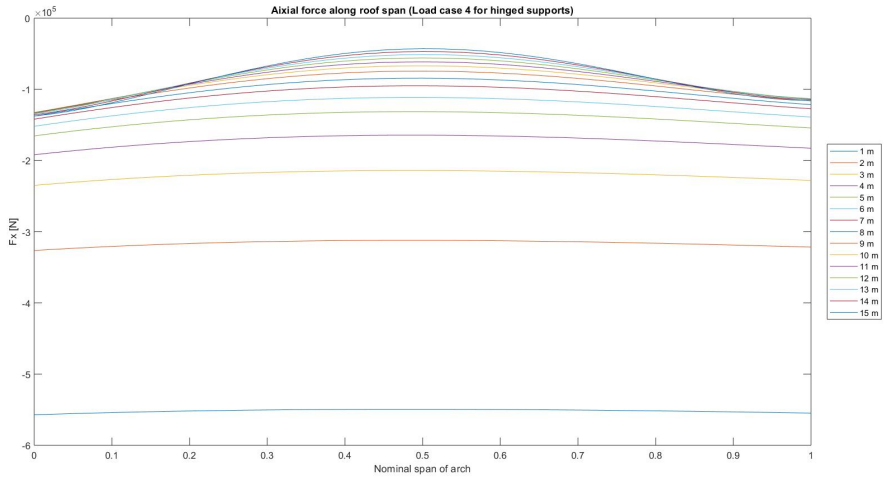

Figure C.15: Load case 4 for two-hinged arches

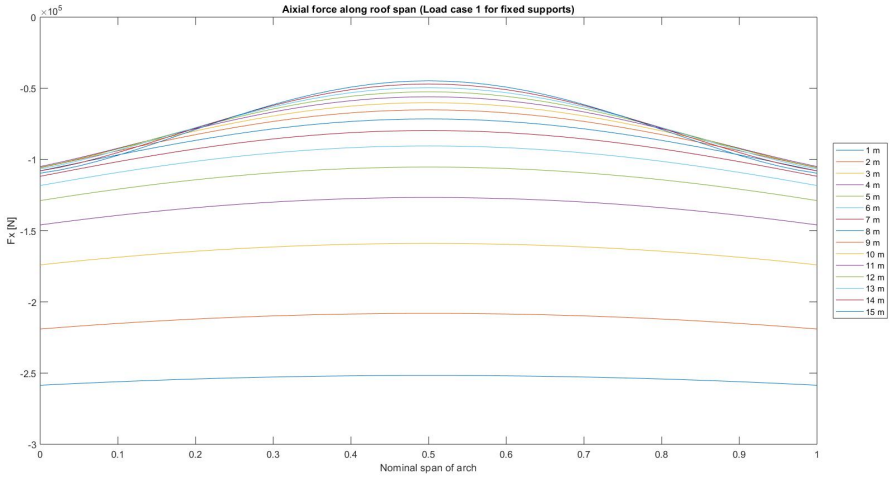

Figure C.16: Load case 1 for fixed arches

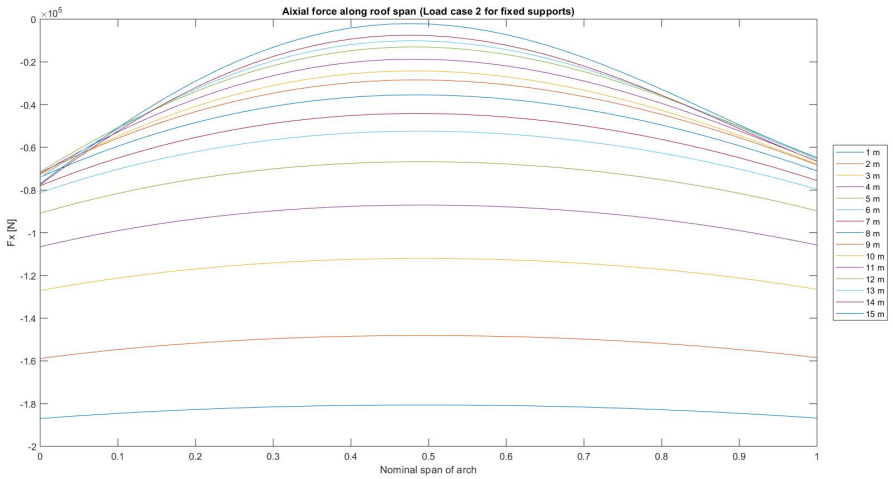

Figure C.17: Load case 2 for fixed arches

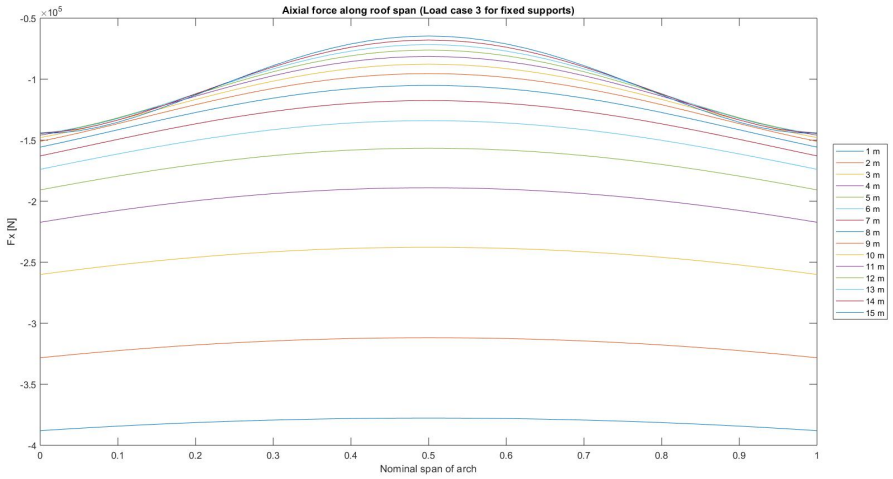

Figure C.18: Load case 3 for fixed arches

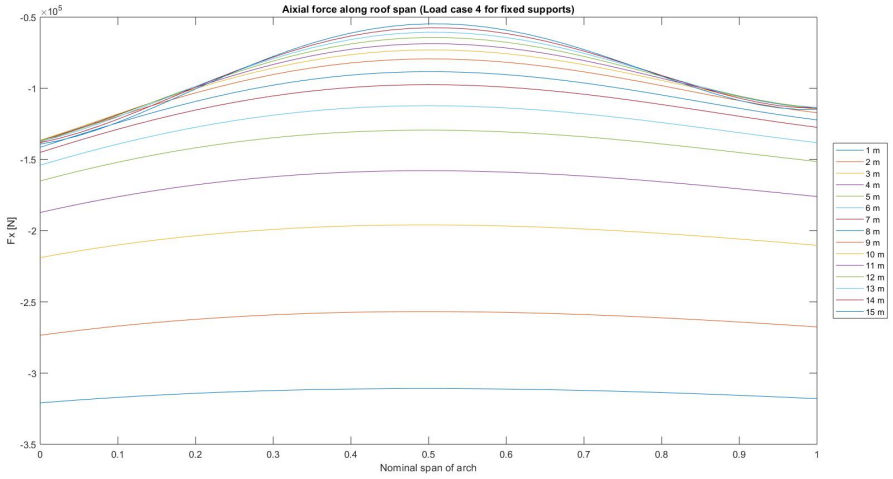

Figure C.19: Load case 4 for fixed arches

C.4. Plot of internal bending moment from GSA solution

```
for iSheet = 1:15
      s_array = xlsread('Moment case2.xlsx',iSheet);
      y = s_array(:,1);
      x = linspace(0,1,length(y))';
      p = polyfit(x,y,4);
      x2 = 0:.025:1;
      y2 = polyval(p,x2);
      plot(x2,y2);
      hold on;
end
 hold off
 xlabel('Nominal span of arch');
 ylabel('Myy [N*m]');
 legend('1 m','2 m','3 m','4 m','5 m','6 m','7 m','8 m','9 m','10 m',...
      '11 m','12 m','13 m','14 m','15 m','Location','eastoutside');
 title('Bending moment along roof span (Load case 2 for hinged supports)')
```

C.5. Plot of axial force from GSA solution

```
for iSheet = 1:15
      s_array = xlsread('Forces case2.xlsx',iSheet);
      y = s_array(:,1);
      x = linspace(0,1,length(y))';
      p = polyfit(x,y,4);
      x2 = 0:.025:1;
      y2 = polyval(p,x2);
      plot(x2,y2);
      hold on;
end
 hold off
 xlabel('Nominal span of arch');
 ylabel('Fx [N]');
 legend('1 m','2 m','3 m','4 m','5 m','6 m','7 m','8 m','9 m','10 m',...
      '11 m','12 m','13 m','14 m','15 m','Location','eastoutside');
 title('Aixial force along roof span (Load case 2 for hinged supports)')
```

C.6. Scatterbar plot1 of parametric component from Ansys solution

```
% for iSheet = 1:15
      x = xlsread('Components parametric.xlsx',3,'H37:H72');
      y = xlsread('Components parametric.xlsx',3,'I37:I72');
      z = xlsread('Components parametric.xlsx',3,'N37:N72');
      scatterbar3(x,y,z,0.01);
% end
%  hold off
 xlabel('1/4 length [m]');
 ylabel('Half height [m]');
 zlabel('Maximum principal stress [MPa]');
%  legend('1 m','2 m','3 m','4 m','5 m','6 m','7 m','8 m','9 m','10 m',...
%       '11 m','12 m','13 m','14 m','15 m','Location','eastoutside');
 title('Fixed supports under load case 4')
```

C.7. Scatterbar plot2 of parametric component from Ansys solution

```
% for iSheet = 1:15
      x = xlsread('Components parametric.xlsx',4,'H37:H72');
      y = xlsread('Components parametric.xlsx',4,'I37:I72');
      z = xlsread('Components parametric.xlsx',4,'N37:N72');
      scatterbar3(x,y,z,0.01);
% end
%  hold off
  xlabel('1/4 length [m]');
  ylabel('Half height [m]');
  zlabel('Maximum principal stress [MPa]');
%  legend('1 m','2 m','3 m','4 m','5 m','6 m','7 m','8 m','9 m','10 m',...
%       '11 m','12 m','13 m','14 m','15 m','Location','eastoutside');
  title('Hinge supports under load case 2')
```

C.8. Height/span ratio parametric study results plot

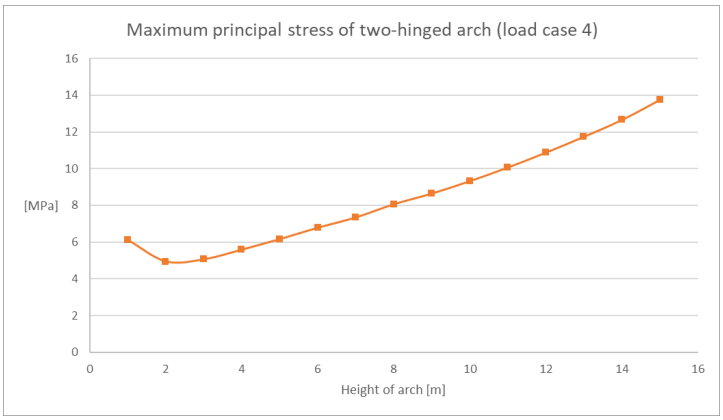

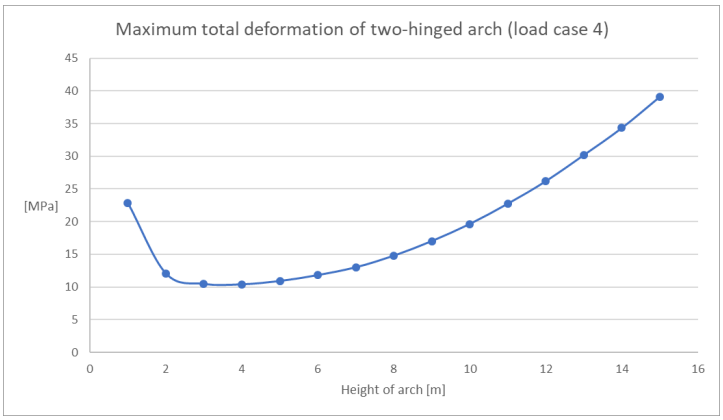


Normal stress maximum of two-hinged arch (load case 4)
[MPa]
0
2
4
6
8
10
12
14
16
Height of arch [m]

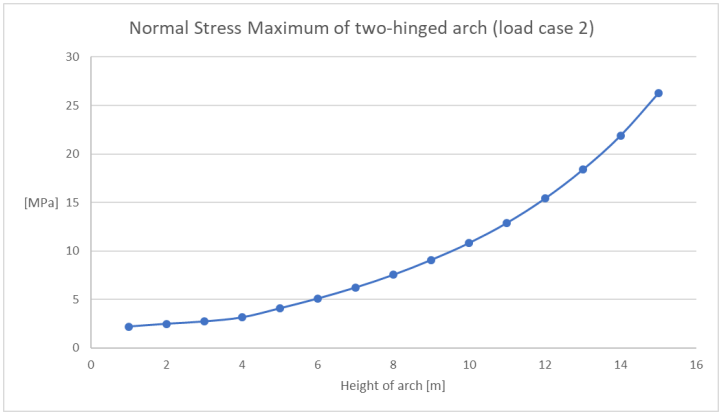
Normal Stress Maximum of two-hinged arch (load case 2)
[MPa]
0
5
10
15
20
25
30
Height of arch [m]

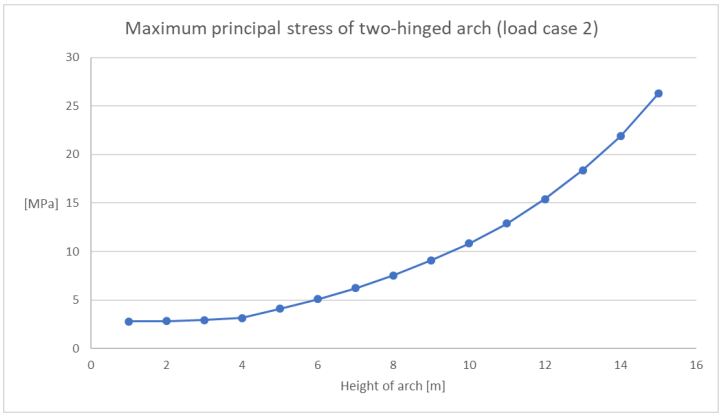
Maximum principal stress of two-hinged arch (load case 2)
[MPa]
0
5
10
15
20
25
30
Height of arch [m]

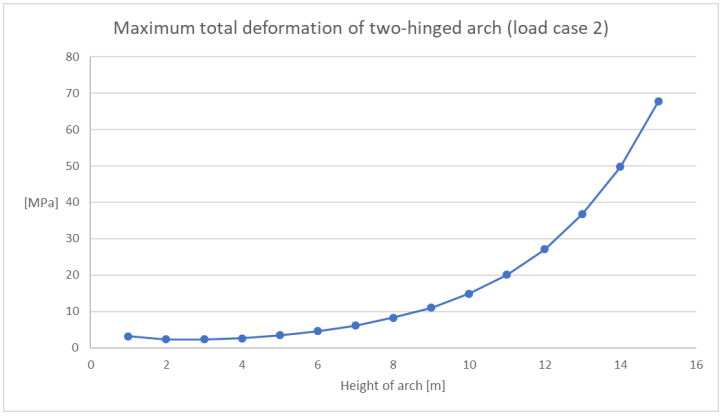
Maximum total deformation of two-hinged arch (load case 2)
[MPa]
0
10
20
30
40
50
60
70
80
Height of arch [m]

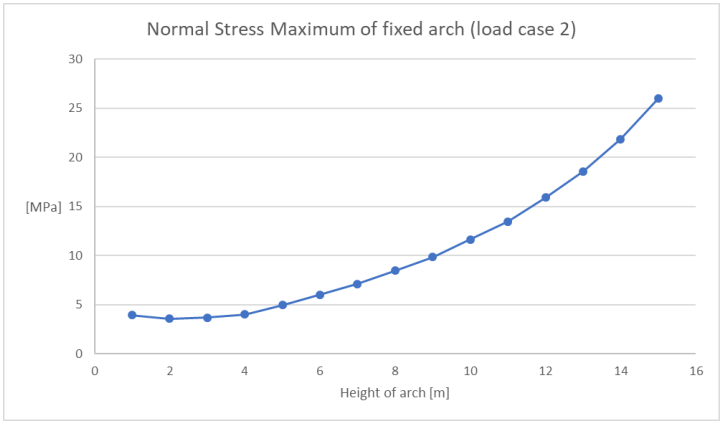
Normal Stress Maximum of fixed arch (load case 2)
[MPa]
Height of arch [m]

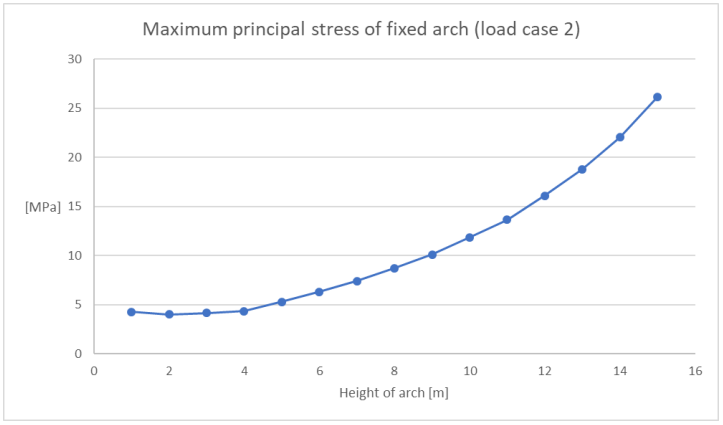
Maximum principal stress of fixed arch (load case 2)
[MPa]
Height of arch [m]

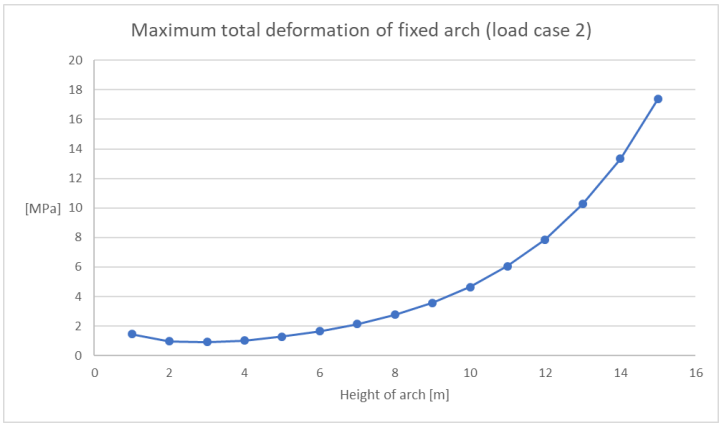
Maximum total deformation of fixed arch (load case 2)
[MPa]
Height of arch [m]

C.9. Cross section parametric study results plot

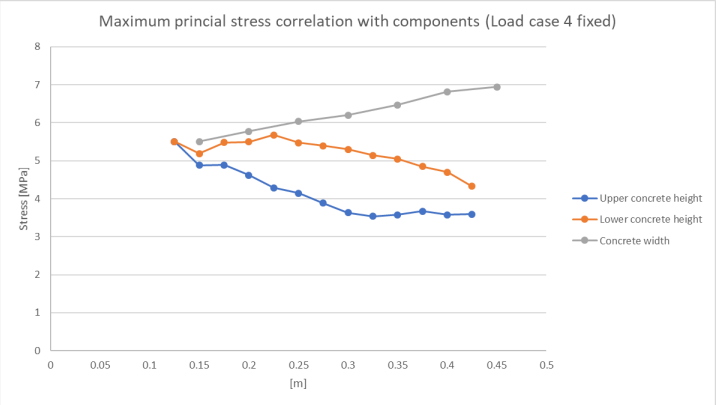

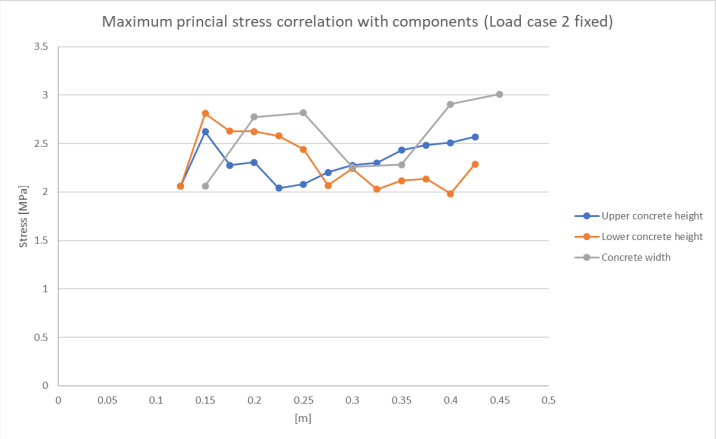

C.10. Correlation curves

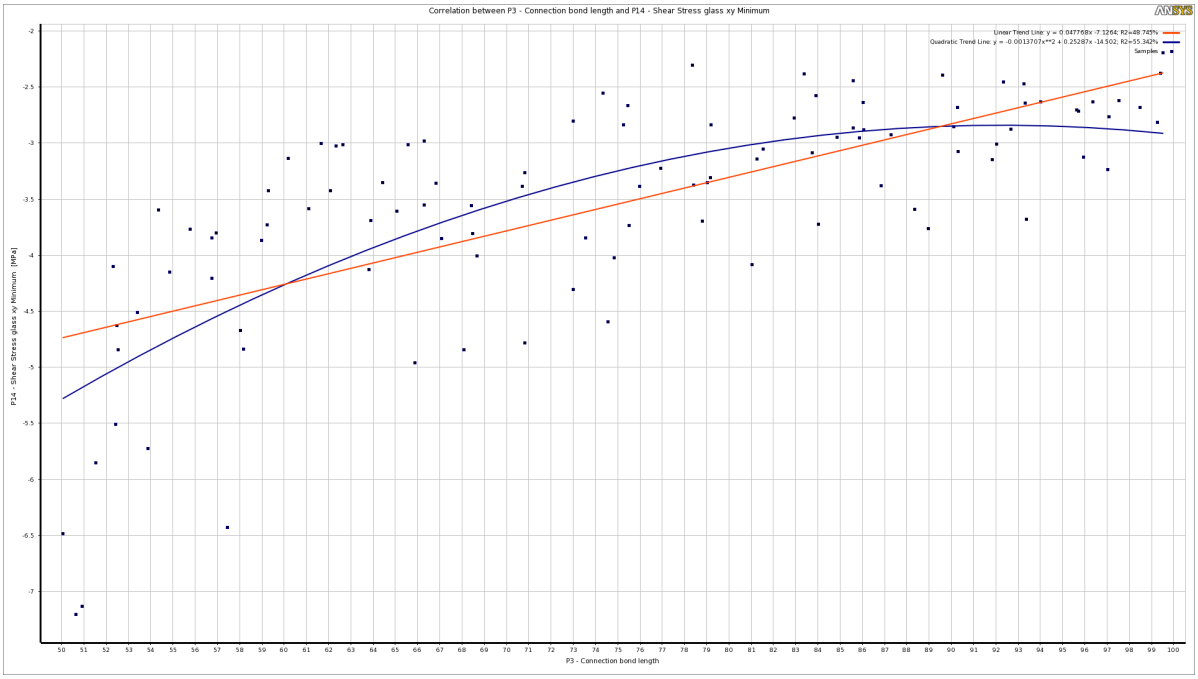
Correlation between P3 - Connection bond length and P14 - Shear Stress glass xy Minimum
Linear Trend Line: y = 0.04776Bx -7.1264; R2=48.745%
Quadratic Trend Line: y = -0.0013707x**2 + 0.25287x -14.502; R2=55.342%
Samples
P14 - Shear Stress glass xy Minimum [MPa]
P3 - Connection bond length

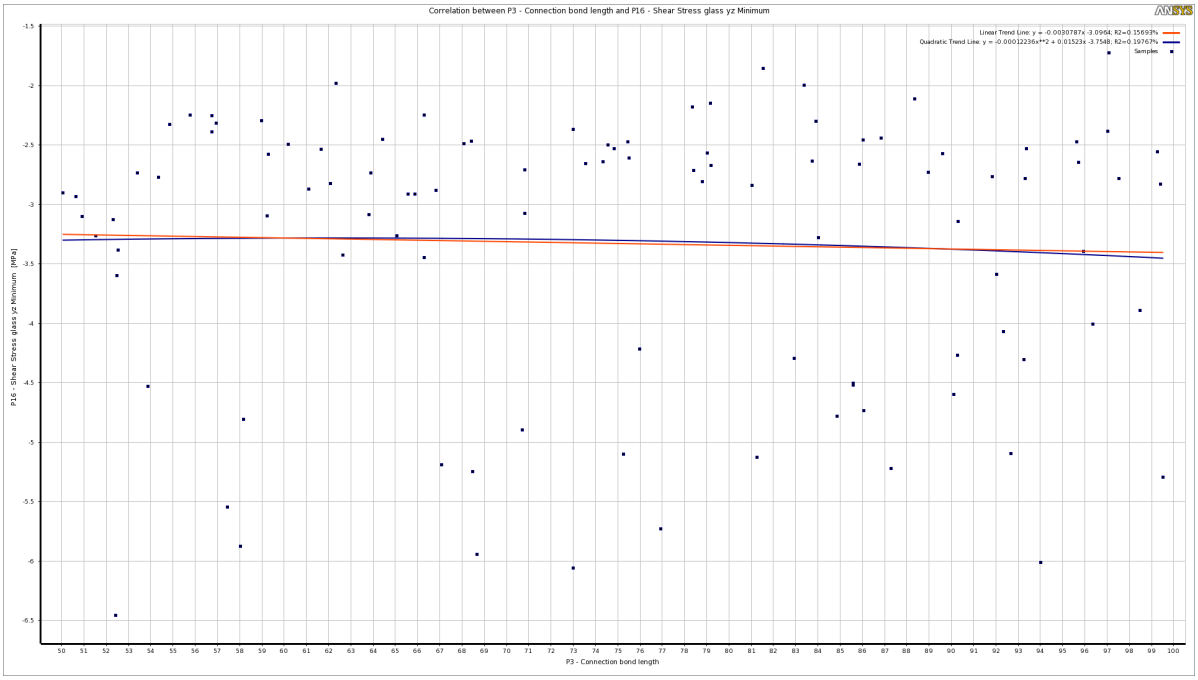
Correlation between P3 - Connection bond length and P16 - Shear Stress glass yz Minimum
Linear Trend Line: y = -0.0030787x -3.0994; R2=0.15693%
Quadratic Trend Line: y = -0.00012236x**2 + 0.01523x -3.7548; R2=0.19767%
Samples
P16 - Shear Stress glass yz Minimum [MPa]
P3 - Connection bond length

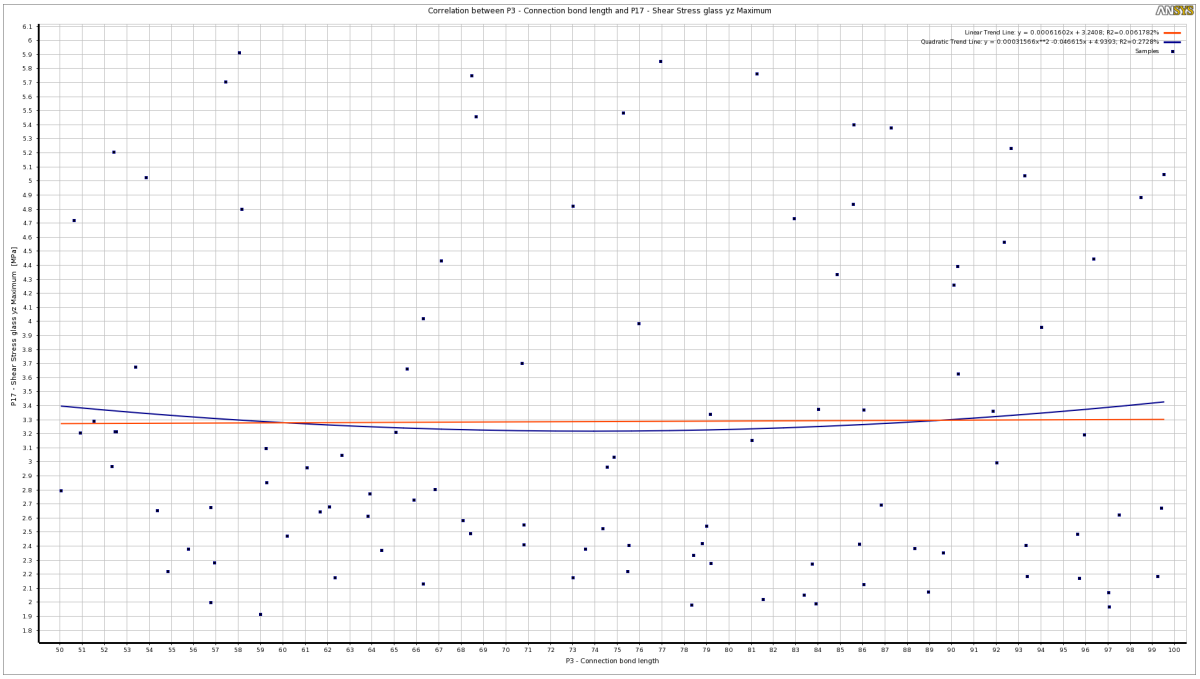
Correlation between P3 - Connection bond length and P17 - Shear Stress glass yz Maximum
Linear Trend Line: y = 0.00061602x + 3.2408; R2=0.0061782%
Quadratic Trend Line: y = 0.00031566x**2 -0.046615x + 4.9393; R2=0.2728%
Samples
P17 - Shear Stress glass yz Maximum [MPa]
P3 - Connection bond length

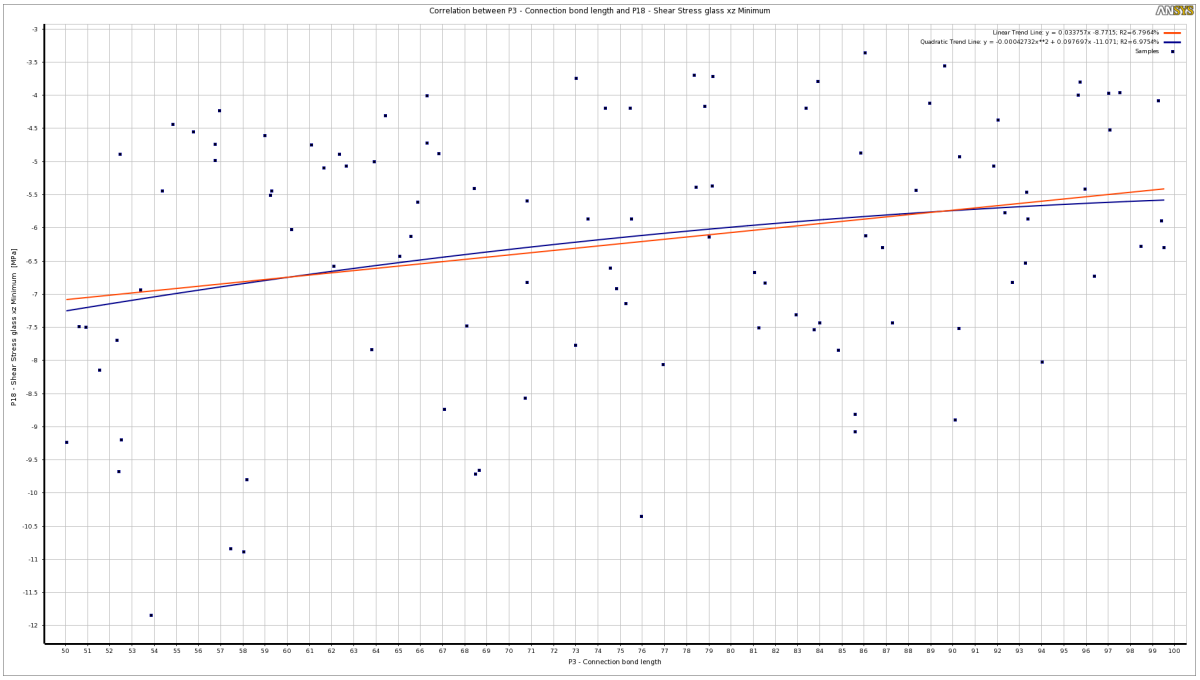
Correlation between P3 - Connection bond length and P18 - Shear Stress glass xz Minimum
Linear Trend Line: y = 0.033757x -8.7715; R2=6.7964%
Quadratic Trend Line: y = -0.00042732x**2 + 0.097697x -11.071; R2=6.9754%
Samples
P18 - Shear Stress glass xz Minimum [MPa]
P3 - Connection bond length

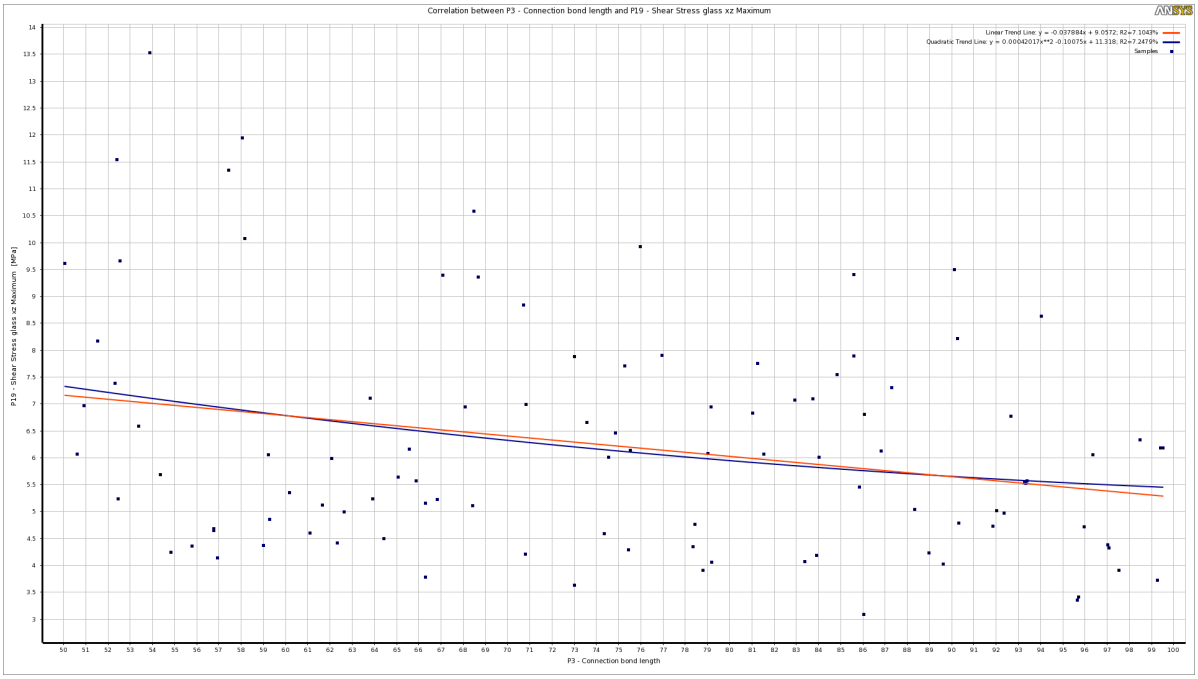
Correlation between P3 - Connection bond length and P19 - Shear Stress glass xz Maximum
Linear Trend Line: y = -0.037884x + 9.0572; R2=7.1043%
Quadratic Trend Line: y = 0.00042017x**2 -0.10075x + 11.318; R2=7.2478%
Samples
P19 - Shear Stress glass xz Maximum [MPa]
P3 - Connection bond length

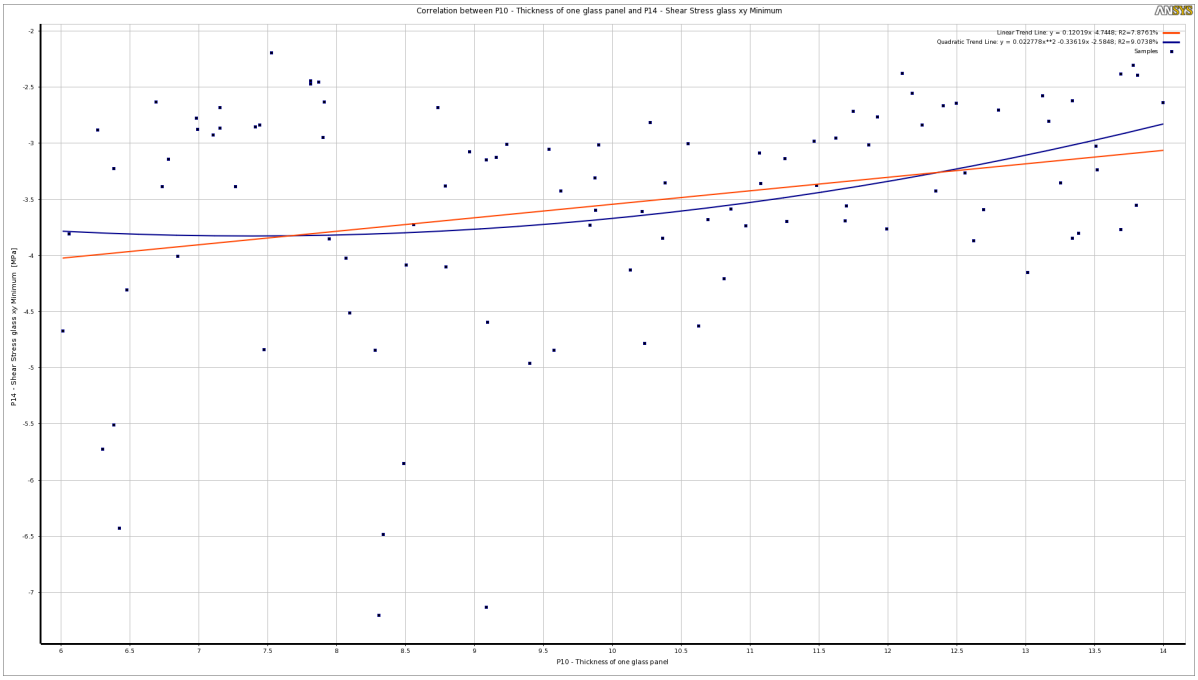
Correlation between P10 - Thickness of one glass panel and P14 - Shear Stress glass xy Minimum
Linear Trend Line: y = 0.12019x -4.7448; R2=7.8761%
Quadratic Trend Line: y = 0.022778x**2 -0.33619x -2.5848; R2=9.0738%
Samples
P14 - Shear Stress glass xy Minimum [MPa]
P10 - Thickness of one glass panel

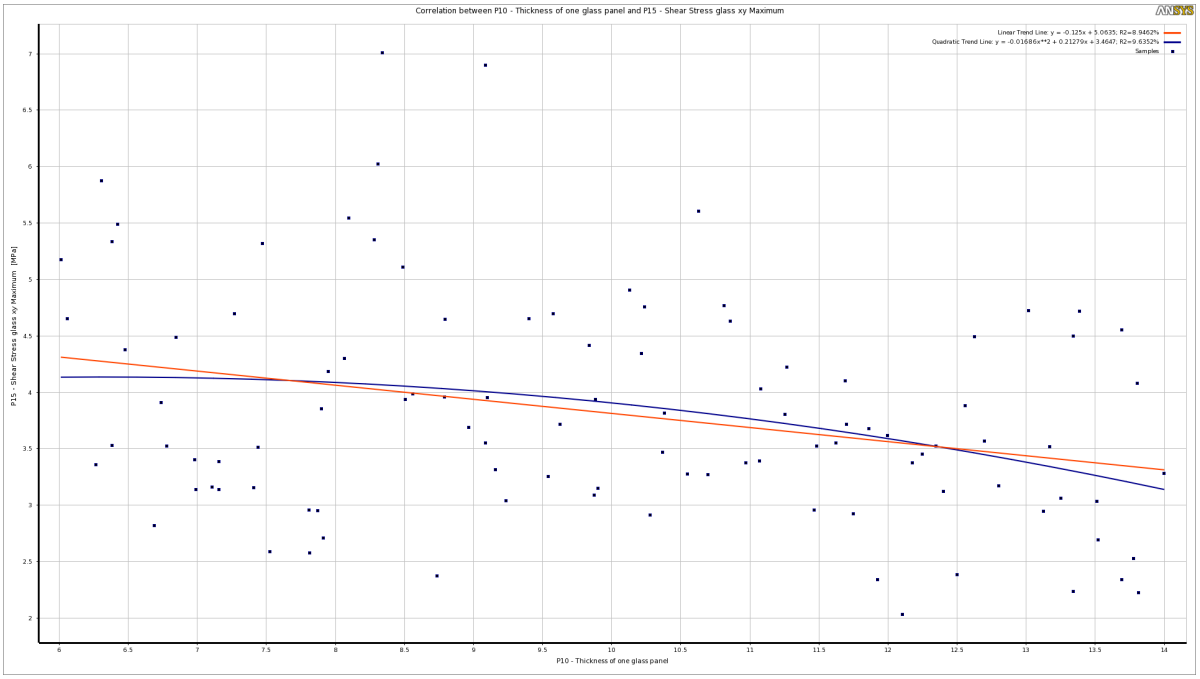
Correlation between P10 - Thickness of one glass panel and P15 - Shear Stress glass xy Maximum
Linear Trend Line: y = -0.125x + 5.0635; R2=8.9462%
Quadratic Trend Line: y = -0.01686x**2 + 0.21279x + 3.4647; R2=9.6352%
Samples
P15 - Shear Stress glass xy Maximum [MPa]
P10 - Thickness of one glass panel

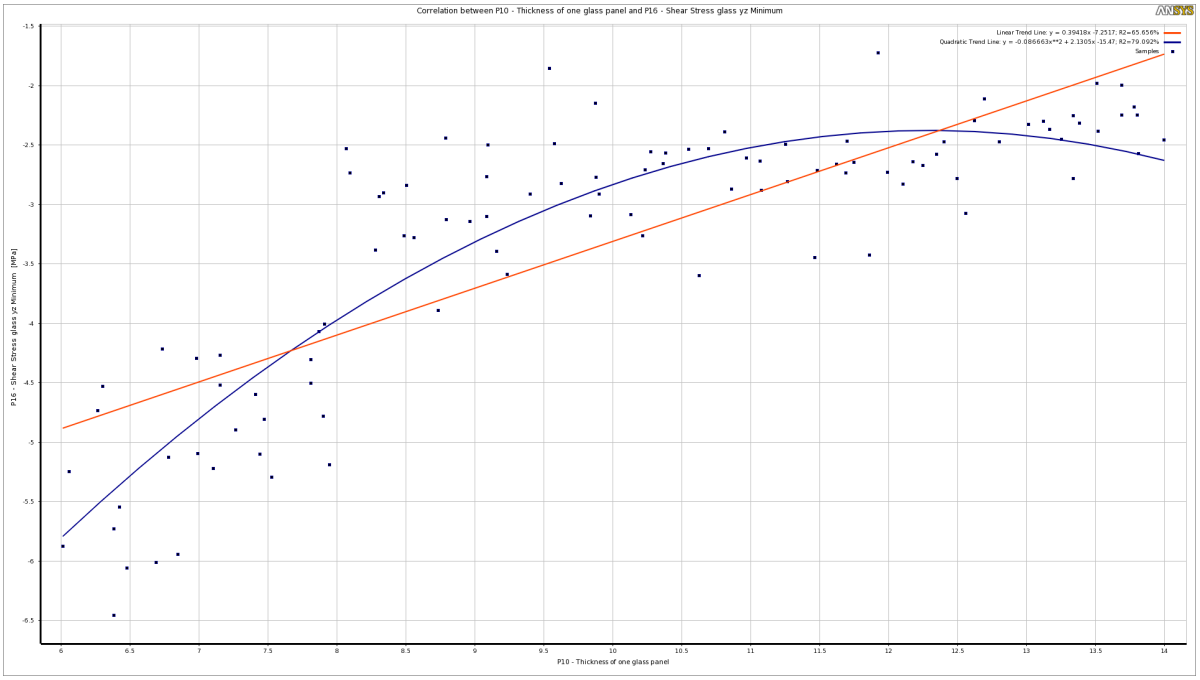
Correlation between P10 - Thickness of one glass panel and P16 - Shear Stress glass yz Minimum
Linear Trend Line: y = 0.39418x -7.2517; R2=65.656%
Quadratic Trend Line: y = -0.086663x**2 + 2.1305x -15.47; R2=79.092%
Samples
P16 - Shear Stress glass yz Minimum [MPa]
P10 - Thickness of one glass panel

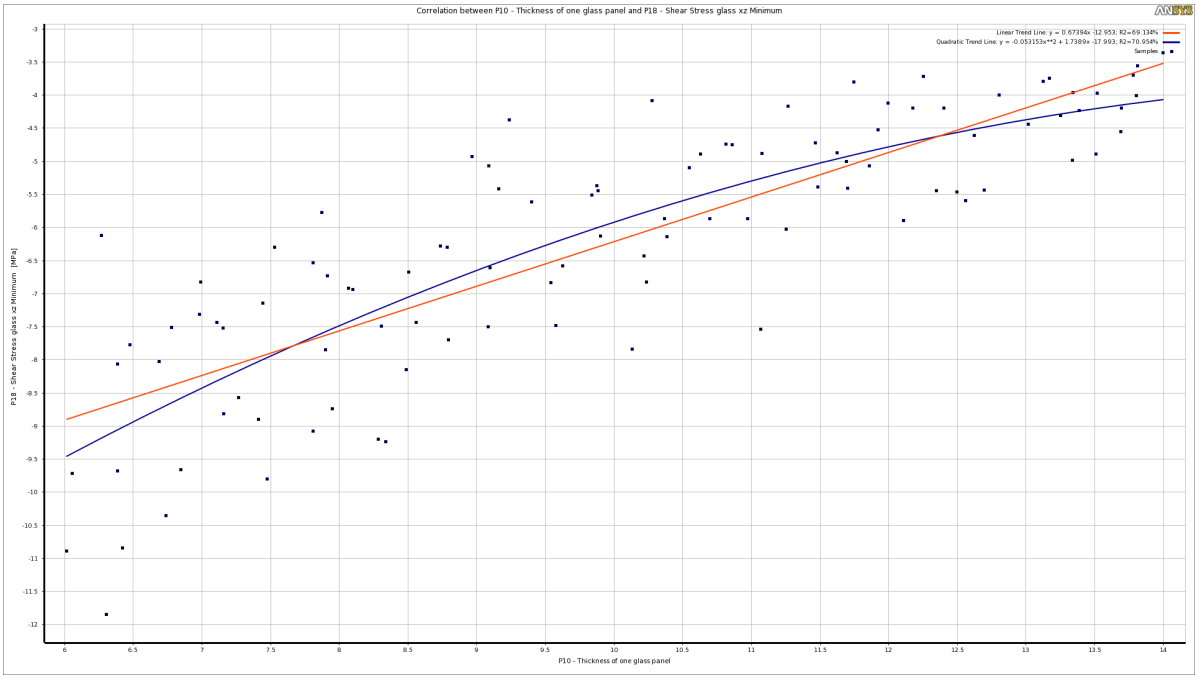
Correlation between P10 - Thickness of one glass panel and P18 - Shear Stress glass xz Minimum
Linear Trend Line: y = 0.6739*x -12.953; R2=69.134%
Quadratic Trend Line: y = -0.053153x**2 + 1.7389x -17.993; R2=70.954%
Samples
P18 - Shear Stress glass xz Minimum [MPa]
P10 - Thickness of one glass panel

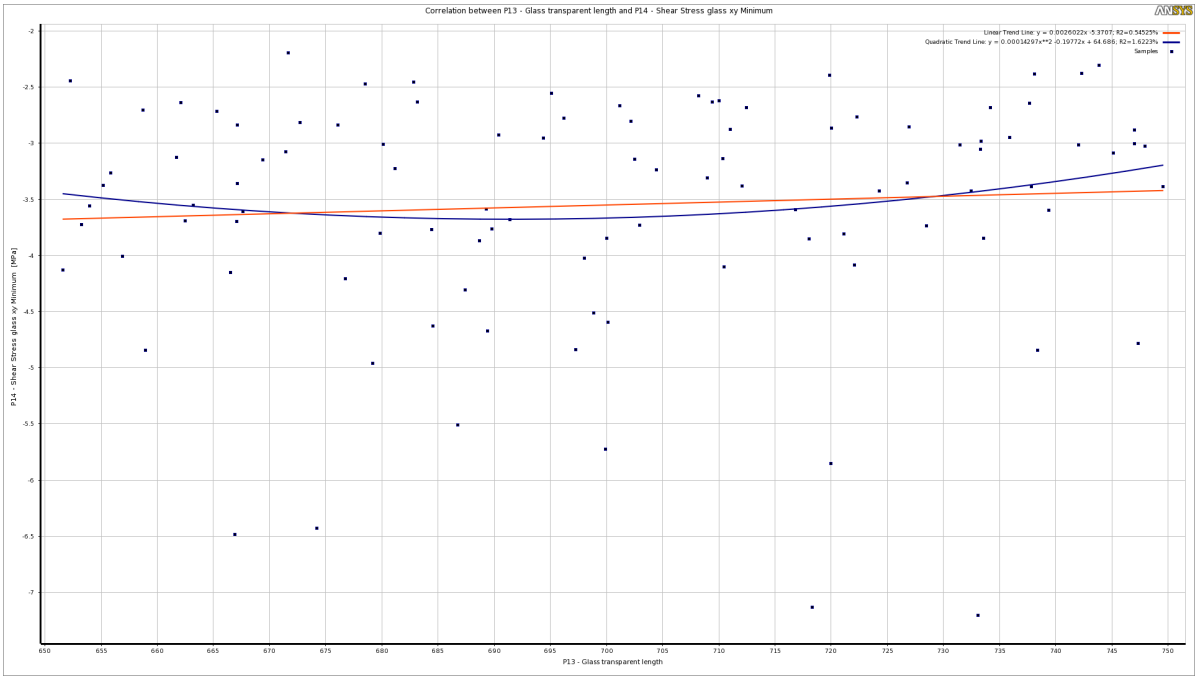
Correlation between P13 - Glass transparent length and P14 - Shear Stress glass xy Minimum
Linear Trend Line: y = 0.0026022x -5.3707; R2=0.54525%
Quadratic Trend Line: y = 0.00014297x**2 -0.19772x + 64.686; R2=1.6223%
Samples
P14 - Shear Stress glass xy Minimum [MPa]
P13 - Glass transparent length

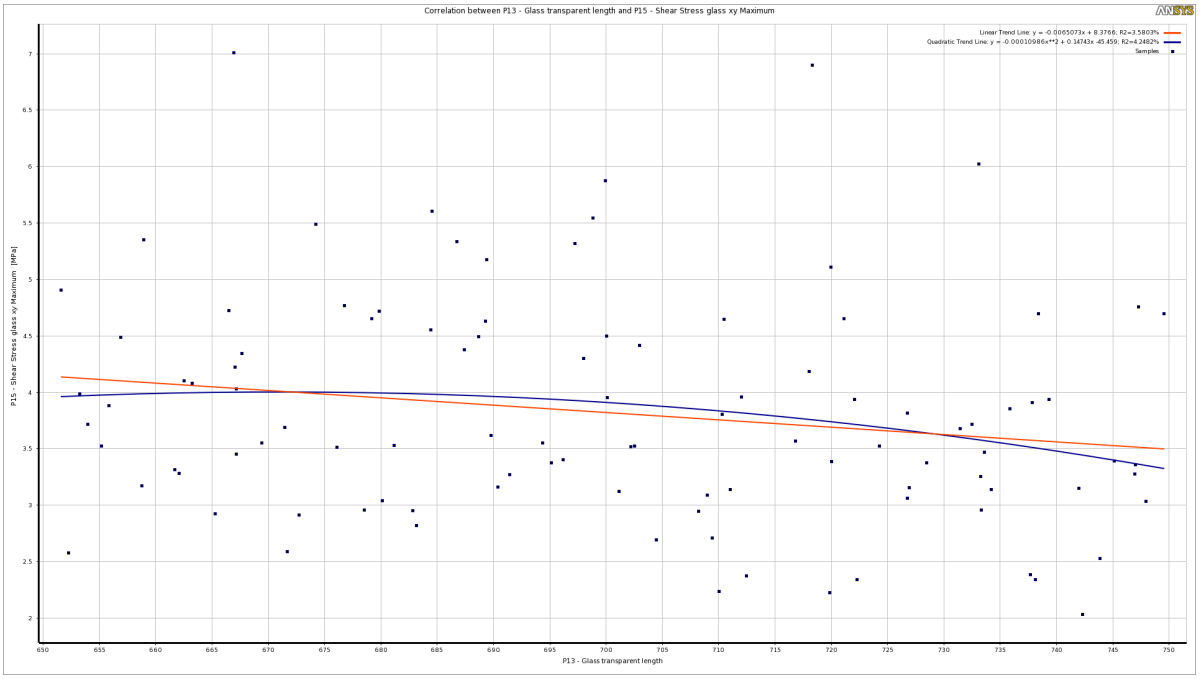
Correlation between P13 - Glass transparent length and P15 - Shear Stress glass xy Maximum
Linear Trend Line: y = -0.0065073x + 8.3766; R2=3.5803%
Quadratic Trend Line: y = -0.00010986x**2 + 0.14743x -45.459; R2=4.2482%
Samples
P15 - Shear Stress glass xy Maximum [MPa]
P13 - Glass transparent length

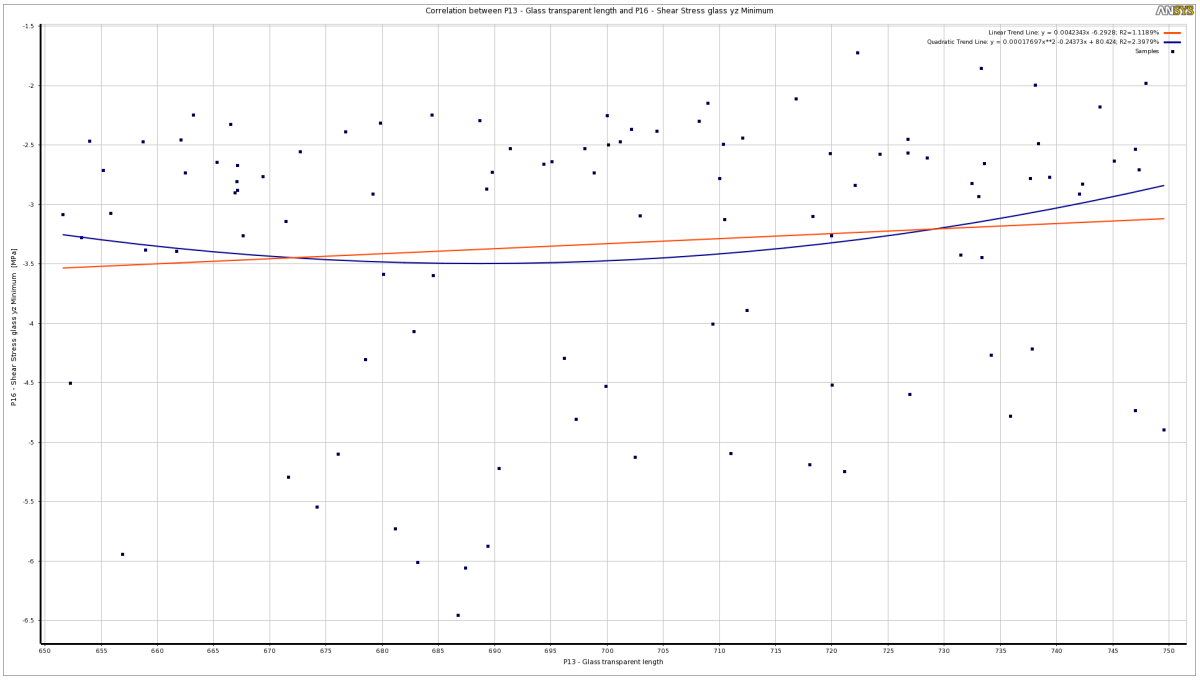
Correlation between P13 - Glass transparent length and P16 - Shear Stress glass yz Minimum
Linear Trend Line: y = 0.0042343x -6.2928; R2=1.1189%
Quadratic Trend Line: y = 0.00017697x**2 -0.24373x + 80.424; R2=2.3979%
Samples
P16 - Shear Stress glass yz Minimum [MPa]
P13 - Glass transparent length

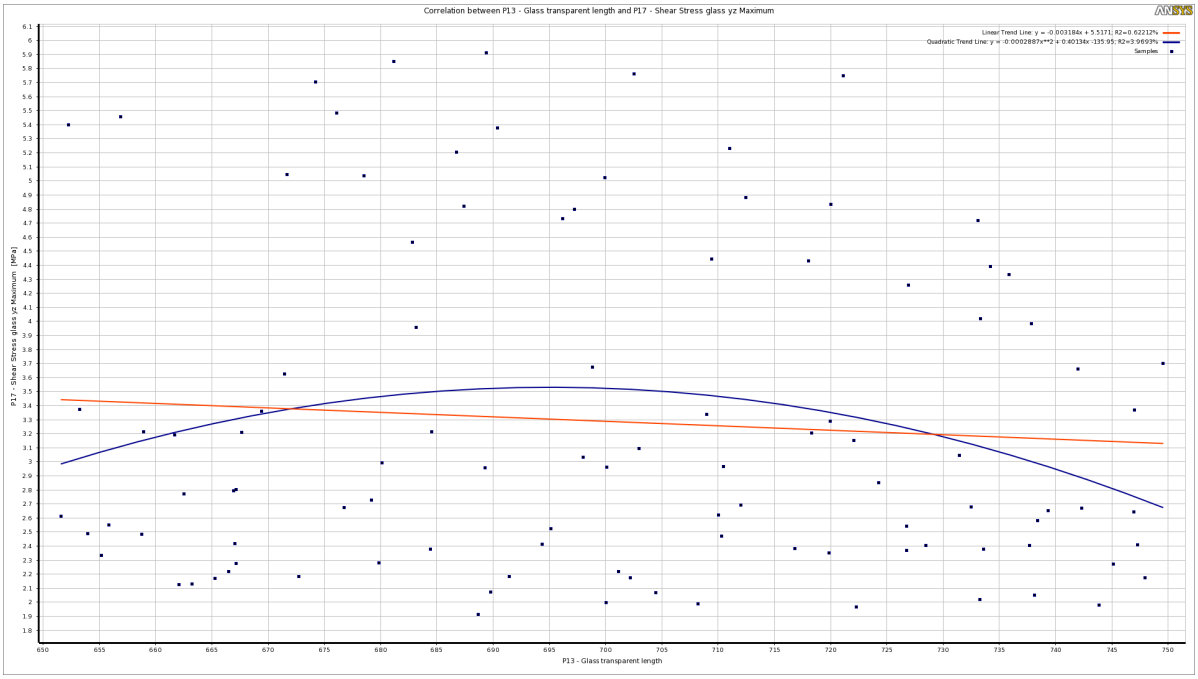
Correlation between P13 - Glass transparent length and P17 - Shear Stress glass yz Maximum
Linear Trend Line: y = -0.003184x + 5.5171; R2=0.62212%
Quadratic Trend Line: y = -0.0002887x**2 + 0.40134x -135.95; R2=3.9693%
Samples
P17 - Shear Stress glass yz Maximum [MPa]
P13 - Glass transparent length

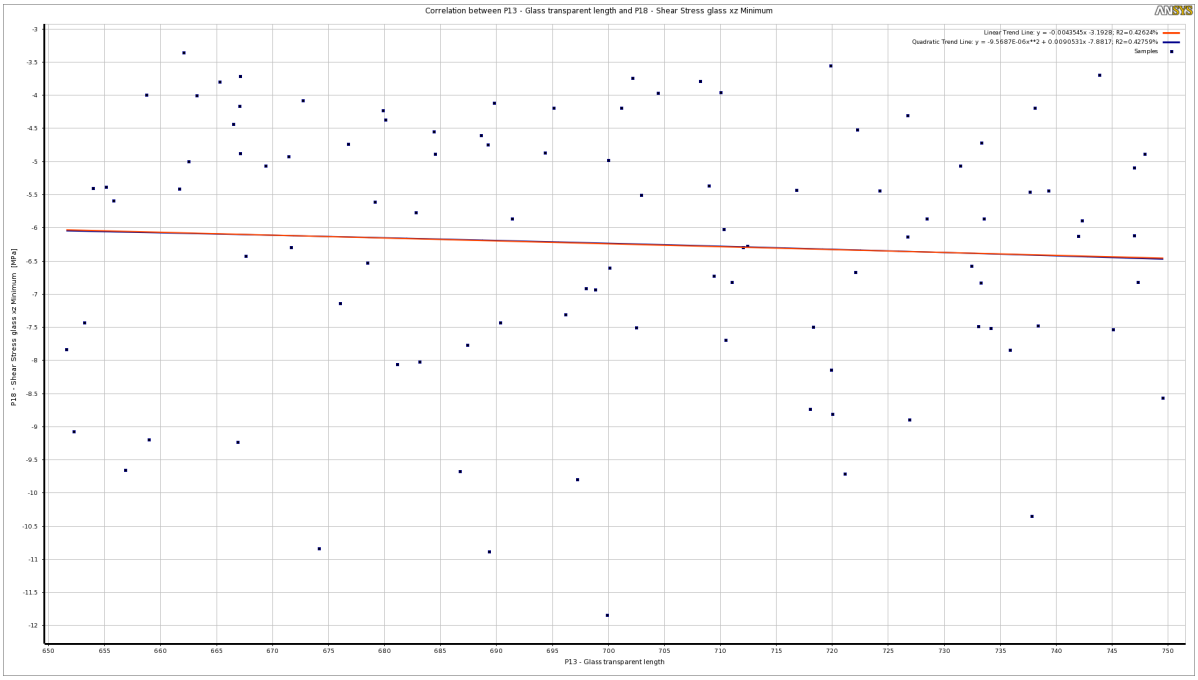
Correlation between P13 - Glass transparent length and P18 - Shear Stress glass xz Minimum
Linear Trend Line: y = -0.0043545x -3.1928; R2=0.42624%
Quadratic Trend Line: y = -9.5687E-06x**2 + 0.0090531x -7.8817; R2=0.42759%
Samples
P18 - Shear Stress glass xz Minimum [MPa]
P13 - Glass transparent length

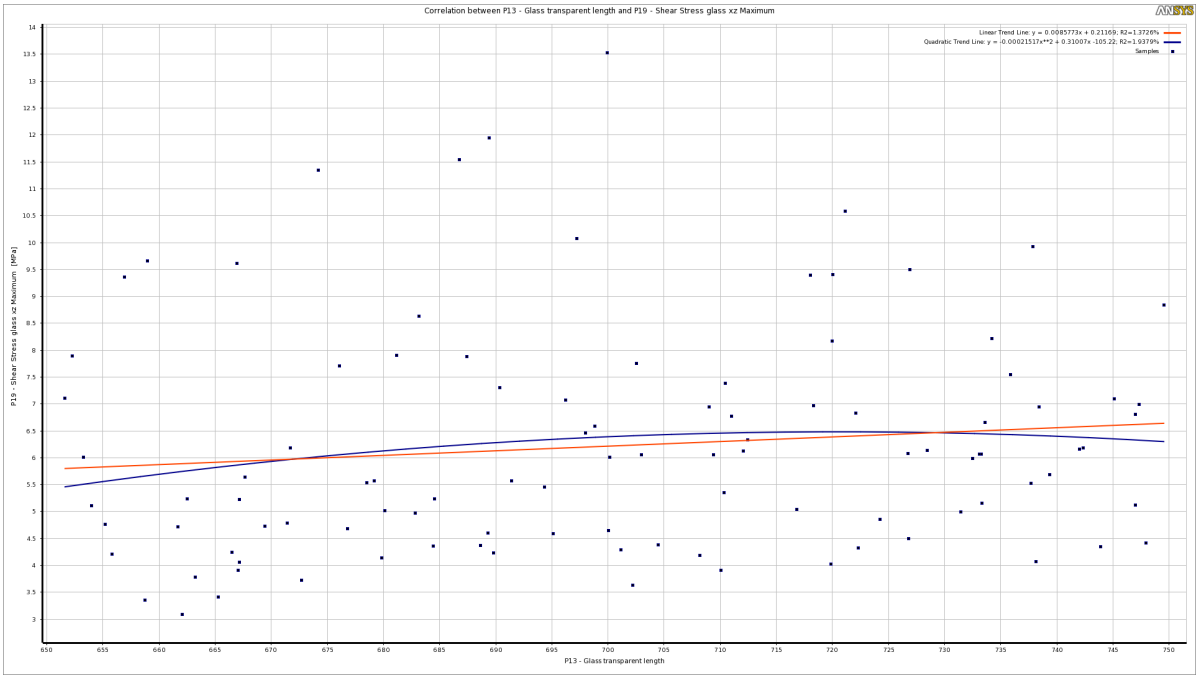
Correlation between P13 - Glass transparent length and P19 - Shear Stress glass xz Maximum
Linear Trend Line: y = 0.0085773x + 0.21169; R2=1.3726%
Quadratic Trend Line: y = -0.00021517x**2 + 0.31007x -105.22; R2=1.9379%
Samples
P19 - Shear Stress glass xz Maximum (MPa)
P13 - Glass transparent length

Bibliography

Sarath Chandra Kumar Bendapudi and P Saha. Contribution of fly ash to the properties of mortar and concrete. *Int J Earth Sci Eng*, 4(06):1017–1023, 2011.

Walairat Bumrongjaroen, Isabelle Muller, Jeffrey Schweitzer, and Richard A Livingston. Application of glass corrosion tests to the reactivity of fly ash. *Northern Kentucky (KY): World of Coal Ash (WOCA)*, 2007.

Paulo L Carvalho, Paulo JS Cruz, and Frederic A Veer. Connecting through the reinforcement - design, testing and construction of a folded reinforced glass structure. *Journal of Facade Design and Engineering*, 2(1-2):109–122, 2014. ISSN 2213-302X.

Sirisala Chandrusha, G Mahaboob Basha, and Shaik Rehana Begum. Behavior of concrete by using waste glass powder and fly ash as a partial replacement of cement. *International Journal of Engineering Science*, 15562, 2017.

Robert E Chapman and Muthiah Kasi. Benefits of using astm building economics standards for the design, construction, and operation of constructed facilities. Report, 2012.

PJS Cruz and I Valente. Experimental analysis on steel reinforced glass beams at different. In *COST Action TU0905 Mid-term Conference on Structural Glass*, page 261. CRC Press. ISBN 1138000442.

Bendz Dale. P. simulation studies of the effects of mineral admixtures on the cement paste-aggregate interfacial zone/p. bendz dale, j. garfodzi edward. *ACI Materials Journal*, 88(8):518–529, 1991.

Institution of Structural Engineers and Institution of Structural Engineers . *Guide to the Structural Use of Adhesives*. Institution of Structural Engineers, 1999. ISBN 9781874266433. URL `https://books.google.nl/books?id=DLW1AAAACAAJ`.

Bernhard Freytag. Glass-concrete composite technology. *Structural Engineering International*, 14(2): 111–117, 2004. ISSN 1016-8664.

Matthias Haldimann, Andreas Luible, and Mauro Overend. *Structural use of glass*, volume 10. Iabse, 2008. ISBN 3857481196.

Frank Kaltenbach. *Translucent materials: glass, plastics, metals*. Walter de Gruyter, 2004. ISBN 3034614322.

PC Louter, JF van Heusden, FA Veer, JNJA Vambersky, HR De Boer, Versteegen, J , and Pieters Bouwtechniek Delft. Post-tensioned glass beams. *Fracture of Nano and Engineering Materials and Structures nd*, 597(8), 2006.

Josef J Ludwig and H-U Weiler. Tragstrukturen aus glas am beispiel einer ganzglastonneschalenkonstruktion ohne tragende stahlunterkonstruktion am maximilianmuseum in augsburg. *Bautechnik*, 77(4):246–249, 2000. ISSN 1437-0999.

Vuk Milošević, Nikola Milošević, and Bojan Milošević. Thrust line dependence on the load and sag. *Journal of faculty of civil engineering ; contemporary achievements in civilengineering*, 25:365–370, 2014.

Philipp Molter and Tina Wolf. Glass-shaping techniques in building construction. *Detail*, pages 178–183, 2011.

Thomas Nelson and Erke Wang. Reliable fe-modeling with ansys. In *International ANSYS Conference*, page 93.

NEN-EN 12390-1. Testing hardened concrete - part 1: Shape, dimensions and other requirements for specimens and moulds. Standard, 2012.

NEN-EN 12390-3. Testing hardened concrete - part 3: Compressive strength of test specimens. Standard, 2009.

NEN-EN 1990. Eurocode - basis of structural design. Standard, 2002.

NEN-EN 1991-1-3. Eurocode 1: Actions on structures - part 1-3: General actions - snow loads. Standard, 2003.

NEN-EN 1991-1-4. Eurocode 1: Actions on structures - part 1-4: General actions - wind actions. Standard, 2005.

NEN-EN 1994-1-1. Eurocode 4: Design of composite steel and concrete structures - part 1-1: General rules and rules for buildings. Standard, 2005.

NEN-EN 450-1. Fly ash for concrete - part 1: Definition, specifications and conformity criteria. Standard, 2012.

Pier Luigi Nervi. *Structures*. F.W. Dodge Corp., New York :, 1956.

Pier Luigi Nervi and Robert Einaudi. *Aesthetics and technology in building*. The Charles Eliot Norton lectures ; 1961-1962; The Charles Eliot Norton lectures ... Harvard University Press, Cambridge, Mass. :, 1965.

Rob Nijsse. Corrugated glass as improvement to the structural resistance of glass. In *IABSE Symposium Report*, volume 96, pages 73–85. International Association for Bridge and Structural Engineering, 2009. ISBN 2221-3783.

Brent Richards. *New glass architecture*. Laurence King Publishing, 2006. ISBN 1856693767.

Christian Schittich and Architektur-Dokumentation Institut für Internationale. *Glass construction manual*. Birkhäuser ; [Springer [distributor], Basel : London :, 2nd, rev. and expanded ed. edition, 2007. ISBN 3764381221 9783764381226 3764382902 9783764382902.

Wolfgang Schueller. *The design of building structures*. Prentice Hall, 1996. ISBN 0133465608.

Trupti Sonavane. *Analysis of Arches*. Thesis, 2014.

Mahesh Varma, RS Jangid, and Siddhartha Ghosh. Thrust line using linear elastic finite element analysis for masonry structures. In *Advanced Materials Research*, volume 133, pages 503–508. Trans Tech Publ. ISBN 0878492399.

FA Veer, MMA Sluis, GJ Hobbelman, and J Zuidema. The use of glass in concrete as reinforcement and aggregate. In *Conf. on the Mechanical Behaviour of Materials (ICM9), Geneva, Switzerland*, pages 1–6.

Ludwig und Weiler and Krippl und Schiele. Maximilian museum in augsburg. *Detail*, pages 873–875, 2001.

Karlhans Wesche. *Fly ash in concrete: properties and performance*, volume 7. CRC Press, 2004. ISBN 0203626419.

Heide Wessely. A second look: Waterloo international terminal in london. *Detail*, pages 1154–1157, 2011.

YL Wong, L Lam, CS Poon, and FP Zhou. Properties of fly ash-modified cement mortar-aggregate interfaces. *Cement and Concrete Research*, 29(12):1905–1913, 1999a. ISSN 0008-8846.

YL Wong, L Lam, CS Poon, and FP Zhou. Properties of fly ash-modified cement mortar-aggregate interfaces. *Cement and Concrete Research*, 29(12):1905–1913, 1999b. ISSN 0008-8846.

Jan Wurm. *Glass structures: design and construction of self-supporting skins*. Walter de Gruyter, 2007. ISBN 3764383178.